論文 / 著書情報
Article / Book Information

題目(和文)	
Title(English)	Theoretical and Experimental Study of the Radiative Ortho-Para Transition in Disulfur Dichloride
著者(和文)	ﾃﾞｰｶﾞﾆﾀﾌﾃｲ ｾﾞｲﾅﾌﾞ
Author(English)	Zeinab Dehghanitafti
出典(和文)	学位:博士(理学), 学位授与機関:東京工業大学, 報告番号:甲第10928号, 授与年月日:2018年7月31日, 学位の種別:課程博士, 審査員:金森 英人,上妻 幹旺,松下 道雄,西田 祐介,相川 清隆,旭 耕一郎,遠藤 泰樹
Citation(English)	Degree:Doctor (Science), Conferring organization: Tokyo Institute of Technology, Report number:甲第10928号, Conferred date:2018/7/31, Degree Type:Course doctor, Examiner:,,,,,,
学位種別(和文)	博士論文
Type(English)	Doctoral Thesis

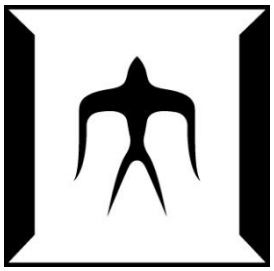

PhD Thesis

Theoretical and Experimental Study of the Radiative Ortho-Para Transition in Disulfur Dichloride

Zeinab DEHGHANI TAFTI

Under supervision of
Associate Professor Hideto KANAMORI

Department of Physics; Condensed Matter Physics
Graduate School of Science and Engineering
Tokyo Institute of Technology
Tokyo, Japan

April 2018

Abstract

Transition between the pure *ortho* and *para* states is theoretically impossible. Nevertheless, some inner perturbation effects, as collision and hyperfine interactions, can change the pure symmetrical character of molecular wave function to an impure character. In such cases, the electric dipole transition between two molecular states with opposite symmetries is theoretically possible, by intensity borrowing.

The present dissertation mainly aimed to respond theoretically and experimentally to this question that "which physical and spectroscopic parameters could determine possibility of the radiative *ortho-para* transition in an asymmetric top molecule via study of S_2Cl_2.

The millimeter wave spectroscopy is done for determination of the spectroscopic parameters of S_2Cl_2. Gas cell and supersonic jet spectroscopies involve the two different experimental setups being applied in the present study. As a result of microwave spectroscopy, all rotational molecular constants including fourth and sixth order centrifugal distortion constants of disulfur dichloride were determined for the first time. The measured frequency region was from 75GHz to 100GHz and the highest determined quantum numbers were $J = 55$ and $K_a = 12$.

Identifying the rotational spectroscopic constants in the millimeter wave region caused the matrix elements of disulfur dichloride molecular Hamiltonian to be calculated. In turn, by knowing the Hamiltonian matrix elements of this molecule, the term energies and molecular wave functions were determined. These molecular wave functions were used in regard with finding the *ortho-para* mixed states. The molecular wave functions were directly used in order to find the *ortho-para* mixing coefficients for the first time.

The study results concerning the *ortho-para* mixed states search reveal the *ortho-para* mixing coefficients for some K_a-doubling states of disulfur dichloride in the millimeter wave region are so high that direct observation of the radiative *ortho-para* transition could be regarded possible. Lists of the *ortho-para* mixed states were given as candidates with respect to direct observation of the *ortho-para* transition. It is worth mentioning that for the first time, a molecule is introduced as a candidate regarding direct observation of the radiative *ortho-para* transition.

As a matter of fact, a criterion is suggested for the *ortho-para* mixing coefficients for the first time. Using this criterion, by knowing the molecular spectroscopic parameters of a molecule, it seems to be possible to predict that whether this molecule serves as a good candidate regarding direct observation of *ortho-para* transitions. Regarding, a simple model for the Hamiltonian matrix, several criteria were derived to have the prediction about the magnitude of the *ortho-para* mixing coefficients. Three parameters were prominently taken into account according to this criterion including: splitting of the *ortho-para K*-doubling states, (ΔE_1), existence of at least the third state in the *ortho-para* mixing process, and the magnitudes of interaction of the third, fourth,… interacting states with the *ortho-para K*-doubling states (h_{op}). For a certain case, the energy difference of the third, fourth,… interacting state with the *ortho-para K*-doubling states, (ΔE_2), determines the magnitude of the *ortho-para* mixing coefficient. Dependency of the *ortho-para* mixing coefficient to *F*, *J* and K_a quantum numbers is demonstrated to be the same as that of ΔE_1, ΔE_2 and h_{op} to these quantum numbers.

Acknowledgements

All praise is to the God the lord of the universe, the compassionate, and the merciful. I should first express my highest gratitude for his blessing and mercy for making this work to be completed.

I also would like to express my thanks to my supervisor, associate professor Hideto Kanamori of the department of condensed matter physics, graduate school of science and engineering, Tokyo institute of technology, for his kind help, guidelines, and support throughout this work, without support of whom this work would barely come into reality.

Also, I appreciate assistance professor Asao Mizoguchi, the member of the Kanamori laboratory who raised criticisms, and shared his points/comments with me throughout this research term in order to improve the quality and standards of the study.

Last but not the least, I have to convey my deep thanks to my little son and daughter for their cooperation without which completion of this work would come too difficult, to my husband for his understanding, patience, and support that made me quite able to keep concentrating on my research throughout these years and in particular to my parents who always teach me the best solution of difficulties.

Table of contents

Chapter 1

Introduction

In this chapter, Section 1-1 presents motivations, objectives and the structure of this dissertation. Section1-2 present a review on previous studies on the *ortho-para* interactions, to which status of the present study is compared. Section 1-3 evaluates the previous spectroscopic studies carried out on disulfur dichloride. Finally, Section 1-4 discusses some important physical properties of S_2Cl_2 since identifying these properties is highly important in the experiment.

1-1 The Objectives and Structure of the Dissertation

According to the Pauli Exclusion Principle, there are restrictions on symmetry properties of molecular wave functions of molecules containing fermions, leading the total molecular wave functions to be classified into two groups named *ortho* and *para* states. Electric dipole transitions between pure *ortho* and pure *para* states are theoretically impossible. Expressing in another way, the *ortho* and *para* states can be treated as two different molecules. Nevertheless, perturbation effects such as collision and hyperfine interactions can change the pure symmetrical character of the molecular wave function. In this respect, the total molecular wave function, as a complete description of a molecule, is a mixture of both *ortho* and *para* states. In this situation, the electric dipole transitions between two molecular states with opposite symmetries are theoretically possible. Intensity borrowing model is a proper description of this forbidden transition. In other words, when an *ortho* state is mixed with a *para* state, the electric dipole transition from this nearby *ortho* state to another *para* state becomes possible by the intensity that is borrowed from the allowed *para-para* transition.

The *ortho-para* transition by the origin of the perturbation has been studied theoretically and experimentally in the molecules, ions and radicals. The experimental observation of this forbidden transition has been reported by the origin of nuclear spin rotational interaction and collision[12-18]. Although the nuclear electric quadruple interaction is recognized as the most important hyperfine interaction in singlet molecules, the *ortho-para* transition due to this interaction has not been reported. An experimental observation of radiative *ortho-para* transition and the prediction of its possibility are an interesting topic in the studies of interstellar media. Analysis of the data obtained from the spectroscopy of molecules in the interstellar media has demonstrated anomalous *ortho* to *para* ratios[1]. The radiative *ortho-para* transition has been investigated in regard to illuminating these anomalous observations[1]. Responding to this question that "Which molecules could have the radiative *ortho-para* transition" assists in improving the theories concerned with the physics of interstellar media. No experimental evidence has been so far reported regarding the radiative *ortho-para* transitions for molecules in their ground electronic state. The main objective of the present dissertation is to assess the

physical and spectroscopic parameters that could determine the possibility of the radiative *ortho-para* transition in an asymmetric top molecule via both theory and experiment.

To achieve this objective, selecting a proper molecule among asymmetric top molecules for the study is important. Mizoguchi et al. observed some unexpected hyperfine splitting in the FTMW centimeter wave spectrum of disulfur dichloride[2]. Furthermore, they proposed a nuclear quadrupole Hamiltonian with off-diagonal terms connecting the *ortho* and *para* states to explain the splitting. The newly-proposed model for the molecular Hamiltonian of S_2Cl_2 could explain the observed hyperfine transitions.

Predicting the new hyperfine splitting patterns in the spectrum of S_2Cl_2 is not the only result of proposing the off-diagonal hyperfine constants in the Hamiltonian of the molecule. The χ_{ab} and χ_{bc} coupling constants playing the main role in the *ortho-para* interactions, make the off-diagonal elements of the hyperfine Hamiltonian matrix comparable to the diagonal elements. Furthermore, the dense spectrum of disulfur dichloride in the millimeter wave region suggests the existence of the molecular states by small magnitude of separation between the *ortho* and *para* states. These two properties would mix the *ortho* and the *para* states. The existence of the mixed *ortho-para* states leads to the non-zero transitions moment between the *ortho* and the *para* states. Therefore, observation of *ortho-para* transitions in the millimeter wave region can be regarded as another evidence for the verification of the newly-proposed Hamiltonian for S_2Cl_2. In addition, the second objective of the present dissertation is to introduce a criterion, which could predict the *ortho-para* mixing coefficients.

To achieve the two mentioned objectives, this study was conducted in two stages. The first stage was the millimeter wave spectroscopy of disulfur dichloride, and the second stage involves the theoretical study of the *ortho-para* interaction in disulfur dichloride. Indeed, the rotational and hyperfine constants obtained in the first stage were also applied in the second stage.

The structure of this dissertation consists as follows. Chapter 1 proposes a review concerning the previous studies conducted on the *ortho-para* interaction in order to provide a background for the study. Moreover, a review on microwave spectroscopy of disulfur dichloride is discussed. Chapter 2 explains the general theories applied in this study, involving the proposed rotational and nuclear quadrupole Hamiltonian for symmetric rotors. In fact, they demonstrate a common way to find the asymmetric top Hamiltonian in the symmetric rotor basis set. In addition, this chapter demonstrates the method to find the transition moment in symmetric and asymmetric top molecules as well as the selection rules. Chapter 3 describes the experimental techniques used in this study, consisting of supersonic jet and gas cell experiments. The techniques applied in these setups are also explained in this chapter, involving supersonic jet expansion, lock-in amplifier, and frequency modulation. Chapter 4 discusses details of millimeter wave spectroscopy of disulfur dichloride. By analyzing the data obtained in this step, the rotational and hyperfine constants of S_2Cl_2 in the millimeter wave region can be obtained. In fact, these spectroscopic constants are utilized in the following chapters to investigate the *ortho-para* interaction. Chapter 5 proposes the *ortho-para* interaction theoretically. The theory of finding the *ortho-para* mixed states is improved, by which a list of *ortho-para* mixed states is calculated. Furthermore, a criterion is given with respect to the prediction of the magnitude of the *ortho-para* mixing coefficients. Finally, Chapter 6 presents a conclusion for the presently reported work and offers some suggestions for future extensions.

1-2 Review of the *Ortho-Para* Interaction Studies

The anomalous specific heat of hydrogen[3] and the line intensity alternation in the molecular spectra[4] of this molecule were two unrelated puzzles at the beginning of 20th century leading to the discovery of two different modifications of hydrogen, that is to say, the spin of proton[5-6].

As a result, the two hydrogen nuclei are distinguished as particles with a half-integer spin value named fermions. Indeed, their wave functions, like any other fermions, obey the Pauli Exclusion Principle[7-8]. According to the Pauli Exclusion Principle, two identical fermions cannot occupy the same quantum state simultaneously. In other words, the total molecular wave function of two fermions is anti-symmetric to the particles exchange. Regarding H_2 molecule, two nuclear spin isomers are distinguished: the *ortho* hydrogen by total spin of $I = 1$ and the *para* hydrogen by total spin of $I = 0$. According to the Pauli Exclusion Principle, the symmetry of molecular wave function upon interchange of two protons allows only odd values of rotational angular momentum (J) for the *ortho* and only even values of J for the *para* nuclear spin combination[6].

The key point in easy separation and conversion of nuclear spin isomers of hydrogen molecules is the large rotational level spacing in this molecule. However, as in polyatomic molecules, the molecular level spacing is not as large as the hydrogen molecules. Therefore, finding a method for nuclear spin separation and conversion was a challenge[9]. Today via improvement of experimental methods such as light induced drift technique[12, 14, 15], separation and conversion of nuclear spin are successfully performed for a number of molecules[12-13, 16-18]. However, in the astrophysics, it is widely assumed that nuclear spin conversion probability is almost zero in the interstellar media[11]. Small level spacing in polyatomic molecules also brought this idea that the nuclear spin isomer conversion rates for these molecules are faster as confirmed by Ozier et al[17]. In fact, they could observe an *ortho-para* transition in this molecule via shifting an *ortho* state of methane molecule to a *para* state using an external magnetic field[19].

Finally, Curl et al. formulated theory of nuclear spin isomer conversion by collision in polyatomic molecules[20]. The validity of this theory has been demonstrated by a series of experiments by Chapovsky and his collaborators[21]. The mechanism of nuclear isomer spin conversion by collision, also named quantum relaxation[22], is based on the intramolecular mixing of *ortho* and *para* states and collisional destruction of the coherence between the states. Formulating the nuclear spin isomer conversion as well as developing experimental techniques to observe them led studies on nuclear spin isomer conversion to be directed to studies of multi-dimensional symmetry polyatomic molecules such as ethylene, C_2H_4[11] with four nuclear spin modifications, benzene, C_6H_6 with six nuclear spin modifications, and ethane, C_2H_6[23] with seven nuclear spin modifications.

As mentioned above, the most studies carried out on the nuclear spin conversion of molecules focused on the mechanism formulation of the nuclear spin conversion via collision and the experimental techniques improvement based on the separation of nuclear spin isomers as well as their conversion. The nuclear spin-rotation hyperfine interaction can be stated as the origin of nuclear spin isomer conversion in all these studies[24-31]. To date, the studied *ortho-para* interactions were not strong enough to lead to the radiative *ortho-para* transition in the ground electronic states of molecules. Moreover, to calculate the *ortho-para* mixing coefficients, all of these studies applied the perturbation theory and thus, no direct calculation of the *ortho-para* mixing coefficients has been reported through wave functions.

The present study intended to investigate $S_2{}^{35}Cl_2$ molecule. The nuclear quadrupole terms in this molecule play the role of the interaction changing the pure symmetry of molecular wave function to impure symmetry. Determination of off-diagonal nuclear quadrupole coupling constant of disulfur dichloride made this molecule a special sample in the nuclear spin conversion studies[2]. The χ_{ab} and χ_{ac} coupling constants, fulfilling the main role in mixing *ortho* and *para* molecular wave functions, make the off-diagonal elements of the hyperfine Hamiltonian matrix of this molecule comparable to the diagonal elements. Like SF_6 molecule that its spin-rotation hyperfine constant value as the origin of the *ortho-para* transition is larger than the centrifugal constants[31], the nuclear quadrupole off-diagonal constants values of $S_2{}^{35}Cl_2$ are larger than its fourth-order and sixth-order centrifugal distortion rotational constants. This can result in a measurable hyperfine splitting pattern in the spectrum of this molecule as well as large value of the *ortho-para* mixing coefficients in the molecular wave functions considered as eigenvectors of the molecular Hamiltonian matrix.

In the current study, for the first time, the *ortho-para* mixing states are calculated directly via the molecular wave functions rather than using the perturbation theory leading the methods to search the *ortho-para* mixing states to be ameliorated. In addition, the *ortho-para* interaction by the origin of the nuclear quadrupole interaction is studied for the first time. Investigating the nuclear quadrupole interaction in disulfur dichloride aims to demonstrate the possibility of the radiative *ortho-para* transition in the ground electronic state of this molecule.

1-3 Review of S_2Cl_2 Spectroscopy

Since the intensity of transitions can get increased via third power of frequencies, one can take the advantage of the millimeter-wave spectroscopy of S_2Cl_2 to bring the observation of weak *ortho-para* transitions closer to the reality. In this study, microwave spectroscopy of disulfur dichloride seems to be inevitable in regard to improving rotational molecular constants to have a proper prediction of *ortho-para* transition frequencies and intensities. In this section, a review is presented regarding the previous studies carried out on S_2Cl_2 spectroscopy.

Beginning of the spectroscopic studies on disulfur dichloride dates back returns to 1930s when there was an interest on the determination of X_2Y_2 molecular structures and as a result, the S_2X_2 molecular structure[33]. Several experimental techniques were used to determine the structure of this molecule, including infrared and Raman spectroscopy as well as electron and X-ray diffractions. Initial Raman spectroscopy of disulfur dichloride revealed that the double bonding between sulfur atoms of this molecule was impossible[34]. Investigations based on the electron diffraction measurements concluded that each sulfur atom is bonded only with one chlorine atom. Further investigations indicated that skew ClSSCl type of configuration for disulfur dichloride was ultimately concluded[33-41].

Two studies were previously conducted on microwave spectroscopy of disulfur dichloride. In initial microwave spectroscopy of this molecule in 1979[42], 8-40 GHz frequency region of centimeter-wave spectrum of S_2Cl_2 was measured. Marsden et al. analyzed these data and determined A, B and C rotational constants for $S_2{}^{35}Cl_2$ and $S_2{}^{35}Cl^{37}Cl$ isotope species as well as diagonal nuclear quadrupole constants for $S_2{}^{35}Cl_2$[42]. Via microwave spectroscopy, they also confirmed the findings of the previous studies[43-44] concerning the abundance of $S_2{}^{35}Cl_2$ and $S_2{}^{35}Cl^{37}Cl$ isotope species.

Mizoguchi et al. reported second and last microwave spectroscopy of S_2Cl_2 in 2008[2]. Using a Fourier transform microwave spectrometer, they measured the centimeter-wave spectrum of $S_2{}^{35}Cl_2$ and $S_2{}^{35}Cl^{37}Cl$ isotope species. Furthermore, using a high resolution technique, they

succeeded in determining hyperfine splitting lines due to off-diagonal nuclear quadrupole constants. Consequently, they could determine the off-diagonal nuclear quadrupole constants values for $S_2{}^{35}Cl_2$ and $S_2{}^{35}Cl^{37}Cl$ isotope species. In addition, they measured the nuclear spin-rotation coupling constants and forth-order centrifugal distortion constants (except δ_K) for both $S_2{}^{35}Cl_2$ and $S_2{}^{35}Cl^{37}Cl$ isotope species. It is worth mentioning that for the first time in the mentioned study, C_2 symmetry configuration for disulfur dichloride could be concluded.

In this study, the microwave spectra of $S_2{}^{35}Cl_2$ and $S_2{}^{35}Cl^{37}Cl$ isotope species in the millimeter wave region were measured. Another innovation was introduced in this study. That is all rotational molecular constants of disulfure dichloride isotopes, including fourth and sixth order centrifugal distortion constants were determined via assignments of transitions applying large values of rotational quantum numbers. Moreover, in the present study, the reliability of the centimeter wave region of nuclear quadrupole constants was confirmed, in the millimeter wave region.

1-4 Physical Properties of S_2Cl_2

Knowledge concerning physical properties of disulfure dichloride is regarded important to design the experimental setup and data analysis. In this section, some physical properties of this molecule are explained.

$S_2{}^{35}Cl^{35}Cl$, $S_2{}^{35}Cl^{37}Cl$ and $S_2{}^{37}Cl^{37}Cl$ involve three isotope species of disulfure dichloride by abundances of 56 %, 38% and 6% [2], respectively. Disulfur Dichloride (S_2Cl_2) is a yellow liquid by the molar mass equal to 135.04 g/mol and density of 1.688 g/cm^3. The melting and boiling points of this substance are reported as 193K and 410.2K, respectively. S_2Cl_2, highly reactive to metals, is soluble in ethanol, benzene, chloroform and CCl_4.

This chiral molecule, with a skew Cl-S-S-Cl type of conformation, has C_2 symmetry along b molecular axis with permanent dipole moment equal to 1.6D. Figure 1.1 demonstrates the S_2Cl_2 configuration schematically. As a matter of fact, the chiral ground electronic potential of this molecule makes this molecule a potential candidate in regard to observing the parity violation[45].

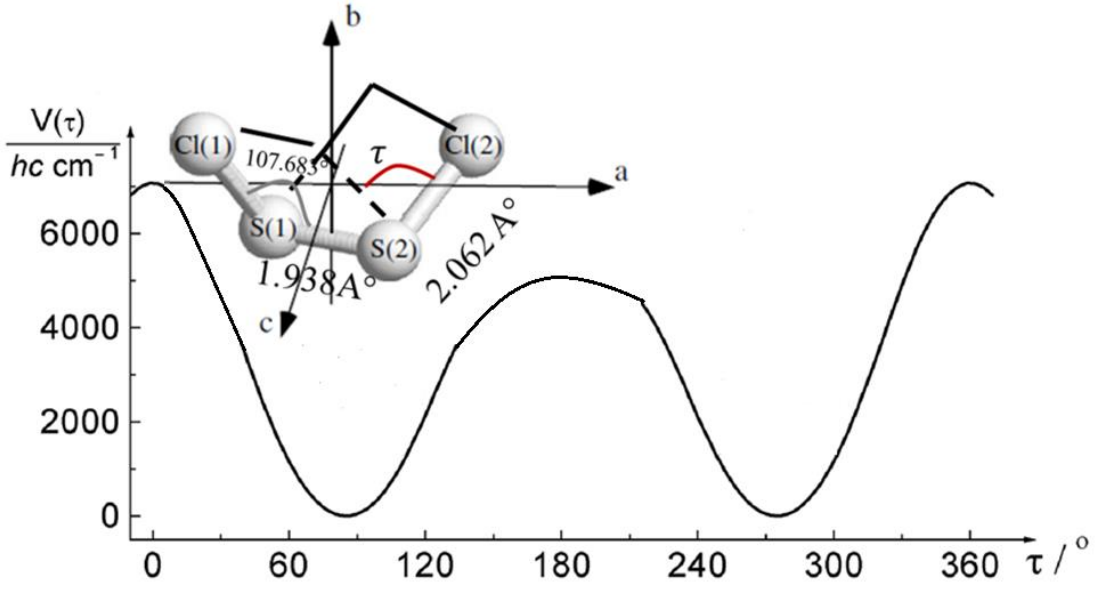

Figure 1.1: Schematic representation of S_2Cl_2symmetry configuration and its chiral ground electronic potential[2, 45]

The vapor pressure of this molecule is of great significance in the experiment data analysis of the current study. Using Antoine equation, vapor pressure can be obtained at different temperatures.

$$\log_{10}(P) = A - (B / (T + C)) \quad (1\text{-}1)$$

Using A, B, C coefficients for a specific temperature in Kelvin, vapor pressure can be obtained in the bar. A, B, C coefficients for S_2Cl_2 are equal to 4.0648, 1417.43 and -61.685, respectively. The validity of these coefficients for temperatures 268.5K to 411.0K is experimentally confirmed [46]. Interested temperatures in this study are 300K (room temperature) and 195K (dry ice temperature). Using Equation 1, the vapor pressure of disulfur dichloride at room temperature and dry ice temperature was equal to 10 Torr and0.0002 Torr, respectively.

Chapter 2

Theory

In this chapter, theories governing this research will be described. However, the theory of the *ortho-para* interaction, as the main object of this research, will be described in Chapter 5. In sections 2-1 and 2-2, rotational and nuclear quadrupole interactions for asymmetric rotors will be discussed respectively, based on which the calculation of the molecular wave functions and term energies of disulfur dichloride will be formed. In order to calculate an *ortho-para* transition moment, the theory of calculating hyperfine transitions moments as well as the selection rules in asymmetric rotors will be required, which are explained in sections 2-3 and 2-4 respectively. It should be noted that the application of these sections will be proposed in Chapters 4 and 5, and the formulas in this chapter will also be used in the Appendix A programs.

2-1 Asymmetric Rotor Hamiltonian (rotational term)

In quantum mechanics, the free rotation of a molecule is described via the moment of inertia. I_a, I_b and I_c denote the moment of inertia around a, b and c axis respectively. These three axes are orthogonal and their origin is the center of mass of the molecule. a, b and c principal axes are chosen in a way that $I_a < I_b < I_c$, conventionally. Therefore, when $I_b \rightarrow I_c$, the prolate symmetric top is approached and when $I_b \rightarrow I_a$, the oblate symmetric top is approached. This behavior of an asymmetric top can be described by *k* parameter:

$$k = (2B - A - C) / (A - C) \tag{2-1}$$

Limiting values for *k* are -1 and 1 which correspond to prolate and oblate symmetric tops respectively. This description of asymmetric top molecules leads to introducing $J_{K_a K_c}$ or $J_{K_{-1} K_1}$ notation concerning the description of an asymmetric top molecule[47].

As rotational angular momentum commutes with Hamiltonian of the asymmetric top molecules, the same as symmetric tops, *J* is considered as a good quantum number in regard to describing these types of molecules. In order to find other quantum numbers for describing asymmetric tops, some explanations will be given as follows.

Hamiltonian of an asymmetric top rotor would be written the same as Hamiltonian of all rigid rotors. By considering centrifugal distortion effects, this Hamiltonian can be written as below in the body-fixed coordinate system[32]:

$$H = AP_z^2 + B\,P_x^2 + C\,P_y^2 - \Delta_J P^4 - \Delta_{JK}\,P^2\,P_z^2 - \Delta_K\,P_z^4 - 2\delta_J\,P^2\,(P_x^2 - P_y^2) - \delta_K\,[P_z^2\,(P_x^2 - P_y^2) + (P_x^2 - P_y^2)\,P_z^2] + H_J P^6 + H_{JK}\,P^4\,P_z^2 + H_{KJ} P^2\,P_z^4 + H_K\,P_z^6 + 2h_J P^4\,(P_x^2 - P_y^2) + h_{JK} P^2\,[P_z^2\,(P_x^2 - P_y^2) + (P_x^2 - P_y^2)\,P_z^2] + h_K\,[P_z^4\,(P_x^2 - P_y^2) + (P_x^2 - P_y^2)\,P_z^4] \tag{2-2}$$

In order to identify term energy and wave functions of an asymmetric top, asymmetric top wave function should be written as linear combination of symmetric top wave functions.

$$|\Psi_{J\,\tau}> = \sum_{K=-J,\ldots J} (a_{JK}\,|\Psi_{JK}>), \qquad (2\text{-}3)$$

where $\tau = K_a - K_c$, $|\Psi_{J\,\tau}>$ and $|\Psi_{JK}>$ involve asymmetric top and symmetric top wave functions, respectively.

Another important issue to be taken into account with respect to finding the term energies and wave functions of an asymmetric top are the way a, b, c principal axes are identified by x, y and z notation in equation 2-2. Regarding asymmetric tops with *k* parameter near to -1, the same as S_2Cl_2 with $k = -0.92$, I^r representation is assumed as the most convenient to determine the term energies and wave functions. In I^r representation, identification of a, b and c principal axes is as below[31]:

$$x \rightarrow b, \quad y \rightarrow c, \quad z \rightarrow a \qquad (2\text{-}4)$$

Although via using 2-2 and 2-3, the term energies and wave functions of an asymmetric rotor can be evaluated, the evaluation can be simplified applying Wang basis set. Details concerning the Wang basis set will be described, in the following.

The Hamiltonian of a rigid asymmetric rotor is invariant under a rotation of 180°, C_2, in regard to any of the principal axes of inertia. It is also invariant under identity operation, E. The set of symmetry operation including E and C_2 about each of axis of inertia form a group that is known as the Four-group and designated by V(a, b, c). These symmetry operations transform the angular momentum in the following manner[32]:

$$\begin{aligned}
&E: \quad P_a \rightarrow P_a,\ P_b \rightarrow P_b,\ P_c \rightarrow P_c \\
&C_2^{a}: P_a \rightarrow P_a,\ P_b \rightarrow -P_b,\ P_c \rightarrow -P_c \\
&C_2^{b}: P_a \rightarrow -P_a,\ P_b \rightarrow P_b,\ -P_c \rightarrow P_c \\
&C_2^{c}: P_a \rightarrow -P_a,\ P_b \rightarrow -P_b,\ P_c \rightarrow P_c
\end{aligned} \qquad (2\text{-}5)$$

The character table of the V(a, b, c) is given in Table 2.1[32].

Table 2.1: Character table of the four group V(a,b,c)[32]

Symmetry species	***E***	C_2^a	C_2^b	C_2^c
A	1	1	1	1
$\mathbf{B_a}$	1	1	-1	-1
$\mathbf{B_b}$	1	-1	1	-1
$\mathbf{B_c}$	1	-1	-1	1

The multiplication table is indicated in Table 2.2[32].

Table 2.2: Multiplication table of the four group V(a,b,c)[32]

	A	**B_a**	**B_b**	**B_c**
A	A	B_a	B_b	B_c
B_a	B_a	A	B_c	B_b
B_b	B_b	B_c	A	B_a
B_c	B_c	B_b	B_a	A

Symmetric rotor wave functions do not belong to the four group, though, their Wang linear combination belongs to the four group[48-49]. Wang linear combination of symmetric rotor wave function can be stated as below[32]:

$$S_{JK\gamma} = (1/\sqrt{2})[\Psi_{JK} + (-1)^{\gamma}\Psi_{J-K}] \quad \text{for } K>0$$
$$S_{J00} = \Psi_{J0} \quad \text{for } K = 0. \qquad (2\text{-}6)$$

Where $\gamma = 0$ is for symmetric Wang functions, whereas $\gamma = 1$ is for antisymmetric Wang functions. Each asymmetric rotor wave function can be written as a linear combination of symmetrized function as expansion 2-7[32].

$$A_{J\tau} = \sum_{K=0,\dots J} (a_{K\tau}^{J} S_{JK\gamma}) \qquad (2\text{-}7)$$

Since symmetrized functions can be classified into symmetric species of asymmetric rotor four group, the sum over K is only over $S_{JK\gamma,}$ which belongs to the same symmetry. As a result, the rotational Hamiltonian would be written as equation 2-8[32].

$$H = E^{+} + O^{+} + E^{-} + O^{-}. \qquad (2\text{-}8)$$

where + and – correspond to evenness and oddness of γ respectively and E and O correspond to the even and odd K respectively. In pure rotational condition, E^{+}, O^{+}, E^{-} and O^{-} are independent, each of which can be calculated and made diagonal separately in order to find their term energies and wave functions. Some portion of each class of Hamiltonian is depicted as matrices in equation 2-9[32].

$$E^{+} = \begin{bmatrix} H_{00} & \sqrt{2}H_{02} & 0 & . & . \\ \sqrt{2}H_{02} & H_{22} & H_{24} & 0 & . \\ 0 & H_{24} & H_{44} & H_{46} & . \\ . & 0 & H_{46} & H_{66} & . \\ . & . & . & . & . \end{bmatrix}$$

$$E^{-}=\begin{bmatrix} H_{22} & H_{24} & 0 & . & . \\ H_{24} & H_{44} & H_{46} & 0 & . \\ 0 & H_{46} & H_{66} & H_{68} & . \\ . & 0 & H_{68} & H_{88} & . \\ . & . & . & . & . \end{bmatrix}$$

$$O^{+}=\begin{bmatrix} H_{11}+H_{-11} & H_{13} & 0 & . & . \\ H_{13} & H_{33} & H_{35} & 0 & . \\ 0 & H_{35} & H_{55} & H_{57} & . \\ . & 0 & H_{57} & H_{77} & . \\ . & . & . & . & . \end{bmatrix}$$

$$O^{-}=\begin{bmatrix} H_{11}-H_{-11} & H_{13} & 0 & . & . \\ H_{13} & H_{33} & H_{35} & 0 & . \\ 0 & H_{35} & H_{55} & H_{57} & . \\ . & 0 & H_{57} & H_{77} & . \\ . & . & . & . & . \end{bmatrix} \qquad (2\text{-}9)$$

Symmetry classification of V(x, y, z), as well as symmetry classification of V(a, b, c) are shown in Tables 2.3 and 2.4 respectively. Utilizing these two tables, asymmetric rotor wave function, corresponded to *K* quantum number, can be found in symmetrized wave function.

Table 2.3: Symmetry classification of submatrices in V(x, y, z)[32]

Sub matrix	***K***	***γ***	***J*+γ**			
			J_{even}	J_{odd}	J_{even}	J_{odd}
$\mathbf{E^{+}}$	e	e	e	o	A	B_z
$\mathbf{E^{-}}$	e	o	o	e	B_z	A
$\mathbf{O^{+}}$	o	e	e	o	B_y	B_x
$\mathbf{O^{-}}$	o	o	o	e	B_x	B_y

Table 2.4: Symmetry classification of V (a, b, c) in I^r representation[32]

Sub-matrix	J_{even}	J_{odd}
E^{+}	A (ee)	B_a (eo)
E^{-}	B_a (eo)	A (ee)
O^{+}	B_c (oe)	B_b (oo)
O^{-}	B_b (oo)	B_c (oe)

Equations and Tables in this section will be applied with respect to the calculation of term energies and molecular wave functions as well as analysis of the observed millimeter wave spectrum of disulfur dichloride. Moreover, the application of this section will be represented in chapters 4 and 5.

2-2 Asymmetric Rotor Hamiltonian (nuclear quadrupole hyperfine term)

Nonspherical distribution of nuclear charge gives rise to the nuclear quadrupole moment. Non-spherical distribution of electronic charge around a nucleus leads to the electric field gradient at the nucleus. The electric field gradient puts a torque on the nuclear that aligns its spin moment in direction of the field gradient. Due to this torque, the spin axis process concerning the direction of the field gradient gives rise to processional frequencies and nuclear quadruple spectra. Nuclear quadrupole interaction, in the language of irreducible tensors, for N coupling nuclei (N>1), is formulated as following[2].

$$H_Q = \sum_{i=1}^{N} Q^2(i) \cdot V^2(i) \tag{2-10}$$

where

$$T^k \cdot U^k = \sum_{q=-k}^{k} (-1)^q T_q U_{-q} \tag{2-11}$$

When coupling energies are the same or nearly similar to this coupling scheme, the following can be employed[32].

$$\begin{aligned} &I_1 + I_2 = \mathcal{J}_2 \\ &\mathcal{J}_2 + I_3 = \mathcal{J}_3 \\ &\vdots \\ &\mathcal{J}_{L-1} + I_L = \mathcal{J}_L \\ &\vdots \\ &\mathcal{J}_{N-1} + I_N = \mathcal{J}_N \\ &J + \mathcal{J}_N = F \end{aligned} \tag{2-12}$$

The basis function in regard to calculating matrix elements of the nuclear quadruple interaction is:

$$|K\, J I_1 I_2 \mathcal{J}_2 \cdots I_L \mathcal{J}_L \cdots I_N \mathcal{J}_N F M_F > \tag{2-13}$$

We have for the matrix elements of quadruple interaction for the Lth coupling nucleus[50].

$$\begin{aligned} &\langle K' J' I_1' I_2' \mathcal{J}_2' \cdots I_L' \mathcal{J}_L' \cdots I_N' \mathcal{J}_N' F' M_F' | Q(L) V(L) | K\, J I_1 I_2 \mathcal{J}_2 \cdots I_L \mathcal{J}_L \cdots I_N \mathcal{J}_N F M_F \rangle = \\ &\delta_{FF'} \delta_{M_F M_F'} (-1)^t \left(eQq_{JJ'}\right)_L f(J') f(I_L) \begin{Bmatrix} \mathrm{F} & \mathcal{J}_N' & \mathrm{J}' \\ 2 & J & \mathcal{J}_N \end{Bmatrix} \Bigg[[(2\mathcal{J}_N + 1)(2\mathcal{J}_N' + 1)]^{1/2} \times \\ &\begin{Bmatrix} \mathrm{I_L} & \mathcal{J}_L' & \mathcal{J}_{L-1} \\ \mathcal{J}_L & \mathrm{I_L} & 2 \end{Bmatrix} \Bigg] \times \prod_{i=L}^{N-1} [(2\mathcal{J}_{i+1} + 1)(2\mathcal{J}_{i+1}' + 1)]^{1/2} \begin{Bmatrix} \mathcal{J}_i' & \mathcal{J}_{i+1}' & I_{i+1} \\ \mathcal{J}_{i+1} & \mathcal{J}_i & 2 \end{Bmatrix} \end{aligned} \tag{2-14}$$

Where

$$t = J + F + I_N + \mathcal{J}_{L-1} + \prod_{i=L}^{N-1}(I_i + \mathcal{J}_{i+1} + \mathcal{J}'_{i+1}) + 2\mathcal{J}'_L$$

$$f(J') = \left[2\begin{pmatrix} J & 2 & J' \\ J & 0 & -J \end{pmatrix}\right]^{-1}$$

$$f(I_L) = \left[2\begin{pmatrix} I_L & 2 & I_L \\ -I_L & 0 & I_L \end{pmatrix}\right]^{-1} \quad (2\text{-}15)$$

In the special case of two identical coupling nuclei, 2-10 can be rewritten as equations 2-16 and 2-17[32] for each nuclear equation.

$$\langle K'J'I_1I_2\mathcal{J}'F'M'_F|Q(1)V(1)|K\,JI_1I_2\mathcal{J}FM_F\rangle = \delta_{FF'}\delta_{M_FM'_F}(-1)^{t_1}\left(eQq_{JJ'}\right)_1 f(J')f(I_1)[(2\mathcal{J}+1)(2\mathcal{J}'+1)]^{1/2}\begin{Bmatrix} \mathrm{F} & \mathcal{J}' & \mathrm{J}' \\ 2 & J & \mathcal{J} \end{Bmatrix}\begin{Bmatrix} I_1 & \mathcal{J}' & I_2 \\ \mathcal{J} & I_1 & 2 \end{Bmatrix} \quad (2\text{-}16)$$

$$\langle K'J'I_1I_2\mathcal{J}'F'M'_F|Q(2)V(2)|K\,JI_1I_2\mathcal{J}FM_F\rangle = \delta_{FF'}\delta_{M_FM'_F}(-1)^{t_2}\left(eQq_{JJ'}\right)_2 f(J')f(I_2)[(2\mathcal{J}+1)(2\mathcal{J}'+1)]^{1/2}\begin{Bmatrix} \mathrm{F} & \mathcal{J}' & \mathrm{J}' \\ 2 & J & \mathcal{J} \end{Bmatrix}\begin{Bmatrix} I_2 & \mathcal{J}' & I_1 \\ \mathcal{J} & I_2 & 2 \end{Bmatrix} \quad (2\text{-}17)$$

With

$$t_1 = J + I_1 + I_2 + \mathcal{J}' + \mathcal{J} + F$$
$$t_2 = J + I_1 + I_2 + 2\mathcal{J}' + F$$
$$\boldsymbol{I_1 + I_2 = \mathcal{J} \equiv I}$$
$$\boldsymbol{I + J = F} \quad (2\text{-}18)$$

Finally, using equations 2-10, 2-11, 2-16 and 2-17, we can write matrix elements of nuclear quadruple Hamiltonian for disulfur dichloride by equation 2-19[2].

$$\left\langle \mathrm{J'K'(I_1I_2)I'F'M'_F}\middle|\mathbf{H_Q}\middle|\mathrm{J\,K(I_1I_2)I\,F\,M_F}\right\rangle = \delta_{\mathrm{F'F}}\delta_{\mathrm{M'_FM_F}}(-1)^{\mathrm{J'+J-K'+I_1+I_2+2I'+F}} \times (1/2)[(2\mathrm{I'}+1)(2\mathrm{I}+1)(2\mathrm{J'}+1)(2\mathrm{J}+1)]^{1/2} \times \begin{Bmatrix} \mathrm{F} & \mathrm{I'} & \mathrm{J'} \\ 2 & \mathrm{J} & \mathrm{I} \end{Bmatrix}\sum_{\mathrm{q}}(-1)^{\mathrm{q}}\begin{pmatrix} \mathrm{J'} & 2 & \mathrm{J} \\ -\mathrm{K'} & -\mathrm{q} & \mathrm{K} \end{pmatrix} \quad (2\text{-}19)$$

In equation 2-10, $\mathrm{eQ_X V^2_{-q}(X)}$ is related to the component of field gradient tensor in the principal inertia axis coordinate as below:

$$\mathrm{eQV^2_0} = (1/2)\mathrm{eQq_{aa}} = (1/2)\chi_{\mathrm{aa}}$$
$$\mathrm{eQV^2_{\pm1}} = \mp(1/\sqrt{6})[\mathrm{eQq_{ab}} \pm \mathrm{i.\,eQq_{ac}}] = \mp(1/\sqrt{6})[\chi_{\mathrm{ab}} \pm \mathrm{i.}\,\chi_{\mathrm{ac}}]$$
$$\mathrm{eQV^2_{\pm2}} = \left(1/2\sqrt{6}\right)[\mathrm{eQq_{bb}} - \mathrm{eQ_{cc}} \pm 2\mathrm{i.\,eQq_{bc}}] = (1/2\sqrt{6})[\chi_{\mathrm{bb}} - \chi_{\mathrm{cc}} \pm 2\mathrm{i.}\,\chi_{\mathrm{bc}}] \quad (2\text{-}20)$$

As S_2Cl_2 has C_2 symmetry along b molecular principle axis, the below relationship between hyperfine constants of nucleus 1 and nucleus 2 can be held[2].

$$\chi_{\mathrm{ii}}(1) = \chi_{\mathrm{ii}}(2)$$
$$\chi_{\mathrm{ab}}(1) = -\chi_{\mathrm{ab}}(2)$$
$$\chi_{\mathrm{ac}}(1) = \chi_{\mathrm{ac}}(2)$$

$$\chi_{\mathrm{bc}}(1) = -\chi_{\mathrm{bc}}(2) \tag{2-21}$$

As *ortho-para* interaction is of interest in this study, obtaining matrix elements of nuclear quadruple Hamiltonian in more details is valuable. C_X is defined as equation 2-22[2].

$$C_X = (-1)^{J'+J-K'+I_1+I_2+2I'+F}\frac{1}{2}[(2I'+1)(2I+1)(2J'+1)(2J+1)]^{\frac{1}{2}} \times \begin{Bmatrix} F & I' & J' \\ 2 & J & I \end{Bmatrix}\begin{Bmatrix} I_X & I' & I_X \\ I & I_X & 2 \end{Bmatrix}\begin{pmatrix} I_X & 2 & I_X \\ -I_X & 0 & I_X \end{pmatrix}^{-1}\delta_{F'F}\delta_{M'_F M_F} \tag{2-22}$$

As nuclear spin angular momentum has the same value, instead of C_1 or C_2, constant C is used in the following formulas. When the Wang basis functions $|JK(I_1I_2)IFM_F\gamma\rangle$ are applied as the basis set, the matrix elements of nuclear quadruple Hamiltonian are as follows[2] using equation 2-20 and 2-21.
For the case $\Delta K = 0$:

$$\langle J'K'(I_1I_2)I'F'M'_F \pm |\mathbf{H}_Q|JK(I_1I_2)IFM_F\gamma\rangle = \frac{C}{2\sqrt{(1+\delta_{K'0})(1+\delta_{K0})}} \times \left\{\begin{pmatrix} J' & 2 & J \\ -K' & 0 & K \end{pmatrix}\frac{1+(-1)^{\Delta J+p}}{2}\left[(-1)^{I'-I}\chi_{aa}(1)+\chi_{aa}(2)\right] \pm \delta_{K1}\begin{pmatrix} J' & 2 & J \\ 1 & -2 & 1 \end{pmatrix}\frac{1+(-1)^{\Delta J+p}}{2\sqrt{6}} \times \{(-1)^{I'-I}[\chi_{bb}(1)-\chi_{cc}(1)]+[\chi_{bb}(2)-\chi_{cc}(2)]\} \pm \delta_{K1}\begin{pmatrix} J' & 2 & J \\ 1 & -2 & 1 \end{pmatrix}\frac{1-(-1)^{\Delta J+p}}{2\sqrt{6}}2i\left[(-1)^{I'-I}\chi_{bc}(1)+\chi_{bc}(2)\right]\right\} \tag{2-23}$$

Where $p = 0$ in the case of $\gamma' = \gamma$, while $p = 1$ for $\gamma' \neq \gamma$.
For $\Delta K = 1$:

$$\langle J'K'(I_1I_2)I'F'M'_F \pm |\mathbf{H}_Q|JK(I_1I_2)IFM_F\gamma\rangle = \frac{C}{2\sqrt{(1+\delta_{K'0})(1+\delta_{K0})}} \times \begin{pmatrix} J' & 2 & J \\ -K' & \mp 1 & K \end{pmatrix}\left\{\pm\frac{1-(-1)^{\Delta J+p}}{\sqrt{6}}\left[(-1)^{I'-I}\chi_{ab}(1)+\chi_{ab}(2)\right]+i\frac{1+(-1)^{\Delta J+p}}{\sqrt{6}}\left[(-1)^{I'-I}\chi_{ac}(1)+\chi_{ac}(2)\right]\right\} \tag{2-24}$$

For $\Delta K = 2$:

$$\langle J'K'(I_1I_2)I'F'M'_F \pm |\mathbf{H}_Q|JK(I_1I_2)IFM_F\gamma\rangle = \frac{C}{2\sqrt{(1+\delta_{K'0})(1+\delta_{K0})}} \times \begin{pmatrix} J' & 2 & J \\ -K' & \mp 2 & K \end{pmatrix} \times \left\{\frac{1+(-1)^{\Delta J+p}}{2\sqrt{6}}\{(-1)^{I'-I}[\chi_{bb}(1)-\chi_{cc}(1)]+[\chi_{bb}(2)-\chi_{cc}(2)]\} \mp i\frac{1-(-1)^{\Delta J+p}}{\sqrt{6}}\left[(-1)^{I'-I}\chi_{bc}(1)+\chi_{bc}(2)\right]\right\} \tag{2-25}$$

The nuclear quadruple Hamiltonian matrix elements, which are not zeros when $\Delta I = |I'-I| = 1$ are responsible for the *ortho-para* interactions. Nonzero elements of the nuclear quadruple Hamiltonian matrix by combining equations 2-21 with 2-25 and assuming that $\chi_{\mathrm{ab}}(1) = \chi_{\mathrm{ab}}$, $\chi_{\mathrm{ac}}(1) = \chi_{\mathrm{ac}}$ and $\chi_{\mathrm{bc}}(1) = \chi_{\mathrm{bc}}$ are:
For the case of $\Delta K = 0$:

$$\langle J'K'(I_1I_2)I'F'M'_F \pm |\mathbf{H}_Q| JK(I_1I_2)IFM_F\gamma\rangle = \frac{c}{2\sqrt{(1+\delta_{K'0})(1+\delta_{K0})}} \times$$

$$\left\{\mp\delta_{K1}\begin{pmatrix} J' & 2 & J \\ 1 & -2 & 1\end{pmatrix}\frac{1-(-1)^{\Delta J+p}}{2\sqrt{6}}2i[2\chi_{bc}]\right\} \quad (2\text{-}26)$$

For $\Delta K = 1$:

$$\langle J'K'(I_1I_2)I'F'M'_F \pm |\mathbf{H}_Q| JK(I_1I_2)IFM_F\gamma\rangle = \frac{c}{2\sqrt{(1+\delta_{K'0})(1+\delta_{K0})}} \times$$

$$\begin{pmatrix} J' & 2 & J \\ -K' & \mp 1 & K\end{pmatrix}\left\{\mp\frac{1-(-1)^{\Delta J+p}}{\sqrt{6}}[2\chi_{ab}]\right\} \quad (2\text{-}27)$$

For $\Delta K = 2$:

$$\langle J'K'(I_1I_2)I'F'M'_F \pm |\mathbf{H}_Q| JK(I_1I_2)IFM_F\gamma\rangle = \frac{c}{2\sqrt{(1+\delta_{K'0})(1+\delta_{K0})}} \times \begin{pmatrix} J' & 2 & J \\ -K' & \mp 2 & K\end{pmatrix} \times$$

$$\left\{\pm i\frac{1-(-1)^{\Delta J+p}}{\sqrt{6}}[2\chi_{bc}(1)]\right\} \quad (2\text{-}28)$$

2-3 Calculating the Hyperfine Transition Moment

If $\mu_q^{(1)}$ shows the components of the irreducible electric dipole moment tensor of the operator regarding the evaluation of line strength of the hyperfine transitions in the equal or nearly equal coupling scheme, the matrix elements of $\langle K'J'I'_1I'_2\mathcal{J}'_2\cdots I'_L\mathcal{J}'_L\cdots I'_N\mathcal{J}'_NF'M'_F\|\mu^{(1)}\|KJI_1I_2\mathcal{J}_2\cdots I_L\mathcal{J}_L\cdots I_N\mathcal{J}_NFM_F\rangle$ must be calculated. It can be demonstrated that[50]:

$$\langle K'J'I'_1I'_2\mathcal{J}'_2\cdots I'_L\mathcal{J}'_L\cdots I'_N\mathcal{J}'_NF'M'_F\|\mu^{(1)}\|KJI_1I_2\mathcal{J}_2\cdots I_L\mathcal{J}_L\cdots I_N\mathcal{J}_NFM_F\rangle =$$
$$(-1)^{J'+\mathcal{J}_N+F+1}[(2F+1)(2F'+1)]^{1/2}\begin{Bmatrix} J' & F' & \mathcal{J}_N \\ F & J & 1\end{Bmatrix}\langle K'J'\|\mu^{(1)}\|KJ\rangle \quad (2\text{-}29)$$

By knowing $\langle K'J'\|\mu^{(1)}\|KJ\rangle$ in I^r representation a transition dipole moment could be calculated. Generally, if for an irreducible tensor $\boldsymbol{T}^{(k)}$ under a rotation of coordinate system, $T_q^{(k)}$ are the components defined with respect to the old coordinate system and $T_{q'}^{\prime(k)}$ are the components relative to the new or rotated coordinate system, we have:

$$T_{q'}^{\prime(k)} = \sum_q T_q^{(k)} D_{qq'}^{(k)} \quad (2\text{-}30)$$

$D_{qq'}^{(k)}$ in equation 2-30 is the $(2k+1)$ dimensional matrix representation of the rotation operator. The matrix elements of this operator in symmetric rotor basis set are given by equation 2-31.

$$\left\langle K'J'M'_J\middle|D_{qq'}^{(k)}\middle|KJM_J\right\rangle = (-1)^{M_J-K}[(2J+1)(2J'+1)]^{1/2} \times$$
$$\begin{pmatrix} J & k & J' \\ M_J & -q & -M'_J\end{pmatrix}\begin{pmatrix} J & k & J' \\ K & -q' & -K'\end{pmatrix} \quad (2\text{-}31)$$

In this discussion, the space-fixed coordinate is designated as (x, y, z) and the body-fixed coordinate is designated as (x', y', z'). In expressing principal axis in I^r representation (x', y', z') is designate as (b, c, a).
The spherical unit vector can be shown by the space-fixed vector as equation 2-32[32].

$$\boldsymbol{e}_0^{(1)} = \boldsymbol{e}_z, \boldsymbol{e}_{\pm 1}^{(1)} = \mp \frac{1}{\sqrt{2}}(\boldsymbol{e}_x \pm i\boldsymbol{e}_y) \tag{2-32}$$

Therefore, the component of a first-rank irreducible tensor like $\mu^{(1)}$ in the spherical unit vector can be rewritten as below[32].

$$\begin{aligned}
\mu_z &= \mu_0^{(1)} \\
\mu_x &= \frac{1}{\sqrt{2}}\left(\mu_{-1}^{(1)} - \mu_1^{(1)}\right) \\
\mu_y &= \frac{i}{\sqrt{2}}\left(\mu_1^{(1)} + \mu_{-1}^{(1)}\right)
\end{aligned} \tag{2-33}$$

The Wigner Eckhart theorem[51] can be introduced as another useful equation. Regarding the basis sets $|JM\rangle$ that involve eigenfunctions of J^2 and J_z, the Wigner Eckhart theorem states by equation 2-34[51]:

$$\left\langle J'M' \middle| T_q^{(k)} \middle| J\ M \right\rangle = (-1)^{J'-M'} \times \begin{pmatrix} J' & k & J \\ -M' & q & M \end{pmatrix} \langle J'M' \| T^{(k)} \| J\ M \rangle \tag{2-34}$$

Using equations 2-30, 2-31 and 2-34 as well as considering orthogonally properties of 3j symbols, equation 2-35 would be obtained[32]:

$$\begin{aligned}
&\left\langle K'J' \middle| \mu_{q'}^{(1)} \middle| KJ \right\rangle = (-1)^{J'-K+1}[(2J+1)(2J'+1)]^{\frac{1}{2}} \\
&\begin{pmatrix} J & 1 & J' \\ K & -q' & -K' \end{pmatrix} \langle K'J' \| \mu^{(1)} \| KJ \rangle
\end{aligned} \tag{2-35}$$

With respect to our interested molecule that its dipole moment is in b principle axis direction, the equation 2-36 will be derived for the hyperfine transition dipole moment:

$$\begin{aligned}
&\langle K'J'I_1'I_2'I'F' \| \mu^{(1)} \| K\,JI_1I_2IF \rangle = \frac{(-1)^{2J'+I+F-K}}{\sqrt{2}}[(2F+1)(2F'+1)(2J+1)(2J'+ \\
&1)]^{\frac{1}{2}} \begin{Bmatrix} J' & F' & \mathcal{J}_N \\ F & J & 1 \end{Bmatrix} \left[\begin{pmatrix} J & 1 & J' \\ K & 1 & -K' \end{pmatrix} - \begin{pmatrix} J & 1 & J' \\ K & -1 & -K' \end{pmatrix} \right] \langle K'J' \| \mu^{(1)} \| K\,J \rangle
\end{aligned} \tag{2-36}$$

2-4 Selection Rules

Conditions, which lead to the vanishing absence in the transition dipole matrix elements, make the selection rules. The component of the dipole moment, along with a space-fixed axis F, can be written as equation 2-37[32].

$$\mu_F = \sum \mu_g \cos(Fg) \tag{2-37}$$

The summation is in g index which shows the principal axis of inertia a, b, c. Matrix element of dipole moment in direction of one of the principal axis of inertia g, in asymmetric rotor basis set is written as equation 2-38[32].

$$< J, K_a, K_c \mid \mu_g \cos(Fg) \mid J', K_a', K_c' > \quad (2\text{-}38)$$

Concerning selection rules in J quantum number, as asymmetric wave function is the summation of symmetric rotor wave function, selection rules are the same as symmetric rotor selection rule; $\Delta J = 0, \pm 1$[32].

Regarding selection rules for K_a and K_c, the expression 2-38 should belong to the symmetry species A in order to have none zero values. As an example, assume that g = a. As the sign of *cos*(Fa) by 180° rotation about b and c axis changes and by 180° rotation about axis a does not change, *cos*(Fa) belongs to the symmetry species B_a. Using the multiplication table, the wave functions which correspond to the $| J, K_a, K_c >$ and $| J', K_a', K_c' >$ should belong to the A and B_a or B_c and B_b symmetry species. This keeps the expression 2-38 belonging to the symmetry species A. Table 2.5 depicts the above discussion in the summary with respect to dipole moment along a, b and c principle axis. Two last columns of Table 2.5 are obtained according to I^r representation.

Table 2.5: Selection rules Table[32]

Dipole moment	**Allowed species**	ΔK_a	ΔK_c
$\mu_a \neq 0$ along the axis of least moment of inertia	$A \leftrightarrow B_a$ $B_c \leftrightarrow B_b$	0, ±2, …	±1, ±3,…
$\mu_b \neq 0$ along the axis of intermediate moment of inertia	$A \leftrightarrow B_b$ $B_a \leftrightarrow B_c$	±1, ±3,…	±1, ±3,…
$\mu_c \neq 0$ along the axis of greatest moment of inertia	$A \leftrightarrow B_c$ $B_a \leftrightarrow B_b$	±1,±3,….	0, ±2, ….

Chapter 3

Experimental Methods

In this chapter, principles of the experimental methods used in this study will be described. In section 3-1, lock-in amplifier and frequency modulation theory are described. In fact, this theory applies the techniques in order to detect a signal buried in noise. Supersonic jet spectroscopy and gas cell spectroscopy involve two different experimental methods utilized in the current study. The supersonic jet principle is described in section 3-2. In addition, section 3-3 presents the supersonic jet spectroscopy experiment in details, and section 3-4 elaborates gas cell spectroscopy.

3-1 Lock-in amplifier and Frequency Modulation Theory

Lock-in amplifier is normally applied when measurement of a small signal buried in noise is desired. In some cases, noise is pure white noise also named Gaussian noise. White noise character changes rapidly and randomly with time and its expectation value will reduce to zero via simple time averaging.

Another type of noise which should be considered is the noise from electronic sources. Regardless of the origin of these noises, that it is an open subject, a great number of studies demonstrate that this noise is proportionate to 1/f, where f is the frequency of the noise repetition. Effect of this noise cannot be reduced by simple time averaging. Multiplication of this noise by a high frequency signal is recognized as a tricky way with respect to reduction of these noises, which can be carried out in a lock-in amplifier[52]. In other words, the lock-in amplifier takes the input signal, multiplies the input signal by the reference signal and finally integrates the multiplication result over a specific time.

Generally, a typical lock-in amplifier consists of five stages as is shown in block diagram in Figure 3.1.Stage 1 is a signal amplifier, involving simply a voltage amplifier combined with the variable filters. Stage 2 is a voltage control oscillator, which is just an oscillator except that it can be synchronized with an external signal both in phase and frequency. Some lock-in amplifiers contain a complete oscillator that needs no external reference. Stage 3, named as the phase sensitive detection, is a circuit that takes two voltages V_1 and V_2 as input and produces a voltage as an output, which is the multiplication of V_1 and V_2. Stage 4 is introduced as the low pass filter by selectable time constants and finally, stage 5 is Dc amplifier, which is simply a low frequency amplifier[55].

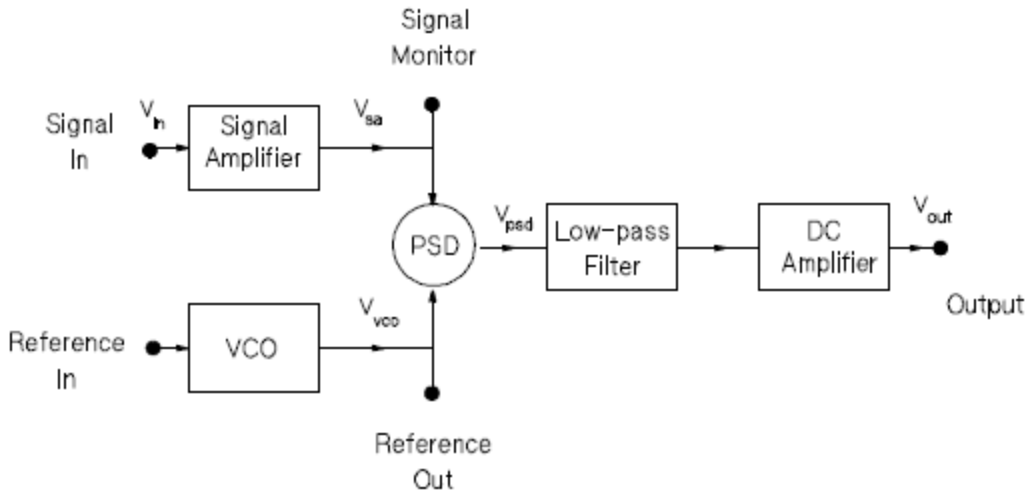

Figure 3.1: Block diagram of a lock-in amplifier[52]

Some mathematical description needs to be presented in order to perceive the frequency modulation concept[53]. Mathematically, the lock-in amplifier can be illustrated as multiplication of the reference and the observed signal as well as an averaging like the integration of this production signal over many periods of the fundamental frequency, T=m/f, where m>>1 is an integer, as is shown in the below equation[53]:

$$S_n = \frac{1}{T}\int_0^T \sin(2\pi n f t + \delta\varphi)\, A\big(\lambda(t)\big) d t\,, \tag{3-1}$$

where $\sin(2\pi ft+\delta\varphi)$ is the reference signal, and $A\big(\lambda(t)\big)$ is the observable, which depends on the parameter $\lambda(t)$. It is worth mentioning that this parameter, in its turn, depends on time. In order to discover the answer of integral (3-1), two expansions demand to be taken into consideration. The expansion into Taylor series of the experimental parameter λ can be stated as the first one, as it is demonstrated in equation 3-2[53].

$$A(\lambda) = \sum_{\vartheta=0}^{\infty} \frac{1}{\vartheta!} A^{(\vartheta)} (\lambda-\lambda_0)^{\vartheta}, \tag{3-2}$$

where $A^{(\vartheta)} = (\partial/\partial\lambda)^{\vartheta} A|_{\lambda=\lambda_0}$, means the ϑ-th derivative of A with respect to the λ, and λ_0 means $\lambda(t=0)$.

The second expansion is the expansion of parameter λ into a Fourier series in time t, as below[53]:

$$\lambda(t) = \sum_{\mu=0}^{\infty} \lambda_\mu \sin(2\pi\mu f + \delta\emptyset_\mu) \tag{3-3}$$

Using equation 3-3, equation 3-2 can be rewritten as equation 3-4[53].

$$A(t)=\sum_{\vartheta=0}^{\infty}\frac{1}{\vartheta!}A^{(\vartheta)}\left(\sum_{\mu=1}^{\infty}\lambda_{\mu}s_{\mu}\right)^{\vartheta}, \quad (3\text{-}4)$$

where

$$s_{\mu}=\sin(2\pi\,\mu\, f\, t+\delta\emptyset_{\mu}) \quad (3\text{-}5)$$

In most real experimental conditions, all $\lambda_{\mu>1}=0$ and we have:

$$\lambda(t)=\lambda_0+\lambda_1\sin(2\pi ft) \quad (3\text{-}6)$$

Using the sum of sine functions rules, orthogonality of sine functions, equation 3-4, and condition 3-6, equation 3-1would be rewritten as below[53]:

$$S_n = A^{(0)}\tilde{s}_n + A^{(1)}\lambda_1(\tilde{s}_{n+1}+\tilde{s}_{n-1}) + \frac{1}{2}A^{(2)}\frac{\lambda_1^2}{2}(\tilde{s}_{n+1+1}+\tilde{s}_{n+1-1}+\tilde{s}_{n-1+1}+\tilde{s}_{n-1-1}) + \frac{1}{6}A^{(3)}\frac{\lambda_1^3}{4}(\tilde{s}_{n+1+1+1}+\tilde{s}_{n+1+1-1}+\cdots)+\cdots \quad (3\text{-}7)$$

where

$$\tilde{s}_{n-1+2}=\sin(2\pi(n-1+2)f\,t+(\delta\emptyset-\delta\emptyset_1+\delta\emptyset_2)-\frac{\pi}{2}(0-1+1)) \quad (3\text{-}8)$$

In frequency modulation, the goal is to observe n-th derivative of A(λ) via a reference frequency of nf.

3-2 Supersonic Jet Expansion

The benefit of free jet expansion in the spectroscopy was first recognized in chemical intermediates investigation in a reaction in 1951[54]. The main feature of the free jet expansion involves a small nozzle orifice that separates a high pressure gas sample behind the nozzle form a downstream region which is kept at a low temperature through vacuum pumping[54].

Pumping speed is identified as the limiting factor in regard to maintaining the proper condition of pressures in the experiment. Via using a pulsed valve on the nozzle, the total gas load on the pump will be limited and to some extent, pumping speed limitations can be overcomed[56].

Figure 3-2 depicts a schematic representation of free jet expansion[57]. As it is shown in the figure, the free jet expansion converts the random thermal motion of gas molecules before the nozzle in the reservoir to a directed motion in front of the nozzle in the region. In other words, free jet expansion monochoromize the gas velocity until it arrives a limiting value.

As the expansion proceeds, Mach number, the ratio of the flow velocity to the local speed of sound, increases dramatically. This can be related to the decreasing local speed of sound, which is proportional to the square root of the temperature. In other words, as the expansion proceeds, temperature decreases. As a result, the local speed of the sound will decrease leading to an increase

in Mach number. However, the decreasing frequency of collision causes a limiting value for the Mach number[58].

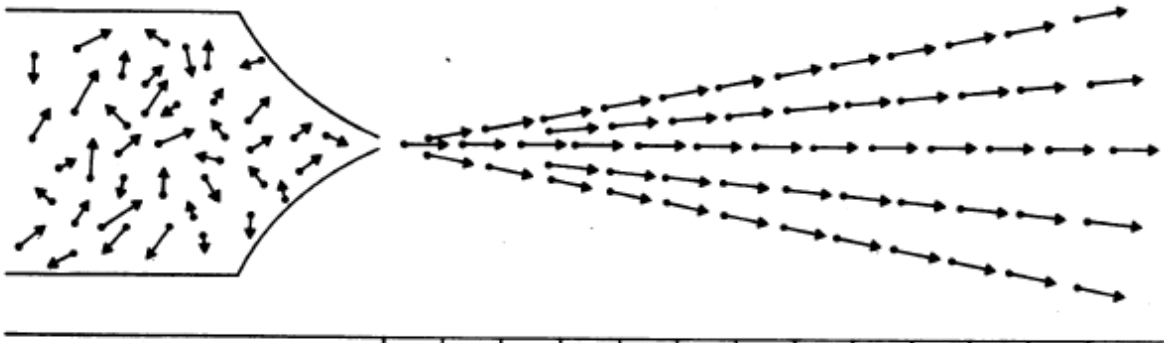

Distance (X/D)	10	20	30	40	50	60
Mach number	15	24	32	38	44	50
Temperature (K)	4.0	1.6	0.9	0.6	0.5	0.4
Density (S.T.P. torr)	15	3.7	1.6	0.9	0.6	0.4
Pressure (mtorr)	150	15	3.5	1.5	0.7	0.4

Figure 3.2: Schematic representation of a free gas jet expansion. X is the downstream distance measured in the unit of nozzle diameter (D). Mach number, temperature, density and pressure in each point are also demonstrated. This figure corresponds to a typical expansion of He gas at the pressure of 10 atmospheres in the room temperature behind the nozzle[57].

Translational temperature values in Figure 3.2 are obtained by knowing the width of the velocity distributions in the expansion region. As the velocity distribution gets narrower, the energies of the collisions, occurring in the expansion, will be lower and thus, lower values will be obtained concerning translational temperature. As a result of the collision, the freedom internal degrees of molecules including vibrational and rotational energy levels will relax toward the translational temperature. Although precise internal-translational temperatures may not be achieved, the rotational-translational temperature equilibrium is normally rapid and rotational temperatures rarely differ greatly from the translational temperatures. It is worth noting that as vibrational temperature often depends on the vibrational structure of the molecule, vibrational-translational temperature equilibrium is not as effective as rotational-translational demonstrating the advantage

of free jet gas expansion in microwave spectroscopy of molecules when low temperature is required.

Cluster formation within the expansion is considered as a limitation on cooling. In clustering, the interatomic binding energy is released and may reappear in the form of translational kinetic energy which reheats the beam and limits the translational temperature. This problem can be solved by seeding the spectroscopic interest molecule in a supersonic jet rare gas beam. Rare gases have weak intermolecular forces and can minimize the clustering[59]. Cluster formation requires at least three-body collisions, whereas cooling the beam requires only two-body collisions. The ratio of three-body to two-body collisions is proportional to the density of molecules. On the other hand, the limiting value of Mach number and cooling temperature are proportional to the density of molecules and diameter of the nozzle. A special cooling temperature, by increasing nozzle diameter and decreasing density of molecules by changing pumping speed minimization of clustering is possible[60].

3-3 Supersonic Jet Spectroscopy Setup

Figure 3.3 illustrates a schematic view of the experimental setup for the supersonic jet spectroscopy. Pure S_2Cl_2 (from Wako Pure Chemical Industries) was used without any further purification. In the supersonic jet experiment, a pulse-jet nozzle (Parker Hannifin) of 0.8 mm orifice was utilized at a repetition rate of 10 Hz. Specified purity Argon gas (99.999 %, from Nippon Sanso Inc.) was bubbled through the liquid sample of S_2Cl_2 and injected into a vacuum chamber evacuated by a 12- inch oil diffusion pump. The back pressure of the nozzle was chosen in order to achieve the strongest absorption signal. The pressure of argon buffer gas was optimized as 0.5 atm for the ${}^rR_4(15)$ transition, which has the rotational term energy corresponding to T = 15K.

A W-band source module (HP83558A) driven by a synthesized sweeper (HP83620) was used. The output radiation power of a few mW was focused via an elliptical mirror (200mm x 150mm) 2.7cm downstream from the pulse valve. The beam waist of MW radiation was 2 cm which was frequency modulated at 47 kHz through the synthesizer. Via applying an Indium Antimonide (InSb) detector (QME-2BI) cooled to liquid Helium temperature, the absorption signal was demodulated by a lock-in amplifier (SRS SR850) twice the modulation frequency (2*f*-detection) with a time constant of 300ms. The operating principle of the detector seems to b same as that of a thermistor. The temperature of the absorber would change through radiation and as a result, the mobility of charge carriers would change resulting in the resistance change and signal detection. In InSb detector at liquid helium temperature (4.2K), as the lattice coupling is weak, the electron-electron interaction time is shorter compared to the electron-phonon interaction time, which can be related to the electrons to be heated beyond the lattice temperature. Hence, the electron mobility and as a result, the conductivity change, as well as a signal, would be detected. The electron-phonon relaxation time constant is held to be reprehensive of the detector speed. At liquid helium temperature, the electron-phonon relaxation time constant for InSb detector is 300ns, that is to say, that the detector possesses a bandwidth of 1MHz[61].

The detected signal was recorded by a digital oscilloscope (TDS5104B, Tektronix Inc.) and sampled for a period of 10 ms with 2 ms delay after opening the pulsed valve, for which the absorption signal was reported to be the strongest.

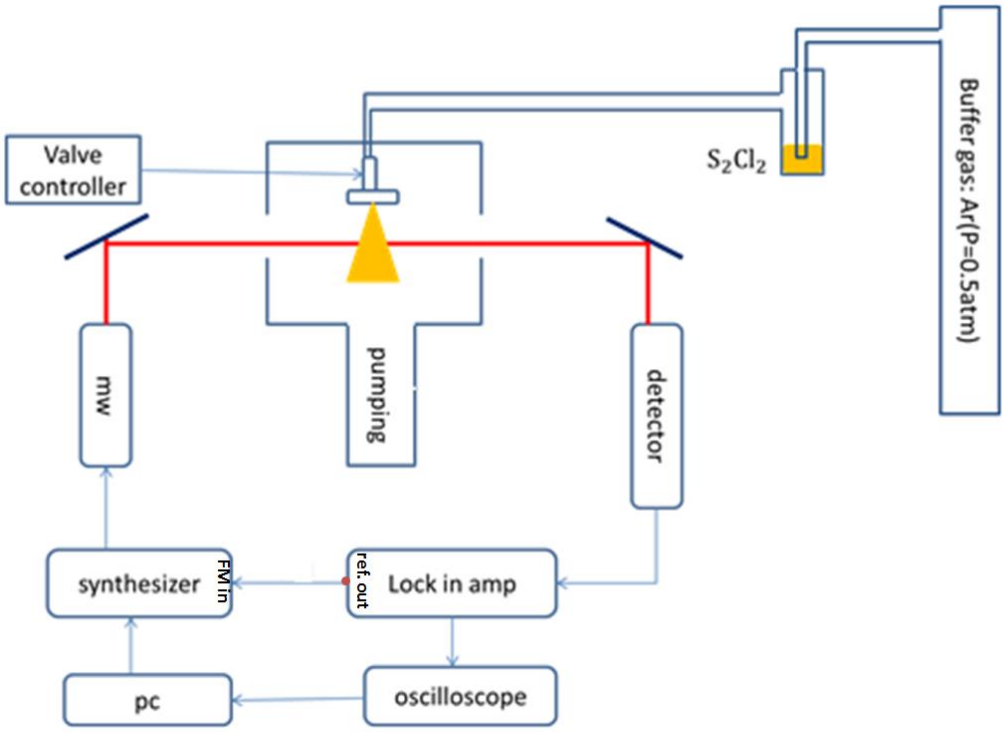

Figure 3.3: Schematic view of jet spectroscopy experimental setup. Mm-wave is shown by a red-colored thick line and electric connections are shown by arrows.

The observed signal on the screen of the oscilloscope is depicted in Figure 3.4. As it is shown in Figure 3.4, a value of 9.2% could be achieved in terms of absorption. The blue color signal in this Figure is related to the voltage, which controls the valve driver. The absorption spectrum appears by a delay relative after opening the pulsed valve.

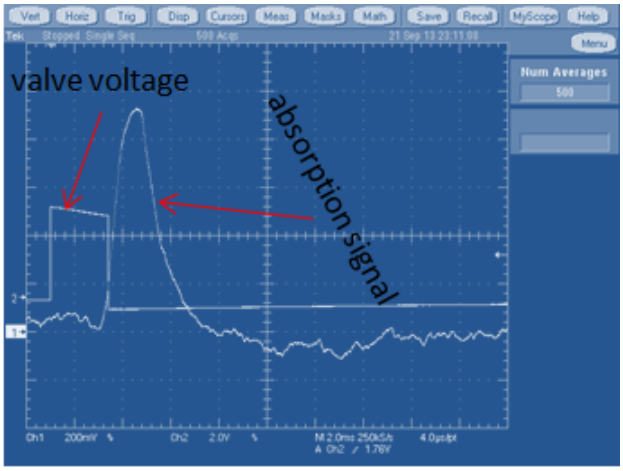

Figure 3.4: Time profile of the absorption spectrum measured directly and the voltage, which controls the nozzle valve, seen in the oscilloscope screen.

Via recording the observed absorption signal (Figure 3.4), the suitable condition with respect to using the gating method was obtained. The time regions selected for the baseline and signal from the time profile of the absorption signal are shown in Figure 3.5. As Figure 3.5 demonstrates, $t_i = 0$ s and $t_f = 0.002$ can be regarded as suitable initial and final points for the baseline. Moreover, $t_i = 0.005$ s and $t_f = 0.007$ were selected as start and end points in order to measure the signal in gating. In fact, in gating method, the area under the baseline, shown by purple lines in the Figure, is subtracted from the area under the signal, shown by red color lines. It should be mentioned, that this procedure was conducted for each mw-frequency. In order to observe the spectrum, the mm-wave frequency was scanned by 0.05 MHz step, while 100 shots of the pulse jet were averaged. As a result, sweeping a 4 MHz region took 15 min.

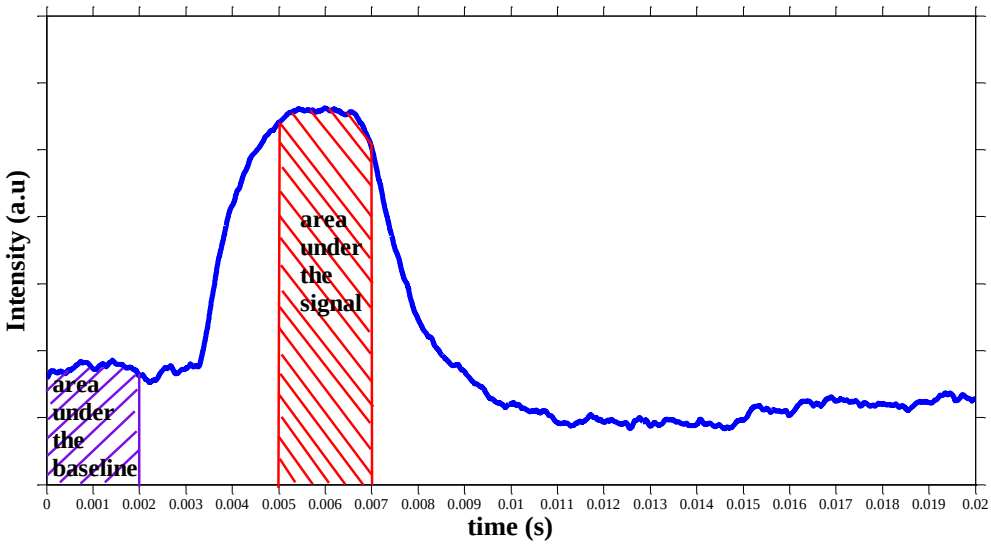

Figure 3.5: Measured time profile. This is averaging of 500 shot. Using time profile time ranges for baseline and signal can be found.

3-4 Gas Cell Spectroscopy Setup

Figure 3.6 displays a schematic view of cell spectroscopy. Gas cell experimentation was carried out through a 3-m Pyrex glass tube with a diameter of 20 cm. The gas cell was surrounded by some dry ice to maintain the temperature at 220K. The sample pressure was maintained at its vapor pressure in 200K using a slow flow as well as continuous pumping. The depth of the frequency modulation was same as that of the supersonic jet experiment. Furthermore, the accuracy of frequency measurements was reported to be~300 kHz.

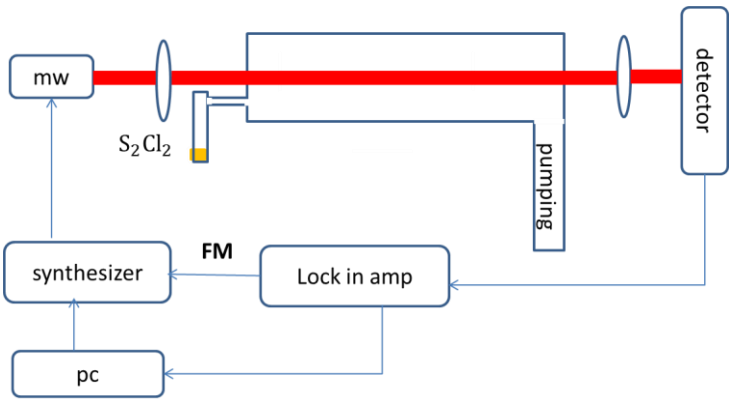

Figure 3.6: Schematic view of the cell spectroscopy experiment. The mm-wave is shown by a red-colored thick line, and electric connections are shown by blue arrows.

Chapter 4

Microwave spectroscopy of S_2Cl_2

Previous studies on the microwave spectroscopy of S_2Cl_2 have been restricted to the centimeter wave region for transitions by frequencies up to 40 GHz. The rotational molecular constants (including the fourth order centrifugal distortion constants) and the nuclear quadruple coupling constants were determined in the centimeter wave region. However, these constants are not enough to predict the transition frequencies in the millimeter wave (mm-wave) region. In this research millimeter wave spectrum of $S_2{}^{35}Cl^{35}Cl$ and $S_2{}^{35}Cl^{37}Cl$ as the two isotope species of disulfur dichloride with the highest abundance are measured. The measured spectrum is in 75 GHz to 100 GHz frequency region. In this chapter, details of rotational spectroscopy of $S_2{}^{35}Cl^{35}Cl$ and $S_2{}^{35}Cl^{37}Cl$ isotope species are explained.

In section 4-1 the millimeter wave spectroscopy of $S_2{}^{35}Cl^{35}Cl$ is described. The measurement is done by two different experimental methods. These two methods are jet spectroscopy and gas cell spectroscopy. Details of data analyzing and results and discussion will be explained in 4-1 sub-sections.

In section 4-2 the millimeter wave spectroscopy of $S_2{}^{35}Cl^{37}Cl$ will be explained. The same as $S_2{}^{35}Cl^{35}Cl$, the data which are measured from jet spectroscopy experiment and gas cell spectroscopy are analyzed for $S_2{}^{35}Cl^{37}Cl$ isotope species. Details of data analyzing and results and discussion will be explained in 4-2 sub-sections.

Analyzing the jet spectroscopy data would be the first step of assignment for both $S_2{}^{35}Cl^{35}Cl$ and $S_2{}^{35}Cl^{37}Cl$ isotope species. By jet experiment, a low temperature of 20K is achieved. In such a low temperature, *Q* branches were measured. Measurement and assignments of *Q* branches was the initial step of millimeter-wave spectroscopy of S_2Cl_2. Totally 38 for $S_2{}^{35}Cl^{35}Cl$ and 40 for $S_2{}^{35}Cl^{37}Cl$ were determined using these data. As the advantage of jet spectroscopy experiment was, in the experiment temperature, the start of *Q*-branches series was measurable and this made *Q*-branches series lines assignments possible in the dense spectrum of disulfur dichloride.

As the second step using new molecular constants which were obtained via the supersonic jet spectroscopy measurement, the measured lines in the gas cell spectroscopy were assigned. In the gas cell spectroscopy totally 179 transitions for $S_2{}^{35}Cl^{35}Cl$ and 51 transitions for $S_2{}^{35}Cl^{37}Cl$ were assigned. K_c-doubling *R*-branch transitions, in the gas cell experiment temperature, play the same role as *Q*-branches series in the jet spectroscopy.

As a result, in the millimeter wave spectroscopy of disulfur dichloride, the transitions with the rotational quantum numbers up to $J = 55$ and $K_a = 12$ were observed for $S_2{}^{35}Cl_2$ and up to $J = 41$ and $K_a = 10$ were observed for $S_2{}^{35}Cl^{37}Cl$. The set of molecular parameters including the sixth-order centrifugal distortion constants were determined for the first time and the reproducibility of the hyperfine pattern was confirmed by using the previous hyperfine constants from reference 32. In section B-1 in the appendix, results of least squares fitting of all observed lines including hyperfine components are shown.

4-1 $S_2{}^{35}Cl_2$ Spectroscopy

The millimeter-wave spectrum of $S_2{}^{35}Cl_2$ is measured by both jet spectroscopy and gas cell spectroscopy methods. Section 4-1-1 corresponds to the results obtained from the supersonic jet spectroscopy. Results which were obtained from the gas cell spectroscopy will be explained in section 4-1-2. Details about experimental methods were explained in Chapter3.

4-1-1 Jet spectroscopy

Disulfur dichloride has a dense microwave spectrum, in room temperature condition. This made the determination of rotational transitions of this molecule in millimeter wave region difficult. As explained in section 3-2, in supersonic jet condition achieving low rotational temperature becomes possible. In low temperatures, transitions with high quantum numbers are not excited. This makes assignments of transitions by rotational term energy corresponding to the low temperatures possible. Using this advantage of jet spectroscopy initial transitions in ${}^rQ_9(J)$ and ${}^rQ_{10}(J)$ series and also *R*- branches transitions with medium J and K_a quantum numbers could be assigned and by assignment of these transitions δ_K forth order centrifugal constants determined for the first time for $S_2{}^{35}Cl_2$ isotope species. Details of the experimental setup were explained in sections 3-1, 3-2 and 3-3. Details about data analyzing and results of this experiment are explained in result and discussion of this part.

Results and Discussion

In total 30 *R*- and 18 *Q*-lines for $S_2{}^{35}Cl_2$ were observed and their central frequencies, ignoring the hyperfine structure are listed in Table 4.1. These transitions were analyzed simultaneously with the transitions measured by FTMW as explained in Ref 32.The least square fitting was weighted by 1.0 for FTMW and 0.01 for our mm-wave work according to the accuracy of each experimental measurement.

Table 4.1: The observed transitions of $S_2{}^{35}Cl_2$ in the supersonic jet experiment[a].

$J'_{K'_aK'_c} - J''_{K''_aK''_c}$	$\nu_{obs.}$/MHz	$\nu_{o\text{-}c}$ /kHz[b]	$J'_{K'_aK'_c} - J''_{K''_aK''_c}$	$\nu_{obs.}$/MHz	$\nu_{o\text{-}c}$ /kHz[b]
$8_{7\,1} - 7_{6\,2}$	75862.6542	19.2	$17_{5\,13} - 16_{4\,12}$	82356.4471	-131.7
$8_{7\,2} - 7_{6\,1}$	75862.6542	19.2	$17_{6\,11} - 16_{5\,12}$	91002.2187	23.6
$8_{8\,0} - 7_{7\,1}$	84290.1207	-13.0	$17_{6\,12} - 16_{5\,11}$	90996.2704	-11.7
$8_{8\,1} - 7_{7\,0}$	84290.1207	-13.0	$17_{7\,11} - 16_{6\,10}$	99481.8676	74.5
$9_{7\,2} - 8_{6\,3}$	78491.3932	-8.0	$17_{7\,10} - 16_{6\,11}$	99481.8676	-61.3
$9_{7\,3} - 8_{6\,2}$	78491.3932	-8.0	$18_{6\,13} - 17_{5\,12}$	93591.3109	72.6
$10_{7\,3} - 9_{6\,4}$	81119.7699	17.1	$13_{10\,3} - 13_{9\,4}$	80100.9271	-48.9
$10_{7\,4} - 9_{6\,3}$	81119.7699	17.2	$13_{10\,4} - 13_{9\,5}$	80100.9271	-48.9
$11_{6\,5} - 10_{5\,6}$	75310.6443	21.2	$14_{10\,4} - 14_{9\,5}$	80098.5671	-33.8
$11_{6\,6} - 10_{5\,5}$	75310.6443	71.4	$14_{10\,5} - 14_{9\,6}$	80098.5671	-33.8
$11_{7\,4} - 10_{6\,5}$	83747.4812	30.6	$15_{10\,5} - 15_{9\,6}$	80095.2310	-23.4
$11_{7\,5} - 10_{6\,4}$	83747.4812	31.0	$15_{10\,6} - 15_{9\,7}$	80095.2310	-23.3
$12_{6\,6} - 11_{5\,7}$	77933.9542	16.5	$19_{10\,9} - 19_{9\,10}$	80068.7021	33.7
$12_{6\,7} - 11_{5\,6}$	77933.9542	150.7	$19_{10\,10} - 19_{9\,11}$	80068.7021	33.7
$13_{6\,7} - 12_{5\,8}$	80554.7429	-73.2	$15_{11\,4} - 15_{10\,5}$	88516.0006	28.7
$14_{6\,8} - 13_{5\,9}$	83172.6360	-49.7	$15_{11\,5} - 15_{10\,6}$	88516.0006	28.7
$14_{6\,9} - 13_{5\,8}$	83171.9142	-37.1	$16_{11\,5} - 16_{10\,6}$	88513.8224	8.9
$15_{5\,10} - 14_{4\,11}$	77307.8974	142.7	$16_{11\,6} - 16_{10\,7}$	88513.8224	8.9
$15_{5\,11} - 14_{4\,10}$	77252.8717	70.0	$17_{11\,6} - 17_{10\,7}$	88510.7738	16.0
$16_{5\,11} - 15_{4\,12}$	79911.0801	19.6	$17_{11\,7} - 17_{10\,8}$	88510.7738	16.0
$16_{5\,12} - 15_{4\,11}$	79816.4151	-19.2	$18_{11\,7} - 18_{10\,8}$	88506.6781	11.6
$16_{7\,9} - 15_{6\,10}$	96865.2142	-2.8	$18_{11\,8} - 18_{10\,9}$	88506.6781	11.6
$16_{7\,10} - 15_{6\,9}$	96865.2142	58.9	$19_{11\,8} - 19_{10\,9}$	88501.4695	76.5
$17_{5\,12} - 16_{4\,13}$	82513.6421	98.6	$19_{11\,9} - 19_{10\,10}$	88501.4695	76.5

[a] All transitions are weighted to be 0.01 relative to the previous cm-wave data[32] with weight=1.
[b] $\nu_{o\text{-}c}$: The difference between the observed frequency and calculation with the molecular constants.

Figure 4.1 shows error distribution of jet spectroscopy least square fitting analysis. $\nu_{o\text{-}c}$ is the difference between the observed frequency and the calculated one by molecular constants which were obtained as the result of least square fitting. As it is expected error distribution of least square fitting has a Gaussian shape, as it is estimated by the red color Gaussian type graph.

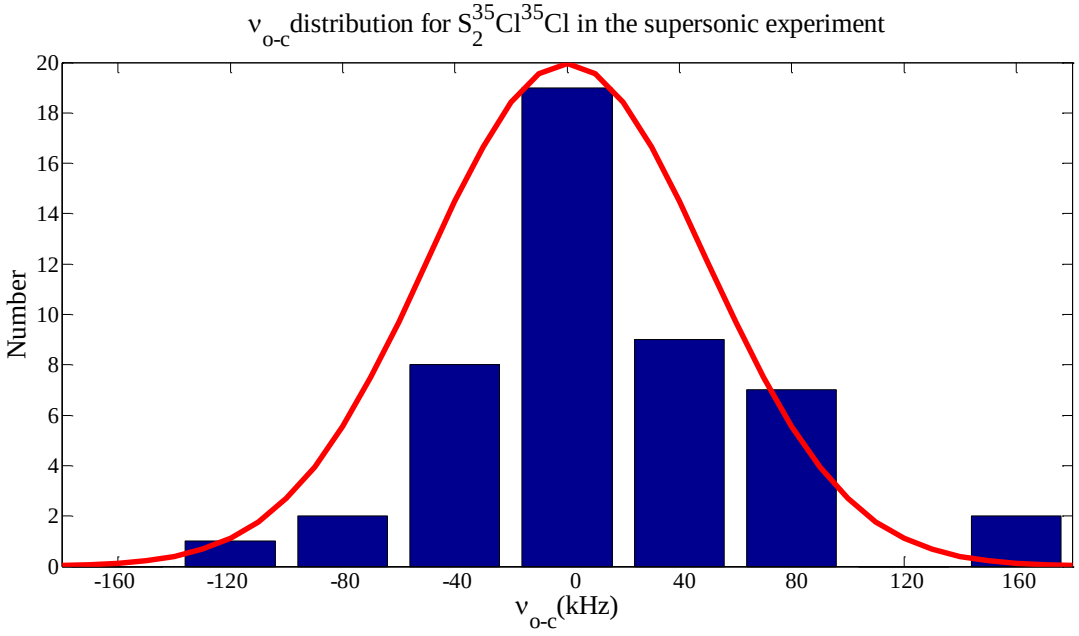

Figure 4.1: Error distribution of jet spectroscopy least square fitting. The distribution is estimated by a Gaussian shape graph which is shown by the red color.

As a result of least squares fitting, the three rotational constants are improved and the fourth-order centrifugal distortion constants including δ_K are determined, which were not determined in the FTMW experiment. These molecular parameters are listed in Table 4.2 as jet spectroscopy. The error of this analysis (0.0039 MHz) is com*para*ble with the experimental error which is about 100 KHz.

Table 4.2: Molecular constants list for $S_2{}^{35}Cl_2$ which obtained from jet experiment data least square fitting and its comparison with FTMW data analysis.

	Jet experiment	**FTMW(Ref 32)**
***A*/MHz**	5533.8964(11)[a]	5533.8937(6)
B/MHz	1393.8436(3)	1393.8461(14)
C/MHz	1232.6728(2)	1232.6697(12)
Δ_J/KHz	0.556(3)	0.568(8)
Δ_{JK}/KHz	-5.115(47)	-5.150(47)
Δ_K/KHz	24.70(25)	24.04(4)
δ_J/KHz	0.144(2)	0.131(6)
δ_K/KHz		1.9(8)
σ_{fit}/MHz	0.0039	0.0036

[a] Numbers in parenthesis denotes one standard deviation of least-squares fitting in the unit of the last significant digit.

The low- *J* transitions in *R*-branch could be observed closely at the position of the predicted frequency. Figure 4.2 shows the observed spectrum of the $^{r}R_5(13)$ transition of $S_2{}^{35}Cl_2$, in which the asymmetric *K*-doubling is resolved, and the positions predicted by the rotational molecular constants from reference 32 are marked by a dotted line. The assignment of the *K*-doubling was also confirmed from the spectral intensity due to the nuclear spin weight of 10: 6. The *ortho* $14_{6,9}$–$13_{5,8}$ transition was observed to be stronger than the *para* $14_{6,8}$–$13_{5,9}$ transition. By adding those observed lines into the least squares analysis, the molecular *para*meters were improved step by step.

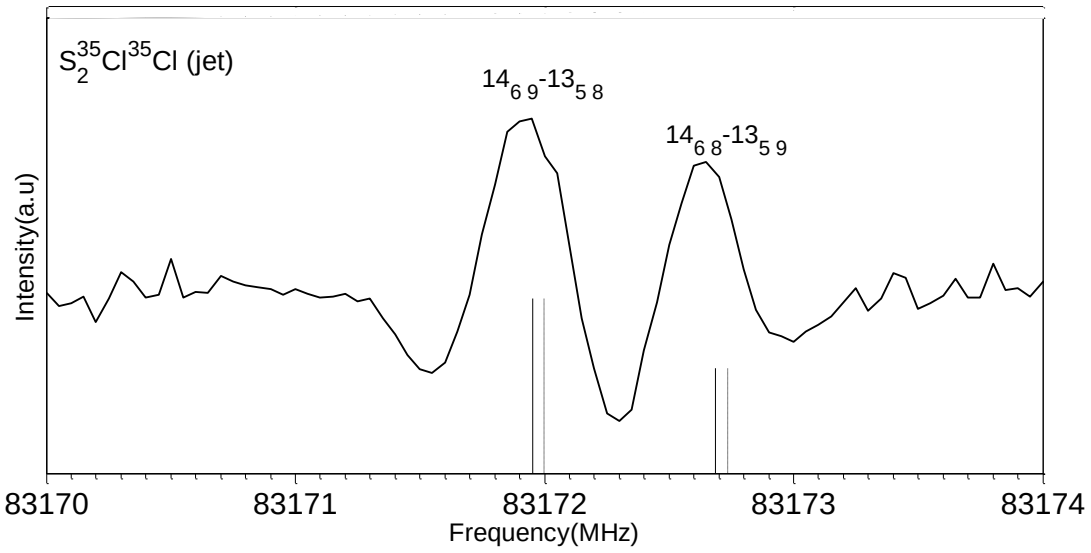

Figure 4.2: An example of middle-*J* transition: $^{r}R_5(13)$ transition of $S_2{}^{35}Cl_2$ observed with the supersonic jet experiment. The frequency positions predicted by the rotational molecular constants of reference 32 and jet experiment, in Table 2.2 are shown with the dashed line and solid line, respectively.

The rotational temperature was also determined from the supersonic jet experiment. From the spectrum intensity distribution of the series of the observed $^{r}Q_9$-branch, the rotational temperature was estimated to be T = 10 to 20K.

The series of $^{r}Q_9(J)$-branches and $^{r}Q_{10}(J)$-branches of $S_2{}^{35}Cl_2$ could be easily observed with a slight shift from the predicted frequencies of the band head by FTMW molecular constants in reference 32. However, these *Q*-branch series appear with a distinct triplet spectral pattern as shown in Figure 4.3.a and Figure 4.3.b. This triplet pattern was attributed to the nuclear quadrupole interaction of the two chlorine nuclei. It was difficult to assign the hyperfine components as they overlapped with other rotational transitions at the band head. All hyperfine

ticks in this Figure correspond to the *ortho-ortho* or *para-para* transitions. This corresponds to the ΔI=0, 2 selection rule for hyperfine transitions. A list of hyperfine transitions in Figure 4.3 could be found in section B-1 of Appendix. The contribution of these hyperfine transitions in the least squares fitting data analysis could also be found in section B-1 of the Appendix.

As seen in Figure 4.3, each line in the series of the ${}^{r}Q_9$-branch ${}^{r}Q_{10}$-branch of $S_2{}^{35}Cl_2$ was observed as a triplet, in which asymmetric *K*-doubling is degenerate. The hyperfine components calculated by using the previous hyperfine constants reported in reference 32 are shown below the observed spectrum in this Figure. Due to the selection rule of $\Delta J = \Delta F$, each rotational transition of $S_2{}^{35}Cl_2$ is composed of 10 or 6 strong components depending on whether it is the *ortho*- or *para*-state. In general, the nuclear quadruple interaction becomes stronger with decreasing *J* and an increase of K_a in the same *J*. Therefore, the K_a/J ratio is a useful *para*meter for estimating the size of the hyperfine splitting. Furthermore, the term values of the hyperfine states in this molecule have a tendency of splitting the components into three bundles. This characteristic mainly comes from the nuclear quadruple interaction *para*meter of χ_{aa} and the separation between the bundles depends on the K_a/J ratio. If the lower state of a ${}^{r}Q$-transition and a ${}^{r}R$-transition is common, the upper state of the ${}^{r}Q$-transition has large K_a'/J' ratio than that of the ${}^{r}R$-transition; that is $(K_a''+1)/J''$ and $(K_a''+1)/(J''+1)$, respectively. Therefore, in general, the three-bundle structure is more easily reflected as a triplet spectral pattern in the ${}^{r}Q$-transition than in the ${}^{r}R$-transition. This is shown in Figure 4.4, for $16_{6,11} - 15_{5,10}$ transition. Although this hyperfine information in the least square analysis is not used, such the line width and line-profile dependence on the K_a/J ratio helps to confirm the assignment of the rotational quantum numbers. As described above, the hyperfine structures observed in the mm-wave region were well reproduced by the nuclear quadruple interaction parameters determined in the previous cm-wave experiment[2].

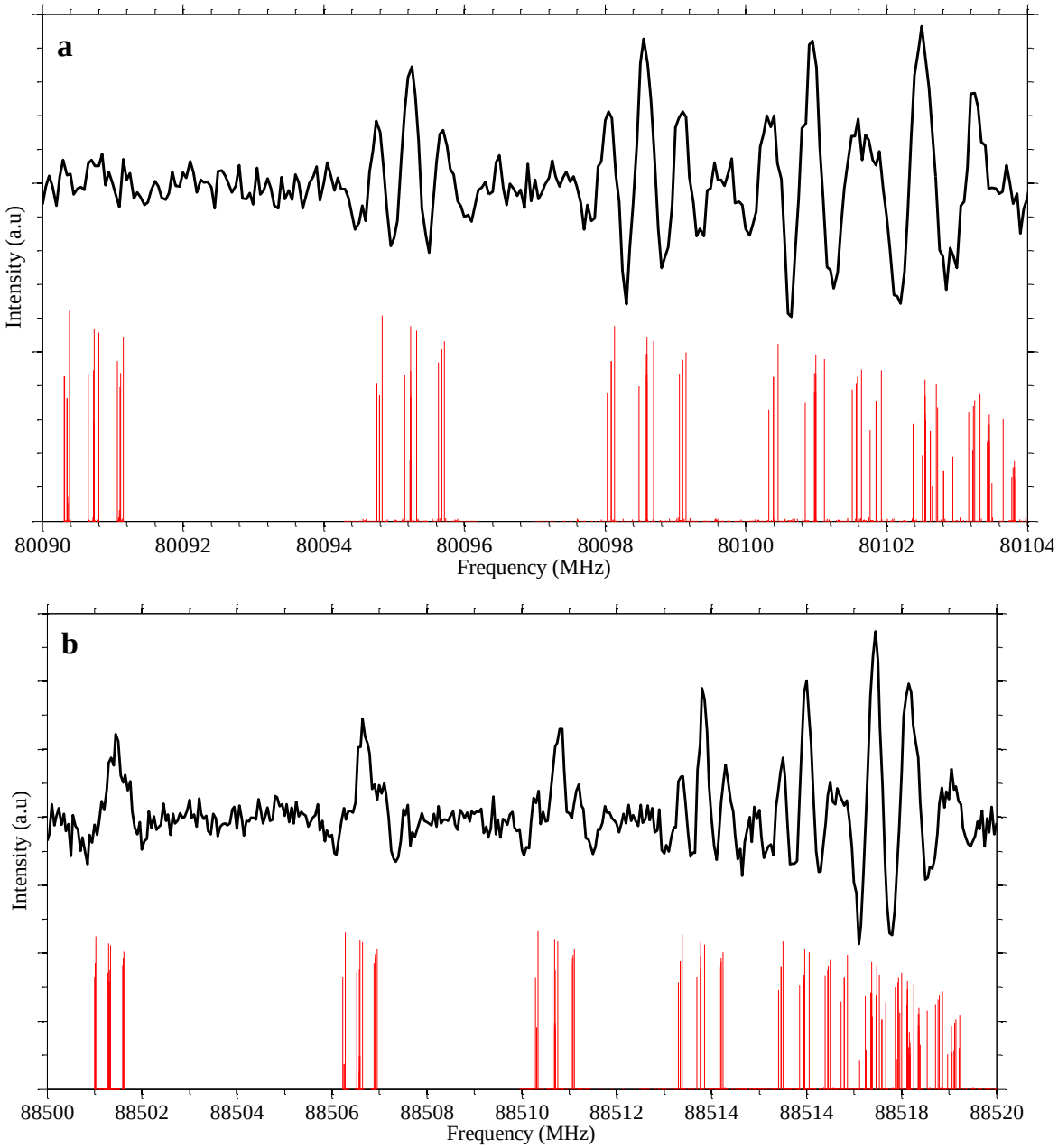

Figure 4.3: Series of $^{r}Q(J)$-branches of $S_2{}^{35}Cl_2$ observed in the supersonic jet experiment. Stick spectrum shows the hyperfine components calculated with the rotational constants from the jet experiment in Table 4.2 and hyperfine constants reported in reference 32. (a) Series of $^{r}Q_9(J)$-branches. (b) Series of $^{r}Q_{10}(J)$-branches.

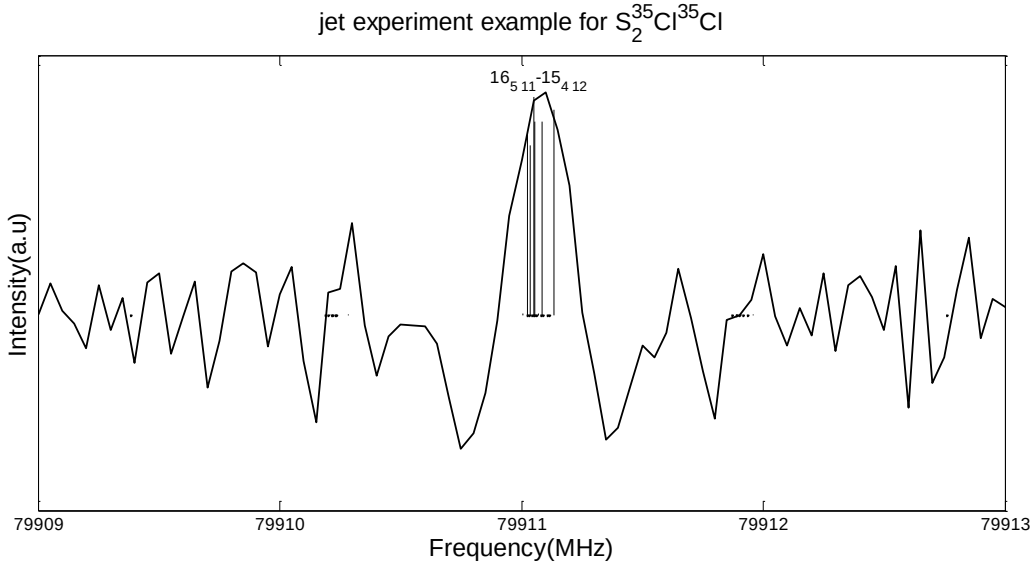

Figure 4.4: *Para* $16_{5,11} - 15_{4,12}$ transition of $S_2{}^{35}Cl_2$ observed with the supersonic jet experiment. Stick lines show the calculated hyperfine structures. Spreading of the hyperfine components depends on the K_a/J ratio.

4-1-2 Cell spectroscopy

In the gas cell spectroscopy by fast scanning condition, despite the reduction of accuracy of the experiment, signal to noise ratio is acceptable for distinguishing microwave transitions. By possibility of fast scanning, measuring all spectrum of disulfur dichloride in a wide frequency region becomes possible. This advantage of gas cell spectroscopy which gives the counties spectrum of S_2Cl_2 leads to the proper assignments of transitions which belong to the K_c-doubling *R*-branches. These kinds of transitions have the high intensity double spectrum pattern in the temperature of the gas cell spectroscopy experiment. Assignments of these transitions have the same role as the assignment of *Q*-branches series in the determining spectroscopic parameters of disulfur dichloride. Details of the experiment were explained in section 3-4. In this experiment, a frequency range of 25 GHz is measured which initialized by 75 GHz and finalized by 100 GHz. Each 100 MHz region is swept in 2s. For getting a better signal to noise ratio 50 scans are averaged. Totally, 179 transitions were determined. All rotational molecular constants of $S_2{}^{35}Cl_2$, including fourth and sixth order centrifugal distortion constants were determined for the first time. The cell spectroscopy measured data are analyzed in three consecutive steps. Details of analysis and discussion on results will be described for each step separately, in result and discussion part.

Results and discussion

The 25 GHz measured spectrum in the gas cell experiment is analyzed in 3 steps. In step 1, K_c-doubling pairs by $K_a' - K_a''$ corresponding to 0-1 and 1-0 played the role the same as *Q*-branch transitions in jet spectroscopy. In this step first nine rotational molecular constants were

determined. In step 2 using predicted pattern obtained from molecular constants of step1 analysis K_c-doubling pairs by $K_a^{'}-K_a^{''}$ corresponding to 2-1 and 1-2 and also 2-3 and 3-2, were determined. In this step least squares fitting analysis, 13 molecular constants were obtained. Finally, in step 3, using the predicted pattern from the molecular constants which were the result of step 2 analysis, transitions which are corresponded to the series of ${}^{r}Q_9(J)$, ${}^{r}Q_{10}(J)$ and ${}^{r}Q_{11}(J)$ are determined by maximum J quantum number equal to 55. In this step of cell experiment data analysis, all rotational molecular constants of $S_2{}^{35}Cl_2$, are determined

Data analysis step 1

K_c - doubling pairs by $K_a^{'}-K_a^{''}$ corresponding to 0-1 and 1-0 R-branch transitions in cell experiment temperature have the highest intensity. Also, in our interested millimeter region, each K_c - doubling transitions are near to each other. So these kinds of transitions are distinguishable between transitions in the dense spectrum of $S_2{}^{35}Cl_2$ for determination. In other words, determining these transitions has the key role in the start of assignments of $S_2{}^{35}Cl_2$ R-branch transitions by high J quantum numbers in the mm-wave region. Totally 16 lines in this step are determined as listed in Table 4.3. These lines are analyzed simultaneously with FTMW experiment lines and jet spectroscopy lines. In the least squares fitting analysis by considering the accuracy of experiment FTMW lines weight is set to 1 and weight of jet experiment and step 1 experiment lines is set to 0.01.

Table 4.3: The observed transitions of $S_2{}^{35}Cl_2$ in the cell experiment, step 1 analysis[a].

$J'_{K'_aK'_c} - J''_{K''_aK''_c}$			$\nu_{obs.}$/MHz	$\nu_{o\text{-}c}$ /kHz[b]	$J'_{K'_aK'_c} - J''_{K''_aK''_c}$			$\nu_{obs.}$/MHz	$\nu_{o\text{-}c}$ /kHz[b]
$31_{0\,31}$	–	$30_{1\,30}$	77219.5509	176.0	$36_{0\,36}$	–	$35_{1\,35}$	89527.1315	35.2
$31_{1\,31}$	–	$30_{0\,30}$	77225.2089	-20.5	$36_{1\,36}$	–	$35_{0\,35}$	89528.1862	30.3
$32_{0\,32}$	–	$31_{1\,31}$	79681.6397	-93.9	$37_{0\,37}$	–	$36_{1\,36}$	91987.5448	-51.6
$32_{1\,32}$	–	$31_{0\,31}$	79685.7982	-106.4	$37_{1\,37}$	–	$36_{0\,36}$	91988.2969	-49.5
$33_{0\,33}$	–	$32_{1\,32}$	82143.6052	-29.8	$38_{0\,38}$	–	$37_{1\,37}$	94447.7982	4.7
$33_{1\,33}$	–	$32_{0\,32}$	82146.5687	-33.3	$38_{1\,38}$	–	$37_{0\,37}$	94448.3430	19.2
$35_{0\,35}$	–	$34_{1\,34}$	87066.4340	151.4	$39_{0\,39}$	–	$38_{1\,38}$	96907.7459	52.9
$35_{1\,35}$	–	$34_{0\,34}$	87067.7385	-39.4	$40_{1\,40}$	–	$39_{0\,39}$	99367.5151	-46.4

[a] All transitions are weighted to be 0.01 relative to the previous cm-wave data[32] with weight=1.

[b] $\nu_{o\text{-}c}$: The difference between the observed frequency and calculation with the molecular constants.

Adding Table 4.3 lines to the least squares fitting analysis leads to find H_J sixth order centrifugal distortion constants. This constant in rotational Hamiltonian is multiplied to the P^6 which itself correspond to the J^6 quantum number in the Hamiltonian matrix in the Wang basis set. As it is expected H_J constant is obtained by adding transitions by high J quantum numbers.

But as K_a quantum numbers in the newly added lines are small, predicting other constants using these lines are not possible. As it is shown in Table 4.4 all other molecular constants except H_J are in the same limit of jet spectroscopy molecular constants. This shows special importance of H_J constant determination in the assignment of transitions with high quantum numbers.

Table 4.4: Molecular constants list for $S_2{}^{35}Cl_2$ which obtained from step1 data least square fitting and its comparison with jet experiment data analysis.

	jet	**Step1**
***A*/MHz**	5533.8937(6)[a]	5533.8938(8)
B/MHz	1393.8461(14)	1393.8460(8)
C/MHz	1232.6697(12)	1232.6698(7)
Δ_J/KHz	0.568(8)	0.568(2)
Δ_{JK}/KHz	-5.150(47)	-5.1454(99)
Δ_K/KHz	24.04(4)	24.0349(89)
δ_J/KHz	0.131(6)	0.1314(8)
δ_K/KHz	1.9(8)	1.9(2)
H_J/Hz		0.0015(3)
σ_{fit}/MHz	0.0036	0.0053

[a] Numbers in parenthesis denotes one standard deviation of least-squares fitting in the unit of the last significant digit.

Figure 4.5 shows the measured spectrum of S_2Cl_2 in the frequency range of 94400 MHz to 94500 MHz. The red color solid lines show the frequencies which correspond to $|38_{1\,38}> - |37_{0\,37}>$ and $|38_{0\,38}> - |37_{1\,37}>$ transitions. These frequencies are obtained by using the molecular constants in the column jet of Table 4.4. The blue color solid lines also show the frequencies which correspond to $|38_{1\,38}> - |37_{0\,37}>$ and $|38_{0\,38}> - |37_{1\,37}>$ transitions. These frequencies are obtained by using the molecular constants in the column step1 of Table 4.4. As it is cleared by H_J constant determination, transitions by high J quantum number and low K_a quantum number became predictable precisely.

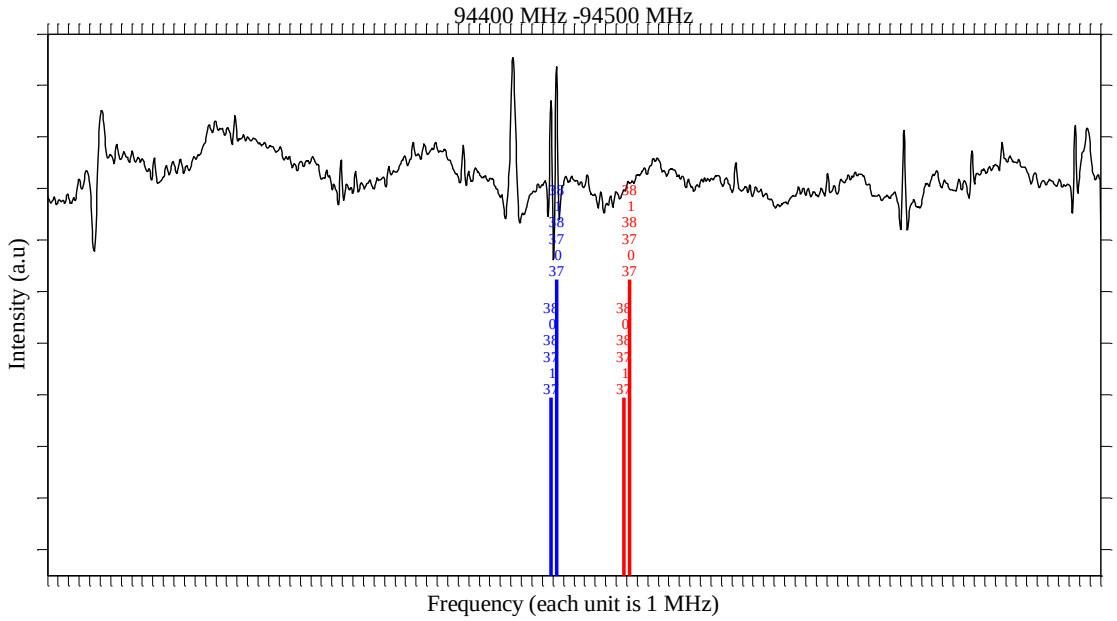

Figure 4.5: Comparison of prediction of the transitions frequencies by the jet experiment molecular constants with the predicted frequencies by step 1 determined molecular constants for $|38_{\ 1\ 38}>$ - $|37_{\ 0\ 37}>$ and $|38_{\ 0\ 38}>$ - $|37_{\ 1\ 37}>$ transitions. Jet prediction is shown by the red solid line and step1 prediction is shown by the blue solid line.

Data analysis step 2

K_c - doubling pairs by $K_a' - K_a''$ corresponding to 2-1 and 1-2 and also 2-3 and 3-2 *R*-branch transitions in this step are determined and added to the jet experiment and step 1 data for the least squares fitting analysis. Totally 19 lines in this step are determined as listed in Table 4.5. These lines are analyzed simultaneously with FTMW experiment, jet spectroscopy and step 1 transitions. In the least squares fitting analysis by considering the accuracy of the experiment, FTMW lines weight is set to 1 and weight of other lines is set to 0.01.

Table 4.5: The observed transitions of $S_2{}^{35}Cl_2$ in the cell experiment, step 2 analysis[a].

$J'_{K'_aK'_c} - J''_{K''_aK''_c}$	$\nu_{obs.}$/MHz	$\nu_{o\text{-}c}$ /kHz[b]	$J'_{K'_aK'_c} - J''_{K''_aK''_c}$	$\nu_{obs.}$/MHz	$\nu_{o\text{-}c}$ /kHz[b]
$31_{1\,30} - 30_{2\,29}$	78791.8398	-90.8	$35_{3\,33} - 34_{2\,32}$	91074.3336	-19.0
$31_{2\,30} - 30_{1\,29}$	79014.4597	19.4	$36_{1\,35} - 35_{2\,34}$	91175.8775	26.6
$32_{1\,31} - 31_{2\,30}$	81279.9535	-53.0	$36_{2\,34} - 35_{3\,33}$	92455.3944	-36.9
$32_{2\,31} - 31_{1\,30}$	81445.4337	53.4	$37_{2\,35} - 36_{3\,34}$	95018.0779	48.3
$33_{1\,32} - 32_{2\,31}$	83760.9579	7.7	$37_{2\,36} - 36_{1\,35}$	93677.3458	-25.2
$33_{2\,32} - 32_{1\,31}$	83883.4930	42.5	$37_{3\,35} - 36_{2\,34}$	95731.6209	26.5
$34_{1\,33} - 33_{2\,32}$	86236.3893	-42.3	$38_{2\,37} - 37_{1\,36}$	96131.5449	31.3
$35_{1\,34} - 34_{2\,33}$	88707.8558	118.5	$39_{1\,38} - 38_{2\,37}$	98567.6108	-12.6
$35_{2\,33} - 34_{3\,32}$	89862.8278	-5.2	$39_{2\,38} - 38_{1\,37}$	98586.6713	-74.6
$35_{2\,34} - 34_{1\,33}$	88774.3266	-29.2			

[a] All transitions are weighted to be 0.01 relative to the previous cm-wave data[32] with weight=1.
[b] $\nu_{o\text{-}c}$:The difference between the observed frequency and calculation with the molecular constants.

Adding lines listed in Table 4.5 to the least squares fitting analysis lead to obtaining 13 rotational molecular constants as listed in Table 4.6.

Table 4.6: Molecular constants list for $S_2{}^{35}Cl_2$ which obtained from step2 data least square fitting and its comparison with step1 data analysis.

	Step1	**Step2**
A/MHz	5533.8938(8)[a]	5533.8939(9)
B/MHz	1393.8460(8)	1393.8460(6)
C/MHz	1232.6698(7)	1232.6706(4)
Δ_J/KHz	0.568(2)	0.569(1)
Δ_{JK}/KHz	-5.1454(99)	-5.134(19)
Δ_K/KHz	24.0349(89)	24.034(37)
δ_J/KHz	0.1314(8)	0.1331(9)
δ_K/KHz	1.9(2)	1.51(7)
H_J/Hz	0.0015(3)	0.0026(9)
H_{JK}/Hz		0.06(4)
H_{KJ}/Hz		-0.23(7)
H_K/Hz		0.3(2)
h_J/Hz		0.0009(5)
σ_{fit}/MHz	0.0053	0.0054

[a] Numbers in parenthesis denotes one standard deviation of least-squares fitting in the unit of the last significant digit.

Data analysis step

In step 3, using the predicted pattern from molecular constants which were the result of step 2 analysis, transitions which correspond to the series of ${}^{r}Q_9(J)$, ${}^{r}Q_{10}(J)$ and ${}^{r}Q_{11}(J)$ are determined by maximum J quantum number equal to 55. The determined lines are listed in Table 4.7.

Table 4-7. The observed transitions of $S_2{}^{35}Cl_2$ in the cell experiment step 3 analysis[a].

$J'_{K'_aK'_c} - J''_{K''_aK''_c}$	$\nu_{obs.}$/MHz	$\nu_{o\text{-}c}$ /kHz[b]	$J'_{K'_aK'_c} - J''_{K''_aK''_c}$	$\nu_{obs.}$/MHz	$\nu_{o\text{-}c}$ /kHz[b]
$20_{10\,10} - 20_{9\,11}$	80057.5490	-120.2	$45_{11\,34} - 45_{10\,35}$	87248.9263	8.0
$20_{10\,11} - 20_{9\,12}$	80057.5490	-120.2	$45_{11\,35} - 45_{10\,36}$	87250.3738	-4.5
$21_{10\,11} - 21_{9\,12}$	80044.4166	-199.3	$46_{11\,36} - 46_{10\,37}$	87122.3179	79.9
$21_{10\,12} - 21_{9\,13}$	80044.4166	-199.3	$47_{11\,37} - 47_{10\,38}$	86984.4015	-48.9
$22_{10\,13} - 22_{9\,14}$	80029.1238	-67.8	$47_{11\,36} - 47_{10\,37}$	86981.0685	-5.8
$22_{10\,12} - 22_{9\,13}$	80029.1238	-67.7	$48_{11\,38} - 48_{10\,39}$	86836.5824	80.7
$23_{10\,13} - 23_{9\,14}$	80011.0471	-101.4	$48_{11\,37} - 48_{10\,38}$	86831.5329	85.9
$23_{10\,14} - 23_{9\,15}$	80011.0471	-101.6	$21_{12\,9} - 21_{11\,10}$	96913.8911	-142.1
$24_{10\,14} - 24_{9\,15}$	79990.1334	-93.1	$21_{12\,10} - 21_{11\,11}$	96913.8911	-142.1
$24_{10\,15} - 24_{9\,16}$	79990.1334	-93.5	$23_{12\,11} - 23_{11\,12}$	96900.9385	-64.4
$27_{10\,17} - 27_{9\,18}$	79907.4217	37.2	$23_{12\,12} - 23_{11\,13}$	96900.9385	-64.3
$27_{10\,18} - 27_{9\,19}$	79907.4217	34.4	$25_{12\,13} - 25_{11\,14}$	96881.9592	-130.7
$28_{10\,18} - 28_{9\,19}$	79871.9809	-93.2	$25_{12\,14} - 25_{11\,15}$	96881.9592	-130.7
$28_{10\,19} - 28_{9\,20}$	79871.9809	-98.7	$27_{12\,15} - 27_{11\,16}$	96856.0247	-56.9
$29_{10\,19} - 29_{9\,20}$	79832.4238	48.0	$27_{12\,16} - 27_{11\,17}$	96856.0247	-56.9
$29_{10\,20} - 29_{9\,21}$	79832.4238	37.7	$28_{12\,16} - 28_{11\,17}$	96839.9861	-22.7
$31_{10\,21} - 31_{9\,22}$	79738.3082	-97.2	$28_{12\,17} - 28_{11\,18}$	96839.9861	-22.7
$31_{10\,22} - 31_{9\,23}$	79738.3082	-131.3	$29_{12\,17} - 29_{11\,18}$	96821.6922	33.0
$33_{10\,23} - 33_{9\,24}$	79622.4375	-29.0	$29_{12\,18} - 29_{11\,19}$	96821.6922	33.1
$33_{10\,24} - 33_{9\,25}$	79622.4375	-133.2	$30_{12\,18} - 30_{11\,19}$	96800.9295	79.1
$35_{10\,25} - 35_{9\,26}$	79481.1250	-90.3	$30_{12\,19} - 30_{11\,20}$	96800.9295	79.1
$35_{10\,26} - 35_{9\,27}$	79481.4738	-38.0	$31_{12\,19} - 31_{11\,20}$	96777.3620	-31.2
$39_{10\,29} - 39_{9\,30}$	79107.3080	113.1	$31_{12\,20} - 31_{11\,21}$	96777.3620	-31.3
$39_{10\,30} - 39_{9\,31}$	79109.2315	42.9	$32_{12\,20} - 32_{11\,21}$	96751.0745	-16.3
$40_{10\,30} - 40_{9\,31}$	78991.2194	-72.0	$32_{12\,21} - 32_{11\,22}$	96751.0745	-16.4
$40_{10\,31} - 40_{9\,32}$	78994.3053	-87.7	$33_{12\,21} - 33_{11\,22}$	96721.9259	187.2
$41_{10\,31} - 41_{9\,32}$	78865.1043	26.3	$33_{12\,22} - 33_{11\,23}$	96721.9259	187.2
$42_{10\,33} - 42_{9\,34}$	78735.0537	67.0	$34_{12\,22} - 34_{11\,23}$	96689.1670	42.8
$43_{10\,33} - 43_{9\,34}$	78578.4440	25.6	$34_{12\,23} - 34_{11\,24}$	96689.1670	42.6
$43_{10\,34} - 43_{9\,35}$	78589.2440	-27.8	$35_{12\,23} - 35_{11\,24}$	96653.1531	126.2
$44_{10\,34} - 44_{9\,35}$	78416.1464	94.8	$35_{12\,24} - 35_{11\,25}$	96653.1531	125.9
$45_{10\,36} - 45_{9\,37}$	78263.0895	-35.4	$36_{12\,24} - 36_{11\,25}$	96613.2977	80.5
$47_{10\,37} - 47_{9\,38}$	77838.2045	129.5	$36_{12\,25} - 36_{11\,26}$	96613.2977	79.9
$47_{10\,38} - 47_{9\,39}$	77887.4813	0.4	$37_{12\,25} - 37_{11\,26}$	96569.3746	-82.3
$48_{10\,39} - 48_{9\,40}$	77680.0967	-51.2	$37_{12\,26} - 37_{11\,27}$	96569.3746	-83.3
$49_{10\,39} - 49_{9\,40}$	77360.1084	-138.5	$38_{12\,26} - 38_{11\,27}$	96521.5648	66.6
$49_{10\,40} - 49_{9\,41}$	77459.6164	96.3	$38_{12\,27} - 38_{11\,28}$	96521.5648	64.9
$25_{11\,14} - 25_{10\,15}$	88435.4155	-84.2	$39_{12\,27} - 39_{11\,28}$	96469.0729	-10.3
$25_{11\,15} - 25_{10\,16}$	88435.4155	-84.2	$39_{12\,28} - 39_{11\,29}$	96469.0729	-13.5

$26_{11\,15}$	–	$26_{10\,16}$	88417.1468	7.9	$41_{12\,29}$	–	$41_{11\,30}$	96349.8582	57.4
$26_{11\,16}$	–	$26_{10\,17}$	88417.1468	7.9	$41_{12\,30}$	–	$41_{11\,31}$	96349.8582	48.0
$28_{11\,18}$	–	$28_{10\,19}$	88372.0998	-114.0	$42_{12\,30}$	–	$42_{11\,31}$	96282.3718	9.2
$28_{11\,17}$	–	$28_{10\,18}$	88372.0998	-113.9	$42_{12\,31}$	–	$42_{11\,32}$	96282.3718	-6.7
$29_{11\,19}$	–	$29_{10\,20}$	88345.0927	-95.4	$43_{12\,31}$	–	$43_{11\,32}$	96209.4134	88.0
$29_{11\,18}$	–	$29_{10\,19}$	88345.0927	-95.1	$43_{12\,32}$	–	$43_{11\,33}$	96209.4134	61.5
$31_{11\,21}$	–	$31_{10\,22}$	88280.7406	-39.6	$44_{12\,32}$	–	$44_{11\,33}$	96130.4323	60.8
$31_{11\,20}$	–	$31_{10\,21}$	88280.7406	-38.6	$44_{12\,33}$	–	$44_{11\,34}$	96130.4323	17.3
$32_{11\,21}$	–	$32_{10\,22}$	88242.9383	66.3	$45_{12\,33}$	–	$45_{11\,34}$	96045.2163	47.9
$32_{11\,22}$	–	$32_{10\,23}$	88242.9383	64.6	$45_{12\,34}$	–	$45_{11\,35}$	96045.2163	-22.8
$34_{11\,23}$	–	$34_{10\,24}$	88154.1674	-85.9	$46_{12\,34}$	–	$46_{11\,35}$	95953.4191	51.9
$34_{11\,24}$	–	$34_{10\,25}$	88154.1674	-91.8	$46_{12\,35}$	–	$46_{11\,36}$	95953.4191	-61.7
$35_{11\,24}$	–	$35_{10\,25}$	88102.9704	25.3	$47_{12\,35}$	–	$47_{11\,36}$	95854.6378	36.2
$35_{11\,25}$	–	$35_{10\,26}$	88102.9704	14.8	$47_{12\,36}$	–	$47_{11\,37}$	95854.6378	-144.1
$36_{11\,25}$	–	$36_{10\,26}$	88046.5316	-18.9	$49_{12\,37}$	–	$49_{11\,38}$	95634.5645	-45.5
$38_{11\,27}$	–	$38_{10\,28}$	87917.2661	115.3	$49_{12\,38}$	–	$49_{11\,39}$	95635.0334	-16.2
$38_{11\,28}$	–	$38_{10\,29}$	87917.2661	61.9	$50_{12\,38}$	–	$50_{11\,39}$	95512.5450	2.6
$39_{11\,28}$	–	$39_{10\,29}$	87843.4752	46.6	$50_{12\,39}$	–	$50_{11\,40}$	95513.2347	16.3
$39_{11\,29}$	–	$39_{10\,30}$	87843.4752	-42.5	$51_{12\,39}$	–	$51_{11\,40}$	95381.7564	-64.7
$40_{11\,29}$	–	$40_{10\,30}$	87763.2724	89.9	$51_{12\,40}$	–	$51_{11\,41}$	95382.7507	-99.7
$40_{11\,30}$	–	$40_{10\,31}$	87763.2730	-56.2	$52_{12\,40}$	–	$52_{11\,41}$	95241.9479	-3.7
$41_{11\,30}$	–	$41_{10\,31}$	87675.9461	-58.7	$52_{12\,41}$	–	$52_{11\,42}$	95243.4641	-39.8
$42_{11\,32}$	–	$42_{10\,33}$	87581.8134	-32.1	$53_{12\,41}$	–	$53_{11\,42}$	95092.3429	-58.6
$43_{11\,32}$	–	$43_{10\,33}$	87479.0347	-66.6	$53_{12\,42}$	–	$53_{11\,43}$	95094.6397	-81.3
$43_{11\,33}$	–	$43_{10\,34}$	87479.6688	-36.5	$55_{12\,43}$	–	$55_{11\,44}$	94762.0156	118.9
$44_{11\,33}$	–	$44_{10\,34}$	87368.3811	-46.7	$55_{12\,44}$	–	$55_{11\,45}$	94766.9638	24.3
$44_{11\,34}$	–	$44_{10\,35}$	87369.3124	-59.8					

[a] All transitions are weighted to be 0.01 relative to the previous cm-wave data[32] with weight=1.
[b] $\nu_{o\text{-}c}$: The difference between the observed frequency and calculation with the molecular constants.

These lines are analyzed simultaneously with FTMW experiment lines, jet spectroscopy and step 1 and 2 lines. In the least squares fitting analysis by considering the accuracy of the experiment, FTMW lines weight is set to 1 and weight of other lines is set to 0.01. This final step of analysis of $S_2{}^{35}Cl_2$ leads to obtaining all rotational molecular constants including forth order and sixth order centrifugal distortion constants for the first time. These constants are listed in Table 4.8.

Table 4.8: Molecular constants list for $S_2{}^{35}Cl_2$ which obtained from step3 data least square fitting and its comparison with step2 data analysis.

	Step2	**Step3**
***A*/MHz**	5533.8939(9)[a]	5533.8962(13)
B/MHz	1393.8460(6)	1393.8478(6)
C/MHz	1232.6706(4)	1232.6699(7)
Δ_J/KHz	0.569(1)	0.572(1)
Δ_{JK}/KHz	-5.134(19)	-5.132(9)
Δ_K/KHz	24.034(37)	24.053(28)
δ_J/KHz	0.1331(9)	0.1329(6)
δ_K/KHz	1.51(7)	2.19(14)
H_J/Hz	0.0026(9)	0.0051(6)
H_{JK}/Hz	0.06(4)	0.31(6)
H_{KJ}/Hz	-0.23(7)	-1.1(2)
H_K/Hz	0.3(2)	0.9(2)
h_J/Hz	0.0009(5)	0.0013(3)
h_{JK}/Hz		0.35(7)
h_K/Hz		11(2)
σ_{fit}/MHz	0.0054	0.0085

[a] Numbers in parenthesis denotes one standard deviation of least-squares fitting in the unit of the last significant digit.

Figures 4.6.a, 4.6.b and 4.6.c show some parts of the observed spectrum of determined *Q*-branch transitions.

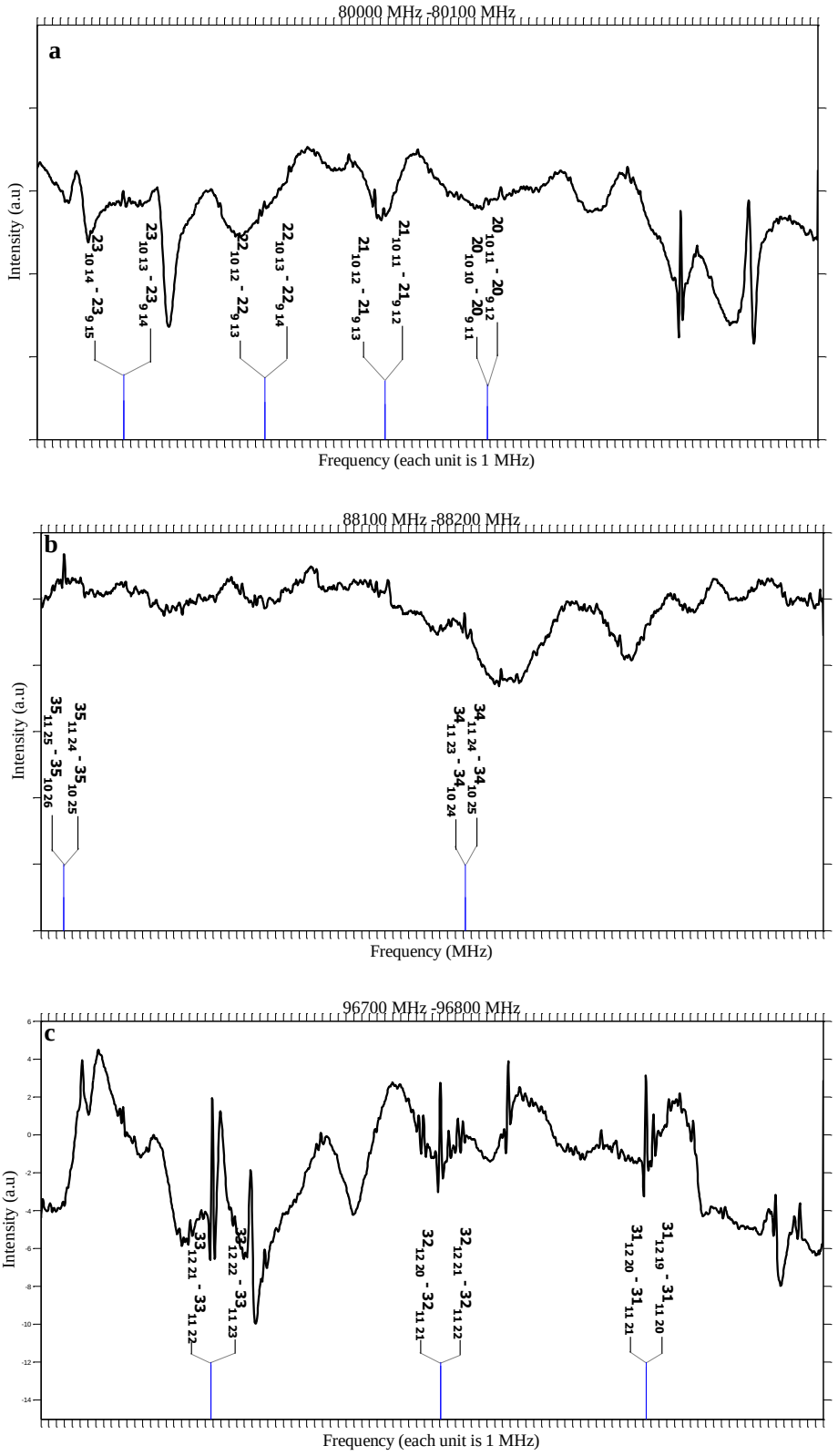

Figure 4.6: Some part of determined *Q*-branch transitions in step 3. (a) series of $^{r}Q_{9}(J)$-branches. (b) series of $^{r}Q_{10}(J)$-branches. (c) series of $^{r}Q_{11}(J)$-branches.

Figure 4-7 shows error distribution of all data including jet spectroscopy and gas cell spectroscopy, at the least square fitting analysis. $\nu_{o\text{-}c}$ is the difference between the observed frequency and the calculated one by molecular constants which were obtained as the result of least square fitting. As it is expected error distribution of least square fitting has a Gaussian shape, as it is estimated by the red color Gaussian type graph.

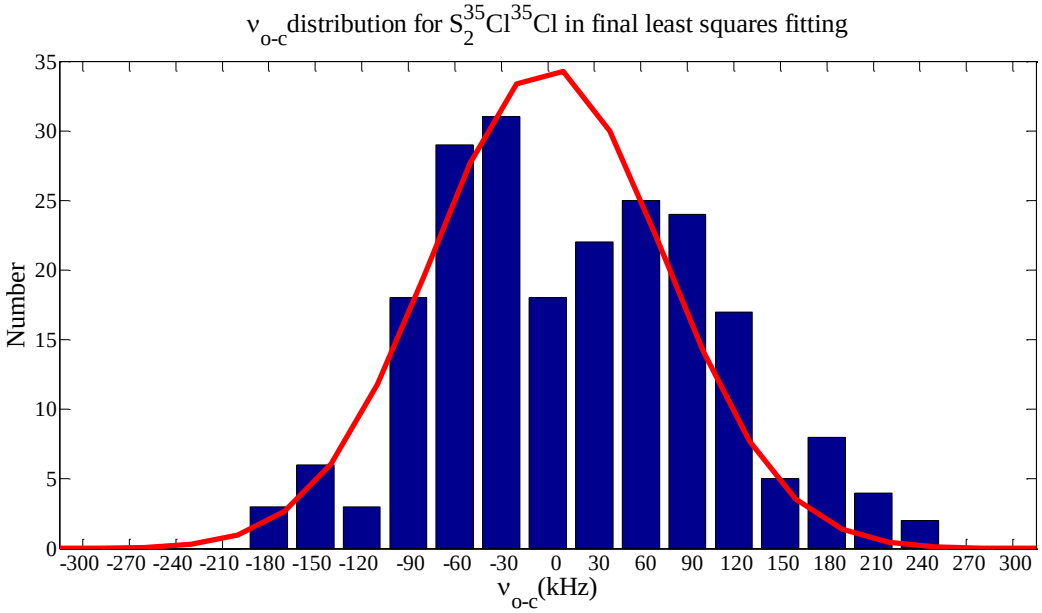

Figure 4.7: Error distribution of final least square fitting analysis. The distribution is estimated by a Gaussian shape graph which is shown by the red color.

In addition to the least squares fitting analysis of the pure rotational transitions, all observed spectrum including hyperfine transitions is also analyzed by least squares fitting. Details and results of this analysis will be discussed in section B-1 in the Appendix.

4-2 $S_2{}^{35}Cl^{37}Cl$ Spectroscopy

The same as the spectrum of $S_2{}^{35}Cl_2$, the spectrum of $S_2{}^{35}Cl^{37}Cl$ is also measured in two different experiment condition. In jet spectroscopy totally 40 lines are determined. Not any new molecular constant can be obtained but by improving the molecular constants which were predicted by FTMW spectroscopy prediction and determination transitions by high J and K_a quantum number become possible. Cell experiment data which were analyzed for $S_2{}^{35}Cl^{37}Cl$ are measured in different experimental conditions. By these data 51 transitions could be determined.

4-2-1 Jet spectroscopy

The transitions corresponding to $S_2{}^{35}Cl^{37}Cl$ isotope species are determined. Details of experiment and data analysis are the same as $S_2{}^{35}Cl_2$ isotope species, as it is explained in section 4-1-1. The result would be explained as follows.

Result and discussion

In total 30 *R*- and 10 *Q*-lines for $S_2{}^{35}Cl^{37}Cl$ were observed and their central frequencies, ignoring the hyperfine structure are listed in Table 4.11.

Table 4.11: The observed transitions of $S_2{}^{35}Cl^{37}Cl$ in the supersonic jet experiment[a].

$J'_{K'_aK'_c} - J''_{K''_aK''_c}$	$\nu_{obs.}$/MHz	$\nu_{o\text{-}c}$ /kHz[b]	$J'_{K'_aK'_c} - J''_{K''_aK''_c}$	$\nu_{obs.}$/MHz	$\nu_{o\text{-}c}$ /kHz[b]
$8_{8\,0} - 7_{7\,1}$	83388.8932	2.9	$15_{7\,9} - 14_{6\,8}$	92980.8807	17.7
$8_{8\,1} - 7_{7\,0}$	83388.8932	2.9	$16_{6\,11} - 15_{5\,10}$	87129.3776	89.1
$9_{8\,1} - 8_{7\,2}$	85953.7153	30.2	$16_{7\,9} - 15_{6\,10}$	95541.3911	-11.4
$9_{8\,2} - 8_{7\,1}$	85953.7153	30.2	$16_{7\,10} - 15_{6\,9}$	95541.3911	43.0
$9_{9\,0} - 8_{8\,1}$	94320.1873	58.5	$17_{6\,11} - 16_{5\,12}$	89678.7619	-98.0
$9_{8\,1} - 8_{7\,0}$	94320.1873	58.5	$17_{6\,12} - 16_{5\,11}$	89673.4668	-88.1
$10_{8\,2} - 9_{7\,3}$	88523.3944	38.5	$17_{7\,10} - 16_{6\,11}$	98099.0919	-116.6
$10_{8\,3} - 9_{7\,2}$	88523.3944	38.5	$17_{7\,11} - 16_{6\,12}$	98099.0919	3.2
$10_{9\,1} - 9_{8\,2}$	96890.3953	61.8	$18_{6\,12} - 17_{5\,13}$	92210.4995	-17.1
$10_{9\,2} - 9_{8\,1}$	96890.3953	61.8	$18_{6\,13} - 17_{5\,12}$	92210.8261	18.5
$11_{8\,3} - 10_{7\,4}$	91092.8041	39.9	$14_{10\,4} - 14_{9\,5}$	79554.9559	-73.4
$11_{8\,4} - 10_{7\,3}$	91092.8041	39.9	$14_{10\,5} - 14_{9\,6}$	79554.9559	-73.3
$11_{9\,2} - 10_{8\,3}$	99460.5077	44.1	$15_{10\,5} - 15_{9\,6}$	79551.9202	-30.4
$11_{9\,3} - 10_{8\,2}$	99460.5077	44.1	$15_{10\,6} - 15_{9\,7}$	79551.9202	-30.4
$14_{6\,8} - 13_{5\,9}$	82025.3107	62.4	$15_{11\,4} - 15_{10\,5}$	87915.2980	45.4
$14_{6\,9} - 13_{5\,8}$	82024.6334	44.0	$15_{11\,5} - 15_{10\,6}$	87915.2980	45.4
$14_{7\,7} - 13_{6\,8}$	90418.1474	51.5	$16_{11\,5} - 16_{10\,6}$	87913.3423	1.3
$14_{7\,8} - 13_{6\,7}$	90418.1474	60.8	$16_{11\,6} - 16_{10\,7}$	87913.3423	1.2
$15_{6\,9} - 14_{5\,10}$	84580.8246	150.6	$17_{11\,6} - 17_{10\,7}$	87910.5349	-52.3
$15_{7\,8} - 14_{6\,9}$	92980.8807	-5.6	$17_{11\,7} - 17_{10\,8}$	87910.5349	-52.3

[a] All transitions are weighted to be 0.01 relative to the previous cm-wave data[32] with weight=1.

[b] $\nu_{o\text{-}c}$: The difference between the observed frequency and calculation with the molecular constants.

These transitions were analyzed simultaneously with the transitions measured by FTMW as explained in reference 32. The least square fitting was weighted by 1.0 for FTMW and 0.01 for

the mm-wave transitions according to the accuracy of each experimental measurement. As a result, the three rotational constants are improved. These molecular parameters are listed in Table 4.12 as jet spectroscopy.

Table 4.12: Molecular constants list for $S_2{}^{35}Cl^{37}Cl$ which obtained from jet experiment data least square fitting and its comparison with FTMW data analysis.

	FTMW	**Jet experiment**
***A*/MHz**	5475.4344(11)	5475.4350(6)
B/MHz	1361.8640(5)	1361.8654(7)
C/MHz	1205.1953(8)	1205.1932(6)
Δ_J/KHz	0.554(9)	0.531(3)
Δ_{JK}/KHz	-4.465(147)	-4.937(13)
Δ_K/KHz	22.68(37)	23.60(2)
δ_J/KHz	0.054(20)	0.114(17)
σ_{fit}/MHz	0.0045	0.0043

[a] Numbers in parenthesis denotes one standard deviation of least-squares fitting in the unit of the last significant digit.

Figures 4.8.a and 4.8.b show ${}^rQ_9(J)$-branches and ${}^rQ_{10}(J)$-branches of $S_2{}^{35}Cl^{37}Cl$ which were observed in the jet spectroscopy.

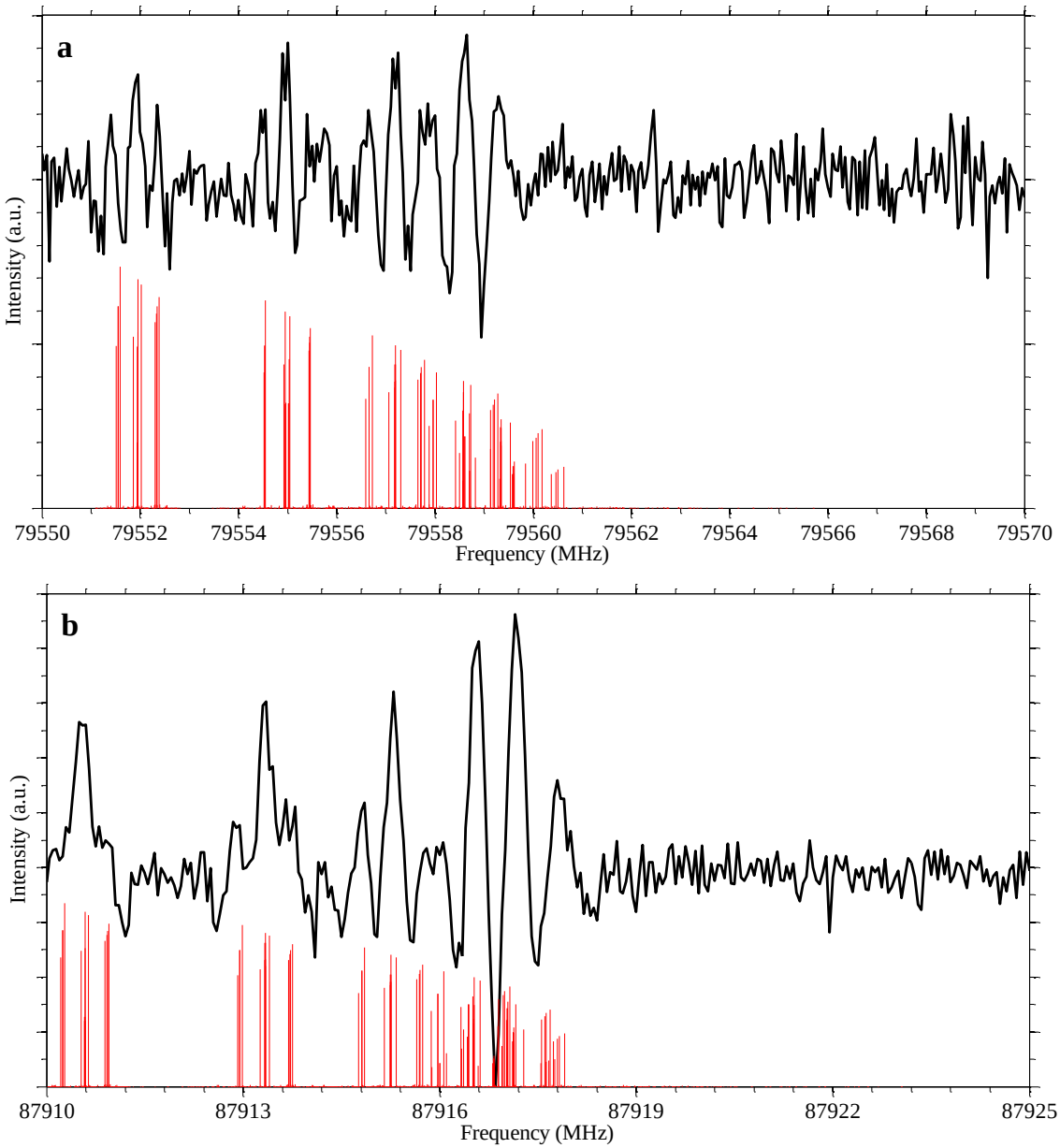

Figure 4.8: Series of ${}^{r}Q(J)$-branches of $S_2{}^{35}Cl{}^{37}Cl$ observed in the supersonic jet experiment. Stick spectrum shows the hyperfine components calculated with the rotational constants from the jet experiment in Table 4.12 and hyperfine constants reported in reference 32. (a) Series of ${}^{r}Q_9(J)$-branches. (b) Series of ${}^{r}Q_{10}(J)$-branches.

4-2-2 Cell Spectroscopy

The experimental setup is the same as what is explained in section 3-2. As the intensity of transitions which correspond to the $S_2{}^{35}Cl{}^{37}Cl$ isotope species are totally low intensity transitions, fast scanning measured spectrum in section 4-1-2 are not suitable for determination

of these transitions. So some selected regions which correspond to the high intensity transitions are selected for measurements with higher accuracy. The measurement was carried out by sweeping the mm-wave frequency over 10 MHz in 150 seconds and 4 scans were averaged to attain a good signal to noise ratio. In results and discussion, there is the list of the determined lines and rotational molecular constants as result of least square fitting analysis of the determined lines.

Results and discussions

Totally 51 lines were determined from the cell spectroscopy data for $S_2{}^{35}Cl^{37}Cl$, as listed in Table 4.13. The highest J quantum number of determined lines is J=40 and the highest K_a quantum number is 12.

Table 4.13: The observed transitions of $S_2{}^{35}Cl^{37}Cl$ in the cell experiment[a].

$J'_{K'_aK'_c} - J''_{K''_aK''_c}$	$\nu_{obs.}$/MHz	$\nu_{o\text{-}c}$ /kHz[b]	$J'_{K'_aK'_c} - J''_{K''_aK''_c}$	$\nu_{obs.}$/MHz	$\nu_{o\text{-}c}$ /kHz[b]
$10_{7\,3} - 9_{6\,4}$	80151.6019	-92.4	$35_{1\,35} - 34_{0\,34}$	85131.3641	5.3
$10_{7\,4} - 9_{6\,3}$	80151.6019	-92.3	$35_{2\,34} - 34_{1\,33}$	86812.6474	148.4
$11_{7\,4} - 10_{6\,5}$	82719.8291	-89.0	$36_{0\,36} - 35_{1\,35}$	87535.6900	4.5
$11_{7\,5} - 10_{6\,4}$	82719.8291	-88.7	$36_{1\,36} - 35_{0\,35}$	87536.8808	-4.4
$12_{6\,6} - 11_{5\,7}$	76904.5742	-80.4	$36_{4\,33} - 35_{3\,32}$	97278.4804	35.7
$12_{6\,7} - 11_{5\,6}$	76904.5742	40.0	$37_{0\,37} - 36_{1\,36}$	89941.3017	-81.3
$12_{7\,5} - 11_{6\,6}$	85287.2030	-60.0	$37_{1\,37} - 36_{0\,36}$	89942.2300	-6.3
$12_{7\,6} - 11_{6\,5}$	85287.2030	-58.8	$37_{2\,36} - 36_{1\,35}$	91604.4582	117.0
$13_{7\,6} - 12_{6\,7}$	87853.3626	-70.1	$37_{2\,35} - 36_{3\,34}$	92877.6106	-124.5
$13_{7\,7} - 12_{6\,6}$	87853.3626	-66.6	$38_{0\,38} - 37_{1\,37}$	92346.7780	2.6
$13_{8\,6} - 12_{7\,5}$	96230.0329	-95.7	$38_{1\,38} - 37_{0\,37}$	92347.3899	8.6
$13_{8\,5} - 12_{7\,6}$	96230.0329	-95.7	$38_{1\,37} - 37_{2\,36}$	93973.6773	19.7
$15_{6\,10} - 14_{5\,9}$	84579.3323	49.6	$38_{2\,37} - 37_{1\,36}$	94003.0395	-131.5
$19_{3\,16} - 18_{2\,17}$	78533.2237	43.5	$39_{0\,39} - 38_{1\,38}$	94751.8435	-25.4
$19_{4\,16} - 18_{3\,15}$	75327.3603	-54.0	$39_{1\,39} - 38_{0\,38}$	94752.3290	30.4
$22_{5\,18} - 21_{4\,17}$	92914.0478	156.0	$39_{1\,38} - 38_{2\,37}$	96381.5563	-46.7
$23_{5\,18} - 22_{4\,19}$	96713.5407	-123.6	$39_{2\,37} - 38_{3\,36}$	97839.4025	77.2
$25_{4\,22} - 24_{3\,21}$	84238.8556	-66.1	$39_{3\,36} - 38_{4\,35}$	97344.2910	23.5
$32_{0\,32} - 31_{1\,31}$	77909.5005	20.0	$40_{0\,40} - 39_{1\,39}$	97156.6412	-24.5
$32_{1\,32} - 31_{0\,31}$	77914.1362	6.7	$40_{1\,40} - 39_{0\,39}$	97157.0656	95.3
$32_{2\,31} - 31_{1\,30}$	79652.4259	6.5	$40_{1\,39} - 39_{2\,38}$	98788.2374	-79.3
$33_{0\,33} - 32_{1\,32}$	80316.5900	-15.6	$26_{10\,16} - 26_{9\,17}$	79404.9432	83.4
$33_{1\,33} - 32_{0\,32}$	80319.9282	1.9	$26_{10\,17} - 26_{9\,18}$	79404.9432	82.2
$34_{0\,34} - 33_{1\,33}$	82723.3230	1.8	$37_{12\,25} - 37_{11\,26}$	95935.4072	-11.6
$34_{1\,34} - 33_{0\,33}$	82725.6787	-11.2	$37_{12\,26} - 37_{11\,27}$	95935.4072	-12.5
$35_{0\,35} - 34_{1\,34}$	85129.6832	11.9			

[a] All transitions are weighted to be 0.01 relative to the previous cm-wave data[32] with weight=1.

[b] $\nu_{o\text{-}c}$: The difference between the observed frequency and calculation with the molecular constants.

These lines are analyzed simultaneously with FTMW experiment lines and jet spectroscopy. In the least squares fitting analysis, by considering the accuracy of the experiment, FTMW lines weight is set to 1 and weight of other lines is set to 0.01. As a result, all molecular constants of $S_2{}^{35}Cl^{37}Cl$ including fourth order and sixth order centrifugal distortion constants determined. This is the first time these molecular constants are introduced for $S_2{}^{35}Cl^{37}Cl$. In Table 4.14 these constants are listed.

Table 4.14: Molecular constants list for $S_2{}^{35}Cl^{37}Cl$ which obtained from gas cell spectroscopy data least square fitting and its comparison with jet experiment data analysis.

	Jet experiment	**Cell experiment**
***A*/MHz**	5475.4350(6)	5475.4349(12)
B/MHz	1361.8654(7)	1361.8651(5)
C/MHz	1205.1932(6)	1205.1908(7)
Δ_J/KHz	0.531(3)	0.511(1)
Δ_{JK}/KHz	-4.937(13)	-4.727(11)
Δ_K/KHz	23.60(2)	23.33(4)
δ_J/KHz	0.114(17)	0.1109(8)
***δ_K*/KHz**		0.6(1)
H_J/Hz		-0.0044(8)
H_{JK}/Hz		1.8(1)
***H_{KJ}*/Hz**		-4.5(3)
***H_K*/Hz**		1.9(3)
***h_J*/Hz**		-0.0015(5)
***h_{JK}*/Hz**		0.12(7)
***h_K*/Hz**		59 (3)
σ_{fit}/MHz	0.0043	0.0067

[a] Numbers in parenthesis denotes one standard deviation of least-squares fitting in the unit of the last significant digit.

The error of the least squares fitting analysis is comparable with experimental error. In Figure 4.9 distribution of $\nu_{o\text{-}c}$ is plotted. As it is expected this distribution can be estimated by a Gaussian graph which is shown in red color. In section B-3 in Appendix, a list of all transitions including $\nu_{o\text{-}c}$ magnitudes from the least squares fitting analysis could be found.

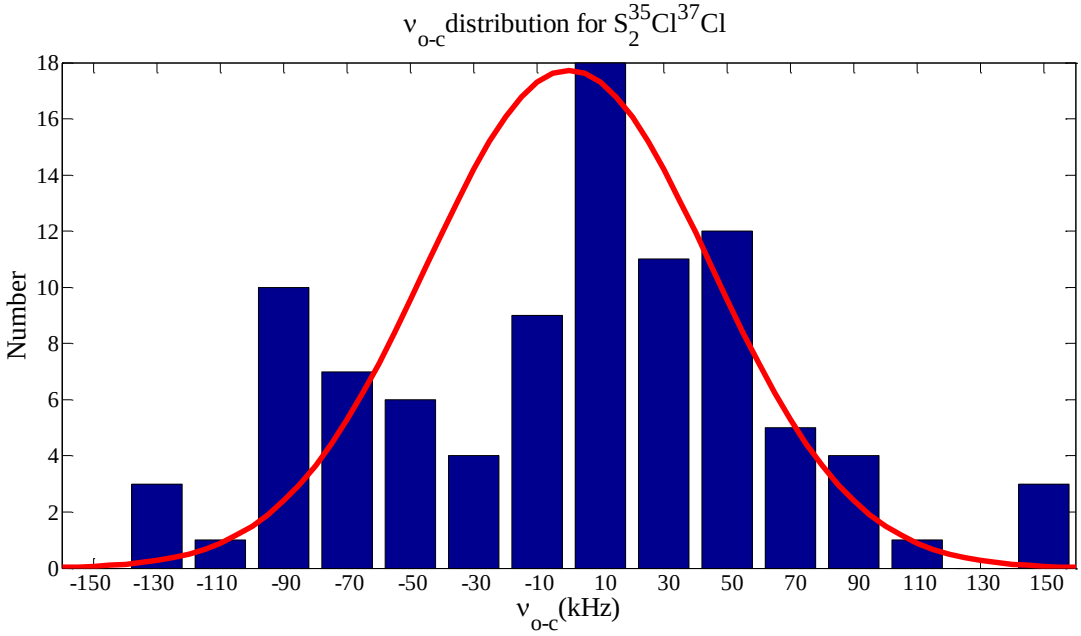

Figure 4.9: The error distribution of final least square fitting data analysis for $S_2{}^{35}Cl^{37}Cl$. The distribution is estimated by a Gaussian shape graph which is shown by the red color.

In Figure 4.10, an example of high-*J* transition, ${}^{r}R_{Kc=0}(37)$ transition of $S_2{}^{35}Cl^{37}Cl$ that is observed with the gas cell experiment is shown. Determining such kind of transitions with high quantum number leads to obtaining sixth order centrifugal distortion constants. The frequency positions predicted by the rotational molecular constants of reference 32, jet spectroscopy, and gas cell spectroscopy are shown with the dotted line, dashed line and solid line, respectively. Although in the jet spectroscopy new molecular constants were not predicted, by the constants which were obtained by analysis of the jet spectroscopy data, the determination of transitions like the one in Figure 4-10 become possible.

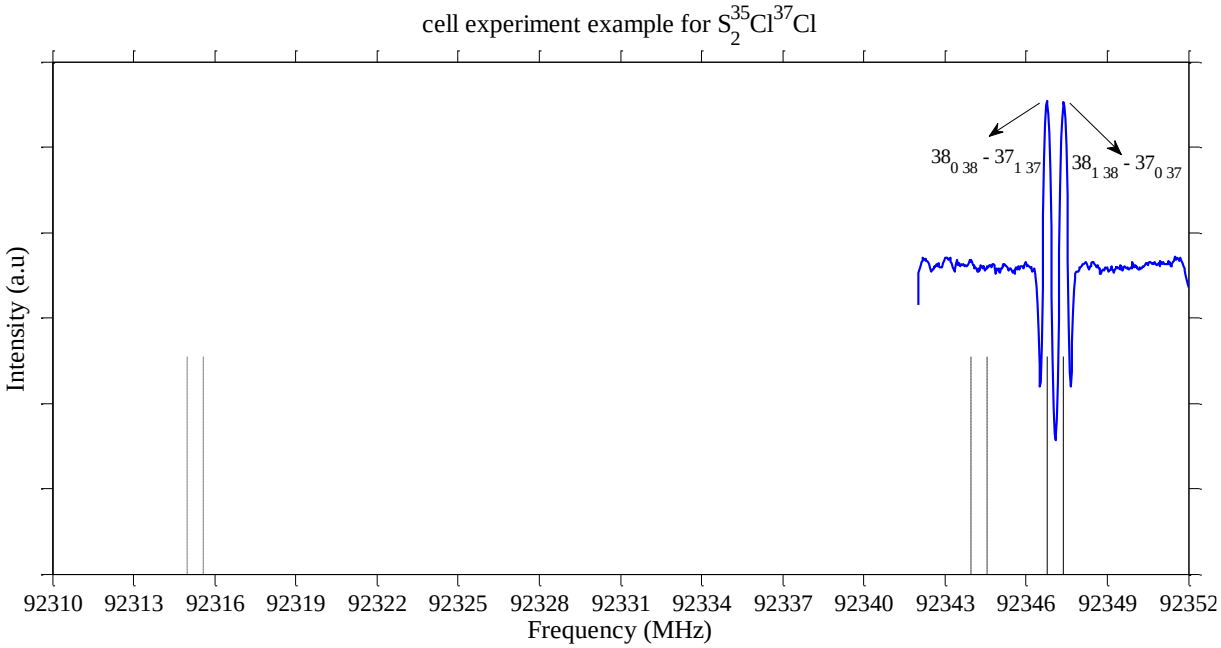

Figure 4.10: An example of high-*J* transition: ${}^{r}R_{Kc=0}(37)$ transition of $S_2{}^{35}Cl^{37}Cl$ observed with the gas cell experiment. The frequency positions predicted by the rotational molecular constants of FTMW jet spectroscopy, and cell spectroscopy are shown with the dotted line, dashed line, and solid line, respectively.

4-3 Investigation of the Signal to Noise Ratio in the Millimeter Wave Spectroscopy of $S_2{}^{35}Cl_2$

In the centimeter wave region, although the intensity of the radiative transitions is small, using a Fourier-transform microwave spectrometer, the sufficient signal to noise ratios for detecting these low intensity transitions has been obtained[2]. The millimeter wave region has special importance in the radiative *ortho-para* transitions studies in S_2Cl_2. However, the FTMW spectrometer in millimeter wave region is not available for some technical reasons. As the intensities of the *ortho-para* hyperfine transitions are small, knowing the best values for S/N ratios leads to predicting that whether an *ortho-para* transition is detectable or not. In this work, to find the best achievable signal to noise ratio values in millimeter wave region, the frequency region of 81118 MHz to 81123 MHz is selected for the measurement. The measurement is done by both gas cell spectroscopy and supersonic pulsed jet spectroscopy. Experimental details are explained in chapter 3. The gas cell spectroscopy had an advantage of achieving higher initial intensity, but unstable baseline and unexpected transition peaks which are related to the high *J* force to do supersonic jet experiment spectroscopy instead.

4-3-1 Calculating the Spectrum Pattern

The transition dipole moments and the frequencies of possible transitions in the frequency region of 81118 MHz to 81123 MHz are calculated to finding the spectrum pattern. Table 4.15 shows a list of possible hyperfine transitions and their frequency and transition moments in this region. By the help of equation 2-35, the transition moment in the direction of principal axis b would be calculated in the symmetrized symmetric rotor basis set. In section A-4 in the appendix, there is the written code for calculating a transition moment.

Table 4.15: List of the hyperfine transitions and their transition moments in 81118 MHz to 81123 MHz frequency region.

Transition	Frequency (MHz)	Transition moment	Transition	Frequency (MHz)	Transition moment
10_{74} 3 13 – 9_{63} 3 12	81119.5030	8.64	10_{74} 3 10 – 9_{63} 3 10	81119.8765	0.29
10_{73} 2 12 – 9_{64} 2 11	81119.7318	8.00	10_{74} 3 11 – 9_{63} 3 11	81120.4883	0.22
10_{74} 3 12 – 9_{63} 3 11	81119.7852	7.80	10_{74} 1 9 – 9_{63} 3 9	81119.9051	0.21
10_{74} 1 11 – 9_{63} 1 10	81119.7280	7.25	10_{74} 3 12 – 9_{63} 3 12	81120.4237	0.20
10_{73} 2 11 – 9_{64} 2 10	81119.7310	7.22	10_{74} 3 7 – 9_{63} 3 7	81118.9854	0.20
10_{74} 3 11 – 9_{63} 3 10	81120.0140	7.13	10_{74} 3 8 – 9_{63} 3 8	81119.5053	0.19
10_{73} 0 10 – 9_{64} 0 9	81119.9880	6.62	10_{74} 3 9 – 9_{63} 3 9	81119.1755	0.15
10_{74} 3 10 – 9_{63} 3 9	81119.9801	6.35	10_{74} 3 8 – 9_{63} 1 8	81119.0029	0.14
10_{73} 2 9 – 9_{64} 2 8	81119.7332	5.88	10_{73} 2 8 – 9_{64} 2 8	81119.7399	0.13
10_{74} 1 9 – 9_{63} 1 8	81119.9566	5.87	10_{73} 2 11 – 9_{64} 2 11	81119.7351	0.13
10_{74} 3 9 – 9_{63} 3 8	81119.7294	5.82	10_{74} 1 11 – 9_{63} 3 11	81119.5617	0.10
10_{73} 2 8 – 9_{64} 2 7	81119.7314	5.30	10_{73} 2 9 – 9_{64} 0 9	81119.1693	0.10
10_{74} 3 8 – 9_{63} 3 7	81119.6731	5.11	10_{74} 1 10 – 9_{63} 1 10	81118.9242	0.10
10_{74} 3 7 – 9_{63} 3 6	81119.4490	4.60	10_{73} 0 10 – 9_{64} 2 10	81120.5476	0.10
10_{73} 2 10 – 9_{64} 2 9	81119.4774	4.08	10_{73} 2 10 – 9_{64} 2 10	81118.9118	0.10
10_{74} 1 10 – 9_{63} 1 9	81119.4773	4.08	10_{74} 3 10 – 9_{63} 1 10	81120.5172	0.07
10_{73} 2 10 – 9_{63} 1 9	81119.4774	2.54	10_{73} 2 9 – 9_{64} 2 9	81120.2945	0.06
10_{74} 1 10 – 9_{64} 2 9	81119.4773	2.54	10_{74} 3 9 – 9_{63} 1 9	81120.2657	0.06

Using Table 4.15 and assuming each transition has a Gaussian shape with FWHM equal to 0.2 MHz, Figure 4.11 is obtained. This magnitude for the FWHM is obtained from the Doppler broadening which is measured in millimeter microwave jet spectroscopy as explained in section 4-1-1.

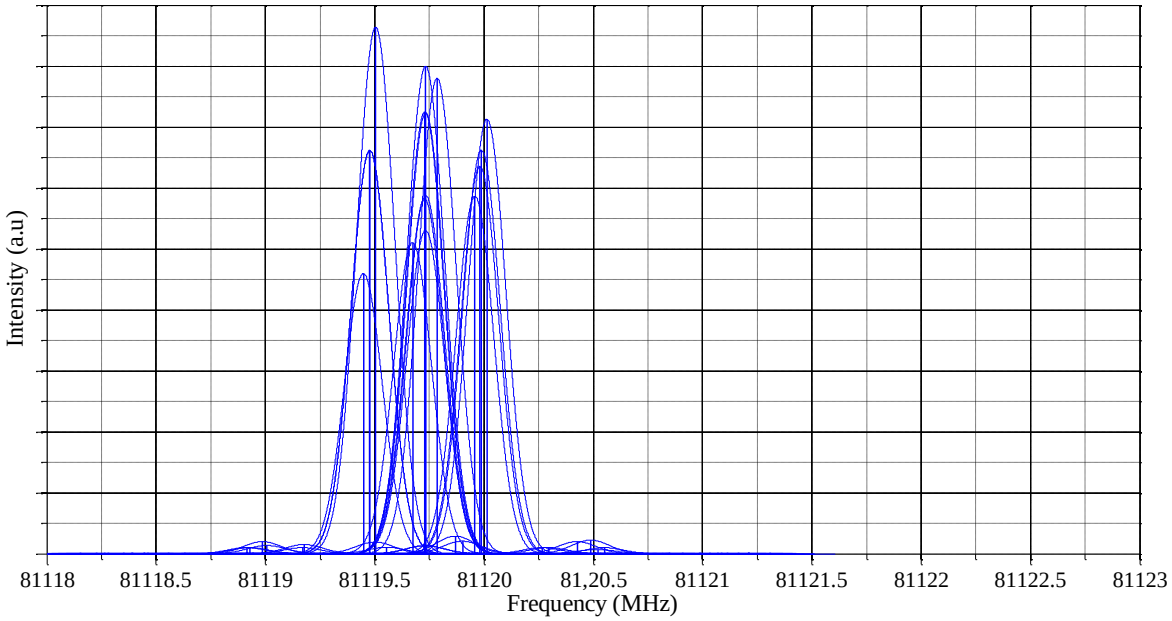

Figure 4.11: the hyperfine radiative transition in the frequency region from 81118 MHz to 81123 MHz. Each line shape is estimated as a Gaussian type by the FWHM equal to 0.2 MHz.

By summation of all peaks in the Figure 4.11 the final spectrum pattern was obtained. It is shown in Figures 4.12.a. Figure 4.12.b is obtained by the second derivative of Figure 4.12.a.

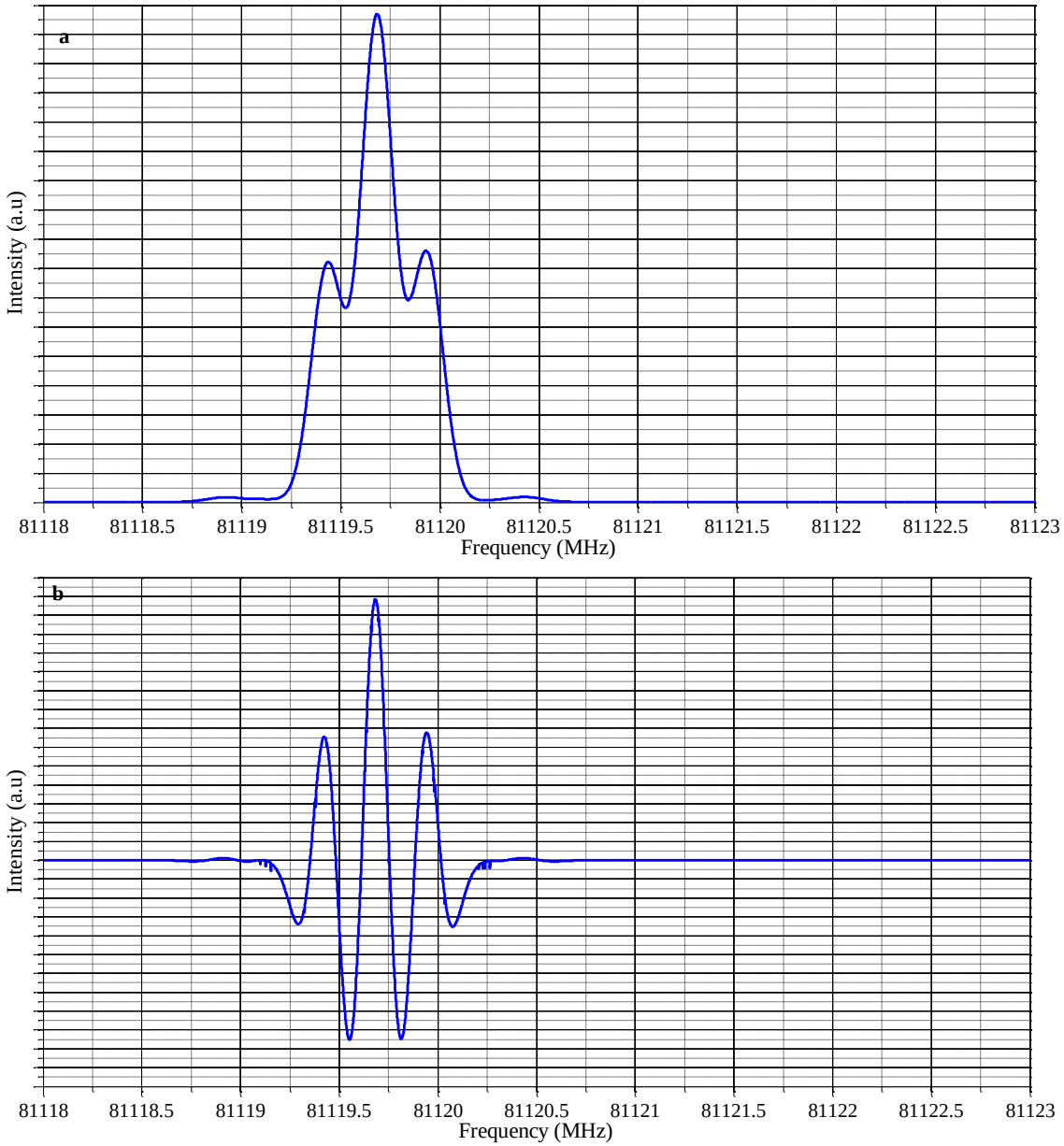

Figure 4.12: (a) Summation of all peaks in Figure 4.11. (b) The second derivative of the spectrum pattern in Figure 4.12.a.

4-3-2 Gas Cell Spectroscopy

Details of the experiment are as explained in section 3-4. The gas cell is covered by a box full of dry ice for keeping the temperature of the experiment the same as dry ice temperature. Dry ice sublimes at 195K at earth atmospheric pressure. As melting point of disulfur dichloride is 193K, it can be assumed that S_2Cl_2 is solid at dry ice temperature. Observing solid S_2Cl_2 in the gas cell during the dry ice temperature experiment confirmed this assumption. As the result,

the only amount of this material which is equal to vapor pressure at dry ice temperature is in the gas cell. S_2Cl_2 vapor pressure at 195K is 0.0002 Torr. Since the pumping speed in the experiment system is less than pumping the 0.0002 Torr material during the experiment time, the pressure inside the gas cell is 0.0002 Torr. Details about data analyzing and results of this experiment are explained in result and discussion of this part.

Results and discussion

Figure 4.13 shows the spectrums which were measured at dry ice temperature.

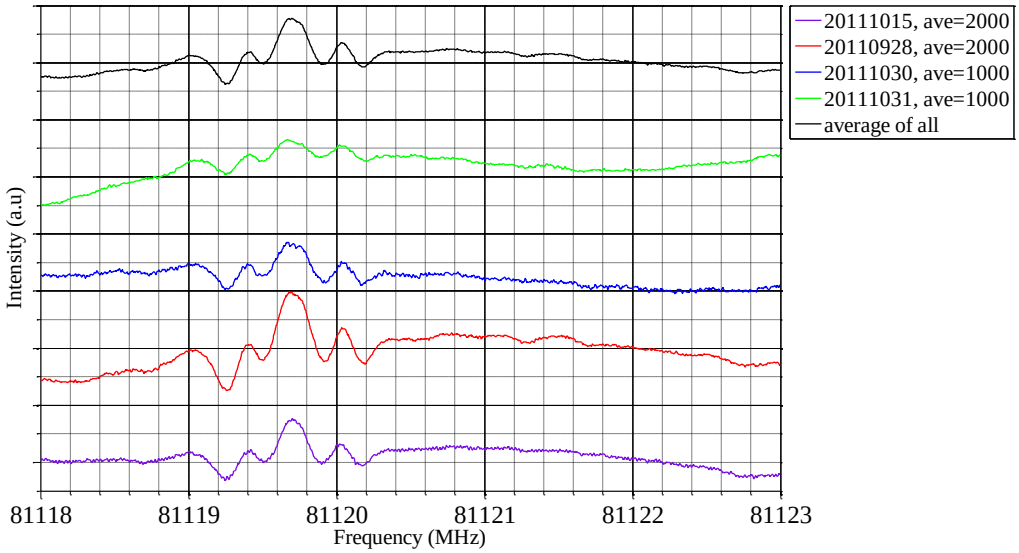

Figure 4.13: Spectrum patterns in 4 different measurements at the $10_{74} - 9_{63}$ and $10_{73} - 9_{64}$ transition. These measurements were done on 4 different days and the average of 2000 or 1000 sweep was recorded. The baselines shown in Figure 4.14 are subtracted from above measurements.

The baseline pattern has an important effect on the final pattern of the measured spectrum. The baseline means the measured pattern without introducing the sample to the experimental setup. This pattern is affected by the alignment. The proper alignment can lead to the stable baseline pattern. In addition to the alignment, electronics and external mechanical noises also have effects on the baseline pattern. As it is shown in Figure 4.14, in four different measurements, there were four different patterns for the baseline. For obtaining Figure 4.13, these patterns are subtracted from the measured spectrum. However, as Figure 4.13 shows, obtaining flat spectrum was not possible. The reason is the difference of real baseline pattern at

the time of measuring the spectrum by introducing sample and the baseline patterns which are measured without introducing sample.

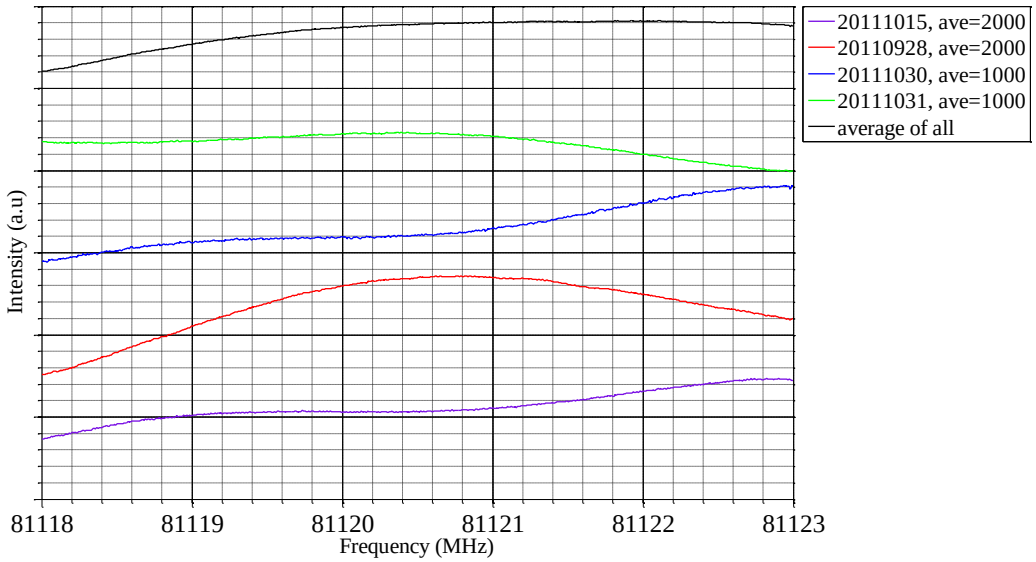

Figure 4.14: The different measured baseline patterns at four different measurements for the subtraction of the spectrums in Figure 4.13.

For achieving the desired signal to noise ratio, averaging is inevitable. On the other hand, by the increase of the number of the averaging, as the time of measurement increases, the baseline pattern may change during the experiment. For decreasing the effect of baseline, the number of averaging was decreased from 2000 times to 10 times for each scan. For achieving the desired signal to noise ratio, 95 measurements were done for signal and 58 measurements were done for the baseline. The baselines were subtracted from the signal and the averaged result is recorded. This result is shown by blue spectrum in the Figure 4.15. In order to reduce the baseline effect and distinguishing the real signal from the noise signals which may be produced by the instability of the baseline, digital filtering of the blue color averaged spectrum was done. At first, low pass FFT filter was used. The result is shown in black in Figure 4.15. As this figure shows, a low pass filter is not enough in making a flat pattern for measured spectrum. Green color spectrum in Figure 4.15 shows the result of a band pass filter. This is the result of low pass filtering and high pass filtering by Gaussian sweep.

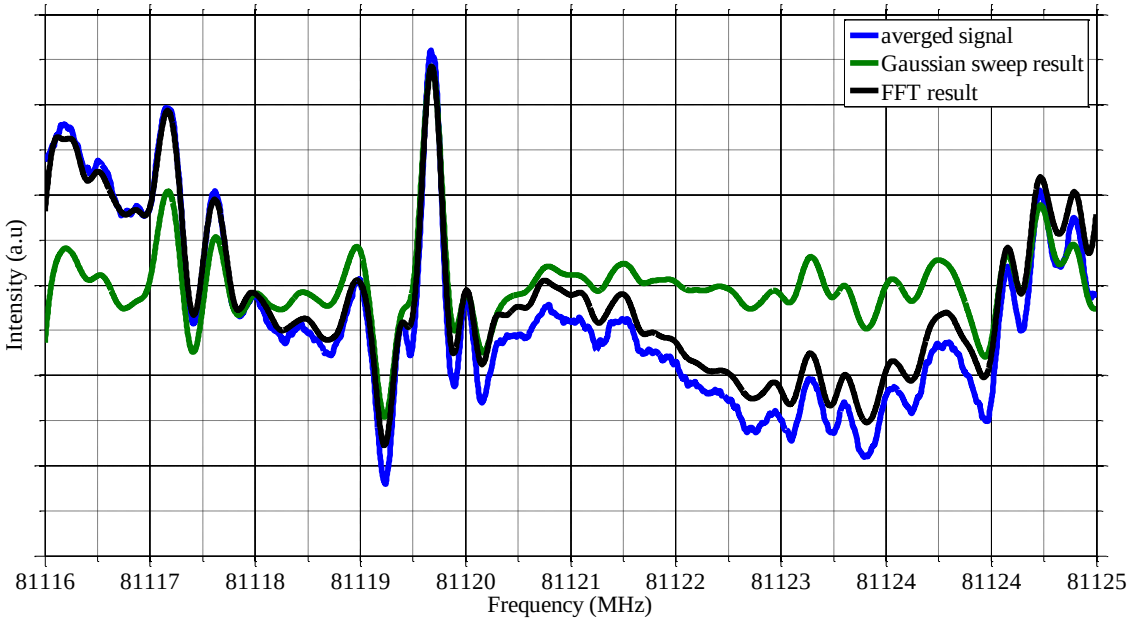

Figure 4.15: Average of 58 baselines and 98 measured signals and their subtraction is shown by the blue color. For having a flat pattern a low pass filter (FFT) and a band pass filter (Gaussian sweep) are performed in the averaged blue color spectrum. They are shown by the black and green color, respectively.

The spectrum which is shown in the Figure 4.16 is the same as green color spectrum in Figure 4.15. This is the final spectrum pattern from cell experiment spectroscopy in the dry ice temperature. As this Figure shows except the predicted peaks there are also unknown peaks. Transitions with high quantum numbers are the main candidates for determining these peaks. As it is shown in this Figure $|69_{11\ 59}> - |\ 69_{10\ 60}>$ transition which is related to the $S_2{}^{35}Cl^{35}Cl$ isotope species and $|66_{6\ 61}> - |\ 66_{5\ 62}>$ transition which is related to the $S_2{}^{35}Cl^{37}Cl$ isotope species are candidates for two peaks in Figure 4.16.

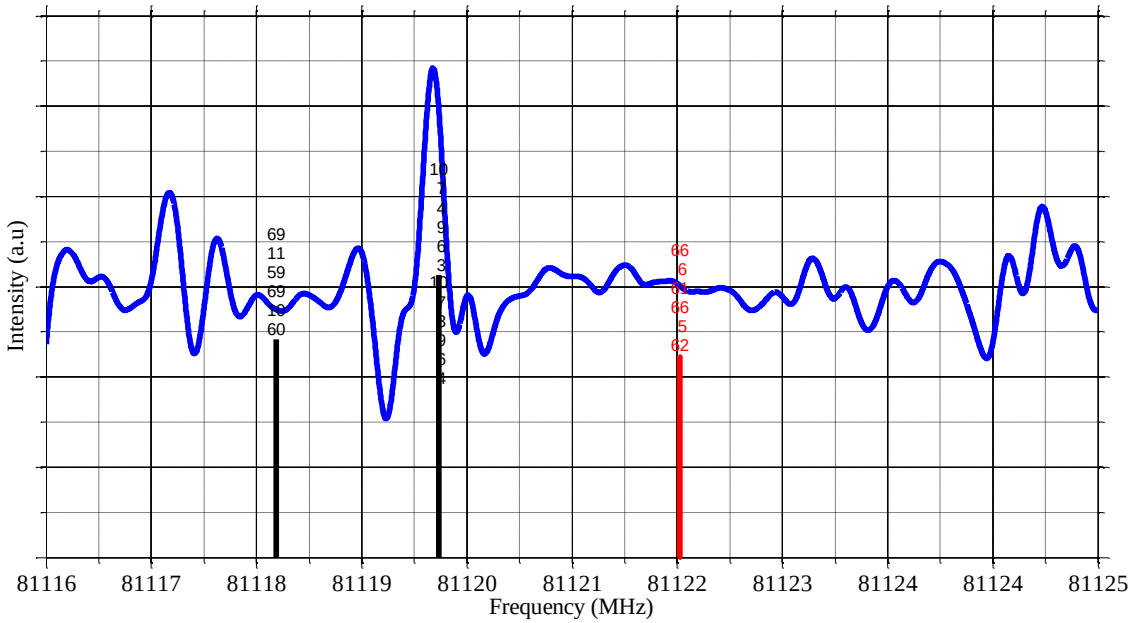

Figure 4.16: Showing probability of the existence of some transitions by high quantum number in the dry ice temperature. $|69_{11\ 59}> - |\ 69_{10\ 60}>$ transition is related to the $S_2{}^{35}Cl^{35}Cl$ isotope species and $|66_{6\ 61}> - |\ 66_{5\ 62}>$ transition is related to the $S_2{}^{35}Cl^{37}Cl$ isotope species. They are shown by the black and red color lines, respectively.

Figure 4.17 shows the comparison of the measured spectrum with the predicted spectrum. The measured spectrum in the gas cell spectroscopy is shown by red color. The predicted spectrum is shown by blue color. As Figure 4.17 shows the relative intensities of three peaks in the measured spectrum are different from the prediction. The triplet pattern is not exact as the prediction. Another difference between the measurement and the prediction is that the magnitude of FWHM of the center peak in the measured spectrum is larger than the prediction. This difference could correspond to the contribution of an unexpected transition in the spectrum pattern. At the temperature of the gas cell spectroscopy experiment, transitions by high quantum numbers could be excited. As these transitions are not determined in the millimeter microwave spectroscopy, in predicting the spectrum pattern they are not considered. As it is interested to be obtained the proper S/N values in the millimeter wave region, having a conclusion that whether some peak is signal or noise is important. So in temperatures as high as the gas cell spectroscopy temperature, determining the transitions by high quantum number is necessary.

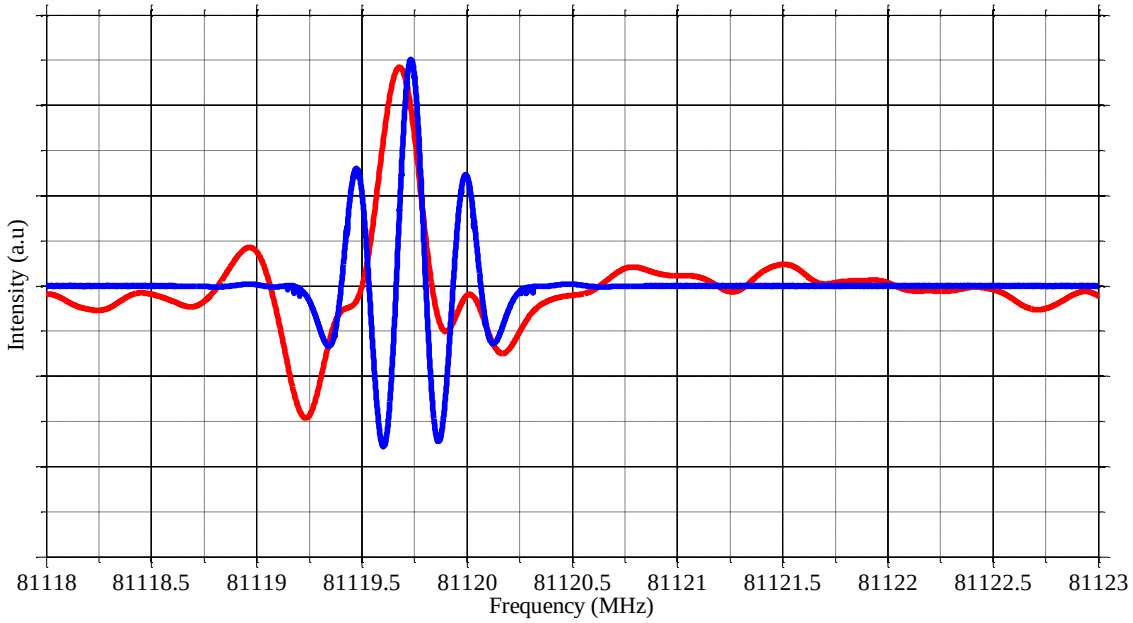

Figure 4.17: Comparison of the measured spectrum in the gas cell spectroscopy (red color) and the predicted spectrum (blue color)

4-3-3 Supersonic Jet Spectroscopy

At low temperatures, the intensity of the target transition increases. So the spectroscopy was done in a pulse jet experiment condition. Another advantage of the pulse jet is an application of the time-resolved spectroscopy. By setting a proper gate, the signal and the baseline can be measured by a very short time difference. So the problem of the unstable baseline was eliminated. Experimental setup and details of the experiment are the same as the mm-wave spectroscopy of normal transitions as explained in chapter 3. At the start of the experiment, the optimum phase and modulation depth were carefully selected.

Results and discussions

The spectra in Figure 4.18 were obtained from the jet spectroscopy of our searching region. 50 shots of the jet were averaged at each frequency without any modulation on the MW source.

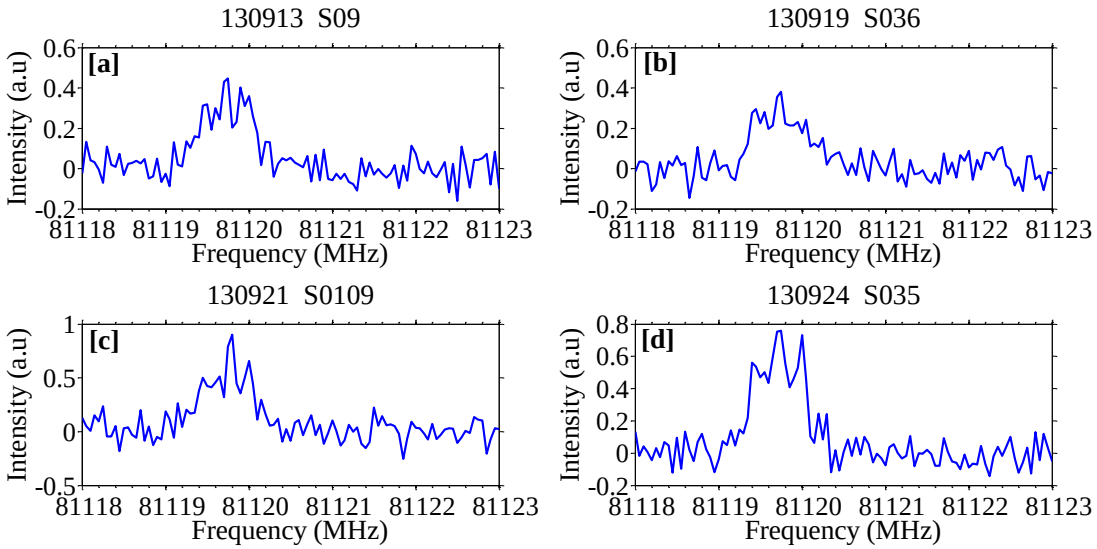

Figure 4.18: Four examples of the measured spectrum. 50 shots of the jet were averaged at each frequency point.

As these spectrums show the signal to noise ratio in each measurement is not enough for distinguishing the low intensity *ortho-para* transitions. For obtaining our desirable signal to noise ratio this experiment is repeated 233 times and the averaged is shown in the Figure 4.19. As it is shown in this figure, the S/N ratio for this experiment is 50.

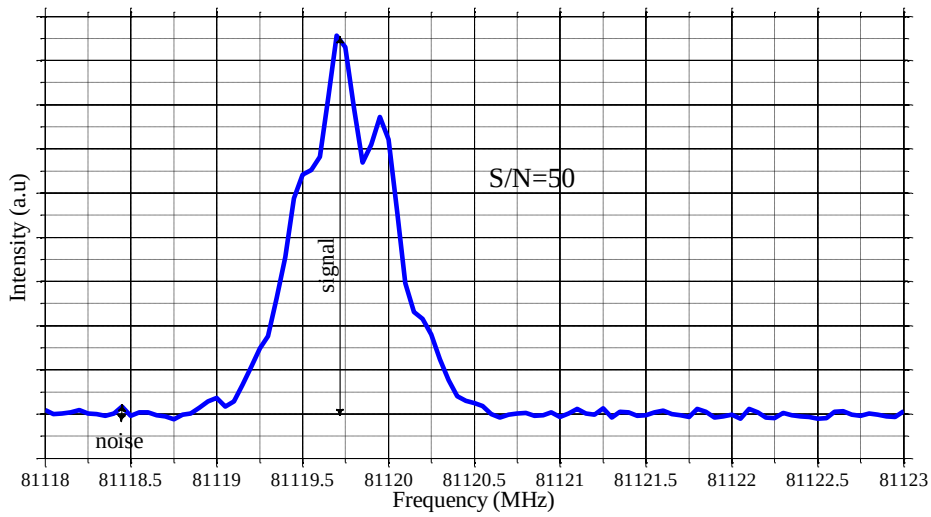

Figure 4.19: Averaging of 233 measurements shown in Figure 4.18. The signal and noise which are considered for finding S/N ratio are shown by the arrows.

In Figure 4.20, the measured spectrum pattern in jet spectroscopy is compared with the predicted pattern. The measured spectrum is shown in red and the predicted spectrum is shown by blue. As Figure 4.20 shows, the intensity of the center peak relative to the two sided peaks is smaller than the prediction. Another different of the measurement and the prediction is that the measured spectrum is wider than the prediction and there are two unexpected shoulders on two sides of the measured spectrum. The predicted pattern shows that the intensity of the left side peak in the triplet pattern would be larger than the intensity of the right side peak. Comparing the intensity of two sided peaks in the red measured spectrum shows the intensity of the left side peak is smaller than the right side peak. On the other hand, the intensity of the center peak relative to the two sided peaks is smaller than the prediction. One possible reason for these differences might be because of shift of the position of the hyperfine transitions relative to the predicted position. Using the experimental methods which are free of Doppler Effect, the hyperfine transitions will be measured by better resolution and this improves the experiment conditions.

Another possible reason could be the estimation of the line shape. As it is explained in section 4-3-1, for calculating the blue color spectrum in Figure 4.20, the line shape of each hyperfine transition is estimated to be Gaussian. If this assumption for line shape changes, the predicted pattern for the spectrum will change. The symmetric shoulders on the two side of the measured spectrum suggest estimating the line shape by shoulders instead of Gaussian type.

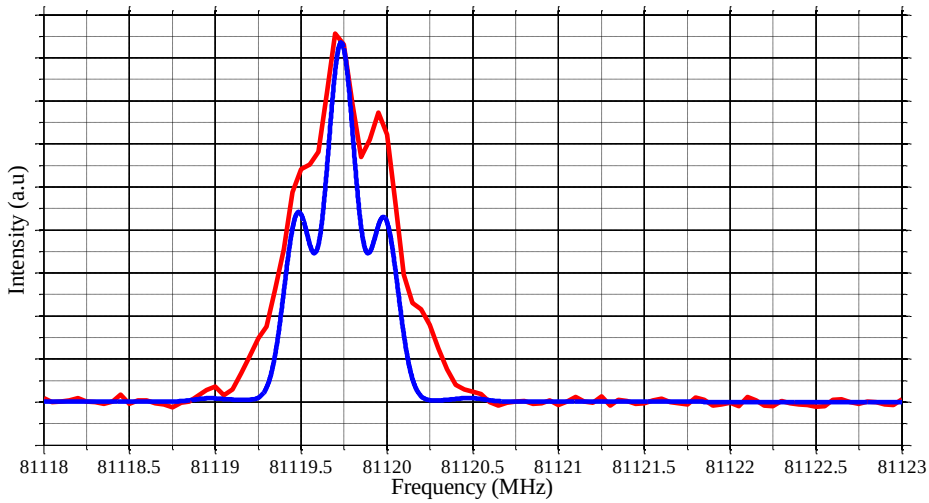

Figure 4.20: Comparison of the final result of the jet spectroscopy with the predicted pattern. The predicted pattern is shown by the blue color. The measured spectrum is shown by the red.

Chapter 5

Theoretical Investigation of the *Ortho-Para* Interaction in S_2Cl_2

Ortho-para transition by the origin of nuclear spin interaction through collisions has been studied in different molecules theoretically. In some cases, experimental observations of them have been reported[12-19]. But, No experimental observation of direct radiative *ortho-para* transition has been reported, yet. The nuclear electric quadrupole interactions could lead to the interaction of *ortho* and *para* states. In S_2Cl_2, this interaction is the most important hyperfine interaction. In 2008, Mizoguchi *et.al* observed unexpected hyperfine splitting in centimeter wave spectrum of S_2Cl_2. They introduced off-diagonal terms of the nuclear quadrupole interaction in the Hamiltonian of S_2Cl_2 and determined the off-diagonal coupling constants. By this effective Hamiltonian including the new off-diagonal hyperfine terms, they could reproduce the observed hyperfine splitting in the spectrum of this molecule[2].

Calculating the hyperfine splitting pattern correctly in the spectrum of S_2Cl_2 would not be the only role of introducing the off-diagonal hyperfine terms in the Hamiltonian. The off-diagonal hyperfine interaction could mix the *ortho* and the *para* states. The existence of the mixed *ortho-para* states would lead to non-zero radiative transition moment between the *ortho* and the *para* states. Observation of the *ortho-para* transition would also be another evidence for verification of the new effective Hamiltonian.

In this chapter, the *ortho-para* mixing coefficients and rotational transition moments in the millimeter wave region are calculated. For calculating the transition moment, the molecular wave functions of the effective Hamiltonian are used directly instead of using a common perturbation theory. The reason is that the common symmetrized symmetric rotor wave functions are not suitable for calculating the *ortho-para* mixing coefficients. In other words, $\boldsymbol{I} = \boldsymbol{I_1} + \boldsymbol{I_2}$ is not a good quantum number for showing the *ortho-para* interacting states. This is because of the contribution of the off-diagonal hyperfine interaction terms in mixing the same symmetry states.

In section 5-1, it is shown that for finding the *ortho-para* mixing coefficients, the projection of the effective wave function on the eigenfunctions of the unperturbed Hamiltonian should be calculated. In section 5-2, details of calculations related to the term energies and wave functions of $S_2{}^{35}Cl_2$ are described and section 5-3 is the results and discussion.

5-1 Theory

$S_2{}^{35}Cl_2$ molecule has two Chlorine atoms with the nuclear spin $I = 3/2$. As a result of the coupling of two Cl nuclei, the magnitude of total nuclear spin is equal to $I = 0,1,2,3$. According

to Pauli exclusion principle, there are restrictions on symmetry properties of molecular wave functions. By these restrictions, the total molecular wave functions are divided into two groups. One group is corresponding to the coupling of the odd-*I* nuclear spin states with $K_a + K_c$ = odd rotational states. These states are known as *ortho* states. The other group is corresponding to the coupling of the even-*I* nuclear spin states with $K_a + K_c$ = even rotational states. These states are known as *para* states. The transition between the pure *ortho* and the pure *para* states is strictly forbidden. Nevertheless, some perturbation effects like hyperfine interactions can change the pure symmetrical character of the molecular wave function to an impure character. It means that the total molecular wave function, as a complete description of a molecule, is a mixture of both the *ortho* and *para* states. In these cases, the radiative transition between two molecular states with opposite symmetries would be theoretically possible. In $S_2{}^{35}Cl_2$, the off-diagonal nuclear quadrupole term is the interaction that can change the pure symmetry of the molecular wave function to the impure symmetry.

The common treatment for calculating the *ortho-para* mixing coefficient in the molecular wave functions is to use the perturbation theory. If H_{OP} shows the perturbed interaction, by perturbation theory for non-degenerated states, the molecular wave function is mixed with an opposite symmetry molecular wave function by a coefficient equal to:

$$\frac{\langle \Psi^O | H_{OP} | \Psi^P \rangle}{E_O - E_P} \tag{5-1}$$

The wave functions and term energies in 5-1 are obtained from the molecular Hamiltonian without the perturbation interaction term. By calculating 5-1, one can find the mixing coefficient between the *ortho* and *para* states. Since the *ortho-para* interacting states of the interest in the previous studies[12-18] are corresponding to the accidentally close levels in the energy and are not degenerate states, using equation 5-1 is applicable in those studies.
However, as in the millimeter wave region, the rotational quantum number of $S_2{}^{35}Cl_2$ become larger than 10, the *K*-doubling states are no more non-degenerate. These *K*-doubling states have the opposite *ortho* and *para* symmetry and can be mixed by a hyperfine interaction. With increasing the *J* quantum number, the *K*-doubling states degenerate more. The non-degenerate perturbation theory is not applicable to calculating the *ortho-para* mixing coefficient for these degenerate states, and a method for the degenerate states are necessary.

In Chapter 4, by microwave spectroscopy of $S_2{}^{35}Cl_2$, the Hamiltonian of this molecule were determined. We describe this Hamiltonian as H_{eff}. This Hamiltonian is an approximation of the true Hamiltonian of the molecule (H_{true}). H_{eff} is determined by least squares fitting analysis of the measured transitions frequencies. So the difference in the eigenvalue of E_{eff} and E_{true} is less than the experimental error.
If the effective Hamiltonian were a good physical approximation of the true Hamiltonian, in addition to reproducibility of eigenvalues, the transition moment would be predicted as well. In other words, experimental measurement of the transition which is predicted by $|\Psi_{eff}\rangle$ would confirm that the wave functions of H_{eff} are more physically close to the true wave functions. So instead of using equation 5-1 for finding the mixing coefficient between the *ortho* and *para* states, the transition moment between molecular states with opposite symmetry will be calculated directly from $|\Psi_{eff}\rangle$. In the following sections, the theory of finding the *ortho* and the *para* mixed states will be described. As described above, the effective molecular Hamiltonian is written as follows:

$$H_{eff} = H_0 + H_{OP}, \tag{5-2}$$

where

$$H_0 = H_{rot} + H^{d}_{hyper} \, . \tag{5-3}$$

In equations 5-2 and 5-3, H_{rot} is the rotational term including centrifugal distortion constants, H^{d}_{hyper} is the diagonal nuclear quadrupole coupling term and H_{OP} is the off-diagonal nuclear quadrupole term. Matrix elements of the Hamiltonian in 5-2 can be written in the symmetric rotor basis set as described in Chapter 2, by equation 2-7. We represent a symmetrized symmetric rotor basis set as below,

$$\{|\chi_i\rangle\} \equiv \left\{|J_{i_{K_i}} I_i F_i, \pm\rangle\right\} = \left\{ \ |J_{i_{K_i}} I_i F_i, \pm\rangle^{P} \right\} \oplus \left\{ \ |J_{i_{K_i}} I_i F_i, \pm\rangle^{O} \right\} \equiv \{ \ |\chi_i\rangle^{P} \} \oplus \{ \ |\chi_i\rangle^{O} \} \tag{5-4}$$

where the superscript *P/O* represents the pure *para/ortho* symmetry. The effective molecular wave function is the solution of equation 5-5.

$$H_{eff}|\Psi_{eff}\rangle = E_{eff}|\Psi_{eff}\rangle \, . \tag{5-5}$$

This wave function would be expanded with the symmetrized symmetric rotor basis set representation as below,

$$|\Psi_{eff}\rangle = \sum_i s_i \, |\chi_i\rangle \, . \tag{5-6}$$

The existence of the symmetrized symmetric rotors basis with the different nuclear spin symmetries in a wave function indicates the impure character of the molecular wave function. In such a condition, to say that the molecular wave function is mostly *para*, it is represented as $|\Psi_{eff}\rangle^{\sim P}$ and if the molecular wave function is mostly *ortho*, it is represented as $|\Psi_{eff}\rangle^{\sim O}$. In fact, some wave functions consist of more than two opposite symmetrized symmetric rotor components. This means that the molecular wave function interacts with more than one opposite symmetry wave functions. In this case, the treatment based on a simple perturbation theory is no more available. The eigenvectors of the molecular wave function should be considered more carefully.

For distinguishing the contribution of each hyperfine term in the molecular wave function, first, the diagonal hyperfine term (H^{d}_{hyper}) is considered. If $|\varphi^{(0)}\rangle$ shows the molecular wave function for H_0 Hamiltonian, it can be expanded to the symmetrized symmetric rotor basis set as follows:

$$|\varphi^{(0)}\rangle \ = \sum_i s_i \, |\chi_i\rangle \ \, . \tag{5-7}$$

$|\varphi^{(0)}\rangle$ is the solution of equation 5-8.

$$H_0|\varphi^{(0)}\rangle = E^{(0)}|\varphi^{(0)}\rangle \, . \tag{5-8}$$

As there is no contribution of *ortho-para* interaction in H_0, $|\varphi^{(0)}\rangle$ has the pure *ortho* or *para* symmetry. So it can be written in one of the following forms:

$$|\varphi^{(0)}\rangle \equiv |\varphi\rangle = \begin{cases} \sum_i {}^{P(0)}s_i \;\; |\chi_i\rangle^P \\ \sum_i {}^{O(0)}s_i \;\; |\chi_i\rangle^O \end{cases} \tag{5-9}$$

Since $\{|\varphi_i\rangle\}$ forms a complete orthogonal basis set, the total molecular wave function $|\Psi_{\text{eff}}\rangle$ for Hamiltonian H_{eff}, could be represented by a basis set whose components are made by $\{|\varphi_i\rangle\}$. Here, we introduce an idea of mostly *ortho* or *para* wave functions for actual hyperfine resolved levels.

$$|\Psi_{\text{eff}}\rangle^{\sim O/P} = \sum_i d_i \, |\varphi_i\rangle = \sum_i {}^P d_i \;\; |\varphi_{\text{i}}\rangle^P + \sum_i {}^O d_i \;\; |\varphi_{\text{i}}\rangle^O \tag{5-10}$$

where, for $|\Psi_{\text{eff}}\rangle^{\sim P}$, $\sum_i \left| {}^O d_i \right|^2 \ll \sum_i \left| {}^P d_i \right|^2$ and for $|\Psi_{\text{eff}}\rangle^{\sim O}$, $\sum_i \left| {}^P d_i \right|^2 \ll \sum_i \left| {}^O d_i \right|^2$.

For example, attendance of $|\varphi_{\text{i}}\rangle^P$ in $|\Psi_{\text{eff}}\rangle^{\sim O}$ leads the non-zero *ortho-para* transition moment whose magnitude is proportional to $|\sum_i {}^P d_i \,|^2$. By knowing $|\Psi_{\text{eff}}\rangle$ from equation 5-6 and $|\varphi_{\text{i}}\rangle^P$ from equation 5-9, ${}^P d_i$ could be derived as follows:

$${}^P d_i = {}^P\langle \varphi_i | \Psi_{\text{eff}}\rangle^{\sim O} \;\; . \tag{5-11}$$

As equation 5-11 shows, the d_i would be obtained by the projecting of $|\Psi_{\text{eff}}\rangle$ onto $|\varphi_i\rangle$. Indeed, by finding the projection of $|\Psi_{\text{eff}}\rangle$ onto $|\varphi\rangle$, the actual *ortho-para* mixing coefficients can be obtained.

In the above approach for finding the *ortho* and *para* mixed states, the eigenfunctions of both H_0 and H_{eff} have to be calculated. As a result, actual *ortho-para* mixed states could be found. By using the projection of the effective wave functions onto $|\varphi\rangle$, the magnitude of the transition moment of an *ortho-para* transition could be approximate by squared values of mixing coefficients. For example, if the initial state in a transition is almost a *para* state ($|\Psi_{\text{eff}}\rangle_i^{\sim P} = c_1|\varphi_1\rangle_i^P + c_2|\varphi_2\rangle_i^O$), and the final state is a pure *ortho* state ($|\varphi\rangle_f^O$), the intensity of $|\Psi_{\text{eff}}\rangle_i^{\sim P} - |\varphi\rangle_f^O$ *ortho-para* transition can be approximated as fallowing:

$$I_{OP} = \left| {}^{\sim P}_i\langle \Psi_{\text{eff}} | \mu | \varphi \rangle_f^O \right|^2 = |c_2|^2 \left| {}^O_i\langle \varphi_2 | \mu | \varphi_2 \rangle_f^O \right|^2$$

In other words, the intensity of $|\Psi_{\text{eff}}\rangle_i^{\sim P} - |\varphi\rangle_f^O$ *ortho-para* transition is borrowed from the intensity of $|\varphi_2\rangle_i^O - |\varphi\rangle_f^O$ normal transition by a coefficient equal to $|c_2|^2$.In this work, we calculated the *ortho-para* transition moment directly from the effective wave functions. The idea of intensity borrowing is only used for physical interpretation like the investigation of quantum number dependency in the *ortho-para* mixing states.

It is also valuable if the *ortho-para* mixing coefficients could be obtained directly from the molecular wave functions. The second approach for finding the *ortho-para* mixing coefficients would be described in the following. In this approach, the molecular wave function which is eigenfunctions of H_{eff} only would be calculated.

Expansion 5-6 also can be written by separating the *ortho* and the *para* symmetrized symmetric rotor basis set:

$$|\Psi_{\text{eff}}\rangle^{\sim O/P} = \sum_i s_i \, |\chi_i\rangle = \sum_i {}^P s_i \;\; |\chi_i\rangle^P \; + \;\; \sum_i {}^O s_i \;\; |\chi_i\rangle^O \tag{5-12}$$

In order to find the mixing coefficient of the total molecular state as a *para* state, we have the following relation by using equations 5-9, 5-11 and 5-12:

$$d_i = {}^{O}\langle\varphi|\Psi\rangle^{P} = \sum_i {}^{O}s_i \, {}^{O(0)}s_i \tag{5-13}$$

As a result, the square of the mixing coefficient is written as below:

$$|d_i|^2 = \left(\sum_i {}^{O}s_i \, {}^{O(0)}s_i\right)^2 = \sum_i({}^{O(0)}s_i)^2 \sum_i({}^{O}s_i)^2 - \sum_i \sum_{j=i+1} \left({}^{O}s_i \, {}^{O(0)}s_i - {}^{O}s_j \, {}^{O(0)}s_j\right)^2 \tag{5-14}$$

As $\sum_i({}^{O(0)}s_i)^2 = 1$ and $\sum_i \sum_{j=i+1} \left({}^{O}s_i \, {}^{O(0)}s_i - {}^{O}s_j \, {}^{O(0)}s_j\right)^2 \ll 1$,

$$|d_i|^2 \approx \sum_i({}^{O}s_i)^2 \tag{5-15}$$

As a result of equation 5-15, square of the *ortho-para* mixing coefficient in a wave function in symmetrized symmetric rotor representation can be calculated. Using equation 5-15, the mixing coefficients for the *ortho-para* transition ($|d_i|^2$) could be also obtained in the common symmetrized symmetric rotor basis set representation without calculating the projection of the molecular wave function on the eigenfunctions of the $\mathrm{H}_0 = \mathrm{H}_{\mathrm{rot}} + \mathrm{H}^{\mathrm{d}}_{\mathrm{hyper}}$ Hamiltonian. As a result, the *ortho* character and *para* character for a molecular wave function can be defined as below:

$$\rho_O = \sum_i |\, {}^{O}s_i|^2 \,, \quad \rho_P = \sum_i |\, {}^{P}s_i|^2 \,. \tag{5-16}$$

In this study, that character of a wave function which has the opposite symmetry of the wave function is named *ortho-para* mixing coefficient and is showed by ρ_{mixing}.

By calculating the *ortho* and *para* characters for a molecular wave function, magnitude of *ortho-para* mixing coefficient for that wave function corresponding *ortho-para* transition could be obtained, but for finding the *ortho-para* mixed states between all basis with opposite symmetries in that wave functions more consideration is needed. The *ortho* and *para* character of all molecular wave functions that their basis representation appears in the interested wave function and have the opposite symmetry should be calculated. The magnitude of the opposite symmetry character in two real *ortho-para* mixed states is the same. So by finding the states having the same magnitude of the opposite symmetry character, two direct interacting *ortho-para* states would be found.

By having above considerations, below approach is introduced for intensity borrowing mechanism in the common symmetrized symmetric rotor basis set for *ortho-para* transitions: Only two opposite symmetry molecular states which have direct *ortho-para* interaction by each other, lead to nonzero dipole moment in intensity borrowing mechanism and all other levels with opposite symmetry which appear in a wave function don't lead to the *ortho-para* transition. In other words, the intensity can be only borrowed from direct interactive pairs not all levels with opposite symmetry which appears in the wave functions. Direct interacting states could be found by calculating the *ortho* and *para* characters. Two opposite symmetry molecular states are direct interacting pairs when they have equal values of mixing character. For an *ortho* state mixing character is the *para* character of that state and for a *para* state the mixing character is the *ortho* character of that molecular state.

5-2 Calculation

In order to study the *ortho-para* interaction, having complete knowledge of eigenenergy and eigenfunction of each $F = J + I$ state is inevitable.
The first step in the calculation is making the Hamiltonian matrix for a certain F. Details about making the Hamiltonian matrix elements were explained in sections 2-1 and 2-2. Using equation 2-2 for the rotational terms and equation 2-18 for the nuclear quadrupole interaction terms, the matrix elements of the Hamiltonian are calculated by using the symmetrized symmetric rotor basis set. In section A-1 in the Appendix, the C++ programming language code which makes the Hamiltonian matrix elements is listed.

The second step of the calculations is to diagonalize the Hamiltonian matrix numerically for finding molecular states term energies and wave functions. Choosing a proper library for diagonalizing the Hamiltonian matrix is important for the precise determination of each molecular state. "Eigen" is an open source C++ library which was used in this research for diagonalizing the Hamiltonian matrix for each F quantum numbers. Treating degenerate eigenenergy and the ability of diagonalization of a complex matrix are two important advantages of this library.

The final step in finding term energies and wave functions of $S_2{}^{35}Cl_2$ is the proper labeling the eigenenergies and eigenvectors which were obtained by making the Hamiltonian matrix diagonal. Details of labeling will be described in section 5-2-1. In section 5-2-2 the results which are obtained from term energies and wave functions of molecular states of $S_2{}^{35}Cl_2$ will be discussed.

5-2-1 Labeling of an Eigenstate

The initial step for the study of the *ortho-para* transitions is to calculate the proper wave functions and energies of each molecular state. For doing that, Hamiltonian of S_2Cl_2 including hyperfine terms should be obtained by calculating matrix elements of this Hamiltonian in symmetric rotor basis set. After calculating the Hamiltonian matrix this Hamiltonian should be made diagonal for obtaining energies and wave functions of each molecular state. In other words, Term energies and wave functions are eigenvalues and eigenfunctions of the Hamiltonian. Different numerical methods are improved and established for making a matrix diagonal and the standard subroutines and libraries according to these methods are introduced for the matrix diagonalization. For making diagonal molecular Hamiltonian of S_2Cl_2 molecule subroutine “Eigen” is used. The advantages of this open-access library for this work are considering degeneracy problem and the ability to make diagonal matrices by complex elements.

The next step after making the Hamiltonian matrix diagonal is proper and correct labeling of each eigenfunction and eigenvalue. This is the most complicated and the most important step of calculating wave functions and energies of all molecular states. Unlike the symmetric-top molecules that their wave functions and energy levels can be obtained analytically, in asymmetric-top molecules, the wave function and energies can be found only numerically. We used A-reduced symmetric rotor Hamiltonian in I^r representation as Table 2.4. The matrix elements are calculated in the Wang basis set using equations 2-6 and 2-7. The asymmetric top rotor states are expanded over the symmetric rotor Wang basis set, as follows:

$$|J_\tau\rangle = \sum_K a_K |J\ K\rangle\ , \tag{5-17}$$

where $\tau = K_\mathrm{a} - K_\mathrm{c}$.

The general strategy for labeling of an eigenstate is to find the biggest eigenvector or the expanded coefficient $|a_K|^2 = a_K a_K^*$. A set of quantum number is chosen as the label of a concerning eigenstate. However, this general strategy just works for small quantum numbers. At large quantum numbers, sometimes it happens to becomes not simple because of large off-diagonal matrix elements of the asymmetric rotor Hamiltonian with hyperfine interactions. For such an eigenstate, the wave function consists several dominant basis. So, it becomes difficult to judge the correct labeling. It is necessary to modify the labeling strategy. This modification is done in three steps as explained in the following sections. In section A-2 in the appendix, the programming codes corresponding to these steps for the labeling are attached.

Step 1: Determination of parity of a wave function

This step is explained by an example of *F*=9 Hamiltonian. As shown in 5-18, it is a linear combination of the symmetrized symmetric rotor basis in Wang representation.

$$\left|J_{K_a\,K_c}\ I\ F\right\rangle = (0.59)\left|9_6\ 1\ 9,+\right\rangle^O + (0.20)\left|9_6\ 3\ 9,+\right\rangle^O + (0.55i)\left|9_6\ 0\ 9,-\right\rangle^P + (0.55i)\left|9_6\ 2\ 9,-\right\rangle^P + \cdots \tag{5-18}$$

The *ortho-para* symmetry of the basis function is defined by Tables 2.3 and 2.4. The biggest expansion coefficient in (5-18) is 0.59 of $|9_{6\,3}\ 1\ 9\rangle^O$ *ortho* states. According to the common strategy for labeling, the eigenstate would be called as the $|9_{6\,3}\ 1\ 9\rangle^O$ *ortho* state. But as the total character of the wave function is *para* (60%), the proper label for this eigenfunction should belong to the *para* state which has the biggest coefficients. So the first modification to the general labeling strategy is determining the *ortho* or the *para* character of the eigenfunction. Then the common labeling strategy would be performed between states with the parity that is the same as the parity of the eigenfunction.

Step 2: Consideration of the second or lower rank coefficients for labeling a wave function

Figure 5.1 shows an example of the participation of more than one symmetric rotor basis in an asymmetric rotor state. This Figure shows $\left|J_{K_a\,K_c}\ I\ F\right\rangle = \left|24_{K\ 24-K}2\ 24\right\rangle$ state which belongs to the E^+ representation in the Wang basis set. Each *K* value shows an asymmetric rotor state. For each state, the highest four $|a_K|^2$ values are shown with different color circles. Blue, red, black and green color circles correspond to the first, second, third and fourth highest value of $|a_K|^2$ in each state, respectively. As seen in Figure 5.1, the portion of the third and fourth components is fairly large at the low *K* values.

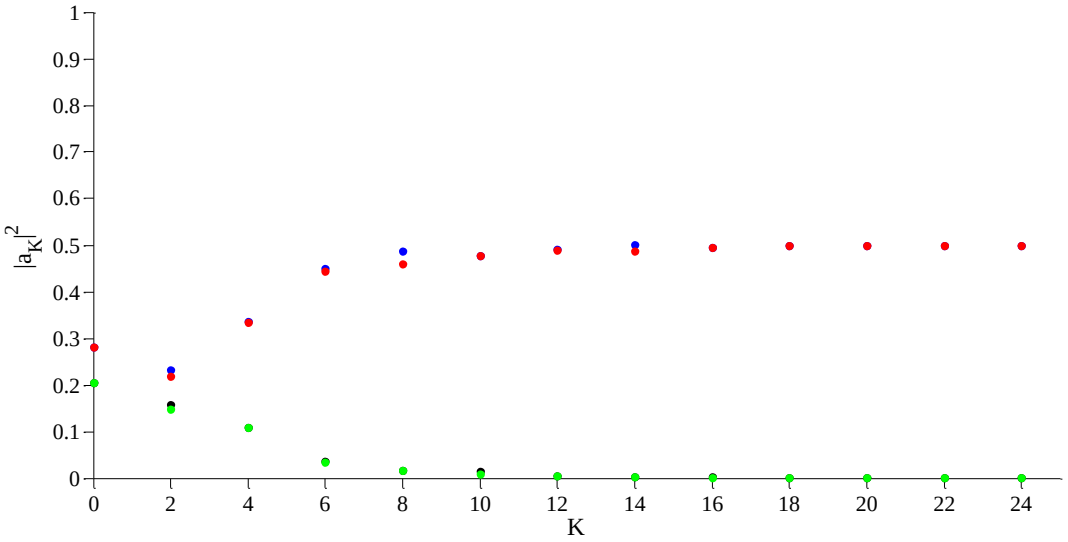

Figure 5.1: The K_a-dependence in the participation of the symmetric rotor basis in the $\left|J_{K_a\,K_c}\;I\;F\right\rangle = \left|24_{K,24-K}2\;24\right\rangle$ state. These states belong to the E^+ representation of the Wang basis set. Each K value in horizontal axis shows the corresponding asymmetric rotor state. For each state, the highest four $|a_K|^2$ values are shown in different color filled circles. Blue, red, black and green color circles belong to first, second, third and fourth highest value of $|a_K|^2$in each state, respectively.

Such a large share of more than one basis in a certain eigenstate leads to a new modification in the labeling strategy. As an example, two eigenfunctions of F=23 state are expanded as below. One is

$$\left|J_{K_a\,K_c}\;I\;F\right\rangle = (-0.75i)\left|24_0\;\;2\;23,+\right\rangle^P + (0.64i)|24_2\;\;2\;23,+\rangle^P + (-0.16i)|24_4\;\;2\;23,+\rangle^P + \cdots\;\;, \tag{5-19}$$

and the other is

$$\left|J_{K_a\,K_c}\;I\;F\right\rangle = (-0.62i)\left|24_0\;\;2\;23,+\right\rangle^P + (-0.60i)|24_2\;\;2\;23,+\rangle^P + (0.48i)|24_4\;\;2\;23,+\rangle^P + \cdots\;\;. \tag{5-20}$$

In both expansions of 5-19 and 5-20, $|24_{0\;24}\;2\;23\rangle^P$ has the largest absolute value of the coefficient. This situation leads to the double labeling problem of $|24_{0\;24}\;2\;23\rangle^P$ for the corresponding eigenfunctions and leads to no labeling of $|24_{2\;22}\;2\;23\rangle^P$for any of the eigen functions. Under such a circumstance, it is necessary to consider the second or lower rank $|a_K|^2$ coefficients. As the absolute value of the coefficient of $|24_{0\;24}\;2\;23\rangle^P$ in (5-19) is larger than that of (5-20), the former should be labeled as $|24_{0\;24}\;2\;23\rangle^P$. By considering the second largest coefficient, expansion (5-20) should be called as $|24_{2\;22}\;2\;23\rangle^P$ for avoiding the labeling duplication.

Step 3: Labeling according to the order of term values

Using equation 2-1, the magnitude of Ray's parameter *k* for disulfur dichloride is -0.92. This fact means that the molecule is near the prolate symmetric top. Generally speaking of such a near prolate symmetric top molecule, the order of term energy is corresponding to the value of $\tau = K_a - K_c$. After considering the wave function as described in the two above sections, the final step in the labeling procedure is checking whether the order of the states with the same *J*, *I*, *F* and the symmetry is correctly sorted by τ.

5-3 Results and Discussion

In this section, the *ortho-para* interaction would be studied using the term energies and molecular wave functions of S_2Cl_2. In section 5-3-1, details in the *ortho-para* mixing coefficients for the molecular wave function of S_2Cl_2 will be described. Using the result of the calculations, a list of the *ortho-para* interacting states is presented. The spectrum pattern of *ortho-para* transition is simulated for nominating the candidate transitions to survey. In section 5-3-2, the method for finding the *ortho-para* mixing states proposed in section 5-1 will be investigated by using some examples. In section 5-3-3, the *ortho-para* interactions and dependence of the *ortho-para* mixing coefficients on the *F*, *J* and K_a quantum numbers will be investigated using the perturbation theorem. In section 5-3-4, a kind of criterion is proposed to find a large *ortho-para* mixing state. And these discussions are summarized in section 5-3-5.

5-3-1 Calculating the *Ortho-Para* Mixing Coefficient

All the term energies and wave functions of $S_2{}^{35}Cl_2$ are calculated for the quantum numbers up to *F*=30 by using the rotational molecular constants listed in column step 3 of Table 4.8 and the hyperfine constants obtained from FTMW spectroscopy of S_2Cl_2 [32]. For all the eigenfunctions of the molecular states with quantum numbers up to *J* = 33 and K_a = 12 and *F* = 30, the *ortho-para* mixing ratio is diagnosed. Totally number of the levels are 7690. The program code for searching the *ortho-para* interacting states is attached in Appendix A-3.

The *ortho-para* mixing coefficient is found by projecting the molecular wave functions on the eigenfunctions of the H_0 Hamiltonian with help of equation 5-13. The mixing characters are also investigated by equation 5-16. The direct *ortho-para* interacting states have been obtained as explained in section 5-1.

The results of these two treatments are the same as it is expected by equation 5-15.

The term energies and the wave functions depend on the Hamiltonian represented by the rotational molecular constants and the nuclear quadrupole constants. So the uncertainty of these constants makes an effect on the uncertainty of term energies and wave function. Although finding an analytical dependence of the term energy and wave function on the molecular parameters is difficult, a propagation of uncertainties of these parameters is possible by numerical treatment. If $y\ (x_1, x_2, \dots, x_n)$shows a function of variables$\{x_1, x_2, \dots, x_n\}$, according to the theory of propagation of uncertainty the uncertainty of *y* could be obtained by equation 5-21[62].

$$\sigma_y = \sum_{i=1}^{n} \left(\frac{dy}{dx_i}\right)^2 {\sigma_{x_i}}^2 + \sum_{i=1}^{n} \sum_{j \neq i}^{n} \left(\frac{dy}{dx_i}\frac{dy}{dx_j}\right) cov(x_i, x_j) \qquad (5\text{-}21)$$

In equation 5-21, σ_y indicate the uncertainty of y, σ_{x_i} indicates the uncertainty of variable x_i and $cov(x_i, x_j)$ indicates the covariance between x_i and x_j. In our problem, x_i denotes the rotational and the nuclear quadrupole constants. The variance and covariance of these constants could be obtained in the least square fitting procedures as explained in chapter 4. Parameter y in equation 5-21 is the term energies of the molecular states. Evaluation of the expression $\frac{dy}{dx_i}$ in equation 5-21 for term energies is possible numerically as follows:

$$\frac{dy}{dx_i} = \frac{y\left(x_1,x_2,\ldots,x_i+\sigma_{x_i},\ldots,x_n\right)-y\left(x_1,x_2,\ldots,x_i-\sigma_{x_i},\ldots,x_n\right)}{2\sigma_{x_i}} \qquad (5\text{-}22)$$

The same as term energies, the uncertainty of coefficients of wave functions could be evaluated by equations 5-21 and 5-22[63]. By using these procedures, the errors are estimated in Table 5.2.

Table 5.1 shows a list of the *ortho-para* mixed pairs, from which transitions occur in the centimeter wave region. The largest mixing coefficient in Table 5.1 is 0.004. This is the first time that such a large value for intensity borrowing coefficient is reported. The value of the *ortho-para* intensity borrowing coefficient is also obtained by equation 5-1. As it is shown in the columns of Table 5.1, these values are equivalent to the mixing coefficients.

For debugging the programming codes in sections A-1 and A-3 in the appendix, the *ortho-para* mixing coefficients are also calculated without the contribution of the off diagonal hyperfine constants in the Hamiltonian. As it is predicted, in the absence of the off-diagonal hyperfine constants, the *ortho-para* mixing coefficients are zero. The *ortho-para* mixing coefficients are also calculated when the only χ_{ac} has the contribution on the Hamiltonian. As it is expected from equations 2-25, 2-26 and 2-27 the *ortho-para* interaction in this condition is also zero. Dependence of the mixing coefficients on the F, J and K_a quantum numbers will be discussed in section 5-3-3

Table 5.1: List of the *ortho-para* mixed states with large mixing coefficients, from which transitions occur in the centimeter wave region.

***ortho-para* levels**	**mixed**	**$\lvert E_O\text{-}E_P\rvert$ (MHz)**	**ρ_{mixing}[a]**	**ρ_{mixing}[b]**	**ρ_{mixing}[c]**	$\lvert\langle\Psi^O\rvert H_{OP}\rvert\Psi^P\rangle\rvert_{pure}$ (MHz)	$\lvert E_O - E_P\rvert_{pure}$ (MHz)	$\left\lvert\frac{\langle\Psi^O\rvert H_{OP}\rvert\Psi^P\rangle}{E_O - E_P}\right\rvert^2_{pure}$
$4_{3\,2}\,3\,6$ –	$4_{3\,1}\,2\,6$	0.1242	0.000	0.000	0.005	0.008	0.1151	0.004
$2_{2\,1}\,3\,4$ –	$2_{2\,0}\,2\,4$	2.9058	0.000	0.000	0.002	0.130	2.8868	0.002
$1_{1\,1}\,2\,3$ –	$1_{1\,0}\,3\,3$	168.4913	0.000	0.000	0.001	6.053	168.2979	0.001
$2_{2\,0}\,2\,3$ –	$2_{2\,1}\,3\,3$	2.3331	0.000	0.000	0.002	0.091	2.3140	0.002
$1_{1\,0}\,1\,2$ –	$1_{1\,1}\,2\,2$	166.2532	0.000	0.000	0.003	8.466	165.0841	0.003
$1_{1\,1}\,2\,2$ –	$1_{1\,0}\,3\,2$	153.1843	0.000	0.000	0.002	6.888	152.5067	0.002
$2_{2\,0}\,0\,2$ –	$2_{2\,1}\,1\,2$	4.5673	0.000	0.000	0.001	0.106	4.5618	0.001
$2_{2\,1}\,3\,2$ –	$2_{2\,0}\,0\,2$	2.2617	0.000	0.000	0.001	0.056	2.2599	0.001
$1_{1\,0}\,1\,1$ –	$1_{1\,1}\,2\,1$	162.1601	0.000	0.000	0.002	6.422	151.4463	0.002
$1_{1\,1}\,0\,1$ –	$1_{1\,0}\,1\,1$	152.2185	0.000	0.000	0.002	6.421	161.3897	0.002
$2_{2\,1}\,1\,1$ –	$2_{2\,0}\,2\,1$	2.9901	0.000	0.000	0.002	0.117	2.9604	0.002

[a] Mixing coefficients values when $\chi_{ab}, \chi_{bc}, \chi_{ac} = 0$.
[b] Mixing coefficients values when χ_{ab} and $\chi_{bc} = 0$.
[c] Mixing coefficients values when $\chi_{ab}, \chi_{bc}, \chi_{ac} \neq 0$.

As the largest value of the *ortho-para* mixing coefficients in the centimeter wave region is 0.004, it is difficult to observe such a low intensity transition using our experimental facilities. Table 5.2 shows a list of *ortho-para* mixed states with $\Delta E_{OP} \geq 0.1$ MHz and the *ortho-para* mixing coefficient larger than 0.001. These *ortho-para* mixed states would lead to the *ortho-para* transition in the millimeter wave region. All the *ortho-para* mixing states in Table 5.2 are degenerate K_a-doubling states. In Table 1.C in Appendix C, there is a list of the *ortho-para* mixed states with the quantum numbers up to $J = 28$, $K_a = 12$ and $F = 25$. As seen in the table, there are the *ortho-para* mixed states, with the *ortho-para* mixing coefficients as large as 0.4 in the mm-wave region.

Table 5.2: List of the *ortho-para* mixed states with the largest value for the *ortho-para* mixing coefficient, from which transitions occurs in the millimeter wave region.

***Para* state**	**Term energy (MHz)**	***Ortho* state**	**Term energy (MHz)**	**$\lvert E_O - E_P \rvert$ (MHz)**	**ρ_{mixing}**
$26_{9\,17}$ 2 24	1265039.040(2.914)[a]	$26_{9\,18}$ 3 24	1265038.475(2.914)	0.565	0.198(4)[b]
$23_{8\,16}$ 2 25	996052.689(1.477)	$23_{8\,15}$ 3 25	996053.287(1.477)	0.598	0.195(4)
$23_{8\,16}$ 2 21	996052.672(1.477)	$23_{8\,15}$ 3 21	996053.476(1.477)	0.804	0.115(3)
$27_{8\,20}$ 2 25	1264766.835(2.791)	$27_{8\,19}$ 3 25	1264767.590(2.791)	0.755	0.108(3)
$20_{7\,13}$ 2 18	759166.853(0.704)	$20_{7\,14}$ 3 18	759167.157(0.704)	0.304	0.092(2)
$24_{7\,17}$ 2 22	996302.213(1.425)	$24_{7\,18}$ 3 22	996301.179(1.425)	1.034	0.059(1)
$17_{6\,12}$ 2 19	554383.477(0.319)	$17_{6\,11}$ 3 19	554383.736(0.319)	0.259	0.039(1)
$20_{6\,14}$ 2 20	704569.595(0.575)	$20_{6\,15}$ 1 20	704569.351(0.575)	0.244	0.0260(7)
$13_{5\,9\,2}$ 15	344839.389(0.116)	$13_{5\,8\,3}$ 15	344839.842(0.116)	0.453	0.0137(3)
$16_{6\,10}$ 2 18	509616.754(0.260)	$16_{6\,11}$ 3 18	509616.410(0.260)	0.344	0.0106(3)
$17_{6\,12}$ 2 15	554383.473(0.319)	$17_{6\,11}$ 3 15	554384.017(0.319)	0.543	0.0105(3)
$23_{7\,17}$ 2 25	933043.171(1.205)	$23_{7\,16}$ 3 25	933043.471(1.205)	0.300	0.0103(3)
$21_{7\,15}$ 2 19	814478.103(0.846)	$21_{7\,14}$ 3 19	814478.376(0.846)	0.273	0.0091(2)
$13_{5\,9\,2}$ 11	344839.419(0.116)	$13_{5\,8\,3}$ 11	344840.183(0.116)	0.764	0.0075(2)
$13_{5\,9}$ 2 13	344840.087(0.116)	$13_{5\,8\,3}$ 13	344839.331(0.116)	0.756	0.0074(2)
$22_{7\,15}$ 2 24	872436.418(1.013)	$22_{7\,16}$ 3 24	872436.155(1.013)	0.263	0.0059(1)
$18_{6\,12}$ 2 16	601797.018(0.390)	$18_{6\,13}$ 3 16	601796.657(0.390)	0.361	0.0049(1)
$10_{4\,6}$ 0 10	212174.351(0.055)	$10_{4\,7\,1}$ 10	212172.071(0.055)	2.280	0.0040(1)
$23_{7\,17}$ 2 21	933043.171(1.205)	$23_{7\,16}$ 3 21	933043.691(1.205)	0.520	0.0038(1)
$10_{4\,6\,2}$ 8	212175.514(0.055)	$10_{4\,7}$ 3 8	212171.514(0.055)	3.999	0.0034(1)
$13_{5\,9}$ 2 12	344839.251(0.116)	$13_{5\,8\,1}$ 12	344839.488(0.116)	0.237	0.00249(4)
$17_{6\,12}$ 0 17	554384.364(0.319)	$17_{6\,11}$ 3 17	554383.006(0.319)	1.357	0.00158(4)
$14_{5\,9}$ 2 12	381707.813(0.144)	$14_{5\,10}$ 3 12	381706.575(0.144)	1.238	0.00128(3)
$26_{7\,19}$ 2 25	1130779.266(1.961)	$26_{7\,20}$ 1 25	1130777.288(1.961)	1.979	0.0013(4)
$19_{6\,14}$ 0 19	651858.242(0.475)	$19_{6\,13}$ 3 19	651857.601(0.475)	0.641	0.00110(3)
$18_{6\,12}$ 2 20	601797.017(0.390)	$18_{6\,13}$ 3 20	601796.381(0.390)	0.637	0.00108(3)

[a] Numbers in parenthesis denotes uncertainty in the unit of MHz.
[b] Numbers in parenthesis denotes uncertainty in the unit of the last significant digit.

Having a large value for the intensity borrowing coefficients is not the only condition for the experimental observation of the *ortho-para* transitions. It should also be considered that whether the *ortho-para* transitions are overlapped with normal transitions or not. So simulation of the hyperfine spectrum pattern including all allowed and forbidden transitions is inevitable. Figures 5.2 and 5.3 show some examples of the calculated spectrum pattern. There is a list of hyperfine transitions for each frequency region in Tables 5.3 and 5.4. The *ortho-para* transitions are highlighted by red color in these tables.

$|24_{7\,18}\ 3\ 22\rangle^{O}$- $|24_{7\,17}\ 2\ 22\rangle^{P}$ *ortho-para* mixing states with the mixing coefficient $\rho_{mixing} = 0.059$, $|24_{7\,18}\ 3\ 24\rangle^{O}$- $|24_{7\,17}\ 2\ 24\rangle^{P}$ *ortho-para* mixing states with the mixing coefficient $\rho_{mixing} = 0.008$ and $|24_{7\,18}\ 1\ 24\rangle^{O}$- $|24_{7\,17}\ 0\ 24\rangle^{P}$ *ortho-para* mixing states with the mixing coefficient $\rho_{mixing} = 0.041$ lead to none zero transition moment for $|24_{7\,18}\ 3\ 22\rangle^{O}$- $|23_{6\,18}\ 2\ 21\rangle^{P}$, $|24_{7\,18}\ 3\ 24\rangle^{O}$- $|23_{6\,18}\ 2\ 25\rangle^{P}$ and $|24_{7\,18}\ 1\ 24\rangle^{O}$- $|23_{6\,18}\ 0\ 23\rangle^{P}$ *ortho-para* transition respectively, as seen in Table 5.3.

Table5.3: List of the *ortho-para* transitions from 117671.5 MHz to 117676.5 MHz frequency region and their intensities.

Transition	Frequency (MHz)	Intensity (a.u)	Transition	Frequency (MH)	Intensity (a.u)
$24_{7\,18}\ 3\ 24$ - $23_{6\,18}\ 2\ 23$	117672.0827	0.07[a]	$24_{7\,17}\ 2\ 24$ - $23_{6\,18}\ 2\ 23$	117674.5568	8.55
$24_{7\,17}\ 0\ 24$ - $23_{6\,18}\ 2\ 23$	117672.7237	0.15	$24_{7\,17}\ 2\ 26$ - $23_{6\,18}\ 2\ 25$	117674.6257	9.15
$24_{7\,18}\ 3\ 26$ - $23_{6\,18}\ 2\ 25$	117673.4379	0.37	$24_{7\,17}\ 2\ 22$ - $23_{6\,18}\ 2\ 22$	117674.6653	0.03
$24_{7\,17}\ 0\ 24$ - $23_{6\,18}\ 2\ 24$	117673.5351	0.02	$24_{7\,17}\ 2\ 22$ - $23_{6\,18}\ 2\ 21$	117674.6750	7.57
$24_{7\,18}\ 3\ 22$ - $23_{6\,18}\ 2\ 21$	117673.6411	0.49[b]	$24_{7\,17}\ 2\ 23$ - $23_{6\,18}\ 2\ 22$	117674.7247	8.38
$24_{7\,17}\ 2\ 23$ - $23_{6\,18}\ 2\ 23$	117673.9480	0.02	$24_{7\,17}\ 2\ 24$ - $23_{6\,18}\ 2\ 24$	117675.3683	0.03
$24_{7\,18}\ 1\ 24$ - $23_{6\,18}\ 2\ 23$	117673.9532	0.01	$24_{7\,17}\ 2\ 23$ - $23_{6\,18}\ 0\ 23$	117675.5342	0.02
$24_{7\,17}\ 2\ 25$ - $23_{6\,18}\ 2\ 25$	117674.0983	0.03	$24_{7\,18}\ 1\ 24$ - $23_{6\,18}\ 0\ 23$	117675.5394	0.35[c]
$24_{7\,17}\ 2\ 25$ - $23_{6\,18}\ 2\ 24$	117674.1152	9.14	$24_{7\,17}\ 2\ 24$ - $23_{6\,18}\ 0\ 23$	117676.1430	0.15
$24_{7\,17}\ 0\ 24$ - $23_{6\,18}\ 0\ 23$	117674.3099	8.28			

[a] $|24_{7\,18}\ 3\ 24\rangle^{O}$- $|24_{7\,17}\ 2\ 24\rangle^{P}$ *ortho-para* mixing states by mixing coefficient $\rho_{mixing} = 0.008$ leads to this transition.

[b] $|24_{7\,18}\ 3\ 22\rangle^{O}$- $|24_{7\,17}\ 2\ 22\rangle^{P}$ *ortho-para* mixing states by mixing coefficient $\rho_{mixing} = 0.059$ leads to this transition.

[c] $|24_{7\,18}\ 1\ 24\rangle^{O}$- $|24_{7\,17}\ 0\ 24\rangle^{P}$ *ortho-para* mixing states by mixing coefficient $\rho_{mixing} = 0.041$ leads to this transition.

Using the transitions in Table5.3, Figure 5.2.a is drawn. By assuming that each transition has a Gaussian shape with FWHM of 100 kHz, Figure 5.2.b is obtained. By summing up these

peaks, Figure 5.2.c is obtained. From this simulation spectrum, it is demanded to have the signal to noise ratios more than 46 in the experimental observation of the *ortho-para* transitions.

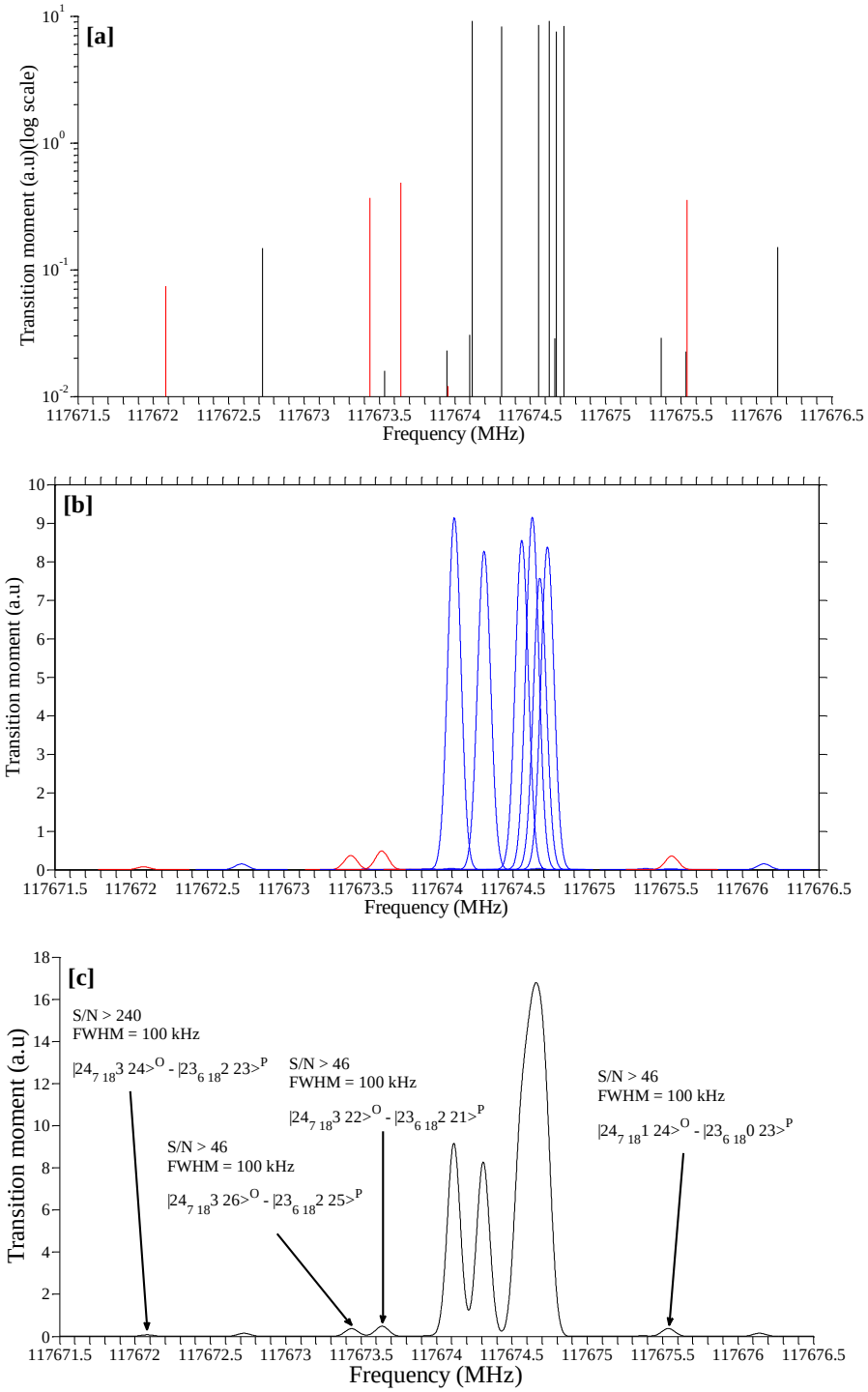

Figure 5.2: (a) Blue and red lines correspond to the normal and *ortho-para* transitions respectively, which are listed in Table 5.3. (b) Each line shape is assumed a Gaussian function with the FWHM of 100 kHz. (c) Summation of all peaks in Figure 5.2.b.

$|24_{7\ 18}\ 3\ 22\rangle^{O}$- $|24_{7\ 17}\ 2\ 22\rangle^{P}$ *ortho-para* mixing states with the mixing coefficient $\rho_{mixing} = 0.059$ and $|24_{7\ 18}\ 1\ 24\rangle^{O}$- $|24_{7\ 17}\ 0\ 24\rangle^{P}$ *ortho-para* mixing states with the mixing coefficient $\rho_{mixing} = 0.041$ lead to none zero transition moment for $|24_{7\ 18}\ 3\ 22\rangle^{O}$- $|24_{6\ 18}\ 2\ 22\rangle^{P}$ and $|24_{7\ 18}\ 1\ 24\rangle^{O}$- $|24_{6\ 18}\ 0\ 24\rangle^{P}$ *ortho-para* transition respectively, in Table 5.4.

Table5.4: List of the hyperfine transitions and their transition moments in 54318.5 MHz to 54323 MHz frequency region.

Transition			Frequency (MHz)	Intensity (a.u)	Transition			Frequency (MHz)	Intensity (a.u)
$24_{7\ 18}\ 3\ 24$	-	$24_{6\ 18}\ 2\ 24$	54318.8388	0.10	$24_{7\ 17}\ 2\ 24$	-	$24_{6\ 18}\ 2\ 24$	54321.31295	11.92
$24_{7\ 17}\ 0\ 24$	-	$24_{6\ 18}\ 2\ 24$	54319.4798	0.22	$24_{7\ 17}\ 2\ 26$	-	$24_{6\ 18}\ 2\ 26$	54321.32797	12.76
$24_{7\ 17}\ 2\ 25$	-	$24_{6\ 18}\ 2\ 24$	54320.0599	0.03	$24_{7\ 17}\ 2\ 26$	-	$24_{6\ 18}\ 2\ 25$	54321.34063	0.04
$24_{7\ 18}\ 3\ 26$	-	$24_{6\ 18}\ 2\ 26$	54320.1402	0.51	$24_{7\ 17}\ 2\ 22$	-	$24_{6\ 18}\ 2\ 23$	54321.37296	0.04
$24_{7\ 17}\ 0\ 24$	-	$24_{6\ 18}\ 2\ 23$	54320.2081	0.02	$24_{7\ 17}\ 2\ 22$	-	$24_{6\ 18}\ 2\ 22$	54321.3801	10.58
$24_{7\ 17}\ 0\ 24$	-	$24_{6\ 18}\ 2\ 25$	54320.2332	0.02	$24_{7\ 17}\ 2\ 23$	-	$24_{6\ 18}\ 2\ 23$	54321.43241	11.68
$24_{7\ 18}\ 3\ 22$	-	$24_{6\ 18}\ 2\ 22$	54320.3462[a]	0.67	$24_{7\ 17}\ 2\ 23$	-	$24_{6\ 18}\ 2\ 22$	54321.43955	0.04
$24_{7\ 17}\ 2\ 23$	-	$24_{6\ 18}\ 2\ 24$	54320.7041	0.03	$24_{7\ 17}\ 2\ 25$	-	$24_{6\ 18}\ 0\ 24$	54321.53958	0.03
$24_{7\ 18}\ 1\ 24$	-	$24_{6\ 18}\ 2\ 24$	54320.7093	0.02	$24_{7\ 17}\ 2\ 24$	-	$24_{6\ 18}\ 2\ 23$	54322.04124	0.04
$24_{7\ 18}\ 1\ 23$	-	$24_{6\ 18}\ 2\ 23$	54320.7709	0.01	$24_{7\ 17}\ 2\ 24$	-	$24_{6\ 18}\ 2\ 25$	54322.06634	0.04
$24_{7\ 17}\ 2\ 25$	-	$24_{6\ 18}\ 2\ 26$	54320.8006	0.04	$24_{7\ 17}\ 2\ 23$	-	$24_{6\ 18}\ 0\ 24$	54322.18382	0.03
$24_{7\ 17}\ 2\ 25$	-	$24_{6\ 18}\ 2\ 25$	54320.8133	12.72	$24_{7\ 18}\ 1\ 24$	-	$24_{6\ 18}\ 0\ 24$	54322.18901[b]	0.50
$24_{7\ 17}\ 0\ 24$	-	$24_{6\ 18}\ 0\ 24$	54320.9595	11.54	$24_{7\ 17}\ 2\ 24$	-	$24_{6\ 18}\ 0\ 24$	54322.79266	0.21

[a] $|24_{7\ 18}\ 3\ 22\rangle^{O}$- $|24_{7\ 17}\ 2\ 22\rangle^{P}$ *ortho-para* mixing states with the mixing coefficient $\rho_{mixing} = 0.059$ leads to this transition.
[b] $|24_{7\ 18}\ 1\ 24\rangle^{O}$- $|24_{7\ 17}\ 0\ 24\rangle^{P}$ *ortho-para* mixing states with the mixing coefficient $\rho_{mixing} = 0.041$ leads to this transition.

Using transitions in Table5.4, Figure 5.3.a is drawn. By assuming that each transition has a Gaussian shape with FWHM of 100 kHz, Figure 5.3.b is obtained. By summation of these peaks, Figure 5.3.c is obtained. From this simulation spectrum, it is demanded to have the signal to noise ratios more than 60 in the experimental observation of the *ortho-para* transitions.
There are more examples of spectrum patterns for the candidate region for experimental observation of the *ortho-para* transitions in Appendix C.

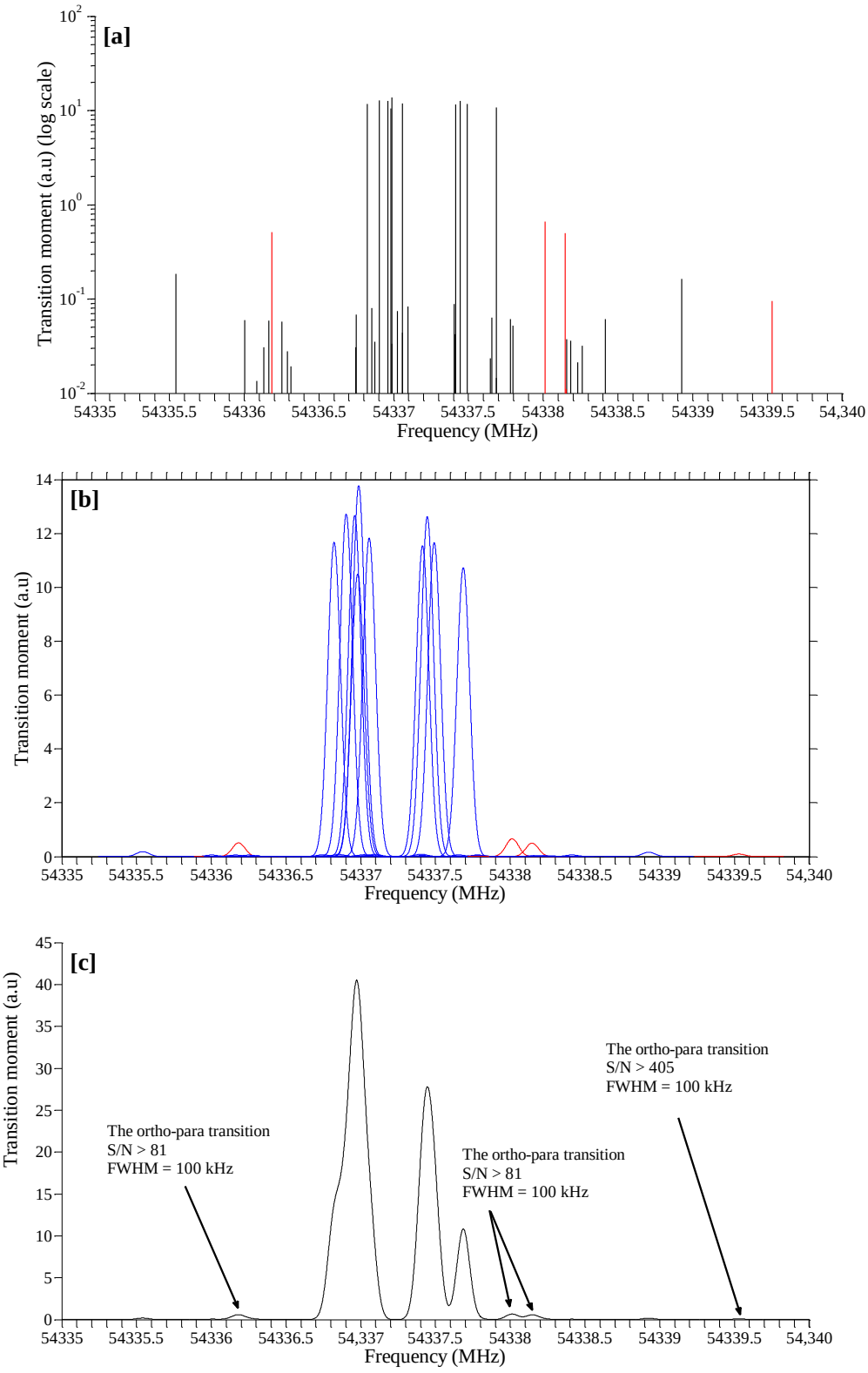

Figure 5.3: (a) Blue and red lines correspond to the normal and *ortho-para* transitions respectively, which are listed in Table 5.4. (b) Each line shape is assumed as a Gaussian function with the FWHM of 100 kHz. (c) Summation of all peaks in Figure 5.3.b.

5-3-2 Investigation of the Proposed Methods for Finding the *Ortho-Para* Mixing Interacting States by Examples.

In this section with some examples, the weakness of the representation of molecular wave function in the common symmetrized symmetric rotor basis set to find the *ortho-para* interacting states is shown. The solution to this weakness will also be explained for those examples.

Indicating the weakness of the common treatment for finding the *ortho-para* transition and its solution by example

Expansions 5-23, 5-25 and 5-26 correspond to the eigenfunctions which are obtained from diagonalization of the Hamiltonian described by equation 5-2. These wave functions are shown in symmetrized symmetric rotor basis set in Wang representation.

$$|9_{6\,3}\ 1\ 9\rangle^{\sim O} = (0.73)|9_6\ \ 1\ 9,+\rangle^O + (0.25)|9_6\ \ 3\ 9,+\rangle^O + (-0.44i)|9_6\ \ 0\ 9,-\rangle^P + (-0.44i)|9_6\ \ 2\ 9,-\rangle^P \quad (5\text{-}23)$$

By the common treatment for finding intensity borrowing coefficients, $|9_{6\,3}\ 1\ 9\rangle^O$ is mixed with $|9_{6\,4}\ 0\ 9\rangle^P$. This mixing leads to an *ortho-para* transition by an intensity that is borrowed from a normal transition by a coefficient equal to $(-0.44i)^2$. $|9_{6\,3}\ 1\ 9\rangle^O$ is also mixed with $|9_{6\,4}\ 2\ 9\rangle^P$. This mixing also leads to an *ortho-para* transition by an intensity that is borrowed from a normal transition by a coefficient equal to $(-0.44i)^2$.
As an example, by considering $\Delta I = 0$ selection rule for the nuclear spin quantum number, the intensity of desired *ortho-para* transition is borrowed from the intensity of the $|10_{7\,3}0\ 10\rangle^P$ - $|9_{6\,3}0\ 9\rangle^P$ normal transition as below:

$$I_{OP} = |\,{}^P\langle 10_{7\,3}0\ 10|\mu|9_{6\,3}1\ 9\rangle^{\sim O}\,|^2 = |\,(-0.44i)\,|^2\,|\,{}^P\langle 10_{7\,3}0\ 10|\mu|9_{6\,4}0\ 9\rangle^P\,|^2 \quad (5\text{-}24)$$

Now intensity borrowing coefficient will be calculated by the new introduced approach for intensity borrowing coefficients for a wave function which is represented in symmetrized symmetric rotor basis set. By this approach, the mixing characters for interacting candidate wave functions should be calculated.
Using expansion 5-23 and equation 5-16, the *ortho* and the *para* character for $|9_{6\,3}\ 1\ 9\rangle^O$ are $\rho_O = 0.6$ and $\rho_P = 0.4$, respectively.
Expansions 5-25 is for $|9_{6\,4}\ 0\ 9\rangle^P$ wave function, in symmetrized symmetric rotor basis set in Wang representation.

$$|9_{6\,4}\ 0\ 9\rangle^{\sim P} = (0.00)|9_6\ \ 1\ 9,+\rangle^O + (-0.00)|9_6\ \ 3\ 9,+\rangle^O + (0.71i)|9_6\ \ 0\ 9,-\rangle^P + (0.70i)|9_6\ \ 2\ 9,-\rangle^P \quad (5\text{-}25)$$

For this wave function, the *ortho* and the *para* characters are $\rho_O = 0.0$ and $\rho_P = 1$, respectively.
Expansion 5-26 is for $|9_{6\,4}\ 2\ 9\rangle^P$ wave function, in the symmetrized symmetric rotor basis set in Wang representation.

$$|9_{6\,4}\ 2\ 9\rangle^{\sim P} = (0.59)|9_6\ \ 1\ 9,+\rangle^O + (0.20)|9_6\ \ 3\ 9,+\rangle^O + (0.54i)|9_6\ \ 0\ 9,-\rangle^P + (0.55i)|9_6\ \ 2\ 9,-\rangle^P \quad (5\text{-}26)$$

For this wave function, the *ortho* and the *para* characters are $\rho_O = 0.4$ and $\rho_P = 0.6$, respectively. According to the newly introduced approach for finding the *ortho-para* mixed states in the symmetrized symmetric rotor basis set $|9_{6\,4}\ 2\ 9\rangle^P$ and $|9_{6\,3}\ 1\ 9\rangle^O$ are the only two *ortho-para* interacting states and unlike the common approach, there is no interaction between $|9_{6\,4}\ 0\ 9\rangle^P$ and $|9_{6\,3}\ 1\ 9\rangle^O$ states.

In order to calculate the intensity borrowing coefficients, we use the concept of the projection of wave function onto the basis functions, which are the eigenfunctions of H_0. Definition of H_0 and its Eigen functions have been provided in the equations 5-3 and 5-8. As it is shown by equation 5-10, the total molecular wave function could be expanded by H_0 eigenfunctions. The representation of $|9_{6\,4}\ 2\ 9\rangle^P$, $|9_{6\,3}\ 1\ 9\rangle^O$ and $|9_{6\,4}\ 2\ 9\rangle^P$ in H_0 eigenfunctions are shown in 5-27, 5-28 and 5-29, respectively. The coefficients are calculated by equation 5-11. The eigenfunctions of H_0 are suffixed by "*d*" in these expansions.

$$|9_{6\,3}\ 1\ 9\rangle^O = (-0.77)|9_{6\,3}\ 1\ 9\rangle_d^O + (0.0)\big|9_{6\,3}\ 3\ 9\rangle_d^O + (0.0)\big|9_{6\,4}\ 0\ 9\rangle_d^P + (-0.63i)|9_{6\,4}\ 2\ 9\rangle_d^P \quad (5\text{-}27)$$

$$|9_{6\,4}\ 0\ 9\rangle^P = (0.00)|9_{6\,3}\ 1\ 9\rangle_d^O + (0.00)\big|9_{6\,3}\ 3\ 9\rangle_d^O + (-0.99i)\big|9_{6\,4}\ 0\ 9\rangle_d^P + (0.00)|9_{6\,4}\ 2\ 9\rangle_d^P \quad (5\text{-}28)$$

$$|9_{6\,4}\ 2\ 9\rangle^P = (-0.63)|9_{6\,3}\ 1\ 9\rangle_d^O + (0.0)\big|9_{6\,3}\ 3\ 9\rangle_d^O + (0.0)\big|9_{6\,4}\ 0\ 9\rangle_d^P + (0.77i)|9_{6\,4}\ 2\ 9\rangle_d^P \quad (5\text{-}29)$$

Meanwhile, the eigenfunctions of H_0 in above expansions are further expanded in Wang basis set, as follows:

$$\big|9_{6\,3}\ 1\ 9\big\rangle_d^O = (-0.94)\big|9_6\ \ 1\ 9,+\big\rangle^O + (-0.32)\big|9_6\ \ 3\ 9,+\big\rangle^O + (0.0.0)\big|9_6\ \ 0\ 9,-\big\rangle^P + (0.00)|9_6\ \ 2\ 9,-\rangle^P \quad (5\text{-}30)$$

$$\big|9_{6\,3}\ 3\ 9\big\rangle_d^O = (-0.32)\big|9_6\ \ 1\ 9,+\big\rangle^O + (-0.94)\big|9_6\ \ 3\ 9,+\big\rangle^O + (0.00)\big|9_6\ \ 0\ 9,-\big\rangle^P + (0.00)|9_6\ \ 2\ 9,-\rangle^P \quad (5\text{-}31)$$

$$\big|9_{6\,4}\ 0\ 9\big\rangle_d^P = (0.00)\big|9_6\ \ 1\ 9,+\big\rangle^O + (0.00)\big|9_6\ \ 3\ 9,+\big\rangle^O + (-0.71)\big|9_6\ \ 0\ 9,-\big\rangle^P + (0.70)|9_6\ \ 2\ 9,-\rangle^P \quad (5\text{-}32)$$

$$\big|9_{6\,4}\ 2\ 9\big\rangle_d^P = (0.00)\big|9_6\ \ 1\ 9,+\big\rangle^O + (0.00)\big|9_6\ \ 3\ 9,+\big\rangle^O + (0.70)\big|9_6\ \ 0\ 9,-\big\rangle^P + (0.71)|9_6\ \ 2\ 9,-\rangle^P \quad (5\text{-}33)$$

As the expansions of 5-27, 5-28 and 5-29 show, only $|9_{6\,4}\ 2\ 9\rangle^P$ and $|9_{6\,3}\ 1\ 9\rangle^O$ have mixed component by opposite symmetries wave functions and there is no *ortho-para* interaction between $|9_{6\,4}\ 0\ 9\rangle^P$ and $|9_{6\,3}\ 1\ 9\rangle^O$. The magnitude of the square of mixing coefficient is 0.4. This value is equal to the mixing character in symmetrized symmetric rotor basis set as expected by equation 5-8.

5-3-3 Investigation on the *Ortho-Para* Mixing Coefficient Dependence on the *F*, *J* and K_a Quantum Numbers by Perturbation Theorem

For finding a physical meaning of the values of *ortho-para* mixing coefficients which are obtained directly from the effective wave function, the dependency of the numerator and dominator of the equation 5-1 on the *J* and K_a quantum numbers was studied, separately.

First, the dependency of the numerator; $\langle \Psi^P | H_{OP} | \Psi^O \rangle$ was studied. According to the equations 2-25, 2-26 and 2-27, the off diagonal hyperfine Hamiltonian matrix elements have nonzero values for ΔK=0, 1, 2. The matrix elements with ΔK=1 multiply by χ_{ab} off diagonal constant and the matrix elements with ΔK=0, 2 multiply by χ_{bc} off diagonal constant. For finding the dependency of the numerator, $|\Psi^O>$ and $|\Psi^P>$ pair should be considered for different conditions of ΔJ and ΔK_a . According to the Tables 5.2 and C.1, the highest intensity borrowing coefficients correspond to the *K*-doubling pairs. The dependency of the numerator, when the off diagonal Hamiltonian matrix is sandwiched between the *K*-doubling states is shown in Figures 5.4.a and 5.5.a. For each *F* quantum number, there are 10 possible combinations of *J* and *I* quantum number values as Table 5.5.

Table 5.5: the possible combination of *J* and *I* quantum number for each *F* quantum number.

J	*F*±2	*F* ±1	*F*
	2	1	0
	3	2	1
		3	2
			3

The dependency of the numerator is considered for each of possible combination of *J* and *I* quantum number in Table 5.5, separately. For each *J* quantum number, the highest value of the numerator corresponds to *K*-doubling states by *K*=1. In Figure 5.4.a, the numerator for *K*-doubling states by *K*=1 are shown. As Figure 5.4.a shows the highest magnitudes of the expectation value of off diagonal hyperfine Hamiltonian is for *J* quantum numbers which are equal to *F*±2. According to Figure 5.4.a, the numerator increases by increasing *F* quantum number for *J*= *F*±2 and *J*= *F*±1. This value decreases when *J*=*F*.

As Figure 5.4.b shows by increasing *F* quantum numbers, term energy differences of the K_a-doubling states increases for all possible combination of *J* and *I* quantum numbers. As Figures 5.4.a and 5.4.b show, by increasing the *F* quantum number the numerator and dominator in equation 5-1 decreases and increases respectively for the condition *J*=*F*. So it can be concluded that when *J*=*F*, by increasing the *F* quantum number the *ortho-para* mixing coefficients decrease. Both numerator and dominator in equation 5-1, by increasing the *F* quantum number

increase for the conditions $J=F\pm1$ and $J=F\pm2$. So having the prediction about the dependency of the *ortho-para* mixing coefficients to the F quantum number is not possible.

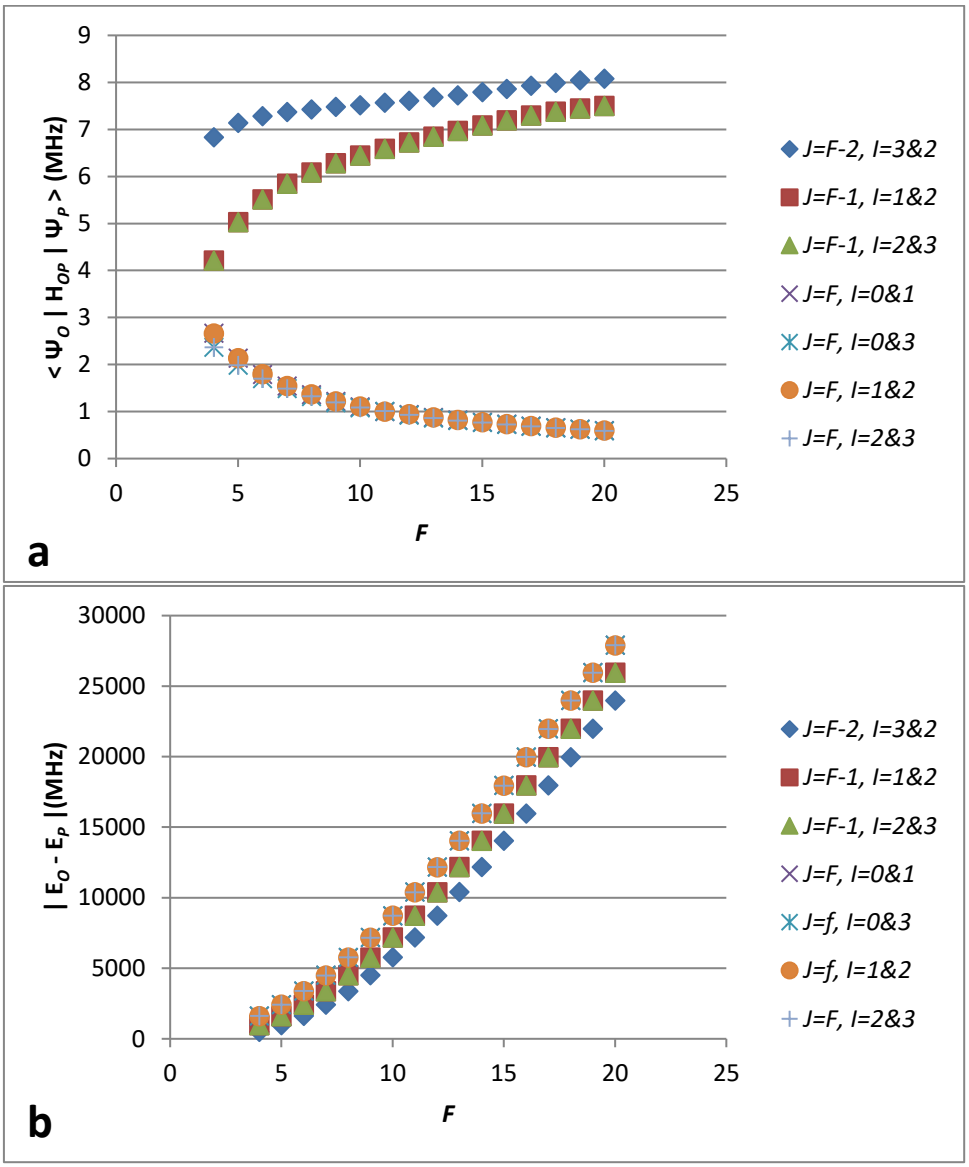

Figure 5.4: (a) $\langle\Psi^P|H_{OP}|\Psi^O\rangle$ versus F quantum number for K_a=1 (b) Term energy differences of *ortho* and *para* states versus F quantum number.

Figures 5.5.a and 5.5.b show the dependency of the $\langle\Psi^P|H_{OP}|\Psi^O\rangle$ and $|E_O - E_P|$ to the K_a quantum number, respectively. In this figure F = 9 is considered. In Figure 5.5.a, all possible combinations of J and I quantum number for F=9 are shown. As Figure 5.5.a and 5.5.b shows

by increasing K_a quantum number, both $\langle \Psi^P | H_{OP} | \Psi^O \rangle$ and $|E_O - E_P|$ decrease. So both numerator and dominator in equation 5-1, by increasing the K_a quantum number increase for all possible combination of J and I quantum numbers. So having the prediction about the dependency of the *ortho-para* mixing coefficients to the K_a quantum number is not possible.

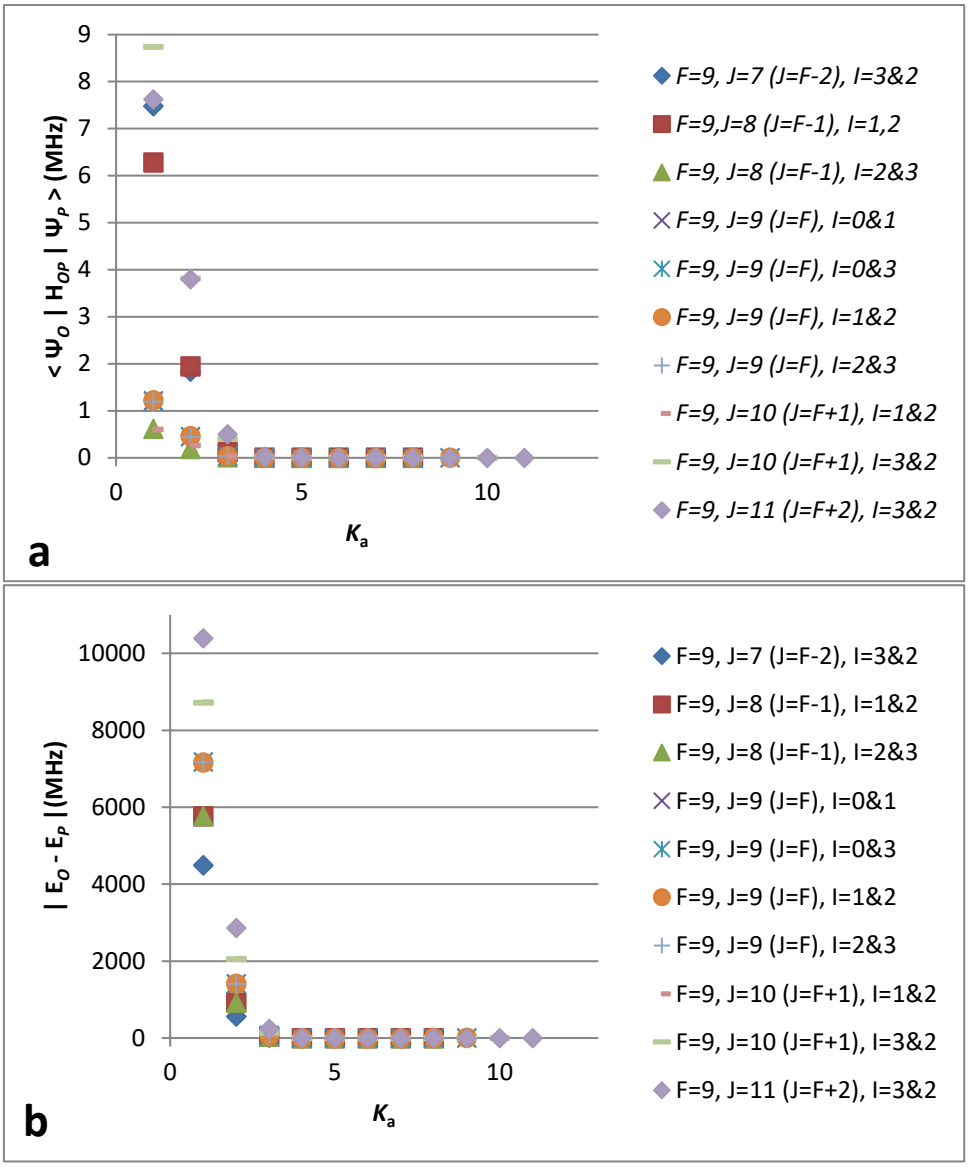

Figure 5.5: (a) $\langle \Psi^P | H_{OP} | \Psi^O \rangle$ versus K_a quantum number for different combinations of J and I quantum numbers, when $F = 9$. (b) Dependency of the term energy differences of the *ortho* and *para* states to the K_a quantum number for different combinations of J and I quantum numbers, when $F = 9$.

To find the criteria in the dependence of equation 5-1 to K_a quantum number further treatment is done as seen in Figure 5.6. Figures 5.6.a and 5.6.b are the same as Figures 5.5.a and 5.5.b, respectively. The only difference is the vertical axis in Figure 5.6 is on the logarithmic scale. Figure 5.6.c is obtained by division of Figure 5.6.a to Figure 5.6.b. As Figure 5.6.c shows, there is not any special rule about the dependence of the vertical axis values to K_a quantum number. So it is concluded that there are no criteria about the dependence of the *ortho-para* mixing coefficient to K_a quantum number.

All ten different combinations of J and I quantum numbers in Figure 5.6 are shown in Figures C.9 to C.18, separately.

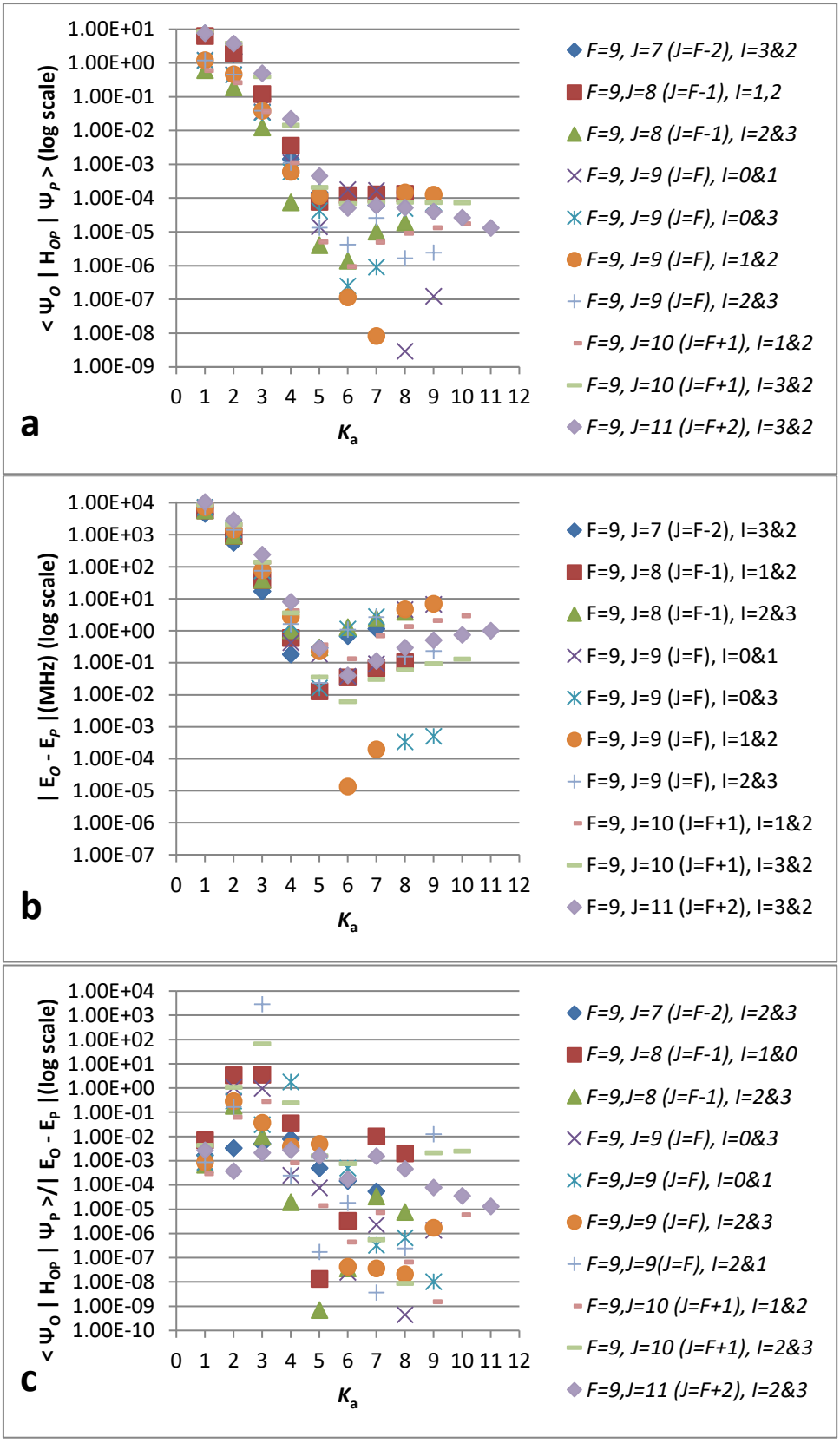

Figure 5.6: (a) $\langle\Psi^P|\mathrm{H}_{OP}|\Psi^O\rangle$ versus K_a quantum number for different combinations of J and I quantum numbers when F=9. (b) $|\mathrm{E}_O - \mathrm{E}_P|$ versus K_a quantum number. (c) $\frac{\langle\Psi^O|\mathrm{H}_{OP}|\Psi^P\rangle}{\mathrm{E}_O-\mathrm{E}_P}$ versus K_a quantum number. The vertical axes are on the logarithmic scale.

5-3-4 Investigation on the *Ortho-Para* Mixing Coefficient Dependence with the Molecular Spectroscopic Constants

As discussed in section 5-3-3, it is not possible to have any clear prospect in the dependence of the *ortho-para* mixing coefficient ρ_{mixing} with F, J and K_a quantum numbers by estimating its value with perturbation theorem. In this section, ρ_{mixing} is calculated by a simplified model of the molecular Hamiltonian matrix. As seen in Tables 5.2 and Table C.1 in the appendix, the significant *ortho-para* mixed states are limited to K-doubling states only. The Hamiltonian matrix element between the *ortho* and *para* states of K-doubling pair does not exist in equation 2-23, because ΔK is zero. It is necessary to have an intermediate state to combine them. So the simplest model for the Hamiltonian is a 3×3 matrix instead of a 2×2 matrix.

Figure 5.7 shows the schematic representation of the interactions between three levels model. These three levels are labeled s A, B and C according to their term energies. The symmetry of A, B and C levels are assumed *ortho*, *para* and *para*, respectively. A and B levels are assumed to be K-doubling states. So there is no interaction between them. The interaction between A and C is described as h_{OP}. The interaction between B and C is described as $h_{PP} = h$. The term energy difference between A and B is described as ΔE_1 and the term energy difference between A and C as ΔE_2.

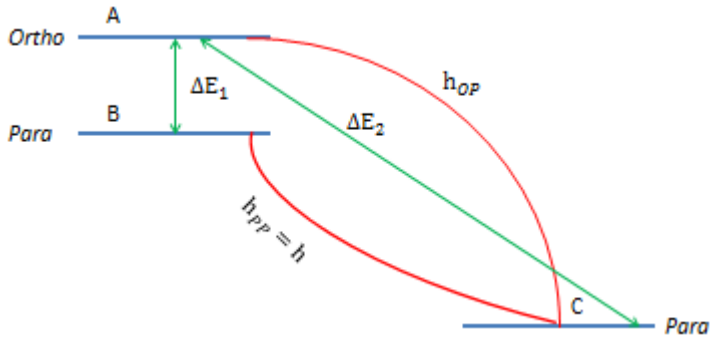

Figure 5.7: The schematic representation of the interaction of three level model.

The molecular Hamiltonian matrix for this model is named as M and is represented as below:

$$M = \begin{bmatrix} A & 0 & h_{OP} \\ 0 & B & h_{PP} \\ h_{OP} & h_{PP} & C \end{bmatrix} = \begin{bmatrix} A & 0 & h_{OP} \\ 0 & A + \Delta E_1 & h \\ h_{OP} & h & A + \Delta E_2 \end{bmatrix} \quad (5\text{-}34)$$

In the case of S_2Cl_2, it should be noticed that the diagonal and off-diagonal hyperfine terms, to say h and h_{op}, have the almost same order of magnitude. This fact is the most important point that we are interested in. The *ortho-para* mixing coefficients for various values of ΔE_1, ΔE_2, h and h_{OP} are systematically calculated by diagonalization of the matrix M, in which the condition of $h = h_{OP}$ is assumed. The result is summarized in Figure 5.8, in which ρ_{mixing} is represented as a function of ΔE_1, while ΔE_2 and h (= h_{OP}) are treated as the parameters.

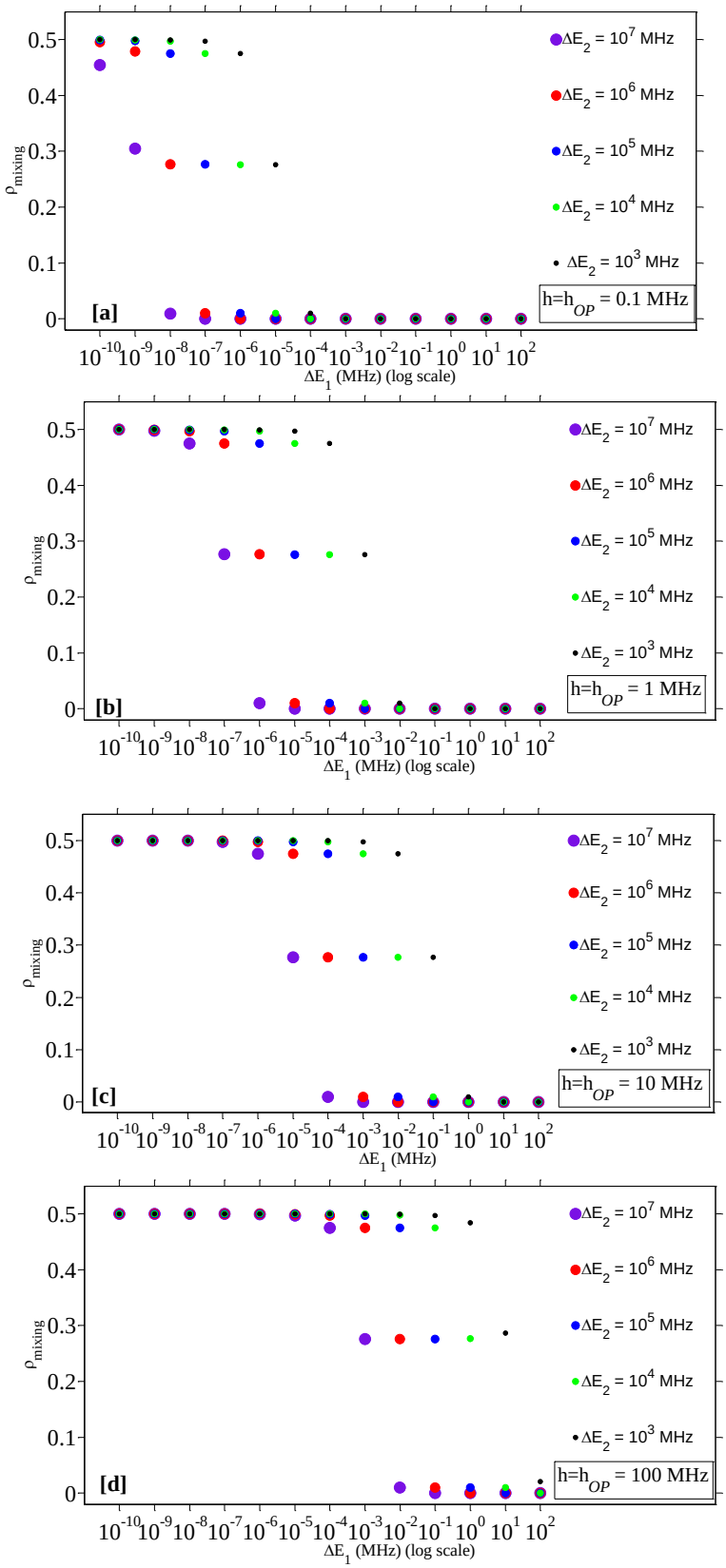

Figure 5.8: Dependence of ρ_{mixing} on ΔE_1 for different values of ΔE_2.(a) h = h_{OP} = 0.1 MHz. (b) h = h_{OP} = 1 MHz. (c) h = h_{OP} = 10 MHz. (d) h = h_{OP} = 100 MHz.

Figure 5.8 shows that larger value of ΔE_2 leads to less mixing of the *ortho* and *para* states. For the experimental observation of the *ortho-para* transitions, it is necessary to consider that those transitions should not overlap with the normal transitions. In other words, the *ortho-para* mixed states with a larger value of ΔE_1 are desirable.

Figure 5.9 shows the relation between h_{OP} and ΔE_1 for various values of ΔE_2, which is extracted from Figure 5.8. As seen in this figure, when h_{OP} becomes larger by one order of magnitude, ΔE_1 becomes smaller by two orders of magnitude.

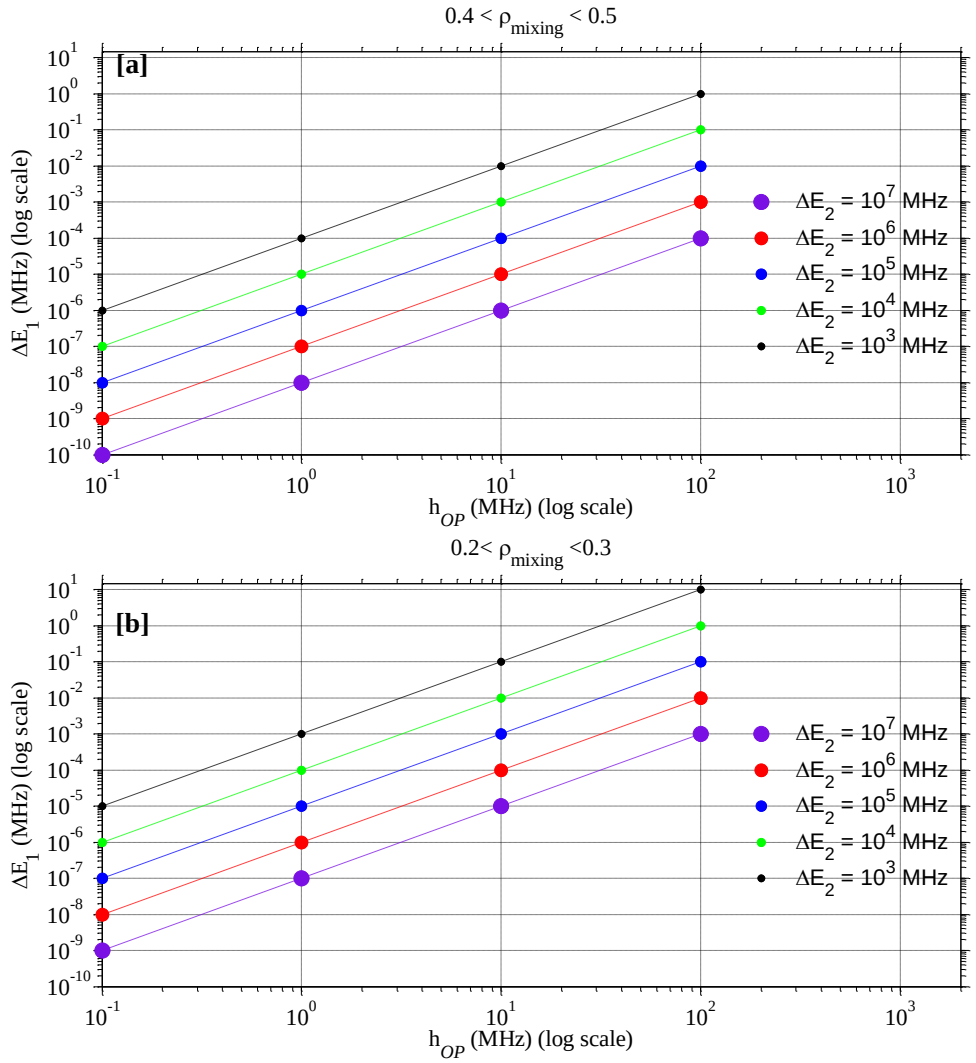

Figure 5.9: The relation between h_{OP} and ΔE_1 for different values of ΔE_2. (a) $0.4 < \rho_{mixing} < 0.5$. (b) $0.2 < \rho_{mixing} < 0.3$.

In the following section, the evaluation of the results obtained from this simplified model is discussed, comparing with a numerical solution of the ρ_{mixing} obtained by using the full-size Hamiltonian matrix.

As an example of the strong mixing case, $|9_{6\,4}\,2\,9\rangle^{\sim P}$ and $|9_{6\,3}\,1\,9\rangle^{\sim O}$ states are considered. These *ortho* and *para* states are mixed with each other with ρ_{mixing} of 0.4 as shown in section 5-3-2. This result was obtained by the eigenfunction analysis of the full-size (150×150) Hamiltonian matrix of the F=9 state. Here, instead of the three-level model, four levels model is introduced because two intermediate states are necessary as C and C′. Thus a 4×4 matrix is reduced from the 150×150 Hamiltonian matrix, in order to validate the simplified model and to understand the roots of the strong mixing.

In the first step, it is necessary to find an intermediate state corresponding to the C-level shown in Fig.5.7. As the intermediate states for these states, $|11_{7\,4}\,3\,9\rangle^{O}$ and $|11_{7\,5}\,2\,9\rangle^{P}$ are selected because the off-diagonal matrix elements are largest in the Wang basis sets. These values are shown as below.

$$^{P}\langle 9_6\,2\,9,-|\mathrm{H}_{OP}|11_7\,3\,9,+\rangle^{O} = 13.2347\ \mathrm{MHz} \tag{5-35}$$

$$^{O}\langle 9_6\,1\,9,+|\mathrm{H}_{OP}|11_7\,2\,9,-\rangle^{P} = 11.3940\ \mathrm{MHz} \tag{5-36}$$

In the case of this 4×4 matrix model, an ordinary perturbation theory is used. The Hamiltonian is represented as $H = H_0 + H_{OP}$, where H_0 is diagonal and H_{OP} is off-diagonal terms concerning the *ortho-para* symmetry. The four components of the basis set are $|9_{6\,3}\,1\,9\rangle_0^O$, $|9_{6\,4}\,2\,9\rangle_0^P$, $|11_{7\,4}\,3\,9\rangle_0^O$ and $|11_{7\,5}\,2\,9\rangle_0^P$, which are the zeroth-order eigenfunction of H_0. Then Hamiltonian matrix is represented as below.

$$\mathrm{M} = \begin{bmatrix} {}_0^O\langle 9_{6\,3}1\,9|H|9_{6\,3}1\,9\rangle_0^O & {}_0^O\langle 9_{6\,3}1\,9|H|9_{6\,4}2\,9\rangle_0^P & {}_0^O\langle 9_{6\,3}1\,9|H|11_{7\,4}3\,9\rangle_0^O & {}_0^O\langle 9_{6\,3}1\,9|H|11_{7\,5}2\,9\rangle_0^P \\ {}_0^P\langle 9_{6\,4}2\,9|H|9_{6\,3}1\,9\rangle_0^O & {}_0^P\langle 9_{6\,4}2\,9|H|9_{6\,4}2\,9\rangle_0^P & {}_0^P\langle 9_{6\,4}2\,9|H|11_{7\,4}3\,9\rangle_0^O & {}_0^P\langle 9_{6\,4}2\,9|H|11_{7\,5}2\,9\rangle_0^P \\ {}_0^O\langle 11_{7\,4}3\,9|H|9_{6\,3}1\,9\rangle_0^O & {}_0^O\langle 11_{7\,4}3\,9|H|9_{6\,4}2\,9\rangle_0^P & {}_0^O\langle 11_{7\,4}3\,9|H|11_{7\,4}3\,9\rangle_0^O & {}_0^O\langle 11_{7\,4}3\,9|H|11_{7\,5}2\,9\rangle_0^P \\ {}_0^P\langle 11_{7\,5}2\,9|H|9_{6\,3}1\,9\rangle_0^O & {}_0^P\langle 11_{7\,5}2\,9|H|9_{6\,4}2\,9\rangle_0^P & {}_0^P\langle 11_{7\,5}2\,9|H|11_{7\,4}3\,9\rangle_0^O & {}_0^P\langle 11_{7\,5}2\,9|H|11_{7\,5}2\,9\rangle_0^P \end{bmatrix} \tag{5-37}$$

The diagonal matrix elements corresponding to the zeroth-order are eigenvalues, and the *ortho-para* matrix elements with the same K_a are zero. Therefore, M is represented as below.

$$\mathrm{M} = \begin{bmatrix} E_1^{(0)} & 0 & {}_0^O\langle 9_{6\,3}1\,9|H|11_{7\,4}3\,9\rangle_0^O & {}_0^O\langle 9_{6\,3}1\,9|H|11_{7\,5}2\,9\rangle_0^P \\ 0 & E_2^{(0)} & {}_0^P\langle 9_{6\,4}2\,9|H|11_{7\,4}3\,9\rangle_0^O & {}_0^P\langle 9_{6\,4}2\,9|H|11_{7\,5}2\,9\rangle_0^P \\ {}_0^O\langle 11_{7\,4}3\,9|H|9_{6\,3}1\,9\rangle_0^O & {}_0^O\langle 11_{7\,4}3\,9|H|9_{6\,4}2\,9\rangle_0^P & E_3^{(0)} & 0 \\ {}_0^P\langle 11_{7\,5}2\,9|H|9_{6\,3}1\,9\rangle_0^O & {}_0^P\langle 11_{7\,5}2\,9|H|9_{6\,4}2\,9\rangle_0^P & 0 & E_4^{(0)} \end{bmatrix} \tag{5-38}$$

By using the mnemonic symbols appeared in 5-34, then M is represented as below.

$$\mathrm{M} = \begin{bmatrix} E_1^{(0)} & 0 & h_{OO}^{(0)} & h_{OP}^{(0)} \\ 0 & E_2^{(0)} & h_{PO}^{(0)} & h_{PP}^{(0)} \\ h_{OO}^{(0)*} & h_{OP}^{(0)*} & E_3^{(0)} & 0 \\ h_{PO}^{(0)*} & h_{PP}^{(0)*} & 0 & E_4^{(0)} \end{bmatrix} \quad (5\text{-}39)$$

The numerical values of (5-39) are quoted from the results of the 150×150 model in which *H* is H_0, and shown as below.

$$\mathrm{M} = \begin{bmatrix} 270174.6526 & 0 & 3.1663\mathrm{i} & 11.3940 \\ 0 & 270174.6526 & 13.2347 & 0 \\ -3.1663\mathrm{i} & 13.2347 & 380218.7431 & 0 \\ 11.3940 & 0 & 0 & 380218.8569 \end{bmatrix} \quad (5\text{-}40)$$

By diagonalization of (5-40), the eigenenergies and eigenfunctions are obtained as below.

$$\mathrm{M_D} = \begin{bmatrix} E_1 = 270174.6516 & 0 & 0 & 0 \\ 0 & E_2 = 270174.6508 & 0 & 0 \\ 0 & 0 & E_3 = 380218.7448 & 0 \\ 0 & 0 & 0 & E_4 = 380218.8581 \end{bmatrix} \quad (5\text{-}41)$$

$$|9_{6\,3}\ 1\ 9\rangle^{\sim O} = (-0.83)\,|9_{6\,3}\ 1\ 9\rangle_0^O - (0.55\mathrm{i})\ |9_{6\,4}\ 2\ 9\rangle_0^P \quad (5\text{-}42)$$

$$|9_{6\,4}\ 2\ 9\rangle^{\sim P} = (-0.55)\,|9_{6\,3}\ 1\ 9\rangle_0^O + (0.83\mathrm{i})\ |9_{6\,4}\ 2\ 9\rangle_0^P \quad (5\text{-}43)$$

$$|11_{7\,4}\ 3\ 9\rangle^{\sim O} = (1)|11_7\ 3\ 9, +\rangle^O \quad (5\text{-}44)$$

$$|11_{7\,5}\ 2\ 9\rangle^{\sim P} = (1)|11_7\ 2\ 9, -\rangle^P \quad (5\text{-}45)$$

As seen in equations 5-42 and 5-43, $|9_{6\,4}\ 2\ 9\rangle^{\sim P}$ and $|9_{6\,3}\ 1\ 9\rangle^{\sim O}$ states are mixed with each other by ρ_{mixing} of 0.30 (=0.55×0.55). Those values are comparable to the result of 150×150 model in which the Hamiltonian is set to *H*. $\Delta E_1^{(0)} (= E_2^{(0)} - E_1^{(0)})$ and $\Delta E_2^{(0)} (= E_3^{(0)} - E_1^{(0)})$ in Matrix M are 10^{-5} MHz and 10^5 MHz respectively and h_{OP} value is approximately about 10 MHz. This condition corresponds to Figure 5.9.a, in which ρ_{mixing} is larger than 0.4 but less than 0.5 ($0.4 < \rho_{mixing} < 0.5$). This value of ρ_{mixing} agrees well to the value of 0.4, which is obtained from diagonalization of the 150×150 molecular Hamiltonian matrix. So it could be concluded that the simplified 4×4 matrix model is a good approximation for ρ_{mixing}.

As seen in figures 5.8 and 5.9, the magnitude of ρ_{mixing} depends on the magnitudes of ΔE_1, ΔE_2 and h_{OP}. The molecular rotational and hyperfine constants determine the magnitudes of ΔE_1, ΔE_2 and h_{OP}. In other words, the molecular rotational and hyperfine constants determine the possibility of experimental observation of the *ortho-para* radiative transition.

The simplified model gives a general view of the three most important parameters which determine the magnitude of ρ_{mixing}. The first parameter is the splitting of the *ortho-para K*-doubling states, (ΔE_1). The second is the energy difference from the intermediate interacting state (ΔE_2). The third is the magnitude of the interaction (h_{op}) with the other *ortho-para K*-doubling states which serve as the intermediate states.

5-3-5 Conclusion in this chapter

The *ortho-para* mixed states of S_2Cl_2 were numerically analyzed. In order to find heavily mixed *ortho-para* states, the molecular wave functions should be expanded on the eigenfunctions of H_0. The numerical calculations become apparent that most significant *ortho-para* mixed states are *K*-doubling pairs. And the magnitudes of the *ortho-para* mixed states estimated by the calculation suggests that the experimental observation of the radiative *ortho-para* transition is possible for S_2Cl_2.

However, there was no criterion for finding a large ρ_{mixing} related with the rotational quantum numbers (J, K_a, K_c, I, F) by using a primitive perturbation method. In order to find the key parameters which determine the magnitude of ρ_{mixing}, a modified subset Hamiltonian matrix model has been introduced. By using this simplified model, we found a criterion for finding a large magnitude of ρ_{mixing}. That is to say, three parameters are important: The first parameter is the splitting of the *ortho-para K*-doubling states (ΔE_1). The second one is the energy difference from the intermediate interacting state (ΔE_2). The third one is magnitudes of interaction between the intermediate state and the *ortho-para K*-doubling states (h_{op}). The dependence of ρ_{mixing} is dominated by these three parameters, which are determined by the molecular constants and quantum numbers (J, K_a, K_c, I, F) of the concerning states.

Chapter 6

Conclusion and Suggestions

The transition between the pure *ortho* and *para* states is theoretically impossible. In other words, the *ortho* states and *para* states could treat as two different molecules. Nevertheless, some internal interaction such as hyperfine interactions can change the pure symmetrical character of the molecular wave function to an impure character, that is to say, the total molecular wave function, as a complete description of a molecule, is a mixture of both the *ortho* and the *para* states. In such cases, the transition between two molecular states with opposite symmetries is theoretically possible. Before this work, no research has been reported focusing on the *ortho-para* interaction via origin of nuclear electric quadrupole interaction, though this interaction is recognized as the most important hyperfine interaction for a molecule without unpaired electrons.

The present dissertation mainly is aimed to respond theoretically and experimentally to a question that "which physical and spectroscopic parameters determine the possibility of the radiative *ortho-para* transition in an asymmetric top molecule?" The microwave spectrum of S_2Cl_2 in the centimeter wave region has revealed strong evidence that suggests the *ortho-para* interaction due to the nuclear quadrupole interaction with off-diagonal terms. Therefore, this molecule has been selected for this study.

As the intensity calculations of the *ortho-para* transitions in the centimeter wave region showed that the magnitudes for the *ortho-para* mixing coefficients are too small for the detection, the microwave spectroscopy of this molecule was extended from the centimeter wave region to the millimeter wave region in this study. The measured frequency region was from 75GHz to 100GHz and the highest determined quantum numbers were $J = 55$ and $K_a = 12$.

As a result of the millimeter spectroscopy, all rotational molecular constants including fourth and sixth order centrifugal distortion constants of S_2Cl_2 were determined for the first time. The measured hyperfine spectrum analysis in the millimeter wave region confirmed that the nuclear quadrupole hyperfine constants, determined in the centimeter wave region in the previous studies, were held to be valid in the millimeter wave region, as well.

The determination of the rotational spectroscopic constants in the millimeter wave region caused the matrix elements of S_2Cl_2 molecular Hamiltonian to be calculated. In turn, by knowing the Hamiltonian matrix elements of this molecule, the term energies and molecular wave functions were determined. These molecular wave functions were used in regard to finding the *ortho-para* mixed states. The molecular wave functions were directly used in order to find the *ortho-para* mixing coefficients for the first time. This approach for searching the *ortho-para* mixed states lead to recognition of the weakness of the representation of the molecular wave function in the common symmetrized symmetric rotor basis set for searching *ortho-para* mixed states. The contribution of diagonal hyperfine interaction in mixing the states via same symmetries was recognized as the reason for this weakness. In order to solve this problem, applying their projection on the eigenfunctions of the Hamiltonian matrix was

proposed as a solution to find the *ortho-para* mixed states rather than using the molecular wave function in the symmetrized symmetric rotor basis set which was made by the contribution of only rotational and diagonal hyperfine constants.

As result, the evaluation of the *ortho-para* mixed states reveals that the *ortho-para* mixing coefficients for some *K*-doubling states in the millimeter wave region are so large that a direct observation of the radiative *ortho-para* transition may become possible. The numerical results were summarized as the lists of the *ortho-para* mixed states for the candidates of experimental observation of the *ortho-para* transition. It is worth mentioning that a molecule without unpaired electron is proposed as a feasible candidate for direct observation of the radiative *ortho-para* transition for the first time.

In order to respond to the question that "which physical and spectroscopic parameters determine the possibility of the radiative *ortho-para* transition in an asymmetric top molecule?", a criterion for evaluation of the *ortho-para* mixing coefficients was investigated.

The first approach using an ordinal perturbation theorem could not demonstrate the general dependence of mixing coefficients on the quantum numbers of a molecular state. The second approach using a three levels interaction mode which includes an intermediate state, a useful criterion was established to have a reliable prediction about the magnitude of the *ortho-para* mixing coefficients. According to this criterion, it is found that three parameters are prominently important. Those are the energy separation of the *ortho-para K*-doubling states (ΔE_1), the magnitude of interaction between the intermediate state and the *ortho-para K*-doubling states (h_{op}), and the energy separation of the intermediate state from the *ortho-para K*-doubling states (ΔE_2). The contribution of these parameters determines the magnitude of the *ortho-para* mixing coefficient. The criterion derived from the three levels interaction model was applied to the actual molecular states and its validity was demonstrated by the example of a 4×4 simplified matrix. As a matter of fact, one criterion is for the first time proposed for the *ortho-para* mixing coefficients. Using this criterion, once molecular spectroscopic parameters of a molecule are known, it is possible to predict that whether this molecule serves as a good candidate regarding direct observation of the *ortho-para* interaction.

Furthermore, the present study was intended for the experimental investigation for the detection of the *ortho-para* transition of S_2Cl_2. As the most of the *ortho-para* mixed states are nearly degenerate or their splitting is too small, utilizing a Doppler free method would be beneficial to detect the *ortho-para* transitions in S_2Cl_2.

References

[1] Tanaka, K., Harada, K., Oka, T., *J. Phys. Chem. A.* 2013, **117**, 9584-9592.

[2] Mizoguchi, A., Ota, S., Kanamori, H., Sumiyoshi, Y., Endo, Y., *J. Mol. Spectrosc.* 2008, **250**, 86-97.

[3] Eucken A. *Sitzber. Preuss. Akad. Wiss*., 1912, **41** .

[4] Mecke *R. Z. f. Physik.*, 1925, **31**,709-712 .

[5] Bonhoefer KF, Harteck P., *Naturwiss.* , 1929, **17**,182.

[6] D.M.Dennison, *Roy. Soc. Proc., A,* 1927, **115**, 483–486.

[7] Dirac, P. A. M. , *Proc. R. Soc. London.*, 1926, **A112**, 661-677.

[8] Heisenberg, W. Mehkorperproblem., *Z. Phys.*, 1926, **38**, 411-426.

[9] Chapovsky, P.L., Hermans, L. J. F., *Annu. Rev. Phys. Chem.*, 1999, **50**, 315.

[10] Chapovsky, P.L., *Sov. Phys. JETP* , 1990,**70** , 5.

[11] Sun, Z.D., Takagi, K., Matsushima, F., *Science*, 2005, **310**,1938-1941.

[12] Chapovsky, P.L. Cosleoou, J. Herlment, F. Khelkhal, M. Legrand, J., *Chem. Phys. Lett.* , 2000, **322**, 424-428.

[13] Peters, G., Schramm, B., *Chem. Phys. Lett.*, 1999, **302**, 181.

[14] Tikonov, V.I., Volkov, A.A., *Science* , 2002,**296**, 2363.

[15] Gel'mukhanov, F.K., Shalagin, A.M., *JETP Lett.*,1979, .**29**, 711.

[16] Nagles, B., Schuurman, M., Chapovsky, PL., Hermans, L.J.F., *Phys. Rev. A* , 1996, **54**, 2050.

[17] Chapovsky, P.L., Cosleou, J., Herlemont, F., Khelkhal, M., Legrand, J., *Chem. Phys. Lett.* , 2000, **322**, 424

[18] Peters, G. Schramn, B. *Chem. Phys. Lett.* , 1992, **302**, 181-186.

[19] I.Ozier, P.Yi, A. Khosla, and N. F. Ramsey, *Phys. Rev. Lett.* , 1970, **24**, 642.

[20] R. F. Curl Jr., J. V. V. Kasper, K. S. Pitzer, *J. Chem. Phys.* , 1967, **46**, 3220.

[21] P. L. Chapovsky, L. J. F. Hermans, *Annu. Rev. Phys. Chem.* , 1999, **50**, 315.

[22] Chapovsky PL. *Physica A* , 1996, **233**, 441-448.

[23] Hougen, J.T., Oka,T., *Science* 2005, **310**, 1913-1914.

[24] Tanaka, K., Hayashi, M., Ohtsuki, M., Harada, K., Tanaka, T., *J. Chem. Phys.*, 2009, **131**, 111101

[25] Hayashi, M., Harada, K., Lavrich, R., Tanaka, T., Tanaka, K., *J. Chem. Phys.* , 2010, **133**, 154303

[26] Pachucki, K. Komasa, J. , *Phys. Rev. A.* 2008, **77**, 030501(R).

[27] Chapovsky, P.L. Ilisa, E. , *Phys. Rev. A.* 2001, **63**, 062505.

[28] Chapovsky, P.L. , *J. Mol. Struct.* 2001, **599**, 337-345.

[29] Miani, A. Tennyson, J. , *J. Chem. Phys.* 2004, **120**, 2732.

[30] Nagles, B. Bakker, P. Hermans, L.J.F. Chapvosky, P.L., *Chem. Phys. Lett.* 1998, **294**, 387-390.

[31] Bordé, J. et al., *Phys. Rev. Lett.* , 1980, **45**, 14.

[32] Gordy, W., Cook, R. L. *Microwave Molecular Spectra*. John Wiley & Sons: New York, 1970.

[33] Bradley, E.B., Mathur, M.S., Frenzel, C.A., *Chem. Phys.* , 1967, **47**, 4325 .

[34] Matossi, F., Aderhold, H., *Z. Physik.* , 1931, **68**, 683.

[35] Morino, Y., Mizushima, S., *Sci. Papers Inst. Phys. Chem. Research* , 1937, **32**, 220 .

[36] Gerding, H., Westrik, R., *Rec. Trav. Chim.* ,1941, **60**, 702.

[37] Gerding, H., Westrik, R., *Rec. Trav. Chim.* ,1942, **61**, 412.

[38] R. Vogel Hogler, *Acta Phys. Austria* , 1948, **1**, 311.

[39] H. J. Bernstein and P. Powling, *J. Chem. Phys.* , 1950, **18**, 1018.

[40] Hirota, E., *Bull. Chem. Soc. Japan* , 1958, **31**, 130.

[41] A. E. Parsons and A. W. Searcy, *J. Chem. Phys.* , 1959, **30**, 1635.

[42] Marsden, C. J.; Brown, R. D.; Godfrey, P. D. , *J. C. S. Chem. Soc.* 1979, **9**, 399-401.

[43] Beagley, B., Eckersley, G.H., Brown, D.P., Tomlinson, D., *Trans. Faraday Soc.*, 1969, **65**, 2300.

[44] Frankiss, S.G., Harrison, D.J., *Spectrochim. Acta*, 1975, **31A**, 131

[45] Berger, R., Gottselig, M., Quack, Willeke, M., *Angew. Chem. Intl. Ed.***,** 2001**, 40**, 4195–4198

[46] Stull, Daniel R., *Ind. Eng. Chem.***,** 1947, **39**, 517-540.

[47] King, G.W., Hainer, R.M., Cross, P.C., *J. Chem. Phys.*, 1943, **11**, 27.

[48] Smith, J.G., Thompson, I., *Mol. Phys.*, 1976, **32**, 1247.

[49] Chang, T.S., Dennison, D.M., *J. Chem. Phys.*, 1953, **21**, 1293.

[50] Cook, R.L., De Lucia, F.C., *Am. J. Phys.*, 1971, **39**, 1533.

[51] Edmonds, A.R., *Angular momentum in quantum mechanics*. Princeton Univ. Press, Princeton, N.J., 1960.

[52] Scofield, J.H., *Am. J. Phys.*, 1994, **62** (2) 129-133.

[53] R. Vogelgesang, *lecture on the Lock-In Amplifier Theory* ,2004 .

[54] Kantrowitz, A., Grey, J., *Rev. Sci. Instrum.* ,1951, **22**, 328.

[55] Van de Meerakker, S.Y.T., Bethlem, H.L., Meijer, G., *Nature physics*, 2008, **4**: 595-602.

[56] Giese, C.F., Gentry, W.R., *Rev. Sci. Instrum.* **49**, 595 (1978);

[57] Miller, T.A., *Science* , 1984, **223**, 4636.

[58] Levy, D.H., *Annu. Rev. Phys. Chem.* 1980, **31**, 197.

[59]) Deursen , A. P. J., Reuss , J. , *J. Chem. Phys.*, 1975, **63**,4559 .

[60] Smalley, R. E., Wharton, L., Levy, D. H., *Acc. Chem. Res.* , 1977, **10**, 139

[61] Indium Antimonide hot electron bolometers. Available at: http://www.terahertz.co.uk/index.php?option=com_content&view=article&id=215&Itemid=594

[62] Ku, H.H., *Journal of Research and National Bureau of Standards*, 1966, **70C.N4**, 263.

[63] Nelson, W.H., *J. Mag. Res.*, 1980, **38**, 71.

Appendix A

Programming Codes

This Appendix includes the programming codes which are used in this work. In section A-1, there is the code for making the molecular Hamiltonian matrix and finding the term energies and molecular wave functions. Details of calculations and application of this code are explained in sections 2-1, 2-2, 2-3 and 5-2. In section A-2, there is the code for labeling the Eigen functions of molecular Hamiltonian. Details of this code are explained in section 5-2-1. In section A-3, there is the code for finding the *ortho-para* mixing states. Details of calculations and application of this code are explained in sections 5-1 and 5-3. In section A-4, there is the code for calculating the transition moment. Details of calculation and application of this code are explained in sections 2-3 and 5-3.

A-1 Making the molecular Hamiltonian and Finding the term energies and molecular functions

```
/*****************************************************************************
In this code, the matrix elements of the Molecular Hamiltonian
would be calculated for each F quantum number.
Hrot: pure rotational Hamiltonian
Hhyper: real hyperfine Hamiltonian
iHyper: complex hyperfine Hamiltonian
Hfina: total molecular Hamiltonian
"Eigen" : name of diagonalization library
D: Eigen values (result of diagonalization of Hamiltonian matrix)
V: Eigen functions (result of diagonalization of Hamiltonian matrix)
energyc: list of molecular functions and term energies for all molecular states.
*****************************************************************************/
#include <stdio.h>
#include <iostream>
#include <fstream>
#include <iomanip>
#include "Eigen"
#include <complex>

using namespace Eigen;
using namespace std;
int even(int);
double absfunc(double);
double maxfunc(double, double);
double minfunc(double, double);
double eQt(double, double, double, double, double, double, double);
double **label(double *e, double *bn[], int r, double *vn[]);
double ** coefread(double *e, double *bn[], int r, double *v[]);
complex<double> **labelc(double *e, double *bn[], int r, double *vn[], complex<double> *v[]);
```

```
double ** labelread(double *e, double *bn[], int r, double *v[]);
extern "C"


int main()
{
        int r, total, i, j;
        double Jcros, JK2p, JK2n, F, Jr, Jc, Ir, Ic, Kr, Kc, I;
        double I1, I2;
        int Fmax;
        double A, B, C, Dj, Djk, Dk, dj, dk, Hj, Hjk, Hkj, Hk, hj, hjk, hk;
        double KayAA, KayAB, KayAC, KayBC, KayBBCC, KayBB, KayCC;
        cout << fixed << setprecision(8);
        A = 5533.89624;      B = 1393.847829;      C = 1232.6699320;
        Dj = 0.00057161;     Djk = -0.00513195;    Dk = 0.0240535;
        dj = 0.000132896;    dk = 0.002186;
        Hj = 0.000000005079; Hjk = 0.00000030674;  Hkj = -0.000001090;
        Hk = 0.000000922;    hj = 0.000000001333;  hjk = 0.0000003486;
        hk = 0.00001121;

        KayAA = -8.0484;     KayBB = -15.722;      KayCC = 23.77;
        KayBBCC = KayBB - KayCC;
        KayAB = -49.24;     KayAC = -23.7;KayBC = -30.27;

        Fmax = 30;
        double a1, a2, a3, jMin, jMax, jMininitial, jMaxinitial;
        int ju, jl, jcounter, kcounter, jtemp, fcounter;
        int *R = new int[Fmax + 1];*R = 1;

        for (fcounter = 0; fcounter <= Fmax; fcounter++){
                F = fcounter;
                cout << "F=" << F << "\n";
                total = 0;
                for (i = 0; i <= 3; i++){
                        I = i;
                        a1 = F + I;a2 = F - I;a3 = I - F;
                        jMininitial = minfunc(a1, a2);
                        jMin = minfunc(a3, jMininitial);
                        jMaxinitial = maxfunc(a1, a2);
                        jMax = maxfunc(a3, jMaxinitial);
                        ju = jMax;
                        jl = jMin;
                        for (jcounter = jl; jcounter <= ju; jcounter++){
                                jtemp = jcounter;
                                if (jtemp % 2 == 0 && i % 2 == 0){
                                        for (kcounter = 0; kcounter <= jtemp; kcounter++){ total
= total + 1; }}
                                if (jtemp % 2 == 1 && i % 2 == 1){
                                        for (kcounter = 0; kcounter <= jtemp; kcounter++){ total
= total + 1; }}
                                if (jtemp % 2 == 0 && i % 2 == 1 && jtemp != 0){
                                        for (kcounter = 1; kcounter <= jtemp; kcounter++){ total
= total + 1; }}
                                if (jtemp % 2 == 1 && i % 2 == 0 && jtemp != 0){
                                        for (kcounter = 1; kcounter <= jtemp; kcounter++){ total
= total + 1; }}
                        }//(jcounter=jMin;jcounter<=jMax;jcounter++)
                }//(i=0;i<=3;i++)
                R[fcounter] = total;
                cout << "rcounter=" << R[fcounter] << "\n";
        }//fcounter

        int dim, tempd;
        dim = 0;tempd = 0;
        for (i = 0; i <= Fmax; i++){ dim = dim + R[i]; }
        double **basisset = 0;
        basisset = new double *[dim];
        for (i = 0; i<dim; i++)basisset[i] = new double[7];
        complex<double> **energyc = 0;
```

```
        energyc = new complex<double> *[dim];
        for (i = 0; i<dim; i++)energyc[i] = new complex<double>[dim + 8];

        I1 = 1.5;I2 = 1.5;
        cout << "start of calculation" << "\n";
        for (fcounter = 0; fcounter <= Fmax; fcounter++){
                r = R[fcounter];F = fcounter;
                double *II = new double[r];*II = 1.0;
                double *JJ = new double[r];*JJ = 1.0;
                double *KK = new double[r];*KK = 1.0;
                int *sym = new int[r];*sym = 1;
                double *Kal = new double[r];*Kal = 1.0;
                double *Kcl = new double[r];*Kcl = 1.0;
                double *op = new double[r];*op = 1.0;

                double *IIt = new double[r];*IIt = 1.0;
                double *JJt = new double[r];*JJt = 1.0;
                double *KKt = new double[r];*KKt = 1.0;
                int *symt = new int[r];*symt = 1;
                total = 0;
                for (i = 0; i <= 3; i++){
                        I = i*1.0;
                        a1 = F + I;a2 = F - I;a3 = I - F;
                        jMininitial = minfunc(a1, a2);
                        jMin = minfunc(a3, jMininitial);
                        jMaxinitial = maxfunc(a1, a2);
                        jMax = maxfunc(a3, jMaxinitial);
                        ju = jMax; jl = jMin;
                        for (jcounter = jl; jcounter <= ju; jcounter++){
                                jtemp = jcounter;
                                if (jtemp % 2 == 0 && i % 2 == 0){
                                        for (kcounter = 0; kcounter <= jtemp; kcounter = kcounter
+ 2){
                                                IIt[total] = I; JJt[total] = jtemp*1.0;
KKt[total] = kcounter*1.0; symt[total] = 0;//E+
                                                total = total + 1;}}
                                if (jtemp % 2 == 1 && i % 2 == 1){
                                        for (kcounter = 0; kcounter <= jtemp; kcounter = kcounter
+ 2){
                                                IIt[total] = I; JJt[total] = jtemp*1.0;
KKt[total] = kcounter*1.0; symt[total] = 0;//E+
                                                total = total + 1;}}
                                if (jtemp % 2 == 0 && i % 2 == 1 && jtemp != 0)  {
                                        for (kcounter = 1; kcounter <= jtemp; kcounter = kcounter
+ 2){
                                                IIt[total] = I; JJt[total] = jtemp*1.0;
KKt[total] = kcounter*1.0; symt[total] = 3;//O-
                                                total = total + 1;}}
                                if (jtemp % 2 == 1 && i % 2 == 0 && jtemp != 0)  {
                                        for (kcounter = 1; kcounter <= jtemp; kcounter = kcounter
+ 2){
                                                IIt[total] = I; JJt[total] = jtemp*1.0;
KKt[total] = kcounter*1.0; symt[total] = 3;//O-
                                                total = total + 1;}}
                                if (jtemp % 2 == 0 && i % 2 == 1 && jtemp != 0){
                                        for (kcounter = 2; kcounter <= jtemp; kcounter = kcounter
+ 2){
                                                IIt[total] = I; JJt[total] = jtemp*1.0;
KKt[total] = kcounter*1.0; symt[total] = 1;//E-
                                                total = total + 1;}}
                                if (jtemp % 2 == 1 && i % 2 == 0 && jtemp != 0){
                                        for (kcounter = 2; kcounter <= jtemp; kcounter = kcounter
+ 2){
                                                IIt[total] = I; JJt[total] = jtemp*1.0;
KKt[total] = kcounter*1.0; symt[total] = 1;//E-
                                                total = total + 1;}}
                                if (jtemp % 2 == 0 && i % 2 == 0){
                                        for (kcounter = 1; kcounter <= jtemp; kcounter = kcounter
+ 2){
```

```
                                                IIt[total] = I; JJt[total] = jtemp*1.0;
KKt[total] = kcounter*1.0; symt[total] = 2;//O+
                                                total = total + 1;}}
                                if (jtemp % 2 == 1 && i % 2 == 1){
                                        for (kcounter = 1; kcounter <= jtemp; kcounter = kcounter
+ 2){
                                                IIt[total] = I; JJt[total] = jtemp*1.0;
KKt[total] = kcounter*1.0; symt[total] = 2;//O+
                                                total = total + 1;}}
                        }//(jcounter=jMin;jcounter<=jMax;jcounter++)
                }//(i=0;i<=3;i++)
                int sepc, sopc, senc, sonc;
                int sep, sop, sen, son;
                sepc = 0; sopc = 0; senc = 0; sonc = 0;
                for (i = 0; i<r; i++){
                        if (symt[i] == 0){ sepc = sepc + 1; }
                        if (symt[i] == 1){ senc = senc + 1; }
                        if (symt[i] == 2){ sopc = sopc + 1; }
                        if (symt[i] == 3){ sonc = sonc + 1; }
                }
                sep = sepc; sop = sopc; sen = senc; son = sonc;
                sepc = 0; sopc = 0; senc = 0; sonc = 0;
                //cout<<son;
                for (i = 0; i<r; i++){ if (symt[i] == 0){ II[sepc] = IIt[i]; JJ[sepc] = JJt[i];
KK[sepc] = KKt[i];
                                                        sym[sepc] = symt[i]; sepc = sepc + 1; }
}
                for (i = 0; i<r; i++){ if (symt[i] == 1){ II[senc + sep] = IIt[i]; JJ[senc + sep]
= JJt[i]; KK[senc + sep] = KKt[i];
                                                        sym[senc + sep] = symt[i]; senc = senc
+ 1; } }
                for (i = 0; i<r; i++){ if (symt[i] == 2){ II[sopc + sep + sen] = IIt[i]; JJ[sopc
+ sep + sen] = JJt[i]; KK[sopc + sep + sen] = KKt[i];
                                                        sym[sopc + sep + sen] = symt[i]; sopc =
sopc + 1; } }
                for (i = 0; i<r; i++){ if (symt[i] == 3){ II[sonc + sep + sen + sop] = IIt[i];
JJ[sonc + sep + sen + sop] = JJt[i]; KK[sonc + sep + sen + sop] = KKt[i];
                                                        sym[sonc + sep + sen + sop] = symt[i];
sonc = sonc + 1; } }
                //making ka & kc and op
                //if ortho:op=1 if para:op=0;
                for (i = 0; i<r; i++){
                        if (sym[i] == 0 || sym[i] == 2){ Kal[i] = KK[i]; Kcl[i] = JJ[i] - Kal[i];
}
                        if (sym[i] == 1 || sym[i] == 3){ Kal[i] = KK[i]; Kcl[i] = JJ[i] + 1 -
Kal[i]; }}//i loop
                for (i = 0; i<r; i++){
                        if (fmod((Kal[i] + Kcl[i]), 2) == 0.0 && fmod(II[i], 2) == 0.0){ op[i] =
0.0; }
                        if (fmod((Kal[i] + Kcl[i]), 2) != 0.0 && fmod(II[i], 2) != 0.0){ op[i] =
1.0; }}

                double **H = 0; //H:hamiltonian for each F
                H = new double *[r];
                for (i = 0; i<r; i++)H[i] = new double[r];
                double **Hrot = 0; //H:rotational hamiltonian
                Hrot = new double *[r];
                for (i = 0; i<r; i++)Hrot[i] = new double[r];
                double **Hhyper = 0; //H:hyperfine hamiltonian
                Hhyper = new double *[r];
                for (i = 0; i<r; i++)Hhyper[i] = new double[r];
                double **iHhyper = 0; //H:imaginary hyperfine hamiltonian
                iHhyper = new double *[r];
                for (i = 0; i<r; i++)iHhyper[i] = new double[r];

                //making rotational hamiltonian
                int symr, symc, midk, jp;
                double add, bave, bdif, ap, bjj, bjj2, bjj4, flkk, fljp;
                for (i = 0; i<r; i++){
```

```
                        Jr = JJ[i]; Kr = KK[i]; Ir = II[i]; symr = sym[i];
                        for (j = 0; j<r; j++){
                                Jc = JJ[j]; Kc = KK[j]; Ic = II[j]; symc = sym[j];
                                if (symc != symr){ Hrot[i][j] = 0; }
                                if (Ir != Ic){ Hrot[i][j] = 0; }
                                if (Jr != Jc){ Hrot[i][j] = 0; }
                                if (Jr == Jc && symr == symc && Ir == Ic){
                                        Jcros = Jr*(Jr + 1);
                                        JK2p = sqrt((Jcros - Kr*(Kr + 1))*(Jcros - (Kr + 1)*(Kr +
2)));//a useful term for calculating elements between K and K+2
                                        JK2n = sqrt((Jcros - Kr*(Kr - 1))*(Jcros - (Kr - 1)*(Kr -
2)));//a useful term for calculating elements between K and K-2
                                        if (Kr == Kc || absfunc(Kr - Kc) == 2){
                                                if (Kr == Kc){
                                                        fljp = Jcros;
                                                        bave = 0.5*(B + C);
                                                        ap = A - bave;
                                                        bdif = 0.25*(B - C);
                                                        add = ((hj*fljp - dj + hjk)*fljp + bdif
- dk + hk)*fljp;
                                                        bjj = ((Hj*fljp - Dj)*fljp + bave)*fljp;
                                                        bjj2 = (Hjk*fljp - Djk)*fljp + ap;
                                                        bjj4 = Hkj*fljp - Dk;

                                                        flkk = Kr*Kr;
                                                        Hrot[i][j] = ((Hk*flkk + bjj4)*flkk +
bjj2)*flkk + bjj;
                                                        if (Kr == 1){
                                                                if (symr == 2) { Hrot[i][j] =
Hrot[i][j] + add; }
                                                                if (symr == 3) { Hrot[i][j] =
Hrot[i][j] - add; }
                                                        }//k=1
                                                }//dk=0
                                                if (absfunc(Kr - Kc) == 2){
                                                        jp = (int)(Jr*(Jr + 1));
                                                        fljp = (double)jp;
                                                        bave = 0.5*(B + C);
                                                        ap = A - bave;
                                                        bdif = 0.25*(B - C);
                                                        add = ((hj*fljp - dj + hjk)*fljp + bdif
- dk + hk)*fljp;
                                                        bjj = (hj*fljp - dj + hjk)*fljp + bdif -
dk + hk;
                                                        bjj2 = hjk*fljp - dk + 6.0*hk;
                                                        midk = (int)((Kr + Kc)) / 2;
                                                        flkk = midk*midk;
                                                        Hrot[i][j] = ((hk*flkk + bjj2)*flkk +
bjj)*sqrt((double)(jp - midk*(midk + 1))*(double)(jp - midk*(midk - 1)));
                                                        if ((Kr == 0) || (Kc == 0)) { Hrot[i][j]
= Hrot[i][j] * sqrt(2.0); }
                                                }//dk=2
                                        }//dk=2 or 0
                                        else{ Hrot[i][j] = 0; }
                                }//(Jr==Jc && symr==symc && Ir==Ic)
                                else{ Hrot[i][j] = 0; }
                        }//j loop
                }// i loop


                double Xap, Xam, Xpbbccp, Xbbccm, Xabp, Xabm, Xacp, Xacm, Xbcp, Xbcm;

                Xap = KayAA*2.0; //  Xa1+Xa2
                Xam = 0.0;  // -Xa1+Xc2
                Xpbbccp = KayBBCC*2.0;//  (Xbb-Xcc)1+(Xbb-Xcc)2
                Xbbccm = 0.0;  // -(Xbb-Xcc)1+(Xbb-Xcc)2
                Xabp = 0.0;    //  Xab1+Xab2
                Xabm = -2.0*KayAB;   // -Xab1+Xab2
                Xacp = 2.0*KayAC;    //  Xac1+Xac2
```

```
                Xacm = 0.0;     // -Xac1+Xac2
                Xbcp = 0.0;     //  Xbc1+Xbc2
                Xbcm = -2.0*KayBC;    // -Xbc1+Xbc2

                double JJ1, JJ2, II1, II2, KK1, KK2, sym1, sym2;
                for (i = 0; i<r; i++)
                {
                        for (j = 0; j<r; j++)
                        {
                                JJ1 = JJ[i]; KK1 = KK[i]; II1 = II[i]; sym1 = sym[i];
                                JJ2 = JJ[j]; KK2 = KK[j]; II2 = II[j]; sym2 = sym[j];
                                if (KK1 - KK2 == 0.0){
                                        if (absfunc(II1 - II2) == 0.0){
                                                if (((sym1 == sym2) && (fmod(absfunc(JJ1 - JJ2),
2) == 0)) || ((abs(sym1 - sym2) == 1) && (fmod(absfunc(JJ1 - JJ2), 2) == 1))){
                                                        Hhyper[i][j] = 0.5*Xap*eQt(JJ1, JJ2,
KK1, KK2, II1, II2, F);
                                                        if (KK1 == 1){
                                                                if (((sym1 == sym2) && (sym1 ==
2)) || ((sym1 != sym2) && (sym1 == 2))){ //[sym1==sym2]=[2,2] or [sym1<=sym2]=[2,3]
                                                                        Hhyper[i][j] =
Hhyper[i][j] + (1 / (2.0*sqrt(6.0))*Xpbbccp*eQt(JJ1, JJ2, -1.0, 1.0, II1, II2, F));}
                                                                if (((sym1 == sym2) && (sym1 ==
3)) || ((sym1 != sym2) && (sym1 == 3))){ //[sym1==sym2]=[3,3]
                                                                        Hhyper[i][j] =
Hhyper[i][j] - (1 / (2.0*sqrt(6.0))*Xpbbccp*eQt(JJ1, JJ2, -1.0, 1.0, II1, II2, F));}
                                                        }//k=1
                                                        iHhyper[i][j] = 0.0;
                                                }//Dsym+dJ:even
                                                if (((sym1 == sym2) && (fmod(absfunc(JJ1 - JJ2),
2) == 1)) || ((abs(sym1 - sym2) == 1) && (fmod(absfunc(JJ1 - JJ2), 2) == 0))){
                                                        if (KK1 == 1){
                                                                if (((sym1 == sym2) && (sym1 ==
2)) || ((sym1 != sym2) && (sym1 == 2))){
                                                                        iHhyper[i][j] = -1 /
(2.0*sqrt(6.0))*2.0*Xbcp*eQt(JJ1, JJ2, -1.0, 1.0, II1, II2, F);}
                                                                if (((sym1 == sym2) && (sym1 ==
3)) || ((sym1 != sym2) && (sym1 == 3))){
                                                                        iHhyper[i][j] = 1 /
(2.0*sqrt(6.0))*2.0*Xbcp*eQt(JJ1, JJ2, -1.0, 1.0, II1, II2, F);}
                                                        }//k=1
                                                        if (KK1 != 1){ iHhyper[i][j] = 0.0; }
                                                        Hhyper[i][j] = 0.0;
                                                }//Dsym+dJ:odd
                                                if (sym1 != sym2 && absfunc(sym1 - sym2) != 1.0){
iHhyper[i][j] = 0.0; Hhyper[i][j] = 0.0; }
                                        }//dI=0

                                        if (absfunc(II1 - II2) == 1.0){
                                                if (((sym1 == sym2) && (fmod(absfunc(JJ1 - JJ2),
2) == 0)) || ((abs(sym1 - sym2) == 1) && (fmod(absfunc(JJ1 - JJ2), 2) == 1))){
                                                        Hhyper[i][j] = 0.5*Xam*eQt(JJ1, JJ2,
KK1, KK2, II1, II2, F);
                                                        if (KK1 == 1){
                                                                if (((sym1 == sym2) && (sym1 ==
2)) || ((sym1 != sym2) && (sym1 == 2))){
                                                                        Hhyper[i][j] =
Hhyper[i][j] + (1 / (2.0*sqrt(6.0))*Xbbccm*eQt(JJ1, JJ2, -1.0, 1.0, II1, II2, F));}
                                                                if (((sym1 == sym2) && (sym1 ==
3)) || ((sym1 != sym2) && (sym1 == 3))){
                                                                        Hhyper[i][j] =
Hhyper[i][j] - (1 / (2.0*sqrt(6.0))*Xbbccm*eQt(JJ1, JJ2, -1.0, 1.0, II1, II2, F));}
                                                        }//k=1
                                                        iHhyper[i][j] = 0.0;
                                                }//Dsym+dJ:even
                                                if (((sym1 == sym2) && (fmod(absfunc(JJ1 - JJ2),
2) == 1)) || ((abs(sym1 - sym2) == 1) && (fmod(absfunc(JJ1 - JJ2), 2) == 0))){
                                                        if (KK1 == 1){
```

```
                                                                        if (((sym1 == sym2) && (sym1 ==
2)) || ((sym1 != sym2) && (sym1 == 2))){
                                                                                iHhyper[i][j] = -1 /
(2.0*sqrt(6.0))*2.0*Xbcm*eQt(JJ1, JJ2, -1.0, 1.0, II1, II2, F);}
                                                                        if (((sym1 == sym2) && (sym1 ==
3)) || ((sym1 != sym2) && (sym1 == 3))){
                                                                                iHhyper[i][j] = 1 /
(2.0*sqrt(6.0))*2.0*Xbcm*eQt(JJ1, JJ2, -1.0, 1.0, II1, II2, F);}
                                                        }//k=1
                                                        if (KK1 != 1){ iHhyper[i][j] = 0.0; }
                                                        Hhyper[i][j] = 0.0;
                                                }//Dsym+dJ:odd
                                                if (sym1 != sym2 && absfunc(sym1 - sym2) != 1.0){
iHhyper[i][j] = 0.0; Hhyper[i][j] = 0.0; }
                                        }//dI=1
                                        if (absfunc(II1 - II2) == 2.0){
                                                if (((sym1 == sym2) && (fmod(absfunc(JJ1 - JJ2),
2) == 0)) || ((abs(sym1 - sym2) == 1) && (fmod(absfunc(JJ1 - JJ2), 2) == 1))){
                                                        Hhyper[i][j] = 0.5*Xap*eQt(JJ1, JJ2,
KK1, KK2, II1, II2, F);
                                                        if (KK1 == 1){
                                                                if (((sym1 == sym2) && (sym1 ==
2)) || ((sym1 != sym2) && (sym1 == 2))){
                                                                        Hhyper[i][j] =
Hhyper[i][j] + (1 / (2 * sqrt(6.0))*Xpbbccp*eQt(JJ1, JJ2, -1.0, 1.0, II1, II2, F));}
                                                                if (((sym1 == sym2) && (sym1 ==
3)) || ((sym1 != sym2) && (sym1 == 3))){
                                                                        Hhyper[i][j] =
Hhyper[i][j] - (1 / (2 * sqrt(6.0))*Xpbbccp*eQt(JJ1, JJ2, -1.0, 1.0, II1, II2, F));}
                                                        }//k=1
                                                        iHhyper[i][j] = 0.0;
                                                }//Dsym+dJ:even
                                                if (((sym1 == sym2) && (fmod(absfunc(JJ1 - JJ2),
2) == 1)) || ((abs(sym1 - sym2) == 1) && (fmod(absfunc(JJ1 - JJ2), 2) == 0))){
                                                        if (KK1 == 1){
                                                                if (((sym1 == sym2) && (sym1 ==
2)) || ((sym1 != sym2) && (sym1 == 2))){
                                                                        iHhyper[i][j] = -1 /
(2.0*sqrt(6.0))*2.0*Xbcp*eQt(JJ1, JJ2, -1.0, 1.0, II1, II2, F);}
                                                                if (((sym1 == sym2) && (sym1 ==
3)) || ((sym1 != sym2) && (sym1 == 3))){
                                                                        iHhyper[i][j] = 1 /
(2.0*sqrt(6.0))*2.0*Xbcp*eQt(JJ1, JJ2, -1.0, 1.0, II1, II2, F);}
                                                        }//k=1;
                                                        if (KK1 != 1){ iHhyper[i][j] = 0.0; }
                                                        Hhyper[i][j] = 0.0;
                                                }////Dsym+dJ:odd
                                                if (sym1 != sym2 && absfunc(sym1 - sym2) != 1.0){
iHhyper[i][j] = 0.0; Hhyper[i][j] = 0.0; }
                                        }//dI=2
                                        if (absfunc(II1 - II2) != 0.0 && absfunc(II1 - II2) !=
1.0 && absfunc(II1 - II2) != 2.0){ iHhyper[i][j] = 0.0; Hhyper[i][j] = 0.0; }
                                }//dK=0
                                if (absfunc(KK1 - KK2) == 1.0){
                                        if (absfunc(II1 - II2) == 0.0){
                                                if (((fmod(absfunc(sym1 - sym2), 2) == 0.0) &&
(fmod(absfunc(JJ1 - JJ2), 2) == 1)) || ((fmod(absfunc(sym1 - sym2), 2) == 1.0) &&
(fmod(absfunc(JJ1 - JJ2), 2) == 0))){
                                                        Hhyper[i][j] = (KK2 - KK1) /
sqrt(6.0)*Xabp*eQt(JJ1, JJ2, KK1, KK2, II1, II2, F);
                                                        iHhyper[i][j] = 0.0;}
                                                if (((fmod(absfunc(sym1 - sym2), 2) == 0.0) &&
(fmod((JJ1 - JJ2), 2) == 0)) || ((fmod(absfunc(sym1 - sym2), 2) == 1.0) && (fmod(absfunc(JJ1 -
JJ2), 2) == 1))){
                                                        iHhyper[i][j] = 1.0 /
sqrt(6.0)*Xacp*eQt(JJ1, JJ2, KK1, KK2, II1, II2, F);
                                        Hhyper[i][j] = 0.0;}
                                                if ((KK1 == 0) || (KK2 == 0)) {
                                                        Hhyper[i][j] = Hhyper[i][j] * sqrt(2.0);
```

```
                                                        iHhyper[i][j] = iHhyper[i][j] *
sqrt(2.0);}
                                        }//dI=0
                                        if (absfunc(II1 - II2) == 1.0){
                                                if (((fmod(absfunc(sym1 - sym2), 2) == 0) &&
(fmod(absfunc(JJ1 - JJ2), 2) == 1)) || ((fmod(absfunc(sym1 - sym2), 2) == 1) && (fmod(absfunc(JJ1
- JJ2), 2) == 0))){
                                                        Hhyper[i][j] = (KK2 - KK1) /
sqrt(6.0)*Xabm*eQt(JJ1, JJ2, KK1, KK2, II1, II2, F);
                                                        iHhyper[i][j] = 0.0;}
                                                if (((fmod(absfunc(sym1 - sym2), 2) == 0) &&
(fmod(absfunc(JJ1 - JJ2), 2) == 0)) || ((fmod(absfunc(sym1 - sym2), 2) == 1) && (fmod(absfunc(JJ1
- JJ2), 2) == 1))){
                                                        iHhyper[i][j] = 1.0 /
sqrt(6.0)*Xacm*eQt(JJ1, JJ2, KK1, KK2, II1, II2, F);
                                                        Hhyper[i][j] = 0.0;}
                                                if ((KK1 == 0) || (KK2 == 0)) {
                                                        Hhyper[i][j] = Hhyper[i][j] * sqrt(2.0);
                                                        iHhyper[i][j] = iHhyper[i][j] *
sqrt(2.0);}
                                        }//dI=1
                                        if (absfunc(II1 - II2) == 2.0){
                                                if (((fmod(absfunc(sym1 - sym2), 2) == 0) &&
(fmod(absfunc(JJ1 - JJ2), 2) == 1)) || ((fmod(absfunc(sym1 - sym2), 2) == 1) && (fmod(absfunc(JJ1
- JJ2), 2) == 0))){
                                                        Hhyper[i][j] = (KK2 - KK1) /
sqrt(6.0)*Xabp*eQt(JJ1, JJ2, KK1, KK2, II1, II2, F);
                                                        iHhyper[i][j] = 0.0;}
                                                if (((fmod(absfunc(sym1 - sym2), 2) == 0) &&
(fmod(absfunc(JJ1 - JJ2), 2) == 0)) || ((fmod(absfunc(sym1 - sym2), 2) == 1) && (fmod(absfunc(JJ1
- JJ2), 2) == 1))){
                                                        iHhyper[i][j] = 1.0 /
sqrt(6.0)*Xacp*eQt(JJ1, JJ2, KK1, KK2, II1, II2, F);
                                                        Hhyper[i][j] = 0.0;}
                                                if ((KK1 == 0) || (KK2 == 0)) {
                                                        Hhyper[i][j] = Hhyper[i][j] * sqrt(2.0);
                                                        iHhyper[i][j] = iHhyper[i][j] *
sqrt(2.0);}
                                        }//dI=2
                                        if (absfunc(II1 - II2) != 0.0 && absfunc(II1 - II2) !=
1.0 && absfunc(II1 - II2) != 2.0){ iHhyper[i][j] = 0.0; Hhyper[i][j] = 0.0; }
                                }//dK=1
                                if (absfunc(KK1 - KK2) == 2.0){
                                        if (absfunc(II1 - II2) == 0.0){
                                                if (((sym1 == sym2) && (fmod(absfunc(JJ1 - JJ2),
2) == 0)) || ((fmod(absfunc(sym1 - sym2), 2) == 1) && (fmod(absfunc(JJ1 - JJ2), 2) == 1))){
                                                        Hhyper[i][j] = 1 / (2 *
sqrt(6.0))*Xpbbccp*eQt(JJ1, JJ2, KK1, KK2, II1, II2, F);
                                                        iHhyper[i][j] = 0.0;}
                                                if (((sym1 == sym2) && (fmod(absfunc(JJ1 - JJ2),
2) == 1)) || ((fmod(absfunc(sym1 - sym2), 2) == 1) && (fmod(absfunc(JJ1 - JJ2), 2) == 0))){
                                                        iHhyper[i][j] = (KK1 - KK2) / (2 *
sqrt(6.0))*Xbcp*eQt(JJ1, JJ2, KK1, KK2, II1, II2, F);
                                                        Hhyper[i][j] = 0.0;}
                                                if (sym1 != sym2 && fmod(absfunc(sym1 - sym2), 2)
!= 1){ iHhyper[i][j] = 0.0; Hhyper[i][j] = 0.0; }
                                                if ((KK1 == 0) || (KK2 == 0)){
                                                        Hhyper[i][j] = Hhyper[i][j] * sqrt(2.0);
                                                        iHhyper[i][j] = iHhyper[i][j] *
sqrt(2.0);}
                                        }//dI=0
                                        if (absfunc(II1 - II2) == 1.0){
                                                if (((sym1 == sym2) && (fmod(absfunc(JJ1 - JJ2),
2) == 0)) || ((fmod(absfunc(sym1 - sym2), 2) == 1) && (fmod(absfunc(JJ1 - JJ2), 2) == 1))){
                                                        Hhyper[i][j] = 1 / (2 *
sqrt(6.0))*Xbbccm*eQt(JJ1, JJ2, KK1, KK2, II1, II2, F);
                                                        iHhyper[i][j] = 0.0;}
                                                if (((sym1 == sym2) && (fmod(absfunc(JJ1 - JJ2),
2) == 1)) || ((fmod(absfunc(sym1 - sym2), 2) == 1) && (fmod(absfunc(JJ1 - JJ2), 2) == 0))){
```

```
                                                        iHhyper[i][j] = (KK1 - KK2) / (2 *
sqrt(6.0))*Xbcm*eQt(JJ1, JJ2, KK1, KK2, II1, II2, F);
                                                        Hhyper[i][j] = 0.0;}
                                                if (sym1 != sym2 && fmod(absfunc(sym1 - sym2), 2)
!= 1){ iHhyper[i][j] = 0.0; Hhyper[i][j] = 0.0; }
                                                if ((KK1 == 0) || (KK2 == 0)){
                                                        Hhyper[i][j] = Hhyper[i][j] * sqrt(2.0);
                                                        iHhyper[i][j] = iHhyper[i][j] *
sqrt(2.0);}
                                        }//dI=1
                                        if (absfunc(II1 - II2) == 2.0){
                                                if (((sym1 == sym2) && (fmod(absfunc(JJ1 - JJ2),
2) == 0)) || ((fmod(absfunc(sym1 - sym2), 2) == 1) && (fmod(absfunc(JJ1 - JJ2), 2) == 1))){
                                                        Hhyper[i][j] = 1 / (2 *
sqrt(6.0))*Xpbbccp*eQt(JJ1, JJ2, KK1, KK2, II1, II2, F);
                                                        iHhyper[i][j] = 0.0;}
                                                if (((sym1 == sym2) && (fmod(absfunc(JJ1 - JJ2),
2) == 1)) || ((fmod(absfunc(sym1 - sym2), 2) == 1) && (fmod(absfunc(JJ1 - JJ2), 2) == 0))){
                                                        iHhyper[i][j] = (KK1 - KK2) / (2 *
sqrt(6.0))*Xbcp*eQt(JJ1, JJ2, KK1, KK2, II1, II2, F);
                                                        Hhyper[i][j] = 0.0;}
                                                if (sym1 != sym2 && fmod(absfunc(sym1 - sym2), 2)
!= 1){ iHhyper[i][j] = 0.0; Hhyper[i][j] = 0.0; }
                                                if ((KK1 == 0) || (KK2 == 0)){
                                                        Hhyper[i][j] = Hhyper[i][j] * sqrt(2.0);
                                                        iHhyper[i][j] = iHhyper[i][j] *
sqrt(2.0);}
                                        }//dI=2
                                        if (absfunc(II1 - II2) != 0.0 && absfunc(II1 - II2) !=
1.0 && absfunc(II1 - II2) != 2.0){ iHhyper[i][j] = 0.0; Hhyper[i][j] = 0.0; }
                                }//dK=2
                                if (absfunc(KK1 - KK2) != 0.0 && absfunc(KK1 - KK2) != 1.0 &&
absfunc(KK1 - KK2) != 2.0){ iHhyper[i][j] = 0.0; Hhyper[i][j] = 0.0; }
                        }// j loop
                }//i loop


                for (i = 0; i<r; i++){ for (j = 0; j<r; j++){ H[i][j] = Hrot[i][j] +
Hhyper[i][j]; } }

                complex <double> **Dfina = 0;
                Dfina = new complex <double> *[r];
                for (i = 0; i<r; i++)Dfina[i] = new complex <double>[r];
                complex <double> **Hfina = 0;
                Hfina = new complex <double> *[r];
                for (i = 0; i<r; i++)Hfina[i] = new complex <double>[r];

                complex<double>Iima = sqrt(complex<double>(-1));
                for (i = 0; i < r; i++){
                        for (j = 0; j < r; j++){
                                Hfina[i][j] = H[i][j] + (Iima * iHhyper[i][j]);}}
                MatrixXcd a(r, r);
                for (i = 0; i<r; i++){
                        for (j = 0; j<r; j++){ a(i, j) = Hfina[i][j]; }}
                ComplexEigenSolver<MatrixXcd> ces(a);

                MatrixXcd D = ces.eigenvalues().asDiagonal();

                MatrixXcd V = ces.eigenvectors();
                for (i = 0; i < r; i++){
                        for (j = 0; j < r; j++){
                                Dfina[i][j] = real(D(i, j));}}
                //new basisset by considering complex hamiltonian
                double *IIn = new double[r];*IIn = 1.0;
                double *JJn = new double[r];*JJn = 1.0;
                double *KKn = new double[r];*KKn = 1.0;
                double *Kan = new double[r];*Kan = 1.0;
                double *Kccn = new double[r];*Kccn = 1.0;
                double *ef = new double[r];*ef = 1.0;
```

```
                int *symn = new int[r];*symn = 1;
                double *opn = new double[r];*opn = 1.0;

                for (i = 0; i<r; i++){
                        IIn[i] = II[i];JJn[i] = JJ[i];KKn[i] = KK[i];Kan[i] = Kal[i];
                        Kccn[i] = Kcl[i];symn[i] = sym[i];opn[i] = op[i];}

                double **bn = 0;
                bn = new double *[r];
                for (i = 0; i<r; i++){ bn[i] = new double[8]; }
                for (i = 0; i<r; i++){ bn[i][0] = JJn[i]; bn[i][1] = Kan[i]; bn[i][2] = Kccn[i];
bn[i][3] = IIn[i]; bn[i][4] = F; bn[i][5] = symn[i]; bn[i][6] = opn[i]; bn[i][7] = i; }
                double *e = new double[r];
                *e = 1.0;
                for (i = 0; i<r; i++){ e[i] = real(D(i, i)); }

                //start of labeling
                complex <double> **vni = 0;
                vni = new complex <double> *[r];
                for (i = 0; i<r; i++)
                        vni[i] = new complex <double>[r];

                for (i = 0; i<r; i++){
                        for (j = 0; j<r; j++){
                                vni[i][j] = V(i, j)*conj(V(i, j));}}

                complex <double> **vn2 = 0;
                vn2 = new complex <double> *[r];
                for (i = 0; i<r; i++)
                        vn2[i] = new complex <double>[r];
                for (i = 0; i<r; i++){ for (j = 0; j<r; j++){ vn2[i][j] = vni[j][i]; } }

                double **vn = 0;
                vn = new double *[r];
                for (i = 0; i<r; i++)
                        vn[i] = new double[r];
                for (i = 0; i<r; i++){ for (j = 0; j<r; j++){ vn[i][j] = real(vn2[i][j]); } }

                complex <double> **v = 0;
                v = new complex <double> *[r];
                for (i = 0; i<r; i++)
                        v[i] = new complex<double>[r];
                for (i = 0; i<r; i++){ for (j = 0; j<r; j++){ v[i][j] = (V(j, i)); } }

                double  **l3 = 0;
                l3 = new double *[r];
                for (i = 0; i<r; i++){ l3[i] = new double[8 + r]; }
                l3 = label(e, bn, r, vn);

                if (F != 0){ tempd = (R[fcounter - 1]) + tempd; }
                for (i = 0; i<r; i++){
                        for (j = 0; j<8 + r; j++){
                                if (fcounter == 0){ energy[i][j] = l3[i][j]; }
                                else{ energy[i + tempd][j] = l3[i][j]; }}//j energy
                }//i energy

                for (i = 0; i<r; i++){
                        if (fcounter == 0){
                                basisset[i][0] = JJn[i]; basisset[i][1] = Kan[i]; basisset[i][2]
= Kccn[i];
                                basisset[i][3] = IIn[i]; basisset[i][4] = F; basisset[i][5] =
opn[i]; basisset[i][6] = symn[i];}
                        else{
                        basisset[i + tempd][0] = JJn[i]; basisset[i + tempd][1] = Kan[i];
basisset[i + tempd][2] = Kccn[i];
                                basisset[i + tempd][3] = IIn[i]; basisset[i + tempd][4] = F;
basisset[i + tempd][5] = opn[i]; basisset[i + tempd][6] = symn[i];}}//i basisset

                for (i = 0; i <r; ++i)
```

```
                        delete[] Hrot[i];delete[] Hrot;
                for (i = 0; i <r; ++i)
                        delete[] H[i];delete[] H;
                for (i = 0; i <r; ++i)
                        delete[] Hhyper[i];delete[] Hhyper;
                for (i = 0; i <r; ++i)
                        delete[] iHhyper[i];delete[] iHhyper;
                for (i = 0; i <r; ++i)
                        delete[] Hfina[i];delete[] Hfina;
                delete[]II; delete[]JJ; delete[]KK; delete[]sym; delete[]Kal; delete[]Kcl;
delete[]op; delete[]IIt; delete[]JJt; delete[]KKt; delete[]symt;
                delete[]IIn; delete[]JJn; delete[]KKn; delete[]Kan; delete[]Kccn; delete[]ef;
delete[]symn; delete[]opn;
        }//fcounter
         cout<<"writing in text files"<<"\n";
        ofstream basisw;
        basisw.open("basissetE0.txt");
        basisw << fixed << setprecision(8);
        for (i = 0; i<dim; i++){
        for (j = 0; j<7; j++){
        basisw << basisset[i][j] << "\t";}
        basisw << "\n";}
        basisw.close();
        ofstream flc;
        flc.open("TermEcE0HL.txt");
        flc << fixed << setprecision(8);
        for (i = 0; i<dim; i++){
                for (j = 0; j<dim + 8; j++){
                        flc << energyc[i][j] << "\t";}
                flc << "\n";}
        flc.close();
}
```

A-2 Labeling

```
#include <stdio.h>
#include <iostream>
#include <iomanip>
#include <fstream>
#include <complex>
using namespace std;
double absfunc(double);
double maxfunc(double, double);
double minfunc(double, double);
complex<double> **labelc(double *e, double *bn[], int r, double *v[], complex<double> *vn[]);
complex<double> **labelc(double *e, double *bn[], int r, double *v[], complex<double> *vn[]){
        int i, j, k, l, F, mc;
        F = bn[0][4];
        complex<double> **l1 = 0;
        l1 = new complex<double> *[r];
        for (i = 0; i<r; i++){ l1[i] = new complex<double>[r + 8]; }

        complex<double> **lf = 0;
        lf = new complex<double> *[r];
        for (i = 0; i<r; i++){ lf[i] = new complex<double>[r + 8]; }

        int *lmarker = new int[r];*lmarker = 0;
        for (i = 0; i<r; i++){ lmarker[i] = -1; }

        int *opEigen = new int[r];*opEigen = 0;

        int *maxcounter = new int[r];*maxcounter = 0;
        for (i = 0; i<r; i++){ maxcounter[i] = 0; }

        double **coefm = 0;coefm = new double *[r];
        for (i = 0; i<r; i++){ coefm[i] = new double[6]; }

        int **indexm = 0;indexm = new int *[r];
        for (i = 0; i<r; i++){ indexm[i] = new int[6]; }

        for (i = 0; i<r; i++){for (j = 0; j<6; j++){ indexm[i][j] = -1; }//j}//i

        for (i = 0; i<r; i++){ opEigen[i] = -1; }

        int npara, northo;
        npara = 0; northo = 0;

        for (i = 0; i<r; i++){if (bn[i][6] == 0){ npara = npara + 1; }
                else{ northo = northo + 1; }}

        double paracoef, orthocoef;
        paracoef = 0; orthocoef = 0;

        for (i = 0; i<r; i++){
                for (j = 0; j<r; j++){
                        if (bn[j][6] == 0){ paracoef = paracoef + v[i][j]; }
                        else{ orthocoef = orthocoef + v[i][j]; }}//j
                if (paracoef>orthocoef){ opEigen[i] = 0; }
                    else{ opEigen[i] = 1; }paracoef = 0.0; orthocoef = 0.0;}//i

        double maxcoef1, maxcoef2, maxcoef3, maxcoef4, maxcoef5, maxcoef6;
        int maxindex1, maxindex2, maxindex3, maxindex4, maxindex5, maxindex6, indexref,
opidentifier;

        maxcoef1 = 0; maxcoef2 = 0; maxcoef3 = 0; maxcoef4 = 0; maxcoef5 = 0; maxcoef6 = 0;
        for (j = 0; j<r; j++){
                for (k = 0; k<r; k++){
                        if (maxcoef1<abs(v[j][k])){ maxcoef1 = abs(v[j][k]); maxindex1 = k; }//if
maxcoef1....}//k
                for (k = 0; k<r; k++){
```

```
                        if (maxcoef2<abs(v[j][k]) && abs(v[j][k]) != maxcoef1){ maxcoef2 =
abs(v[j][k]); maxindex2 = k; }}//k
                for (k = 0; k<r; k++){
                        if (maxcoef3<abs(v[j][k]) && abs(v[j][k]) != maxcoef2 && abs(v[j][k]) !=
maxcoef1){ maxcoef3 = abs(v[j][k]); maxindex3 = k; }}//k
                for (k = 0; k<r; k++){
                        if (maxcoef4<abs(v[j][k]) && abs(v[j][k]) != maxcoef2 && abs(v[j][k]) !=
maxcoef1 && abs(v[j][k]) != maxcoef3){ maxcoef4 = abs(v[j][k]); maxindex4 = k; }}//k
                for (k = 0; k<r; k++){
                        if (maxcoef5<abs(v[j][k]) && abs(v[j][k]) != maxcoef2 && abs(v[j][k]) !=
maxcoef1 && abs(v[j][k]) != maxcoef3 && abs(v[j][k]) != maxcoef4){ maxcoef5 = abs(v[j][k]);
maxindex5 = k; }}//k
                for (k = 0; k<r; k++){
                        if (maxcoef6<abs(v[j][k]) && abs(v[j][k]) != maxcoef2 && abs(v[j][k]) !=
maxcoef1 && abs(v[j][k]) != maxcoef3 && abs(v[j][k]) != maxcoef4 && abs(v[j][k]) != maxcoef5){
maxcoef6 = abs(v[j][k]); maxindex6 = k; }}//k
                indexm[j][0] = maxindex1; indexm[j][1] = maxindex2; indexm[j][2] = maxindex3;
indexm[j][3] = maxindex4; indexm[j][4] = maxindex5; indexm[j][5] = maxindex6;
                coefm[j][0] = maxcoef1; coefm[j][1] = maxcoef2; coefm[j][2] = maxcoef3;
coefm[j][3] = maxcoef4; coefm[j][4] = maxcoef5; coefm[j][5] = maxcoef6;
                maxcoef1 = 0; maxcoef2 = 0; maxcoef3 = 0; maxcoef4 = 0; maxcoef5 = 0; maxcoef6 =
0;}//j
        maxindex1 = 0; maxindex2 = 0; maxindex3 = 0; maxindex4 = 0; maxindex5 = 0; maxindex6 = 0;
        maxcoef1 = 0; maxcoef2 = 0; maxcoef3 = 0; maxcoef4 = 0; maxcoef5 = 0; maxcoef6 = 0;
        for (i = 0; i<r; i++){
                l1[i][0] = bn[i][0]; l1[i][1] = bn[i][1]; l1[i][2] = bn[i][2];
                l1[i][3] = bn[i][3]; l1[i][4] = bn[i][4]; l1[i][5] = bn[i][5];//sym
                l1[i][6] = bn[i][6];}

        int counter, tempcounter, jcounter;
        tempcounter = 0;
        //max1
        for (i = 0; i < r; i++){
                opidentifier = bn[i][6];indexref = i;
                for (j = 0; j < r; j++){
                        if (indexm[j][0] == indexref && opEigen[j] == opidentifier){
maxcounter[i] = maxcounter[i] + 1; }}//j
                counter = maxcounter[i];
                if (counter != 0)
                {double *tempcoef = new double[counter];*tempcoef = 0;
                int *tempindex = new int[counter];*tempindex = 0;
                for (j = 0; j < r; j++){
                                if (indexm[j][0] == indexref && opEigen[j] == opidentifier){
tempcoef[tempcounter] = coefm[j][0]; tempindex[tempcounter] = j; tempcounter = tempcounter + 1;
}}//j
                        if (i == 0){
                                for (j = 0; j < counter; j++){ if (tempcoef[j] >= maxcoef1){
maxcoef1 = tempcoef[j]; lmarker[i] = tempindex[j]; } }
                                jcounter = lmarker[i];
                                l1[i][7] = e[jcounter]; for (l = 8; l<r + 8; l++){ l1[i][l] =
vn[jcounter][l - 8]; }
                                maxcoef1 = 0;}//i==0
                        if (i != 0){mc = 0;
                                for (j = 0; j < counter; j++){
                                        for (k = 0; k < r; k++){
                                                if (tempindex[j] == lmarker[k]){ mc = mc + 1;
}}//k}//j
                                if (mc == 0){
                                        for (j = 0; j < counter; j++){ if (tempcoef[j] >=
maxcoef1){ maxcoef1 = tempcoef[j]; lmarker[i] = tempindex[j]; } }
                                        jcounter = lmarker[i];
                                        l1[i][7] = e[jcounter]; for (l = 8; l<r + 8; l++){
l1[i][l] = vn[jcounter][l - 8]; }
                                        maxcoef1 = 0;}}}//counter!=0
                maxcoef1 = 0;tempcounter = 0;}//i
        maxcoef1 = 0; tempcounter = 0;
        //max2
        for (i = 0; i < r; i++){
                if (lmarker[i] == -1){
```

```
                        opidentifier = bn[i][6];indexref = i;
                        maxcounter[i] = 0;maxcoef1 = 0; tempcounter = 0;
                        for (j = 0; j < r; j++){mc = 0;
                                if (indexm[j][1] == indexref && opEigen[j] == opidentifier){
                                        for (k = 0; k < r; k++){ if (j == lmarker[k]){ mc = mc +
1; } }
                                        if (mc == 0){maxcounter[i] = maxcounter[i] + 1;}}}//j
                        counter = maxcounter[i];
                        if (counter != 0){
                                double *tempcoef = new double[counter];*tempcoef = 0;
                                int *tempindex = new int[counter];*tempindex = 0;
                                for (j = 0; j < r; j++){mc = 0;
                                        if (indexm[j][1] == indexref && opEigen[j] ==
opidentifier){
                                                for (k = 0; k < r; k++){ if (j == lmarker[k]){ mc
= mc + 1; } }
                                                if (mc == 0){
                                                        tempcoef[tempcounter] = coefm[j][1];
tempindex[tempcounter] = j;
                                                        tempcounter = tempcounter + 1;}}}//j
                                for (j = 0; j < counter; j++){ if (tempcoef[j] >= maxcoef1){
maxcoef1 = tempcoef[j]; lmarker[i] = tempindex[j]; } }
                                jcounter = lmarker[i];
                                l1[i][7] = e[jcounter]; for (l = 8; l < r + 8; l++){ l1[i][l] =
vn[jcounter][l - 8]; }
                                maxcoef1 = 0;}}//lmarker[i]
                maxcoef1 = 0;tempcounter = 0;}//i
        maxcoef1 = 0; tempcounter = 0;
        //max3
        for (i = 0; i < r; i++){
                if (lmarker[i] == -1){
                        opidentifier = bn[i][6];indexref = i;maxcounter[i] = 0;
                        maxcoef1 = 0; tempcounter = 0;
                        for (j = 0; j < r; j++){mc = 0;
                                if (indexm[j][2] == indexref && opEigen[j] == opidentifier){
                                        for (k = 0; k < r; k++){ if (j == lmarker[k]){ mc = mc +
1; } }
                                        if (mc == 0){maxcounter[i] = maxcounter[i] + 1;}}}//j
                        counter = maxcounter[i];
                        if (counter != 0){
                                double *tempcoef = new double[counter];*tempcoef = 0;
                                int *tempindex = new int[counter];*tempindex = 0;
                                for (j = 0; j < r; j++){mc = 0;
                                        if (indexm[j][2] == indexref && opEigen[j] ==
opidentifier){
                                                for (k = 0; k < r; k++){ if (j == lmarker[k]){ mc
= mc + 1; } }
                                                if (mc == 0){
                                                        tempcoef[tempcounter] = coefm[j][2];
tempindex[tempcounter] = j;
                                                        tempcounter = tempcounter + 1;}}}//j
                                for (j = 0; j < counter; j++){ if (tempcoef[j] >= maxcoef1){
maxcoef1 = tempcoef[j]; lmarker[i] = tempindex[j]; } }
                                jcounter = lmarker[i];
                                l1[i][7] = e[jcounter]; for (l = 8; l < r + 8; l++){ l1[i][l] =
vn[jcounter][l - 8]; }
                                maxcoef1 = 0;}}//lmarker[i]
                maxcoef1 = 0;tempcounter = 0;}//i
        maxcoef1 = 0; tempcounter = 0;
        //max4
        for (i = 0; i < r; i++){
                if (lmarker[i] == -1){
                        opidentifier = bn[i][6];indexref = i;maxcounter[i] = 0;
                        maxcoef1 = 0; tempcounter = 0;
                        for (j = 0; j < r; j++){mc = 0;
                                if (indexm[j][3] == indexref && opEigen[j] == opidentifier){
                                        for (k = 0; k < r; k++){ if (j == lmarker[k]){ mc = mc +
1; } }
                                        if (mc == 0){maxcounter[i] = maxcounter[i] + 1;}}}//j
```

```
                        counter = maxcounter[i];
                        if (counter != 0){
                                double *tempcoef = new double[counter];*tempcoef = 0;
                                int *tempindex = new int[counter];*tempindex = 0;
                                for (j = 0; j < r; j++){mc = 0;
                                        if (indexm[j][3] == indexref && opEigen[j] ==
opidentifier){
                                                for (k = 0; k < r; k++){ if (j == lmarker[k]){ mc
= mc + 1; } }
                                                if (mc == 0){
                                                        tempcoef[tempcounter] = coefm[j][3];
tempindex[tempcounter] = j;
                                                        tempcounter = tempcounter + 1;}}}//j
                                for (j = 0; j < counter; j++){ if (tempcoef[j] >= maxcoef1){
maxcoef1 = tempcoef[j]; lmarker[i] = tempindex[j]; } }
                                jcounter = lmarker[i];
                                l1[i][7] = e[jcounter]; for (l = 8; l < r + 8; l++){ l1[i][l] =
vn[jcounter][l - 8]; }
                                maxcoef1 = 0;}}//lmarker[i]
                maxcoef1 = 0;tempcounter = 0;}//i
        maxcoef1 = 0; tempcounter = 0;
        //max5
        for (i = 0; i < r; i++){
                if (lmarker[i] == -1){
                        opidentifier = bn[i][6];indexref = i;maxcounter[i] = 0;
                        maxcoef1 = 0; tempcounter = 0;
                        for (j = 0; j < r; j++){mc = 0;
                                if (indexm[j][4] == indexref && opEigen[j] == opidentifier){
                                        for (k = 0; k < r; k++){ if (j == lmarker[k]){ mc = mc +
1; } }
                                        if (mc == 0){maxcounter[i] = maxcounter[i] + 1;}}}//j
                        counter = maxcounter[i];
                        if (counter != 0){
                                double *tempcoef = new double[counter];*tempcoef = 0;
                                int *tempindex = new int[counter];*tempindex = 0;
                                for (j = 0; j < r; j++){mc = 0;
                                        if (indexm[j][4] == indexref && opEigen[j] ==
opidentifier){
                                                for (k = 0; k < r; k++){ if (j == lmarker[k]){ mc
= mc + 1; } }
                                                if (mc == 0){
                                                        tempcoef[tempcounter] = coefm[j][4];
tempindex[tempcounter] = j;
                                                        tempcounter = tempcounter + 1;}}}//j
                                for (j = 0; j < counter; j++){ if (tempcoef[j] >= maxcoef1){
maxcoef1 = tempcoef[j]; lmarker[i] = tempindex[j]; } }
                                jcounter = lmarker[i];
                                l1[i][7] = e[jcounter]; for (l = 8; l < r + 8; l++){ l1[i][l] =
vn[jcounter][l - 8]; }
                                maxcoef1 = 0;}}//lmarker[i]
                maxcoef1 = 0;tempcounter = 0;}//i
        maxcoef1 = 0; tempcounter = 0;
        //max6
        for (i = 0; i < r; i++){
                if (lmarker[i] == -1){
                        opidentifier = bn[i][6];indexref = i;maxcounter[i] = 0;
                        maxcoef1 = 0; tempcounter = 0;
                        for (j = 0; j < r; j++){mc = 0;
                                if (indexm[j][5] == indexref && opEigen[j] == opidentifier){
                                        for (k = 0; k < r; k++){ if (j == lmarker[k]){ mc = mc +
1; } }
                                        if (mc == 0){maxcounter[i] = maxcounter[i] + 1;}}}//j
                        counter = maxcounter[i];
                        if (counter != 0){
                                double *tempcoef = new double[counter];*tempcoef = 0;
                                int *tempindex = new int[counter];*tempindex = 0;
                                for (j = 0; j < r; j++){mc = 0;
                                        if (indexm[j][5] == indexref && opEigen[j] ==
opidentifier){
```

```
                                                for (k = 0; k < r; k++){ if (j == lmarker[k]){ mc
= mc + 1; } }
                                                if (mc == 0){
                                                        tempcoef[tempcounter] = coefm[j][5];
tempindex[tempcounter] = j;
                                                        tempcounter = tempcounter + 1;}}//j
                                        for (j = 0; j < counter; j++){ if (tempcoef[j] >= maxcoef1){
maxcoef1 = tempcoef[j]; lmarker[i] = tempindex[j]; } }
                                        jcounter = lmarker[i];
                                        l1[i][7] = e[jcounter]; for (l = 8; l < r + 8; l++){ l1[i][l] =
vn[jcounter][l - 8]; }
                                        maxcoef1 = 0;}}//lmarker[i]
                        maxcoef1 = 0;tempcounter = 0;}//i
                maxcoef1 = 0; tempcounter = 0;
                for (i = 0; i<r; i++){ for (j = 0; j<r + 8; j++){ lf[i][j] = l1[i][j]; } }
                for (i = 0; i<r; i++){ if (lmarker[i] == -1){ cout << "there is bug for F=" << bn[1][4] <<
"and basis number=" << i << "\n"; } }
                maxcoef1 = 0; maxcoef2 = 0; maxcoef3 = 0; maxcoef4 = 0;

                return lf;}
```

A-3 Finding the *ortho-para* mixed states

```
#include <stdio.h>
#include <iostream>
#include <fstream>
#include <iomanip>
#include <complex>
#include <math.h>
using namespace std;
double maxfunc(double, double);
double minfunc(double, double);
int main(){
        int i, j;
        int const Fmax = 30;
        int dim[Fmax + 1][2];
        ifstream indim;
        indim.open("dim.txt");
        for (i = 0; i<Fmax + 1; i++){ for (j = 0; j<2; j++){ indim >> dim[i][j]; } }
        int totald;totald = 0;
        for (i = 0; i <= Fmax; i++){ totald = totald + dim[i][1];
        cout << "totald=" << totald << "\n";
        double **energy = 0; //energy:termenergy and wavefunction
        energy = new double *[totald];
        for (i = 0; i<totald; i++)energy[i] = new double[11];
        double **basisset = 0; //basissetbasisset = new double *[totald];
        for (i = 0; i<totald; i++)basisset[i] = new double[7];
        ifstream inenergy;
        inenergy.open("opcharE.txt");
        for (i = 0; i<totald; i++){ for (j = 0; j<11; j++){ inenergy >> energy[i][j]; } }
        ifstream inbasis;
        inbasis.open("basisset.txt");
        for (i = 0; i<totald; i++){ for (j = 0; j<7; j++){ inbasis >> basisset[i][j]; } }
        cout << "end of reading input files" << "\n";
        double dEcrit, opcrit, cu, cl;
        dEcrit = 1e-16;opcrit = 1e-4;cl = 0.002;cu = 1 - cl;
        cout << "dEcrit=" << dEcrit << "\n";
        int opcount;opcount = 0;
        for (i = 0; i < totald; i++){
                for (j = 0; j <totald; j++){
                        if (energy[i][4] == energy[j][4] && energy[i][6] != energy[j][6] &&
abs(energy[i][8] - energy[j][9]) <= 1e-3 && energy[i][8] >= cl && energy[i][8] <= cu)
                        {opcount = opcount + 1;}}}//i
        cout << "opcount=" << opcount << "\n";
        double **op = 0; op = new double *[opcount];
        for (i = 0; i<opcount; i++)op[i] = new double[17];
        opcount = 0;
        for (i = 0; i < totald; i++){
                for (j = 0; j < totald; j++){
                        if (energy[i][4] == energy[j][4] && energy[i][6] != energy[j][6] &&
abs(energy[i][8] - energy[j][9]) <= 1e-3 && energy[i][8] >= cl && energy[i][8] <= cu)
                        {
                                op[opcount][0] = energy[i][0]; op[opcount][1] = energy[i][1];
op[opcount][2] = energy[i][2];
                                op[opcount][3] = energy[i][3]; op[opcount][4] = energy[i][4];
op[opcount][5] = energy[i][6];
                                op[opcount][6] = energy[i][7];
                                op[opcount][7] = energy[j][0]; op[opcount][8] = energy[j][1];
op[opcount][9] = energy[j][2];
                                op[opcount][10] = energy[j][3]; op[opcount][11] = energy[j][4];
op[opcount][12] = energy[j][6];
                                op[opcount][13] = energy[j][7];
                                op[opcount][14] = energy[i][8];
                                op[opcount][15] = abs(energy[i][7] - energy[j][7]);
                                op[opcount][16] = energy[j][8];
                                opcount = opcount + 1;}}}//i
        cout << "opcount=" << opcount << "\n";
        ofstream orthpara;
```

```
        orthpara.open("OPE.txt");
        orthpara << fixed << setprecision(8);
        orthpara << "J" << "\t" << "Ka" << "\t" << "Kc" << "\t" << "I" << "\t" << "F" << "\t" <<
"op" << "\t" << "termvalue" << "\t" << "J" << "\t" << "Ka" << "\t" << "Kc" << "\t" << "I" << "\t"
<< "F" << "\t" << "op" << "\t" << "termvalue" << "\t" << "mixing ratio" << "\t" << "dEop" << "\t"
<< "dJ" << "\n";
        for (i = 0; i<opcount; i++){
                for (j = 0; j<17; j++){ orthpara << op[i][j] << "\t"; }
                orthpara << "\n";}
        orthpara.close();
        int jutemp, kautemp, kcutemp, iutemp, futemp;
        int jltemp, kaltemp, kcltemp, iltemp, fltemp;
        int transcount;
        int jtemp, katemp, kctemp;
        transcount = 0;
        for (i = 0; i<opcount; i++){
                if (op[i][15] >= dEcrit){
                        jutemp = op[i][7]; kautemp = op[i][8]; kcutemp = op[i][9]; iutemp =
op[i][10]; futemp = op[i][11];
                        jtemp = jutemp; katemp = kautemp + 1; kctemp = kcutemp + 1;
                        if ((katemp + kctemp == jtemp) || (katemp + kctemp == jtemp + 1)){
transcount = transcount + 1; }
                        jtemp = jutemp; katemp = kautemp + 1; kctemp = kcutemp - 1;
                        if ((katemp + kctemp == jtemp) || (katemp + kctemp == jtemp + 1)){
transcount = transcount + 1; }
                        jtemp = jutemp; katemp = kautemp - 1; kctemp = kcutemp + 1;
                        if ((katemp + kctemp == jtemp) || (katemp + kctemp == jtemp + 1)){
transcount = transcount + 1; }
                        jtemp = jutemp; katemp = kautemp - 1; kctemp = kcutemp - 1;
                        if ((katemp + kctemp == jtemp) || (katemp + kctemp == jtemp + 1)){
transcount = transcount + 1; }
                        jtemp = jutemp - 1; katemp = kautemp + 1; kctemp = kcutemp + 1;
                        if ((katemp + kctemp == jtemp) || (katemp + kctemp == jtemp + 1)){
transcount = transcount + 1; }
                        jtemp = jutemp - 1; katemp = kautemp + 1; kctemp = kcutemp - 1;
                        if ((katemp + kctemp == jtemp) || (katemp + kctemp == jtemp + 1)){
transcount = transcount + 1; }
                        jtemp = jutemp - 1; katemp = kautemp - 1; kctemp = kcutemp + 1;
                        if ((katemp + kctemp == jtemp) || (katemp + kctemp == jtemp + 1)){
transcount = transcount + 1; }
                        jtemp = jutemp - 1; katemp = kautemp - 1; kctemp = kcutemp - 1;
                        if ((katemp + kctemp == jtemp) || (katemp + kctemp == jtemp + 1)){
transcount = transcount + 1; }
                        jtemp = jutemp + 1; katemp = kautemp + 1; kctemp = kcutemp + 1;
                        if ((katemp + kctemp == jtemp) || (katemp + kctemp == jtemp + 1)){
transcount = transcount + 1; }
                        jtemp = jutemp + 1; katemp = kautemp + 1; kctemp = kcutemp - 1;
                        if ((katemp + kctemp == jtemp) || (katemp + kctemp == jtemp + 1)){
transcount = transcount + 1; }
                        jtemp = jutemp + 1; katemp = kautemp - 1; kctemp = kcutemp + 1;
                        if ((katemp + kctemp == jtemp) || (katemp + kctemp == jtemp + 1)){
transcount = transcount + 1; }
                        jtemp = jutemp + 1; katemp = kautemp - 1; kctemp = kcutemp - 1;
                        if ((katemp + kctemp == jtemp) || (katemp + kctemp == jtemp + 1)){
transcount = transcount + 1; }
                }}//i
        cout << "transcount=" << transcount << "\n";
        double **trans = 0;trans = new double *[transcount];
        for (i = 0; i<transcount; i++)trans[i] = new double[18];
        transcount = 0;
        for (i = 0; i<opcount; i++){
                if (op[i][15] >= dEcrit){
                        jutemp = op[i][7]; kautemp = op[i][8]; kcutemp = op[i][9]; iutemp =
op[i][10]; futemp = op[i][11];
                        jtemp = jutemp; katemp = kautemp + 1; kctemp = kcutemp + 1;
                        if ((katemp + kctemp == jtemp) || (katemp + kctemp == jtemp + 1)){
                                jltemp = jtemp; kaltemp = katemp, kcltemp = kctemp, iltemp =
iutemp, fltemp = futemp;
```

```
                                trans[transcount][0] = jutemp; trans[transcount][1] = kautemp;
trans[transcount][2] = kcutemp;
                                trans[transcount][3] = iutemp; trans[transcount][4] = futemp;
trans[transcount][5] = op[i][13];
                                trans[transcount][6] = jltemp; trans[transcount][7] = kaltemp;
trans[transcount][8] = kcltemp;
                                trans[transcount][9] = iltemp; trans[transcount][10] = fltemp;
                                trans[transcount][11] = op[i][0]; trans[transcount][12] =
op[i][1]; trans[transcount][13] = op[i][2];
                                trans[transcount][14] = op[i][3]; trans[transcount][15] =
op[i][4]; trans[transcount][16] = op[i][6];
                                trans[transcount][17] = op[i][14];
                                transcount = transcount + 1;}
                        jtemp = jutemp; katemp = kautemp + 1; kctemp = kcutemp - 1;
                        if ((katemp + kctemp == jtemp) || (katemp + kctemp == jtemp + 1)){
                                jltemp = jtemp; kaltemp = katemp, kcltemp = kctemp, iltemp =
iutemp, fltemp = futemp;
                                trans[transcount][0] = jutemp; trans[transcount][1] = kautemp;
trans[transcount][2] = kcutemp;
                                trans[transcount][3] = iutemp; trans[transcount][4] = futemp;
trans[transcount][5] = op[i][13];
                                trans[transcount][6] = jltemp; trans[transcount][7] = kaltemp;
trans[transcount][8] = kcltemp;
                                trans[transcount][9] = iltemp; trans[transcount][10] = fltemp;
                                trans[transcount][11] = op[i][0]; trans[transcount][12] =
op[i][1]; trans[transcount][13] = op[i][2];
                                trans[transcount][14] = op[i][3]; trans[transcount][15] =
op[i][4]; trans[transcount][16] = op[i][6];
                                trans[transcount][17] = op[i][14];
                                transcount = transcount + 1;}
                        jtemp = jutemp; katemp = kautemp - 1; kctemp = kcutemp + 1;
                        if ((katemp + kctemp == jtemp) || (katemp + kctemp == jtemp + 1)){
                                jltemp = jtemp; kaltemp = katemp, kcltemp = kctemp, iltemp =
iutemp, fltemp = futemp;
                                trans[transcount][0] = jutemp; trans[transcount][1] = kautemp;
trans[transcount][2] = kcutemp;
                                trans[transcount][3] = iutemp; trans[transcount][4] = futemp;
trans[transcount][5] = op[i][13];
                                trans[transcount][6] = jltemp; trans[transcount][7] = kaltemp;
trans[transcount][8] = kcltemp;
                                trans[transcount][9] = iltemp; trans[transcount][10] = fltemp;
                                trans[transcount][11] = op[i][0]; trans[transcount][12] =
op[i][1]; trans[transcount][13] = op[i][2];
                                trans[transcount][14] = op[i][3]; trans[transcount][15] =
op[i][4]; trans[transcount][16] = op[i][6];
                                trans[transcount][17] = op[i][14];
                                transcount = transcount + 1;}
                        jtemp = jutemp; katemp = kautemp - 1; kctemp = kcutemp - 1;
                        if ((katemp + kctemp == jtemp) || (katemp + kctemp == jtemp + 1)){
                                jltemp = jtemp; kaltemp = katemp, kcltemp = kctemp, iltemp =
iutemp, fltemp = futemp;
                                trans[transcount][0] = jutemp; trans[transcount][1] = kautemp;
trans[transcount][2] = kcutemp;
                                trans[transcount][3] = iutemp; trans[transcount][4] = futemp;
trans[transcount][5] = op[i][13];
                                trans[transcount][6] = jltemp; trans[transcount][7] = kaltemp;
trans[transcount][8] = kcltemp;
                                trans[transcount][9] = iltemp; trans[transcount][10] = fltemp;
                                trans[transcount][11] = op[i][0]; trans[transcount][12] =
op[i][1]; trans[transcount][13] = op[i][2];
                                trans[transcount][14] = op[i][3]; trans[transcount][15] =
op[i][4]; trans[transcount][16] = op[i][6];
                                trans[transcount][17] = op[i][14];
                                transcount = transcount + 1;}
                        jtemp = jutemp - 1; katemp = kautemp + 1; kctemp = kcutemp + 1;
                        if ((katemp + kctemp == jtemp) || (katemp + kctemp == jtemp + 1)){
                                jltemp = jtemp; kaltemp = katemp, kcltemp = kctemp, iltemp =
iutemp, fltemp = futemp - 1;
```

```
                                trans[transcount][0] = jutemp; trans[transcount][1] = kautemp;
trans[transcount][2] = kcutemp;
                                trans[transcount][3] = iutemp; trans[transcount][4] = futemp;
trans[transcount][5] = op[i][13];
                                trans[transcount][6] = jltemp; trans[transcount][7] = kaltemp;
trans[transcount][8] = kcltemp;
                                trans[transcount][9] = iltemp; trans[transcount][10] = fltemp;
                                trans[transcount][11] = op[i][0]; trans[transcount][12] =
op[i][1]; trans[transcount][13] = op[i][2];
                                trans[transcount][14] = op[i][3]; trans[transcount][15] =
op[i][4]; trans[transcount][16] = op[i][6];
                                trans[transcount][17] = op[i][14];
                                transcount = transcount + 1;}
                        jtemp = jutemp - 1; katemp = kautemp + 1; kctemp = kcutemp - 1;
                        if ((katemp + kctemp == jtemp) || (katemp + kctemp == jtemp + 1)){
                                jltemp = jtemp; kaltemp = katemp, kcltemp = kctemp, iltemp =
iutemp, fltemp = futemp - 1;
                                trans[transcount][0] = jutemp; trans[transcount][1] = kautemp;
trans[transcount][2] = kcutemp;
                                trans[transcount][3] = iutemp; trans[transcount][4] = futemp;
trans[transcount][5] = op[i][13];
                                trans[transcount][6] = jltemp; trans[transcount][7] = kaltemp;
trans[transcount][8] = kcltemp;
                                trans[transcount][9] = iltemp; trans[transcount][10] = fltemp;
                                trans[transcount][11] = op[i][0]; trans[transcount][12] =
op[i][1]; trans[transcount][13] = op[i][2];
                                trans[transcount][14] = op[i][3]; trans[transcount][15] =
op[i][4]; trans[transcount][16] = op[i][6];
                                trans[transcount][17] = op[i][14];
                                transcount = transcount + 1;}
                        jtemp = jutemp - 1; katemp = kautemp - 1; kctemp = kcutemp + 1;
                        if ((katemp + kctemp == jtemp) || (katemp + kctemp == jtemp + 1)){
                                jltemp = jtemp; kaltemp = katemp, kcltemp = kctemp, iltemp =
iutemp, fltemp = futemp - 1;
                                trans[transcount][0] = jutemp; trans[transcount][1] = kautemp;
trans[transcount][2] = kcutemp;
                                trans[transcount][3] = iutemp; trans[transcount][4] = futemp;
trans[transcount][5] = op[i][13];
                                trans[transcount][6] = jltemp; trans[transcount][7] = kaltemp;
trans[transcount][8] = kcltemp;
                                trans[transcount][9] = iltemp; trans[transcount][10] = fltemp;
                                trans[transcount][11] = op[i][0]; trans[transcount][12] =
op[i][1]; trans[transcount][13] = op[i][2];
                                trans[transcount][14] = op[i][3]; trans[transcount][15] =
op[i][4]; trans[transcount][16] = op[i][6];
                                trans[transcount][17] = op[i][14];
                                transcount = transcount + 1;}
                        jtemp = jutemp - 1; katemp = kautemp - 1; kctemp = kcutemp - 1;
                        if ((katemp + kctemp == jtemp) || (katemp + kctemp == jtemp + 1)){
                                jltemp = jtemp; kaltemp = katemp, kcltemp = kctemp, iltemp =
iutemp, fltemp = futemp - 1;
                                trans[transcount][0] = jutemp; trans[transcount][1] = kautemp;
trans[transcount][2] = kcutemp;
                                trans[transcount][3] = iutemp; trans[transcount][4] = futemp;
trans[transcount][5] = op[i][13];
                                trans[transcount][6] = jltemp; trans[transcount][7] = kaltemp;
trans[transcount][8] = kcltemp;
                                trans[transcount][9] = iltemp; trans[transcount][10] = fltemp;
                                trans[transcount][11] = op[i][0]; trans[transcount][12] =
op[i][1]; trans[transcount][13] = op[i][2];
                                trans[transcount][14] = op[i][3]; trans[transcount][15] =
op[i][4]; trans[transcount][16] = op[i][6];
                                trans[transcount][17] = op[i][14];
                                transcount = transcount + 1;}
                        jtemp = jutemp + 1; katemp = kautemp + 1; kctemp = kcutemp + 1;
                        if ((katemp + kctemp == jtemp) || (katemp + kctemp == jtemp + 1)){
                                jltemp = jtemp; kaltemp = katemp, kcltemp = kctemp, iltemp =
iutemp, fltemp = futemp + 1;
```

```
                                trans[transcount][0] = jutemp; trans[transcount][1] = kautemp;
trans[transcount][2] = kcutemp;
                                trans[transcount][3] = iutemp; trans[transcount][4] = futemp;
trans[transcount][5] = op[i][13];
                                trans[transcount][6] = jltemp; trans[transcount][7] = kaltemp;
trans[transcount][8] = kcltemp;
                                trans[transcount][9] = iltemp; trans[transcount][10] = fltemp;
                                trans[transcount][11] = op[i][0]; trans[transcount][12] =
op[i][1]; trans[transcount][13] = op[i][2];
                                trans[transcount][14] = op[i][3]; trans[transcount][15] =
op[i][4]; trans[transcount][16] = op[i][6];
                                trans[transcount][17] = op[i][14];
                                transcount = transcount + 1;}
                        jtemp = jutemp + 1; katemp = kautemp + 1; kctemp = kcutemp - 1;
                        if ((katemp + kctemp == jtemp) || (katemp + kctemp == jtemp + 1)){
                                jltemp = jtemp; kaltemp = katemp, kcltemp = kctemp, iltemp =
iutemp, fltemp = futemp + 1;
                                trans[transcount][0] = jutemp; trans[transcount][1] = kautemp;
trans[transcount][2] = kcutemp;
                                trans[transcount][3] = iutemp; trans[transcount][4] = futemp;
trans[transcount][5] = op[i][13];
                                trans[transcount][6] = jltemp; trans[transcount][7] = kaltemp;
trans[transcount][8] = kcltemp;
                                trans[transcount][9] = iltemp; trans[transcount][10] = fltemp;
                                trans[transcount][11] = op[i][0]; trans[transcount][12] =
op[i][1]; trans[transcount][13] = op[i][2];
                                trans[transcount][14] = op[i][3]; trans[transcount][15] =
op[i][4]; trans[transcount][16] = op[i][6];
                                trans[transcount][17] = op[i][14];
                                transcount = transcount + 1;}
                        jtemp = jutemp + 1; katemp = kautemp - 1; kctemp = kcutemp + 1;
                        if ((katemp + kctemp == jtemp) || (katemp + kctemp == jtemp + 1)){
                                jltemp = jtemp; kaltemp = katemp, kcltemp = kctemp, iltemp =
iutemp, fltemp = futemp + 1;
                                trans[transcount][0] = jutemp; trans[transcount][1] = kautemp;
trans[transcount][2] = kcutemp;
                                trans[transcount][3] = iutemp; trans[transcount][4] = futemp;
trans[transcount][5] = op[i][13];
                                trans[transcount][6] = jltemp; trans[transcount][7] = kaltemp;
trans[transcount][8] = kcltemp;
                                trans[transcount][9] = iltemp; trans[transcount][10] = fltemp;
                                trans[transcount][11] = op[i][0]; trans[transcount][12] =
op[i][1]; trans[transcount][13] = op[i][2];
                                trans[transcount][14] = op[i][3]; trans[transcount][15] =
op[i][4]; trans[transcount][16] = op[i][6];
                                trans[transcount][17] = op[i][14];
                                transcount = transcount + 1;}
                        jtemp = jutemp + 1; katemp = kautemp - 1; kctemp = kcutemp - 1;
                        if ((katemp + kctemp == jtemp) || (katemp + kctemp == jtemp + 1)){
                                jltemp = jtemp; kaltemp = katemp, kcltemp = kctemp, iltemp =
iutemp, fltemp = futemp + 1;
                                trans[transcount][0] = jutemp; trans[transcount][1] = kautemp;
trans[transcount][2] = kcutemp;
                                trans[transcount][3] = iutemp; trans[transcount][4] = futemp;
trans[transcount][5] = op[i][13];
                                trans[transcount][6] = jltemp; trans[transcount][7] = kaltemp;
trans[transcount][8] = kcltemp;
                                trans[transcount][9] = iltemp; trans[transcount][10] = fltemp;
                                trans[transcount][11] = op[i][0]; trans[transcount][12] =
op[i][1]; trans[transcount][13] = op[i][2];
                                trans[transcount][14] = op[i][3]; trans[transcount][15] =
op[i][4]; trans[transcount][16] = op[i][6];
                                trans[transcount][17] = op[i][14];
                                transcount = transcount + 1;}}}//i
        cout << "transcount=" << transcount << "\n";
        ofstream optrans;
        optrans.open("OPtransE.txt");
        optrans << fixed << setprecision(8);
```

```
        optrans << "Junormal" << "\t" << "Kaunormal" << "\t" << "Kcunormal" << "\t" << "Iunormal"
<< "\t" << "Funormal" << "\t" << "termunormal" << "\t" << "jlnormal" << "\t" << "kalnormal" <<
"\t" << "kclnormal" << "\t" << "Ilnormal" << "\t" << "Flnormal" << "\t" << "Jf" << "\t" << "Kaf"
<< "\t" << "Kcf" << "\t" << "If" << "\t" << "Ff" << "\t" << "termf" << "\t" << "mixing" << "\n";
        for (i = 0; i<transcount; i++){
                for (j = 0; j<18; j++){ optrans << trans[i][j] << "\t"; }
                optrans << "\n";}
        optrans.close();
}//main int
```

A-4 calculation of the transition moment

```
#include <stdio.h>
#include <iostream>
#include <fstream>
#include <iomanip>
#include <complex>
#include <math.h>
using namespace std;
double dipole(int, int, int, int, int, int, int, int);
double maxfunc(double, double);
double minfunc(double, double);
int main(){
        int const c = 10;
        int const r = 256;
        double lines[r][c];
        double finten[r][14];
        int i, j;
        int const Fmax = 30;
        int dim[Fmax + 1][2];
        cout << fixed << setprecision(18);
        ifstream inlines;
        inlines.open("input.txt");
        for (i = 0; i<r; i++){ for (j = 0; j<c; j++){ inlines >> lines[i][j]; } }
        for (i = 0; i<r; i++){ for (j = 0; j<c; j++){ finten[i][j] = lines[i][j]; } }
        ifstream indim;
        indim.open("20141205dim.txt");
        for (i = 0; i<Fmax + 1; i++){ for (j = 0; j<2; j++){ indim >> dim[i][j]; } }
        int totald;totald = 0;
        for (i = 0; i <= Fmax; i++){ totald = totald + dim[i][1]; }
        cout << "totald=" << totald << "\n";
        complex <double> **energyc = 0; //energy:termenergy and wavefunction
        energyc = new complex <double> *[totald];
        for (i = 0; i<totald; i++)energyc[i] = new complex <double>[totald + 8];
        double **basisset = 0; basisset = new double *[totald];
        for (i = 0; i<totald; i++)basisset[i] = new double[7];
        ifstream inenergy;
        inenergy.open("termEcE0.txt");
        for (i = 0; i<totald; i++){ for (j = 0; j<totald + 8; j++){ inenergy >> energyc[i][j]; } }
        ifstream inbasis;
        inbasis.open("20141205basisset.txt");
        for (i = 0; i<totald; i++){ for (j = 0; j<7; j++){ inbasis >> basisset[i][j]; } }
        cout << "end of reding input files" << "\n";
        //start of calculating intensity
        double Fmax1, Fmax2, fmax, Fmin1, Fmin2, fmin;
        Fmin1 = lines[0][4]; Fmin2 = lines[0][4]; Fmax1 = 0; Fmax2 = 0;
        for (i = 0; i<r; i++){
                Fmax1 = maxfunc(lines[i][4], Fmax1); Fmax2 = maxfunc(lines[i][9], Fmax2);
                Fmin1 = minfunc(lines[i][4], Fmin1); Fmin2 = minfunc(lines[i][9], Fmin2);}
        fmax = maxfunc(Fmax1, Fmax2); fmin = minfunc(Fmin1, Fmin2);
        cout << "fmin=" << fmin << "\t" << "fmax=" << fmax << "\n";
        int lindex, uindex, lcounter;
        int Ju, Jl, Kau, Kal, Kcu, Kcl, IIu, IIl, Fu, Fl;
        int du, dl;
        lindex = 0;uindex = 0;
        for (i = 0; i<fmin; i++){ lindex = lindex + dim[i][1]; }
        for (i = 0; i<fmax + 1; i++){ uindex = uindex + dim[i][1]; }
        lindex = (lindex);uindex = (uindex)-1;
        cout << "indexu=" << uindex << "\t" << "indexl=" << lindex << "\n";
        for (lcounter = 0; lcounter<r; lcounter++){
                Ju = lines[lcounter][0]; Kau = lines[lcounter][1]; Kcu = lines[lcounter][2]; IIu
= lines[lcounter][3]; Fu = lines[lcounter][4];
                Jl = lines[lcounter][5]; Kal = lines[lcounter][6]; Kcl = lines[lcounter][7]; IIl
= lines[lcounter][8]; Fl = lines[lcounter][9];
                for (i = fmin; i <= fmax; i++){
                        if (Fu == dim[i][0]){ du = dim[i][1]; }
                        if (Fl == dim[i][0]){ dl = dim[i][1]; }}
```

```
		int *ju = new int[du]; *ju = 1;
		int *kau = new int[du]; *kau = 1;
		int *kcu = new int[du]; *kcu = 1;
		int *Iu = new int[du]; *Iu = 1;
		int *symu = new int[du]; *symu = 1;
		int *jl = new int[dl]; *jl = 1;
		int *kal = new int[dl]; *kal = 1;
		int *kcl = new int[dl]; *kcl = 1;
		int *Il = new int[dl]; *Il = 1;
		int *syml = new int[dl]; *syml = 1;
		complex <double> *coefu = new complex <double>[du]; *coefu = 0.0;
		complex <double> *coefl = new complex <double>[dl]; *coefl = 0.0;
		int uc, lc;
		uc = 0; lc = 0;
		double Eu, El, T1, T2;
		T1 = 4.17e+5;//20k jet exp
		T2 = 4.17E+6;//200K cell exp
		for (i = lindex; i <= uindex; i++){
			if (Fu == basisset[i][4]){
				ju[uc] = basisset[i][0]; kau[uc] = basisset[i][1]; kcu[uc] =
basisset[i][2];
				Iu[uc] = basisset[i][3]; symu[uc] = basisset[i][6]; uc = uc + 1;}
			if (Fl == basisset[i][4]){
				jl[lc] = basisset[i][0]; kal[lc] = basisset[i][1]; kcl[lc] =
basisset[i][2];
				Il[lc] = basisset[i][3]; syml[lc] = basisset[i][6]; lc = lc +
1;}}
		for (i = lindex; i <= uindex; i++){
			if (Ju == real(energyc[i][0]) && Kau == real(energyc[i][1]) && Kcu ==
real(energyc[i][2]) && IIu == real(energyc[i][3]) && Fu == real(energyc[i][4]))
			{for (j = 0; j<du; j++){ coefu[j] = energyc[i][j + 8]; }Eu =
real(energyc[i][7]);}
			if (Jl == real(energyc[i][0]) && Kal == real(energyc[i][1]) && Kcl ==
real(energyc[i][2]) && IIl == real(energyc[i][3]) && Fl == real(energyc[i][4]))
			{for (j = 0; j<dl; j++){ coefl[j] = energyc[i][j + 8]; }El =
real(energyc[i][7]);}}
		double re, im, intensity;
		re = 0;im = 0;
		double factor2, factor1;
		int lg, ug, type;
		double siu, sil, sisum;
		for (i = 0; i<du; i++){
			for (j = 0; j<dl; j++){
				if (abs(kau[i] - kal[j]) % 2 == 0){
					if ((symu[i] == syml[j]) && (abs(ju[i] - jl[j]) == 1)){
type = 0; } //0 means a type
					if ((abs(symu[i] - syml[j]) % 2 == 1) && (abs(ju[i] -
jl[j]) == 0)){ type = 0; }}
				if (abs(kau[i] - kal[j]) % 2 == 1){
					if ((abs(symu[i] - syml[j]) % 2 == 0) && (abs(ju[i] -
jl[j]) == 1)){ type = -1; } //-1 means c type
					if ((abs(symu[i] - syml[j]) % 2 == 1) && (abs(ju[i] -
jl[j]) == 0)){ type = -1; }
					if ((abs(symu[i] - syml[j]) % 2 == 0) && (abs(ju[i] -
jl[j]) == 0)){ type = 1; }// 1 means b type
					if ((abs(symu[i] - syml[j]) % 2 == 1) && (abs(ju[i] -
jl[j]) == 1)){ type = 1; }
					if ((abs(ju[i] - jl[j]) != 1) && (abs(ju[i] - jl[j]) !=
0)){ type = 2; } }
				factor1 = (real(coefu[i]) * real(coefl[j])) +
(imag(coefu[i])*imag(coefl[j]));
				factor2 = (real(coefl[j]) * imag(coefu[i])) -
(real(coefu[i])*imag(coefl[j]));
				if (symu[i] % 2 == 0){ ug = 0; }else{ ug = 1; }
				if (syml[j] % 2 == 0){ lg = 0; }else{ lg = 1; }
				if (ug == 0){ siu = 1; }else{ siu = -1; }
				if (lg == 0){ sil = 1; }else{ sil = -1; }
				if ((ug + lg) % 2 == 0){ sisum = 1; }else{ sisum = -1; }
				if (kau[i] * kal[j] != 0){
```

```
                                        re = re + ((factor1 / 2)*(dipole(ju[i], jl[j], kau[i],
kal[j], Iu[i], Il[j], Fu, Fl)
                                                + siu*dipole(ju[i], jl[j], -kau[i], kal[j],
Iu[i], Il[j], Fu, Fl)
                                                + sil*dipole(ju[i], jl[j], kau[i], -kal[j],
Iu[i], Il[j], Fu, Fl)
                                                + sisum*dipole(ju[i], jl[j], -kau[i], -kal[j],
Iu[i], Il[j], Fu, Fl)));}
                                if (kau[i] == 0 && kal[j] != 0){
                                        re = re + ((factor1 / sqrt(2.0))*(dipole(ju[i], jl[j], 0,
kal[j], Iu[i], Il[j], Fu, Fl)
                                                + sil*dipole(ju[i], jl[j], 0, -kal[j], Iu[i],
Il[j], Fu, Fl)));}
                                if (kau[i] != 0 && kal[j] == 0){
                                        re = re + ((factor1 / sqrt(2.0))*(dipole(ju[i], jl[j],
kau[i], 0, Iu[i], Il[j], Fu, Fl)
                                                + siu*dipole(ju[i], jl[j], -kau[i], 0, Iu[i],
Il[j], Fu, Fl)));}
                                if (kau[i] == 0 && kal[i] == 0){
                                        re = re + (factor1*dipole(ju[i], jl[j], 0, 0, Iu[i],
Il[j], Fu, Fl));}
                                if (kau[i] * kal[j] != 0){
                                        im = im + ((factor2 / 2)*(dipole(ju[i], jl[j], kau[i],
kal[j], Iu[i], Il[j], Fu, Fl)
                                                + siu*dipole(ju[i], jl[j], -kau[i], kal[j],
Iu[i], Il[j], Fu, Fl)
                                                + sil*dipole(ju[i], jl[j], kau[i], -kal[j],
Iu[i], Il[j], Fu, Fl)
                                                + sisum*dipole(ju[i], jl[j], -kau[i], -kal[j],
Iu[i], Il[j], Fu, Fl)));}
                                if (kau[i] == 0 && kal[j] != 0){
                                        im = im + ((factor2 / sqrt(2.0))*(dipole(ju[i], jl[j], 0,
kal[j], Iu[i], Il[j], Fu, Fl)
                                                + sil*dipole(ju[i], jl[j], 0, -kal[j], Iu[i],
Il[j], Fu, Fl)));}
                                if (kau[i] != 0 && kal[j] == 0){
                                        im = im + ((factor2 / sqrt(2.0))*(dipole(ju[i], jl[j],
kau[i], 0, Iu[i], Il[j], Fu, Fl)
                                                + siu*dipole(ju[i], jl[j], -kau[i], 0, Iu[i],
Il[j], Fu, Fl)));}
                                if (kau[i] == 0 && kal[j] == 0){
                                        im = im + ((factor2)*(dipole(ju[i], jl[j], 0, 0, Iu[i],
Il[j], Fu, Fl)));}
                        }}// end i loop
                intensity = re*re + im*im;
                cout << "end of intensity for l=" << lcounter << "\n";
                finten[lcounter][10] = Eu - El;finten[lcounter][11] = intensity;
                finten[lcounter][12] = intensity*exp(-El / T2);finten[lcounter][13] =
intensity*exp(-El / T1);
        }//lcounter read each transition
        cout << "writing in text files" << "\n";
        ofstream intensityw;
        intensityw.open("output.txt");
        for (i = 0; i<r; i++){
                for (j = 0; j<14; j++){
                        intensityw << finten[i][j] << "\t";}
                intensityw << "\n";}
        intensityw.close();
        extern "C"
                double six_J(double A, double B, double C, double D, double E, double F);
        extern "C"
                double three_J(double J1, double J2, double J3, double M1, double M2, double M3);
        double dipole(int, int, int, int, int, int, int, int);
        double dipole(int ju, int jl, int ku, int kl, int Iu, int Il, int Fu, int Fl){
                double ans, si1, si2, sqrtterm, sixjterm;
                if ((Iu + Fl + 1 - kl + 1) % 2 == 0){ si1 = 1.0; }else{ si1 = -1.0; }
                if ((Iu + Fl + 1 - kl - 1) % 2 == 0){ si2 = 1.0; }else{ si2 = -1.0; }
                sqrtterm = (2 * Fu + 1)*(2 * Fl + 1)*(2 * ju + 1)*(2 * jl + 1);sqrtterm =
sqrt(sqrtterm);
```

```
                sixjterm = six_J(ju, Fu, Il, Fl, jl, 1.0);
                if (Iu != Il){ ans = 0; }
                else{
                        ans = sqrtterm*sixjterm*((-si1*three_J(ju, 1.0, jl, -ku, 1.0, kl)) +
(si2*three_J(ju, 1.0, jl, -ku, -1.0, kl))) / sqrt(2.0);
                }//else
                return ans;}
}//end of code int main
```

Appendix B

Least squares Fitting Analysis of Hyperfine Components

In the millimeter microwave spectroscopy of disulfur dichloride, as it is shown in Figures 4.3 in Chapter 4 and Figure 6.8 in Chapter 6, hyperfine splitting of transitions is observed as triplet spectrum patterns. In data analysis in Chapter 4, frequency of the center peak in each triplet spectrum is assumed as the observed frequency of the pure rotational transitions which are corresponded to the triplet pattern.

In this section, least square fitting analysis is done for all observe hyperfine components. In this analysis the observed hyperfine components by FTMW experiment are also considered[32]. By considering the accuracy of experiments, weight of FTMW data is assumed to be equal to 1 and weight of millimeter wave spectroscopy data is assumed to be equal to 0.01. By this assumption for weights, the weights of hyperfine components which are corresponded to each peak are chosen in a way that the sum of their weights is equal to the 0.01. Table B.1 and Table B.2 shows the list of all transitions which are included in the least squares fitting analysis. The observed frequency of each transition and $\nu_{o\text{-}c}$ magnitudes are also listed in these Tables. The assumed weight for each transition can be seen in these Tables. All transitions in these two Tables are included in the data analysis. The result of data analysis for hyperfine transitions is listed in Table B.1 and for normal transitions is listed in Table B.2. In Table B.3, the rotational molecular constants and hyperfine constants which are obtained from least squares fitting analysis are listed. The hyperfine constants which are obtained by millimeter-wave data analysis and FTMW data analysis[32] are compared in Table B.4. As Table B.4 shows, the hyperfine constants which are predicted by millimeter-wave data analysis are inside the prediction of the hyperfine constants by FTMW data analysis[32].

Table B.1: result of least squares fitting data analysis for hyperfine transitions.

$J'_{K'_aK'_c} - J''_{K''_aK''_c}$	$\nu_{obs.}$/MHz	ν_{o-c} /MHz[b]	weight	$J'_{K'_aK'_c} - J''_{K''_aK''_c}$	$\nu_{obs.}$/MHz	ν_{o-c} /MHz[b]	weight
$1_{11}2\ 1 - 0_{00}0\ 0$	6761.3020	0.0011	1.0000	$15_{106}2\ 13 - 15_{972}13$	80095.2205	0.0342	0.0013
$1_{11}2\ 1 - 0_{00}2\ 2$	6761.3540	0.0055	1.0000	$15_{106}2\ 16 - 15_{972}16$	80095.2205	0.0341	0.0013
$1_{11}2\ 2 - 0_{00}2\ 2$	6765.8590	-0.0040	1.0000	$15_{105}3\ 17 - 15_{963}17$	80095.2205	-0.0441	0.0013
$1_{11}2\ 3 - 0_{00}2\ 2$	6766.3770	0.0021	1.0000	$15_{105}3\ 14 - 15_{963}14$	80095.7125	0.1315	0.0025
$1_{11}0\ 1 - 0_{00}0\ 0$	6771.2440	0.0016	1.0000	$15_{105}3\ 15 - 15_{963}15$	80095.7125	0.0976	0.0025
$1_{11}0\ 1 - 0_{00}2\ 2$	6771.2840	-0.0061	1.0000	$15_{106}0\ 15 - 15_{970}15$	80095.7125	0.0866	0.0025
$1_{10}3\ 2 - 1_{01}1\ 2$	4293.8670	0.0061	1.0000	$15_{105}3\ 16 - 15_{963}16$	80095.7125	0.0483	0.0025
$1_{10}1\ 1 - 1_{01}3\ 2$	4294.0700	0.0043	1.0000	$14_{105}3\ 11 - 14_{963}11$	80098.0206	0.0456	0.0025
$1_{10}3\ 2 - 1_{01}3\ 3$	4294.9440	0.0036	1.0000	$14_{105}1\ 14 - 14_{961}14$	80098.0206	-0.0056	0.0025
$1_{10}1\ 1 - 1_{01}1\ 1$	4295.4010	0.0047	1.0000	$14_{104}2\ 14 - 14_{952}14$	80098.0206	-0.0055	0.0025
$1_{10}3\ 4 - 1_{01}3\ 4$	4297.9530	0.0017	1.0000	$14_{105}3\ 17 - 14_{963}17$	80098.0206	-0.0512	0.0025
$1_{10}1\ 1 - 1_{01}1\ 2$	4298.3290	0.0065	1.0000	$14_{105}3\ 12 - 14_{963}12$	80098.5536	0.1266	0.0013
$1_{10}1\ 1 - 1_{01}1\ 0$	4300.2000	0.0033	1.0000	$14_{105}1\ 15 - 14_{961}15$	80098.5536	0.0235	0.0013
$1_{10}3\ 4 - 1_{01}3\ 3$	4301.2000	0.0045	1.0000	$14_{105}3\ 13 - 14_{963}13$	80098.5536	0.0233	0.0013
$1_{10}1\ 2 - 1_{01}3\ 2$	4302.6720	-0.0013	1.0000	$14_{104}2\ 16 - 14_{952}16$	80098.5536	0.0207	0.0013
$1_{10}1\ 2 - 1_{01}1\ 1$	4304.0060	0.0021	1.0000	$14_{104}2\ 15 - 14_{952}15$	80098.5536	0.0191	0.0013
$1_{10}3\ 3 - 1_{01}3\ 2$	4305.4250	0.0029	1.0000	$14_{104}2\ 13 - 14_{952}13$	80098.5536	0.0168	0.0013
$1_{10}1\ 2 - 1_{01}1\ 2$	4306.9320	0.0019	1.0000	$14_{104}2\ 12 - 14_{952}12$	80098.5536	0.0140	0.0013
$1_{10}3\ 3 - 1_{01}3\ 4$	4307.5160	0.0019	1.0000	$14_{105}3\ 16 - 14_{963}16$	80098.5536	-0.0791	0.0013
$1_{10}1\ 2 - 1_{01}3\ 3$	4308.0100	0.0005	1.0000	$14_{105}1\ 13 - 14_{961}13$	80099.0873	0.0937	0.0025
$1_{10}1\ 0 - 1_{01}1\ 1$	4308.6560	0.0082	1.0000	$14_{105}3\ 14 - 14_{963}14$	80099.0873	0.0542	0.0025
$1_{10}3\ 3 - 1_{01}1\ 2$	4309.6840	0.0051	1.0000	$14_{104}0\ 14 - 14_{950}14$	80099.0873	0.0401	0.0025
$1_{10}3\ 3 - 1_{01}3\ 3$	4310.6710	-0.0873	1.0000	$14_{105}3\ 15 - 14_{963}15$	80099.0873	-0.0055	0.0025
$2_{20}0\ 2 - 1_{11}0\ 1$	17992.8800	0.0053	1.0000	$13_{103}3\ 10 - 13_{943}10$	80100.3409	0.0823	0.0025
$2_{20}2\ 1 - 1_{11}0\ 1$	17995.2530	-0.0002	1.0000	$13_{103}1\ 13 - 13_{941}13$	80100.3409	0.0105	0.0025
$2_{20}2\ 0 - 1_{11}0\ 1$	17995.2830	0.0057	1.0000	$13_{104}0\ 13 - 13_{952}13$	80100.3409	0.0104	0.0025
$2_{20}2\ 2 - 1_{11}0\ 1$	17997.5790	0.0060	1.0000	$13_{103}3\ 16 - 13_{943}16$	80100.3409	-0.0540	0.0025
$2_{20}0\ 2 - 1_{11}2\ 3$	17997.7920	0.0021	1.0000	$13_{103}3\ 11 - 13_{943}11$	80100.9289	0.1478	0.0013
$2_{20}0\ 2 - 1_{11}2\ 2$	17998.3020	0.0002	1.0000	$13_{103}3\ 12 - 13_{943}12$	80100.9289	0.0159	0.0013
$2_{20}2\ 4 - 1_{11}2\ 3$	18000.1410	-0.0017	1.0000	$13_{103}1\ 14 - 13_{941}14$	80100.9289	0.0134	0.0013
$2_{20}2\ 3 - 1_{11}2\ 2$	18000.6550	0.0024	1.0000	$13_{104}2\ 11 - 13_{952}11$	80100.9289	0.0057	0.0013
$2_{20}2\ 1 - 1_{11}2\ 2$	18000.6800	-0.0003	1.0000	$13_{104}2\ 14 - 13_{952}14$	80100.9289	0.0019	0.0013
$2_{20}2\ 2 - 1_{11}2\ 3$	18002.4890	0.0008	1.0000	$13_{104}2\ 12 - 13_{952}12$	80100.9289	0.0002	0.0013

$2_{20}0\ 2$	–	$1_{11}2\ 1$	18002.8250	0.0088	1.0000	$13_{104}2\ 15$	–	$13_{952}15$	80100.9289	0.0000	0.0013
$2_{20}2\ 2$	–	$1_{11}2\ 2$	18002.9990	-0.0011	1.0000	$13_{103}3\ 15$	–	$13_{943}15$	80100.9289	-0.1229	0.0013
$2_{20}2\ 1$	–	$1_{11}2\ 1$	18005.1880	-0.0068	1.0000	$13_{103}1\ 12$	–	$13_{941}12$	80101.6494	0.2009	0.0013
$2_{20}2\ 0$	–	$1_{11}2\ 1$	18005.2140	-0.0048	1.0000	$13_{103}3\ 13$	–	$13_{943}13$	80101.6494	0.1475	0.0013
$2_{20}2\ 2$	–	$1_{11}2\ 1$	18007.5130	-0.0016	1.0000	$13_{104}2\ 13$	–	$13_{950}13$	80101.6494	0.1268	0.0013
$2_{21}1\ 2$	–	$1_{10}3\ 3$	17824.7300	-0.0008	1.0000	$13_{103}3\ 14$	–	$13_{943}14$	80101.6494	0.0654	0.0013
$2_{21}1\ 3$	–	$1_{10}3\ 3$	17826.4560	0.0006	1.0000	$12_{103}3\ 9$	–	$12_{943}9$	80101.6494	-0.0515	0.0013
$2_{21}1\ 1$	–	$1_{10}1\ 0$	17826.7860	-0.0039	1.0000	$12_{103}1\ 12$	–	$12_{941}12$	80101.6494	-0.1326	0.0013
$2_{21}3\ 1$	–	$1_{10}1\ 2$	17826.9740	-0.0159	1.0000	$12_{103}3\ 15$	–	$12_{943}15$	80101.6494	-0.2035	0.0013
$2_{21}3\ 2$	–	$1_{10}3\ 3$	17827.0350	0.0018	1.0000	$12_{103}3\ 10$	–	$12_{943}10$	80102.4999	0.1911	0.0008
$2_{21}3\ 4$	–	$1_{10}3\ 3$	17828.7410	-0.0022	1.0000	$11_{101}3\ 8$	–	$11_{923}8$	80102.4999	0.0648	0.0008
$2_{21}1\ 3$	–	$1_{10}1\ 2$	17829.2090	0.0048	1.0000	$12_{103}3\ 11$	–	$12_{943}11$	80102.4999	0.0264	0.0008
$2_{21}3\ 3$	–	$1_{10}3\ 3$	17829.3160	0.0000	1.0000	$12_{102}2\ 14$	–	$12_{932}14$	80102.4999	0.0236	0.0008
$2_{21}3\ 2$	–	$1_{10}1\ 2$	17829.7820	0.0000	1.0000	$12_{102}2\ 13$	–	$12_{932}13$	80102.4999	0.0236	0.0008
$2_{21}3\ 3$	–	$1_{10}1\ 2$	17832.0620	-0.0028	1.0000	$12_{103}1\ 13$	–	$12_{941}13$	80102.4999	0.0224	0.0008
$2_{21}3\ 5$	–	$1_{10}3\ 4$	17835.4210	0.0027	1.0000	$12_{102}2\ 11$	–	$12_{932}11$	80102.4999	0.0188	0.0008
$2_{21}1\ 2$	–	$1_{10}1\ 1$	17836.0860	-0.0011	1.0000	$12_{102}2\ 10$	–	$12_{932}10$	80102.4999	0.0091	0.0008
$2_{21}3\ 4$	–	$1_{10}3\ 4$	17838.3050	-0.0011	1.0000	$11_{101}1\ 11$	–	$11_{921}11$	80102.4999	-0.0505	0.0008
$2_{21}3\ 2$	–	$1_{10}1\ 1$	17838.4080	0.0184	1.0000	$12_{103}3\ 14$	–	$12_{943}14$	80102.4999	-0.1341	0.0008
$2_{21}3\ 3$	–	$1_{10}3\ 4$	17838.8750	-0.0038	1.0000	$11_{101}3\ 14$	–	$11_{923}14$	80102.4999	-0.1514	0.0008
$2_{21}1\ 1$	–	$1_{10}1\ 1$	17840.0480	0.0066	1.0000	$12_{103}1\ 11$	–	$12_{941}11$	80103.2575	0.1547	0.0083
$2_{21}3\ 1$	–	$1_{10}3\ 2$	17840.0480	-0.0110	1.0000	$11_{101}3\ 9$	–	$11_{923}9$	80103.2575	0.1092	0.0083
$2_{21}1\ 2$	–	$1_{10}3\ 2$	17840.5470	-0.0018	1.0000	$12_{103}3\ 12$	–	$12_{943}12$	80103.2575	0.0971	0.0083
$2_{21}1\ 3$	–	$1_{10}3\ 2$	17842.2740	0.0007	1.0000	$12_{103}3\ 13$	–	$12_{943}13$	80103.2575	0.0023	0.0083
$2_{21}3\ 2$	–	$1_{10}3\ 2$	17842.8480	-0.0032	1.0000	$11_{101}3\ 10$	–	$11_{923}10$	80103.2575	-0.1049	0.0083
$2_{21}3\ 1$	–	$2_{12}3\ 1$	12892.4750	-0.0067	1.0000	$11_{101}1\ 12$	–	$11_{921}12$	80103.2575	-0.1124	0.0083
$2_{21}1\ 2$	–	$2_{12}3\ 1$	12892.9680	-0.0034	1.0000	$11_{102}2\ 12$	–	$11_{932}12$	80103.2575	-0.1269	0.0083
$2_{21}3\ 1$	–	$2_{12}1\ 2$	12893.9660	-0.0108	1.0000	$11_{102}2\ 13$	–	$11_{932}13$	80103.2575	-0.1281	0.0083
$2_{21}1\ 2$	–	$2_{12}1\ 2$	12894.4620	-0.0046	1.0000	$11_{102}2\ 9$	–	$11_{932}9$	80103.2575	-0.1283	0.0083
$2_{21}3\ 2$	–	$2_{12}3\ 1$	12895.2700	-0.0038	1.0000	$11_{102}2\ 10$	–	$11_{932}10$	80103.2575	-0.1296	0.0083
$2_{21}1\ 3$	–	$2_{12}1\ 2$	12896.1880	-0.0031	1.0000	$10_{743}7$	–	$9_{633}6$	81119.4024	-0.0448	0.0025

$2_{21}3\,2$	–	$2_{12}1\,2$	12896.7640	-0.0050	1.0000	$10_{741}10$	–	$9_{631}9$	81119.4024	-0.0726	0.0025
$2_{21}1\,1$	–	$2_{12}1\,2$	12898.4180	-0.0028	1.0000	$10_{732}10$	–	$9_{642}9$	81119.4024	-0.0740	0.0025
$2_{21}3\,5$	–	$2_{12}3\,5$	12898.8780	-0.0018	1.0000	$10_{743}13$	–	$9_{633}12$	81119.4024	-0.0988	0.0025
$2_{21}1\,2$	–	$2_{12}1\,3$	12899.4400	-0.0023	1.0000	$10_{743}8$	–	$9_{633}7$	81119.6700	-0.0010	0.0013
$2_{21}3\,1$	–	$2_{12}3\,2$	12900.6320	-0.0042	1.0000	$10_{741}11$	–	$9_{631}10$	81119.6700	-0.0562	0.0013
$2_{21}1\,2$	–	$2_{12}3\,2$	12901.1190	-0.0069	1.0000	$10_{743}9$	–	$9_{633}8$	81119.6700	-0.0573	0.0013
$2_{21}1\,3$	–	$2_{12}1\,3$	12901.1670	0.0001	1.0000	$10_{732}11$	–	$9_{642}10$	81119.6700	-0.0594	0.0013
$2_{21}3\,4$	–	$2_{12}3\,5$	12901.7610	-0.0065	1.0000	$10_{732}8$	–	$9_{642}7$	81119.6700	-0.0596	0.0013
$2_{21}1\,3$	–	$2_{12}3\,2$	12902.8540	0.0035	1.0000	$10_{732}12$	–	$9_{642}11$	81119.6700	-0.0600	0.0013
$2_{21}3\,4$	–	$2_{12}1\,3$	12903.4580	0.0033	1.0000	$10_{732}9$	–	$9_{642}8$	81119.6700	-0.0617	0.0013
$2_{21}3\,3$	–	$2_{12}1\,3$	12904.0240	-0.0035	1.0000	$10_{743}12$	–	$9_{633}11$	81119.6700	-0.1132	0.0013
$2_{21}1\,1$	–	$2_{12}3\,2$	12905.0820	0.0018	1.0000	$10_{741}9$	–	$9_{631}8$	81119.9150	-0.0396	0.0025
$2_{21}3\,3$	–	$2_{12}3\,2$	12905.7090	-0.0021	1.0000	$10_{743}10$	–	$9_{633}9$	81119.9150	-0.0630	0.0025
$2_{21}1\,2$	–	$2_{12}1\,1$	12906.0760	0.0049	1.0000	$10_{730}10$	–	$9_{640}9$	81119.9150	-0.0712	0.0025
$2_{21}3\,5$	–	$2_{12}3\,4$	12907.4490	0.0045	1.0000	$10_{743}11$	–	$9_{633}10$	81119.9150	-0.0969	0.0025
$2_{21}1\,3$	–	$2_{12}3\,4$	12908.0460	0.0016	1.0000	$17_{1163}14$	–	$17_{1073}14$	88510.3402	0.0676	0.0025
$2_{21}3\,2$	–	$2_{12}1\,1$	12908.3780	0.0044	1.0000	$17_{1161}17$	–	$17_{1071}17$	88510.3402	0.0371	0.0025
$2_{21}1\,3$	–	$2_{12}3\,3$	12909.6990	0.0051	1.0000	$17_{1172}17$	–	$17_{1082}17$	88510.3402	0.0371	0.0025
$2_{21}1\,1$	–	$2_{12}1\,1$	12910.0290	0.0036	1.0000	$17_{1163}20$	–	$17_{1073}20$	88510.3402	0.0095	0.0025
$2_{21}3\,2$	–	$2_{12}3\,3$	12910.2710	-0.0007	1.0000	$17_{1163}15$	–	$17_{1073}15$	88510.7829	0.1660	0.0013
$2_{21}3\,4$	–	$2_{12}3\,4$	12910.3360	0.0037	1.0000	$17_{1161}18$	–	$17_{1071}18$	88510.7829	0.1078	0.0013
$2_{21}3\,3$	–	$2_{12}3\,4$	12910.9020	-0.0030	1.0000	$17_{1161}16$	–	$17_{1071}16$	88510.7829	0.1068	0.0013
$2_{21}3\,4$	–	$2_{12}3\,3$	12911.9850	0.0032	1.0000	$17_{1172}19$	–	$17_{1082}19$	88510.7829	0.1031	0.0013
$2_{21}3\,3$	–	$2_{12}3\,3$	12912.5560	0.0015	1.0000	$17_{1172}15$	–	$17_{1082}15$	88510.7829	0.0979	0.0013
$3_{13}2\,3$	–	$2_{02}2\,3$	11611.4550	-0.0004	1.0000	$17_{1172}18$	–	$17_{1082}18$	88510.7829	0.0975	0.0013
$3_{13}2\,3$	–	$2_{02}0\,2$	11613.8460	-0.0022	1.0000	$17_{1172}16$	–	$17_{1082}16$	88510.7829	0.0962	0.0013
$3_{13}2\,2$	–	$2_{02}2\,2$	11615.7840	0.0012	1.0000	$17_{1163}19$	–	$17_{1073}19$	88510.7829	0.0411	0.0013
$3_{13}2\,1$	–	$2_{02}2\,0$	11617.8930	-0.0018	1.0000	$17_{1163}16$	–	17_{1073}	88511.1840	0.1539	0.0025

$3_{13}2\ 4$	–	$2_{02}2\ 3$	11618.1750	0.0046	1.0000	$17_{116}3\ 17$	–	$17_{107}3\ 16$	88511.1840	0.1287	0.0025
$3_{13}2\ 2$	–	$2_{02}2\ 1$	11618.2380	-0.0205	1.0000	$17_{117}0\ 17$	–	$17_{108}0\ 17$	88511.1840	0.1217	0.0025
$3_{13}2\ 5$	–	$2_{02}2\ 4$	11618.3210	0.0013	1.0000	$17_{116}3\ 18$	–	$17_{107}3\ 17$	88511.1840	0.0936	0.0025
$3_{13}2\ 4$	–	$2_{02}2\ 4$	11618.3690	0.0103	1.0000	$16_{116}3\ 13$	–	$16_{107}3\ 18$	88513.3562	0.0714	0.0025
$3_{13}2\ 2$	–	$2_{02}0\ 2$	11620.4940	0.0007	1.0000	$16_{116}1\ 16$	–	$16_{107}1\ 13$	88513.3562	0.0324	0.0025
$3_{13}0\ 3$	–	$2_{02}2\ 2$	11622.5700	0.0034	1.0000	$16_{115}2\ 16$	–	$16_{106}2\ 16$	88513.3562	0.0324	0.0025
$3_{13}0\ 3$	–	$2_{02}2\ 3$	11624.8880	0.0037	1.0000	$16_{116}3\ 19$	–	$16_{107}3\ 19$	88513.3562	-0.0030	0.0025
$4_{23}3\ 2$	–	$4_{14}3\ 1$	13466.9770	-0.0002	1.0000	$16_{116}3\ 14$	–	$16_{107}3\ 14$	88513.8299	0.1551	0.0013
$4_{23}3\ 1$	–	$4_{14}3\ 1$	13467.4580	-0.0030	1.0000	$16_{116}1\ 17$	–	$16_{107}1\ 17$	88513.8299	0.0775	0.0013
$4_{23}1\ 4$	–	$4_{14}1\ 4$	13469.8850	-0.0021	1.0000	$16_{116}1\ 15$	–	$16_{107}1\ 15$	88513.8299	0.0774	0.0013
$4_{23}3\ 3$	–	$4_{14}3\ 2$	13470.3790	0.0036	1.0000	$16_{115}2\ 18$	–	$16_{106}2\ 18$	88513.8299	0.0746	0.0013
$4_{23}3\ 6$	–	$4_{14}3\ 7$	13470.5210	-0.0042	1.0000	$16_{115}2\ 17$	–	$16_{106}2\ 17$	88513.8299	0.0746	0.0013
$4_{23}3\ 2$	–	$4_{14}3\ 2$	13470.8350	0.0005	1.0000	$16_{115}2\ 15$	–	$16_{106}2\ 15$	88513.8299	0.0724	0.0013
$4_{23}3\ 1$	–	$4_{14}3\ 2$	13471.3130	-0.0053	1.0000	$16_{115}2\ 14$	–	$16_{106}2\ 14$	88513.8299	0.0720	0.0013
$4_{23}3\ 7$	–	$4_{14}3\ 7$	13471.6680	-0.0016	1.0000	$16_{116}3\ 18$	–	$16_{107}3\ 18$	88513.8299	-0.0001	0.0013
$4_{23}3\ 4$	–	$4_{14}3\ 3$	13473.3250	0.0039	1.0000	$16_{116}3\ 15$	–	$16_{107}3\ 15$	88514.3149	0.1659	0.0025
$4_{23}3\ 3$	–	$4_{14}3\ 3$	13474.1190	0.0019	1.0000	$16_{116}3\ 16$	–	$16_{107}3\ 16$	88514.3149	0.1343	0.0025
$4_{23}3\ 2$	–	$4_{14}3\ 3$	13474.5750	-0.0012	1.0000	$16_{115}0\ 16$	–	$16_{106}0\ 16$	88514.3149	0.1248	0.0025
$4_{23}1\ 5$	–	$4_{14}1\ 5$	13475.5710	-0.0001	1.0000	$16_{116}3\ 17$	–	$16_{107}3\ 17$	88514.3149	0.0893	0.0025
$4_{23}1\ 4$	–	$4_{14}1\ 5$	13476.1760	-0.0007	1.0000	$15_{114}3\ 12$	–	$15_{105}3\ 12$	88515.4701	0.0774	0.0025
$4_{23}3\ 5$	–	$4_{14}3\ 6$	13478.6120	0.0029	1.0000	$15_{114}1\ 15$	–	$15_{105}1\ 15$	88515.4701	0.0238	0.0025
$4_{23}3\ 6$	–	$4_{14}3\ 6$	13479.1950	0.0022	1.0000	$15_{115}0\ 15$	–	$15_{106}2\ 15$	88515.4701	0.0237	0.0025
$4_{23}3\ 5$	–	$4_{14}3\ 4$	13479.7020	0.0088	1.0000	$15_{114}3\ 18$	–	$15_{105}3\ 18$	88515.4701	-0.0253	0.0025
$4_{23}3\ 4$	–	$4_{14}3\ 4$	13480.1940	0.0045	1.0000	$15_{114}3\ 13$	–	$15_{105}3\ 13$	88516.0060	0.1696	0.0013
$4_{23}1\ 3$	–	$4_{14}1\ 3$	13480.3500	0.0013	1.0000	$15_{114}1\ 14$	–	$15_{105}1\ 14$	88516.0060	0.0729	0.0013
$4_{23}3\ 3$	–	$4_{14}3\ 4$	13480.9860	0.0004	1.0000	$15_{114}1\ 16$	–	$15_{105}1\ 16$	88516.0060	0.0720	0.0013
$4_{23}3\ 5$	–	$4_{14}3\ 5$	13483.1310	0.0029	1.0000	$15_{115}2\ 13$	–	$15_{106}2\ 13$	88516.0060	0.0674	0.0013

$4_{23}3\,4$	–	$4_{14}3\,5$	13483.6280	0.0036	1.0000	$15_{11\,5}2\,16$	–	$15_{10\,6}2\,16$	88516.0060	0.0611	0.0013
$4_{23}3\,6$	–	$4_{14}3\,5$	13483.7220	0.0102	1.0000	$15_{11\,5}2\,14$	–	$15_{10\,6}2\,14$	88516.0060	0.0601	0.0013
$5_{15}2\,5$	–	$4_{04}2\,5$	16174.9910	-0.0022	1.0000	$15_{11\,5}2\,17$	–	$15_{10\,6}2\,17$	88516.0060	0.0593	0.0013
$5_{15}2\,5$	–	$4_{04}0\,4$	16177.8730	-0.0012	1.0000	$15_{11\,4}3\,17$	–	$15_{10\,5}3\,17$	88516.0060	-0.0305	0.0013
$5_{15}2\,4$	–	$4_{04}2\,4$	16179.0990	-0.0024	1.0000	$15_{11\,4}3\,14$	–	$15_{10\,5}3\,14$	88516.5079	0.1240	0.0013
$5_{15}2\,4$	–	$4_{04}2\,3$	16182.0150	0.0069	1.0000	$15_{11\,4}3\,15$	–	$15_{10\,5}3\,15$	88516.5079	0.0818	0.0013
$5_{15}2\,3$	–	$4_{04}2\,2$	16182.0150	0.0013	1.0000	$15_{11\,5}2\,15$	–	$15_{10\,6}0\,15$	88516.5079	0.0682	0.0013
$5_{15}2\,7$	–	$4_{04}2\,6$	16182.0830	0.0019	1.0000	$15_{11\,4}3\,16$	–	$15_{10\,5}3\,16$	88516.5079	0.0211	0.0013
$5_{15}2\,6$	–	$4_{04}2\,5$	16182.1640	0.0021	1.0000	$14_{11\,4}3\,11$	–	$14_{10\,5}3\,11$	88516.5079	-0.2114	0.0013
$5_{15}2\,4$	–	$4_{04}0\,4$	16184.9060	-0.0007	1.0000	$14_{11\,4}1\,14$	–	$14_{10\,5}1\,14$	88516.5079	-0.2779	0.0013
$5_{15}0\,5$	–	$4_{04}2\,4$	16186.2360	0.0012	1.0000	$14_{11\,4}3\,17$	–	$14_{10\,5}3\,17$	88516.5079	-0.3381	0.0013
$5_{15}0\,5$	–	$4_{04}2\,5$	16189.1610	0.0018	1.0000	$14_{11\,4}3\,12$	–	$14_{10\,5}3\,12$	88517.4392	0.2123	0.0006
$6_{06}2\,5$	–	$5_{15}0\,5$	12453.1710	-0.0021	1.0000	$14_{11\,4}3\,13$	–	$14_{10\,5}3\,13$	88517.4392	0.0927	0.0006
$6_{06}2\,6$	–	$5_{15}2\,6$	12456.3180	-0.0056	1.0000	$14_{11\,4}1\,15$	–	$14_{10\,5}1\,15$	88517.4392	0.0899	0.0006
$6_{06}0\,6$	–	$5_{15}0\,5$	12457.0360	-0.0036	1.0000	$14_{11\,3}2\,12$	–	$14_{10\,4}2\,12$	88517.4392	0.0857	0.0006
$6_{06}2\,7$	–	$5_{15}2\,6$	12460.1850	0.0003	1.0000	$14_{11\,3}2\,15$	–	$14_{10\,4}2\,15$	88517.4392	0.0797	0.0006
$6_{06}2\,8$	–	$5_{15}2\,7$	12460.2600	0.0015	1.0000	$14_{11\,3}2\,13$	–	$14_{10\,4}2\,13$	88517.4392	0.0780	0.0006
$6_{06}2\,4$	–	$5_{15}2\,3$	12460.3060	0.0032	1.0000	$14_{11\,3}2\,16$	–	$14_{10\,4}2\,16$	88517.4392	0.0760	0.0006
$6_{06}2\,5$	–	$5_{15}2\,4$	12460.3060	-0.0005	1.0000	$13_{11\,2}3\,10$	–	$13_{10\,3}3\,10$	88517.4392	0.0583	0.0006
$6_{06}2\,6$	–	$5_{15}2\,5$	12463.4900	-0.0022	1.0000	$13_{11\,2}1\,13$	–	$13_{10\,3}1\,13$	88517.4392	-0.0183	0.0006
$6_{06}0\,6$	–	$5_{15}2\,6$	12464.0320	-0.0049	1.0000	$14_{11\,4}3\,16$	–	$14_{10\,5}3\,16$	88517.4392	-0.0342	0.0006
$11_{29}3\,8$	–	$10_{38}3\,7$	9900.5300	0.0036	1.0000	$12_{11\,2}3\,9$	–	$12_{10\,3}3\,9$	88517.4392	-0.0446	0.0006
$11_{29}1\,11$	–	$10_{38}1\,10$	9900.9080	0.0017	1.0000	$13_{11\,2}3\,16$	–	$13_{10\,3}3\,16$	88517.4392	-0.0868	0.0006
$11_{29}3\,14$	–	$10_{38}3\,13$	9901.2390	0.0025	1.0000	$12_{11\,2}1\,12$	–	$12_{10\,3}1\,12$	88517.4392	-0.1435	0.0006
$11_{29}3\,9$	–	$10_{38}3\,8$	9902.9740	-0.0002	1.0000	$13_{11\,2}3\,11$	–	$13_{10\,3}3\,11$	88518.1588	0.1936	0.0005
$11_{29}1\,12$	–	$10_{38}1\,11$	9903.7820	-0.0042	1.0000	$14_{11\,4}3\,15$	–	$14_{10\,5}3\,15$	88518.1588	0.1697	0.0005
$11_{29}3\,10$	–	$10_{38}3\,9$	9903.8100	0.0036	1.0000	$13_{11\,2}3\,12$	–	$13_{10\,3}3\,12$	88518.1588	0.0473	0.0005
$11_{29}3$	–	$10_{38}3$	9904.5820	-0.0016	1.0000	$13_{11\,2}1\,14$	–	$13_{10\,3}1$	88518.1588	0.0444	0.0005

$11_{29}1_{13}$	–	$10_{38}1_{12}$	9906.3880	-0.0026	1.0000	$13_{113}2\ 14_{14}$	–	$13_{104}2$	88518.1588	0.0366	0.0005
$11_{29}3_{10}$	–	$10_{38}3_{9}$	9906.6980	0.0011	1.0000	$13_{113}2\ 15_{14}$	–	$13_{104}2$	88518.1588	0.0359	0.0005
$11_{29}3_{11}$	–	$10_{38}3_{10}$	9907.2320	-0.0030	1.0000	$13_{113}2\ 11_{15}$	–	$13_{104}2$	88518.1588	0.0345	0.0005
$15_{105}3_{12}$	–	15_{963}_{12}	80094.7438	0.0409	0.0025	$13_{113}2\ 12_{11}$	–	$13_{104}2$	88518.1588	0.0344	0.0005
$15_{105}1_{15}$	–	15_{961}_{15}	80094.7438	-0.0015	0.0025	$12_{112}3\ 10_{12}$	–	$12_{103}3$	88518.1588	-0.0027	0.0005
$15_{106}2_{15}$	–	15_{972}_{15}	80094.7438	-0.0016	0.0025	$13_{112}3\ 15_{15}$	–	$13_{103}3$	88518.1588	-0.1022	0.0005
$15_{105}3_{18}$	–	15_{963}_{18}	80094.7438	-0.0398	0.0025	$12_{112}3\ 11_{11}$	–	$12_{103}3$	88518.1588	-0.1878	0.0005
$15_{105}3_{13}$	–	15_{963}_{13}	80095.2205	0.1243	0.0013	$12_{112}1\ 13_{13}$	–	$12_{103}1$	88518.1588	-0.1930	0.0005
$15_{105}1_{16}$	–	15_{961}_{16}	80095.2205	0.0428	0.0013	$12_{111}2\ 13_{13}$	–	$12_{102}2$	88518.1588	-0.2048	0.0005
$15_{105}1_{14}$	–	15_{961}_{14}	80095.2205	0.0399	0.0013	$12_{111}2\ 10_{10}$	–	$12_{102}2$	88518.1588	-0.2058	0.0005
$15_{106}2_{17}$	–	15_{972}_{17}	80095.2205	0.0365	0.0013	$12_{111}2\ 14_{14}$	–	$12_{102}2$	88518.1588	-0.2059	0.0005
$15_{106}2_{14}$	–	15_{972}_{14}	80095.2205	0.0344	0.0013	$12_{111}2\ 11_{11}$	–	$12_{102}2$	88518.1588	-0.2070	0.0005

Table B.2: result of least squares fitting data analysis for normal transitions.

$J'_{K'_aK'_c} - J''_{K''_aK''_c}$	$\nu_{obs.}$/MHz	ν_{o-c} /MHz[b]	weight	$J'_{K'_aK'_c} - J''_{K''_aK''_c}$	$\nu_{obs.}$/MHz	ν_{o-c} /MHz[b]	weight
$8_{7\,1} - 7_{6\,2}$	75862.6542	0.0525	0.0100	$26_{11\,16} - 26_{10\,17}$	88417.1468	0.0171	0.0100
$8_{7\,2} - 7_{6\,1}$	75862.6542	0.0525	0.0100	$28_{11\,18} - 28_{10\,19}$	88372.0998	-0.1047	0.0100
$8_{8\,0} - 7_{7\,1}$	84290.1207	0.0301	0.0100	$28_{11\,17} - 28_{10\,18}$	88372.0998	-0.1046	0.0100
$8_{8\,1} - 7_{7\,0}$	84290.1207	0.0301	0.0100	$29_{11\,19} - 29_{10\,20}$	88345.0927	-0.0862	0.0100
$9_{7\,2} - 8_{6\,3}$	78491.3932	0.0190	0.0100	$29_{11\,18} - 29_{10\,19}$	88345.0927	-0.0859	0.0100
$9_{7\,3} - 8_{6\,2}$	78491.3932	0.0190	0.0100	$31_{11\,21} - 31_{10\,22}$	88280.7406	-0.0308	0.0100
$10_{7\,3} - 9_{6\,4}$	81119.7699	0.0384	0.0100	$31_{11\,20} - 31_{10\,21}$	88280.7406	-0.0299	0.0100
$10_{7\,4} - 9_{6\,3}$	81119.7699	0.0385	0.0100	$32_{11\,21} - 32_{10\,22}$	88242.9383	0.0746	0.0100
$11_{6\,5} - 10_{5\,6}$	75310.6443	0.0188	0.0100	$32_{11\,22} - 32_{10\,23}$	88242.9383	0.0729	0.0100
$11_{6\,6} - 10_{5\,5}$	75310.6443	0.0692	0.0100	$34_{11\,23} - 34_{10\,24}$	88154.1674	-0.0787	0.0100
$11_{7\,4} - 10_{6\,5}$	83747.4812	0.0467	0.0100	$34_{11\,24} - 34_{10\,25}$	88154.1674	-0.0846	0.0100
$11_{7\,5} - 10_{6\,4}$	83747.4812	0.0471	0.0100	$35_{11\,24} - 35_{10\,25}$	88102.9704	0.0317	0.0100
$12_{6\,6} - 11_{5\,7}$	77933.9542	0.0088	0.0100	$35_{11\,25} - 35_{10\,26}$	88102.9704	0.0213	0.0100
$12_{6\,7} - 11_{5\,6}$	77933.9542	0.1433	0.0100	$36_{11\,25} - 36_{10\,26}$	88046.5316	-0.0134	0.0100
$13_{6\,7} - 12_{5\,8}$	80554.7429	-0.0857	0.0100	$38_{11\,27} - 38_{10\,28}$	87917.2661	0.1181	0.0100
$14_{6\,8} - 13_{5\,9}$	83172.6360	-0.0666	0.0100	$38_{11\,28} - 38_{10\,29}$	87917.2661	0.0648	0.0100
$14_{6\,9} - 13_{5\,8}$	83171.9142	-0.0521	0.0100	$39_{11\,28} - 39_{10\,29}$	87843.4752	0.0477	0.0100
$15_{5\,10} - 14_{4\,11}$	77307.8974	0.0857	0.0100	$39_{11\,29} - 39_{10\,30}$	87843.4752	-0.0415	0.0100
$15_{5\,11} - 14_{4\,10}$	77252.8717	0.0665	0.0100	$40_{11\,29} - 40_{10\,30}$	87763.2724	0.0888	0.0100
$16_{5\,11} - 15_{4\,12}$	79911.0801	-0.0568	0.0100	$40_{11\,30} - 40_{10\,31}$	87763.2730	-0.0573	0.0100
$16_{5\,12} - 15_{4\,11}$	79816.4151	-0.0091	0.0100	$41_{11\,30} - 41_{10\,31}$	87675.9461	-0.0624	0.0100
$16_{7\,9} - 15_{6\,10}$	96865.2142	-0.0005	0.0100	$42_{11\,32} - 42_{10\,33}$	87581.8134	-0.0392	0.0100
$16_{7\,10} - 15_{6\,9}$	96865.2142	0.0615	0.0100	$43_{11\,32} - 43_{10\,33}$	87479.0347	-0.0771	0.0100
$17_{5\,12} - 16_{4\,13}$	82513.6421	-0.0040	0.0100	$43_{11\,33} - 43_{10\,34}$	87479.6688	-0.0475	0.0100
$17_{5\,13} - 16_{4\,12}$	82356.4471	-0.1004	0.0100	$44_{11\,33} - 44_{10\,34}$	87368.3811	-0.0616	0.0100
$17_{6\,11} - 16_{5\,12}$	91002.2187	-0.0056	0.0100	$44_{11\,34} - 44_{10\,35}$	87369.3124	-0.0756	0.0100
$17_{6\,12} - 16_{5\,11}$	90996.2704	-0.0284	0.0100	$45_{11\,34} - 45_{10\,35}$	87248.9263	-0.0120	0.0100
$17_{7\,11} - 16_{6\,10}$	99481.8676	0.0774	0.0100	$45_{11\,35} - 45_{10\,36}$	87250.3738	-0.0261	0.0100
$17_{7\,10} - 16_{6\,11}$	99481.8676	-0.0589	0.0100	$46_{11\,36} - 46_{10\,37}$	87122.3179	0.0513	0.0100
$18_{6\,13} - 17_{5\,12}$	93591.3109	0.0596	0.0100	$47_{11\,37} - 47_{10\,38}$	86984.4015	-0.0860	0.0100
$31_{0\,31} - 30_{1\,30}$	77219.5509	0.1652	0.0100	$47_{11\,36} - 47_{10\,37}$	86981.0685	-0.0384	0.0100
$31_{1\,31} - 30_{0\,30}$	77225.2089	-0.0284	0.0100	$48_{11\,38} - 48_{10\,39}$	86836.5824	0.0333	0.0100

$32_{0\,32}$	–	$31_{1\,31}$	79681.6397	-0.1005	0.0100	$48_{11\,37}$	–	$48_{10\,38}$	86831.5329	0.0457	0.0100
$32_{1\,32}$	–	$31_{0\,31}$	79685.7982	-0.1106	0.0100	$21_{12\,10}$	–	$21_{11\,11}$	96913.8911	-0.1305	0.0100
$33_{0\,33}$	–	$32_{1\,32}$	82143.6052	-0.0326	0.0100	$21_{12\,9}$	–	$21_{11\,10}$	96913.8911	-0.1305	0.0100
$33_{1\,33}$	–	$32_{0\,32}$	82146.5687	-0.0343	0.0100	$23_{12\,11}$	–	$23_{11\,12}$	96900.9385	-0.0563	0.0100
$35_{0\,35}$	–	$34_{1\,34}$	87066.4340	0.1543	0.0100	$23_{12\,12}$	–	$23_{11\,13}$	96900.9385	-0.0563	0.0100
$35_{1\,35}$	–	$34_{0\,34}$	87067.7385	-0.0355	0.0100	$25_{12\,13}$	–	$25_{11\,14}$	96881.9592	-0.1264	0.0100
$36_{0\,36}$	–	$35_{1\,35}$	89527.1315	0.0393	0.0100	$25_{12\,14}$	–	$25_{11\,15}$	96881.9592	-0.1264	0.0100
$36_{1\,36}$	–	$35_{0\,35}$	89528.1862	0.0352	0.0100	$27_{12\,15}$	–	$27_{11\,16}$	96856.0247	-0.0567	0.0100
$37_{0\,37}$	–	$36_{1\,36}$	91987.5448	-0.0476	0.0100	$27_{12\,16}$	–	$27_{11\,17}$	96856.0247	-0.0567	0.0100
$37_{1\,37}$	–	$36_{0\,36}$	91988.2969	-0.0449	0.0100	$28_{12\,16}$	–	$28_{11\,17}$	96839.9861	-0.0245	0.0100
$38_{0\,38}$	–	$37_{1\,37}$	94447.7982	0.0070	0.0100	$28_{12\,17}$	–	$28_{11\,18}$	96839.9861	-0.0245	0.0100
$38_{1\,38}$	–	$37_{0\,37}$	94448.3430	0.0219	0.0100	$29_{12\,17}$	–	$29_{11\,18}$	96821.6922	0.0293	0.0100
$39_{0\,39}$	–	$38_{1\,38}$	96907.7459	0.0514	0.0100	$29_{12\,18}$	–	$29_{11\,19}$	96821.6922	0.0293	0.0100
$40_{1\,40}$	–	$39_{0\,39}$	99367.5151	-0.0538	0.0100	$30_{12\,18}$	–	$30_{11\,19}$	96800.9295	0.0734	0.0100
$19_{10\,9}$	–	$19_{9\,10}$	80068.7021	0.1247	0.0100	$30_{12\,19}$	–	$30_{11\,20}$	96800.9295	0.0734	0.0100
$19_{10\,10}$	–	$19_{9\,11}$	80068.7021	0.1247	0.0100	$31_{12\,19}$	–	$31_{11\,20}$	96777.3620	-0.0388	0.0100
$20_{10\,10}$	–	$20_{9\,11}$	80057.5490	-0.1086	0.0100	$31_{12\,20}$	–	$31_{11\,21}$	96777.3620	-0.0388	0.0100
$20_{10\,11}$	–	$20_{9\,12}$	80057.5490	-0.1086	0.0100	$32_{12\,20}$	–	$32_{11\,21}$	96751.0745	-0.0256	0.0100
$21_{10\,11}$	–	$21_{9\,12}$	80044.4166	-0.1853	0.0100	$32_{12\,21}$	–	$32_{11\,22}$	96751.0745	-0.0256	0.0100
$21_{10\,12}$	–	$21_{9\,13}$	80044.4166	-0.1854	0.0100	$33_{12\,21}$	–	$33_{11\,22}$	96721.9259	0.1764	0.0100
$22_{10\,13}$	–	$22_{9\,14}$	80029.1238	-0.0515	0.0100	$33_{12\,22}$	–	$33_{11\,23}$	96721.9259	0.1763	0.0100
$22_{10\,12}$	–	$22_{9\,13}$	80029.1238	-0.0514	0.0100	$34_{12\,22}$	–	$34_{11\,23}$	96689.1670	0.0305	0.0100
$23_{10\,13}$	–	$23_{9\,14}$	80011.0471	-0.0827	0.0100	$34_{12\,23}$	–	$34_{11\,24}$	96689.1670	0.0303	0.0100
$23_{10\,14}$	–	$23_{9\,15}$	80011.0471	-0.0828	0.0100	$35_{12\,23}$	–	$35_{11\,24}$	96653.1531	0.1127	0.0100
$24_{10\,14}$	–	$24_{9\,15}$	79990.1334	-0.0720	0.0100	$35_{12\,24}$	–	$35_{11\,25}$	96653.1531	0.1124	0.0100
$24_{10\,15}$	–	$24_{9\,16}$	79990.1334	-0.0723	0.0100	$36_{12\,24}$	–	$36_{11\,25}$	96613.2977	0.0660	0.0100
$27_{10\,17}$	–	$27_{9\,18}$	79907.4217	0.0654	0.0100	$36_{12\,25}$	–	$36_{11\,26}$	96613.2977	0.0654	0.0100
$27_{10\,18}$	–	$27_{9\,19}$	79907.4217	0.0626	0.0100	$37_{12\,25}$	–	$37_{11\,26}$	96569.3746	-0.0975	0.0100
$28_{10\,18}$	–	$28_{9\,19}$	79871.9809	-0.0627	0.0100	$37_{12\,26}$	–	$37_{11\,27}$	96569.3746	-0.0985	0.0100
$28_{10\,19}$	–	$28_{9\,20}$	79871.9809	-0.0682	0.0100	$38_{12\,26}$	–	$38_{11\,27}$	96521.5648	0.0510	0.0100
$29_{10\,19}$	–	$29_{9\,20}$	79832.4238	0.0807	0.0100	$38_{12\,27}$	–	$38_{11\,28}$	96521.5648	0.0492	0.0100
$29_{10\,20}$	–	$29_{9\,21}$	79832.4238	0.0704	0.0100	$39_{12\,27}$	–	$39_{11\,28}$	96469.0729	-0.0261	0.0100
$31_{10\,21}$	–	$31_{9\,22}$	79738.3082	-0.0602	0.0100	$39_{12\,28}$	–	$39_{11\,29}$	96469.0729	-0.0293	0.0100
$31_{10\,22}$	–	$31_{9\,23}$	79738.3082	-0.0942	0.0100	$41_{12\,29}$	–	$41_{11\,30}$	96349.8582	0.0424	0.0100
$33_{10\,23}$	–	$33_{9\,24}$	79622.4375	0.0118	0.0100	$41_{12\,30}$	–	$41_{11\,31}$	96349.8582	0.0330	0.0100

$33_{10\,24}$	–	$33_{9\,25}$	79622.4375	-0.0923	0.0100	$42_{12\,30}$	–	$42_{11\,31}$	96282.3718	-0.0050	0.0100
$35_{10\,25}$	–	$35_{9\,26}$	79481.1250	-0.0465	0.0100	$42_{12\,31}$	–	$42_{11\,32}$	96282.3718	-0.0209	0.0100
$35_{10\,26}$	–	$35_{9\,27}$	79481.4738	0.0059	0.0100	$43_{12\,31}$	–	$43_{11\,32}$	96209.4134	0.0751	0.0100
$39_{10\,29}$	–	$39_{9\,30}$	79107.3080	0.1580	0.0100	$43_{12\,32}$	–	$43_{11\,33}$	96209.4134	0.0486	0.0100
$39_{10\,30}$	–	$39_{9\,31}$	79109.2315	0.0879	0.0100	$44_{12\,32}$	–	$44_{11\,33}$	96130.4323	0.0495	0.0100
$40_{10\,30}$	–	$40_{9\,31}$	78991.2194	-0.0282	0.0100	$44_{12\,33}$	–	$44_{11\,34}$	96130.4323	0.0059	0.0100
$40_{10\,31}$	–	$40_{9\,32}$	78994.3053	-0.0441	0.0100	$45_{12\,33}$	–	$45_{11\,34}$	96045.2163	0.0387	0.0100
$41_{10\,31}$	–	$41_{9\,32}$	78865.1043	0.0680	0.0100	$45_{12\,34}$	–	$45_{11\,35}$	96045.2163	-0.0322	0.0100
$42_{10\,33}$	–	$42_{9\,34}$	78735.0537	0.1044	0.0100	$46_{12\,34}$	–	$46_{11\,35}$	95953.4191	0.0450	0.0100
$43_{10\,33}$	–	$43_{9\,34}$	78578.4440	0.0607	0.0100	$46_{12\,35}$	–	$46_{11\,36}$	95953.4191	-0.0688	0.0100
$43_{10\,34}$	–	$43_{9\,35}$	78589.2440	0.0043	0.0100	$47_{12\,35}$	–	$47_{11\,36}$	95854.6378	0.0321	0.0100
$44_{10\,34}$	–	$44_{9\,35}$	78416.1464	0.1254	0.0100	$47_{12\,36}$	–	$47_{11\,37}$	95854.6378	-0.1486	0.0100
$45_{10\,36}$	–	$45_{9\,37}$	78263.0895	-0.0205	0.0100	$49_{12\,37}$	–	$49_{11\,38}$	95634.5645	-0.0428	0.0100
$47_{10\,37}$	–	$47_{9\,38}$	77838.2045	0.1435	0.0100	$49_{12\,38}$	–	$49_{11\,39}$	95635.0334	-0.0147	0.0100
$47_{10\,38}$	–	$47_{9\,39}$	77887.4813	-0.0146	0.0100	$50_{12\,38}$	–	$50_{11\,39}$	95512.5450	0.0093	0.0100
$48_{10\,39}$	–	$48_{9\,40}$	77680.0967	-0.0883	0.0100	$50_{12\,39}$	–	$50_{11\,40}$	95513.2347	0.0210	0.0100
$49_{10\,39}$	–	$49_{9\,40}$	77360.1084	-0.1318	0.0100	$51_{12\,39}$	–	$51_{11\,40}$	95381.7564	-0.0534	0.0100
$49_{10\,40}$	–	$49_{9\,41}$	77459.6164	0.0307	0.0100	$51_{12\,40}$	–	$51_{11\,41}$	95382.7507	-0.0916	0.0100
$18_{11\,7}$	–	$18_{10\,8}$	88506.6781	0.1083	0.0100	$52_{12\,40}$	–	$52_{11\,41}$	95241.9479	0.0128	0.0100
$18_{11\,8}$	–	$18_{10\,9}$	88506.6781	0.1083	0.0100	$52_{12\,41}$	–	$52_{11\,42}$	95243.4641	-0.0284	0.0100
$19_{11\,8}$	–	$19_{10\,9}$	88501.4695	0.1911	0.0100	$53_{12\,41}$	–	$53_{11\,42}$	95092.3429	-0.0360	0.0100
$19_{11\,9}$	–	$19_{10\,10}$	88501.4695	0.1911	0.0100	$53_{12\,42}$	–	$53_{11\,43}$	95094.6397	-0.0667	0.0100
$25_{11\,14}$	–	$25_{10\,15}$	88435.4155	-0.0751	0.0100	$55_{12\,43}$	–	$55_{11\,44}$	94762.0156	0.1572	0.0100
$25_{11\,15}$	–	$25_{10\,16}$	88435.4155	-0.0751	0.0100	$55_{12\,44}$	–	$55_{11\,45}$	94766.9638	0.0438	0.0100
$26_{11\,15}$	–	$26_{10\,16}$	88417.1468	0.0172	0.0100						

Table B.3: the molecular constants from least squares fitting data analysis.

	mm
A/MHz	5533.8935(3)[a]
B/MHz	1393.8474(3)
C/MHz	1232.6674(3)
Δ_J/KHz	0.5676(10)
Δ_{JK}/KHz	-5.153(9)
Δ_K/KHz	24.04(2)
δ_J/KHz	0.1300(6)
δ_K/KHz	2.9094(1)
H_J/Hz	0.0042(7)
H_{JK}/Hz	0.49(8)
H_{KJ}/Hz	-1.6(2)
H_K/Hz	1.2(2)
h_J/Hz	0.0008(5)
h_{JK}/Hz	0.5(1)
h_K/Hz	18(2)
χ_{aa}/MHz	-8.044(6)
χ_{bb}/MHz	-15.72(1)
χ_{cc}/MHz	23.77(1)
χ_{ab}/MHz	-49.3(2)
χ_{ac}/MHz	-22.6(9)
χ_{bc}/MHz	-30.34(9)
σ_{fit}/MHz	0.0071

[a] Numbers in parenthesis denotes one standard deviation of least-squares fitting in the unit of the last significant digit.

Table B.4: comparison of result of least squares fitting data analysis of millimeter wave data and FTMW data for hyperfine constants.

	mm	FTMW[32]
χ_{aa}/MHz	-8.044(6)[a]	-8.0484(17)
χ_{bb}/MHz	-15.72(1)	-15.722(3)
χ_{cc}/MHz	23.77(1)	23.770(3)
χ_{ab}/MHz	-49.3(2)	-49.24(8)
χ_{ac}/MHz	-22.6(9)	-23.7(3)
χ_{bc}/MHz	-30.34(9)	-30.27(3)

[a] Numbers in parenthesis denotes one standard deviation of least-squares fitting in the unit of the last significant digit.

Appendix C

Theoretical Investigation of the *Ortho-Para* Interaction in S_2Cl_2

This appendix includes two sections. Section C-1 includes the list of the *ortho-para* mixed states and the calculated pattern of several candidate regions for experimental observation of the *ortho-para* transients. Section C-2 includes figures that show the dependency of the *ortho-para* mixing coefficients using the perturbation theorem.

C-1 Introducing the *ortho-para* interacting states

This section is an appendix for section 5-3-1. Table C.1 shows a list of the *ortho-para* mixed states by the *ortho-para* mixing coefficients $\rho_{mixing} > 0.001$. The *ortho-para* mixed states in this table are almost degenerate *K*-doubling states. These *ortho-para* mixed states lead to the *ortho-para* transitions in the millimeter wave region.

Table C.1: List of the *ortho-para* mixed states with the large ρ_{mixing} value, $\rho_{mixing} > 0.001$.

***Para* state**	**Term energy (MHz)**	***Ortho* state**	**Term energy (MHz)**	**$\lvert E_O - E_P \rvert$ (MHz)**	**ρ_{mixing}**
$18_{11\,7}\,2\,19$	959872.84(1.325)[a]	$18_{11\,8}\,1\,19$	959872.838(1.325)	0.003	0.486(3)[b]
$22_{12\,10}\,2\,21$	1272463.038(2.931)	$22_{12\,11}\,1\,21$	1272463.038(2.931)	0.000	0.466(5)
$17_{10\,8}\,2\,17$	824024.629(0.869)	$17_{10\,7}\,1\,17$	824024.629(0.869)	0.000	0.46(11)
$13_{7\,7\,2}\,14$	445967.573(0.187)	$13_{7\,6\,1}\,14$	445967.575(0.187)	0.002	0.458(4)
$15_{9\,7\,2}\,16$	657146.156(0.48)	$15_{9\,6\,1}\,16$	657146.159(0.48)	0.003	0.436(4)
$20_{12\,8}\,2\,20$	1159364.813(2.248)	$20_{12\,9}\,1\,20$	1159364.813(2.248)	0.000	0.43(11)
$12_{7\,5\,2}\,11$	411776.143(0.16)	$12_{7\,6\,3}\,11$	411776.147(0.16)	0.004	0.423(4)
$14_{8\,6\,2}\,14$	546028.349(0.301)	$14_{8\,7\,1}\,14$	546028.35(0.301)	0.001	0.406(10)
$9_{6\,4\,2}\,9$	270174.753(0.076)	$9_{6\,3\,1}\,9$	270174.753(0.076)	0.000	0.395(7)
$20_{12\,8}\,2\,19$	1159365.049(2.248)	$20_{12\,9}\,1\,19$	1159365.052(2.248)	0.004	0.381(4)
$22_{12\,10}\,2\,23$	1272463.043(2.931)	$22_{12\,11}\,1\,23$	1272463.043(2.931)	0.000	0.374(6)
$10_{6\,4\,2}\,11$	296471.551(0.086)	$10_{6\,5\,1}\,11$	296471.547(0.086)	0.004	0.368(2)
$17_{12\,6}\,2\,16$	1009462.223(1.563)	$17_{12\,5}\,1\,16$	1009462.245(1.563)	0.022	0.35(4)
$12_{7\,5\,2}\,12$	411776.063(0.16)	$12_{7\,6\,1}\,12$	411776.063(0.16)	0.000	0.339(11)
$15_{9\,7\,2}\,14$	657146.154(0.48)	$15_{9\,6\,1}\,14$	657146.151(0.48)	0.003	0.33(2)
$20_{11\,9}\,2\,19$	1062446.362(1.75)	$20_{11\,10}\,1\,19$	1062446.361(1.75)	0.001	0.323(5)
$15_{9\,7\,2}\,15$	657145.944(0.48)	$15_{9\,6\,1}\,15$	657145.944(0.48)	0.000	0.308(10)
$20_{12\,8}\,2\,21$	1159365.052(2.248)	$20_{12\,9}\,1\,21$	1159365.056(2.248)	0.004	0.299(4)
$17_{10\,8}\,2\,16$	824024.776(0.869)	$17_{10\,7}\,1\,16$	824024.782(0.869)	0.006	0.29(4)
$12_{7\,5\,2}\,13$	411776.15(0.16)	$12_{7\,6\,1}\,13$	411776.155(0.16)	0.005	0.286(4)
$11_{6\,6\,2}\,10$	325401.977(0.1)	$11_{6\,5\,3}\,10$	325401.96(0.1)	0.017	0.281(5)
$17_{12\,6}\,2\,18$	1009462.222(1.563)	$17_{12\,5}\,1\,18$	1009462.248(1.563)	0.026	0.277(4)
$18_{11\,7}\,2\,17$	959872.836(1.325)	$18_{11\,8}\,1\,17$	959872.834(1.325)	0.003	0.274(1)
$19_{12\,8}\,2\,20$	1106765.27(1.981)	$19_{12\,7}\,1\,20$	1106765.268(1.981)	0.003	0.247(1)
$21_{7\,15}\,2\,23$	814478.092(0.846)	$21_{7\,14}\,3\,23$	814478.148(0.846)	0.056	0.244(4)
$17_{10\,8}\,2\,18$	824024.78(0.869)	$17_{10\,7}\,1\,18$	824024.787(0.869)	0.007	0.241(4)
$20_{11\,9}\,2\,21$	1062446.367(1.75)	$20_{11\,10}\,1\,21$	1062446.366(1.75)	0.001	0.24(5)
$13_{8\,6\,2}\,14$	509210.02(0.259)	$13_{8\,5\,1}\,14$	509210.017(0.259)	0.003	0.239(1)
$18_{7\,11}\,2\,19$	656478.815(0.48)	$18_{7\,12}\,1\,19$	656478.81(0.48)	0.005	0.236(1)
$22_{7\,15}\,2\,20$	872436.429(1.013)	$22_{7\,16}\,3\,20$	872436.375(1.013)	0.053	0.231(2)
$16_{10\,6}\,2\,17$	779316.665(0.755)	$16_{10\,7}\,1\,17$	779316.662(0.755)	0.003	0.219(2)
$11_{6\,6\,2}\,12$	325401.991(0.1)	$11_{6\,5\,1}\,12$	325401.968(0.1)	0.023	0.215(4)

$9_{7\,3\,2}$ 10	325003.447(0.113)	$9_{7\,2\,1}$ 10	325003.419(0.113)	0.028	0.206(2)
$14_{8\,6\,2}$ 13	546028.374(0.301)	$14_{8\,7\,3}$ 13	546028.389(0.301)	0.015	0.193(4)
$13_{7\,7\,2}$ 12	445967.564(0.187)	$13_{7\,6\,3}$ 12	445967.566(0.187)	0.002	0.188(1)
$14_{8\,6\,2}$ 15	546028.379(0.301)	$14_{8\,7\,1}$ 15	546028.397(0.301)	0.018	0.185(4)
$22_{8\,14}$ 2 23	935489.845(1.244)	$22_{8\,15}$ 1 23	935489.851(1.244)	0.006	0.183(3)
$18_{10\,8}$ 2 19	871366.27(1.007)	$18_{10\,9}$ 1 19	871366.268(1.007)	0.002	0.182(4)
$14_{10\,4}$ 2 15	697798.288(0.587)	$14_{10\,5}$ 1 15	697798.279(0.587)	0.009	0.174(2)
$19_{11\,9}$ 2 20	1009843.011(1.519)	$19_{11\,8}$ 1 20	1009842.982(1.519)	0.029	0.165(4)
$18_{11\,7}$ 2 18	959872.537(1.325)	$18_{11\,8}$ 1 18	959872.537(1.325)	0.000	0.165(5)
$19_{11\,9}$ 2 18	1009843.004(1.519)	$19_{11\,8}$ 1 18	1009842.978(1.519)	0.026	0.165(4)
$16_{9\,7\,2}$ 15	699225.972(0.558)	$16_{9\,8\,1}$ 15	699225.966(0.558)	0.006	0.153(4)
$21_{12\,10}$ 2 22	1214597.521(2.563)	$21_{12\,9}$ 1 22	1214597.517(2.563)	0.004	0.135(3)
$21_{12\,10}$ 2 20	1214597.516(2.563)	$21_{12\,9}$ 1 20	1214597.513(2.563)	0.004	0.128(3)
$17_{12\,6}$ 2 17	1009461.281(1.563)	$17_{12\,5}$ 1 17	1009461.281(1.563)	0.000	0.121(2)
$17_{11\,7}$ 2 18	912535.47(1.163)	$17_{11\,6}$ 1 18	912535.467(1.163)	0.004	0.112(1)
$18_{12\,6}$ 2 19	1056797.787(1.755)	$18_{12\,7}$ 1 19	1056797.783(1.755)	0.004	0.11(1)
$19_{12\,8}$ 2 18	1106765.267(1.981)	$19_{12\,7}$ 1 18	1106765.264(1.981)	0.003	0.101(1)
$18_{7\,11}$ 2 17	656478.772(0.48)	$18_{7\,12}$ 1 17	656478.769(0.48)	0.003	0.096(1)
$15_{8\,8\,2}$ 16	585480.984(0.353)	$15_{8\,7\,1}$ 16	585480.985(0.353)	0.001	0.093(1)
$11_{5\,7\,2}$ 13	279033.934(0.078)	$11_{5\,6\,3}$ 13	279033.917(0.078)	0.017	0.093(2)
$16_{11\,5}$ 2 17	867830.424(1.029)	$16_{11\,6}$ 1 17	867830.418(1.029)	0.006	0.09(1)
$22_{8\,14}$ 2 20	935489.829(1.244)	$22_{8\,15}$ 3 20	935489.905(1.244)	0.077	0.082(1)
$14_{9\,5\,2}$ 15	617699.756(0.418)	$14_{9\,6\,1}$ 15	617699.751(0.418)	0.005	0.077(1)
$10_{6\,4\,2}$ 9	296471.543(0.086)	$10_{6\,5\,3}$ 9	296471.538(0.086)	0.005	0.073(1)
$16_{10\,6}$ 2 15	779316.661(0.755)	$16_{10\,7}$ 1 15	779316.657(0.755)	0.004	0.072(1)
$13_{8\,6\,2}$ 13	509209.727(0.259)	$13_{8\,5\,1}$ 13	509209.727(0.259)	0.000	0.064(2)
$11_{7\,5\,2}$ 12	380218.978(0.139)	$11_{7\,4\,1}$ 12	380218.972(0.139)	0.006	0.064(1)
$13_{8\,6\,2}$ 12	509210.015(0.259)	$13_{8\,5\,3}$ 12	509210.01(0.259)	0.005	0.059(1)
$21_{8\,14}$ 2 22	877569.291(1.043)	$21_{8\,13}$ 1 22	877569.301(1.043)	0.010	0.055(1)
$16_{9\,7\,2}$ 14	699225.979(0.558)	$16_{9\,8\,3}$ 14	699225.978(0.558)	0.001	0.054(4)
$15_{10\,6}$ 2 16	737241.342(0.662)	$15_{10\,5}$ 1 16	737241.337(0.662)	0.006	0.053(1)
$14_{10\,4}$ 2 13	697798.287(0.587)	$14_{10\,5}$ 3 13	697798.273(0.587)	0.014	0.049(1)
$22_{8\,14}$ 2 21	935489.771(1.244)	$22_{8\,15}$ 1 21	935489.773(1.244)	0.002	0.041(0)
$18_{12\,6}$ 2 17	1056797.785(1.755)	$18_{12\,7}$ 1 17	1056797.779(1.755)	0.006	0.039(1)
$17_{11\,7}$ 2 16	912535.468(1.163)	$17_{11\,6}$ 1 16	912535.462(1.163)	0.005	0.037(1)

$12_{9\,3\,2}$ 13	546704.59(0.329)	$12_{9\,4\,1}$ 13	546704.558(0.329)	0.032	0.035(1)
$8_{5\,3\,2}$ 9	200116.576(0.047)	$8_{5\,4\,1}$ 9	200116.565(0.047)	0.011	0.035(1)
$16_{10\,6}$ 2 16	779316.285(0.755)	$16_{10\,7}$ 1 16	779316.285(0.755)	0.000	0.033(1)
$16_{9\,7\,2}$ 18	699225.967(0.558)	$16_{9\,8\,3}$ 18	699225.964(0.558)	0.002	0.033(1)
$9_{7\,3\,2}$ 8	325003.448(0.113)	$9_{7\,2\,3}$ 8	325003.395(0.113)	0.053	0.03(1)
$13_{9\,5\,2}$ 14	580886.099(0.368)	$13_{9\,4\,1}$ 14	580886.089(0.368)	0.009	0.029(1)
$16_{11\,5}$ 2 15	867830.423(1.029)	$16_{11\,6}$ 1 15	867830.414(1.029)	0.009	0.028(1)
$23_{8\,16}$ 2 22	996053.352(1.477)	$23_{8\,15}$ 1 22	996053.372(1.477)	0.020	0.028(1)
$12_{8\,4\,2}$ 13	475025.022(0.227)	$12_{8\,5\,1}$ 13	475025.014(0.227)	0.008	0.028(1)
$19_{12\,8}$ 2 19	1106764.829(1.981)	$19_{12\,7}$ 1 19	1106764.829(1.981)	0.000	0.027(1)
$9_{5\,5\,2}$ 10	223786.147(0.054)	$9_{5\,4\,1}$ 10	223786.173(0.054)	0.026	0.023(1)
$11_{8\,4\,2}$ 12	443472.624(0.203)	$11_{8\,3\,1}$ 12	443472.608(0.203)	0.016	0.023(0)
$12_{6\,6\,2}$ 13	356967.865(0.118)	$12_{6\,7\,1}$ 13	356967.867(0.118)	0.002	0.023(1)
$21_{8\,14}$ 2 20	877569.253(1.043)	$21_{8\,13}$ 1 20	877569.262(1.043)	0.009	0.023(0)
$14_{9\,5\,2}$ 13	617699.752(0.418)	$14_{9\,6\,3}$ 13	617699.745(0.418)	0.007	0.02(0)
$17_{9\,9\,2}$ 18	743939.896(0.655)	$17_{9\,8\,1}$ 18	743939.897(0.655)	0.001	0.019(0)
$14_{8\,6\,2}$ 12	546028.382(0.301)	$14_{8\,7\,3}$ 12	546028.37(0.301)	0.012	0.018(1)
$9_{6\,4\,2}$ 10	270175.319(0.076)	$9_{6\,3\,1}$ 10	270175.307(0.076)	0.012	0.018(0)
$15_{11\,5}$ 2 16	825757.29(0.917)	$15_{11\,4}$ 1 16	825757.274(0.917)	0.016	0.016(0)
$16_{7\,9\,2}$ 17	564358.423(0.324)	$16_{7\,10}$ 1 17	564358.428(0.324)	0.004	0.016(0)
$15_{10\,6}$ 2 14	737241.34(0.662)	$15_{10\,5}$ 1 14	737241.331(0.662)	0.009	0.015(0)
$12_{9\,3\,2}$ 11	546704.587(0.329)	$12_{9\,4\,3}$ 11	546704.546(0.329)	0.041	0.015(0)
$17_{9\,9\,2}$ 16	743939.888(0.655)	$17_{9\,8\,1}$ 16	743939.89(0.655)	0.002	0.015(0)
$20_{7\,13}$ 2 21	759166.875(0.704)	$20_{7\,14}$ 1 21	759166.817(0.704)	0.058	0.013(0)
$14_{8\,6\,2}$ 16	546028.391(0.301)	$14_{8\,7\,3}$ 16	546028.396(0.301)	0.005	0.012(0)
$11_{7\,5\,2}$ 11	380218.575(0.139)	$11_{7\,4\,1}$ 11	380218.575(0.139)	0.000	0.012(0)
$10_{7\,3\,2}$ 11	351295.05(0.124)	$10_{7\,4\,1}$ 11	351295.035(0.124)	0.015	0.011(0)
$20_{8\,12}$ 2 21	822290.523(0.871)	$20_{8\,13}$ 1 21	822290.527(0.871)	0.004	0.011(0)
$11_{7\,5\,2}$ 10	380218.973(0.139)	$11_{7\,4\,3}$ 10	380218.962(0.139)	0.011	0.011(0)
$15_{6\,10}$ 2 17	467493.289(0.212)	$15_{6\,9\,3}$ 17	467493.196(0.212)	0.093	0.011(0)
$18_{7\,11}$ 2 16	656478.807(0.48)	$18_{7\,12}$ 3 16	656478.904(0.48)	0.097	0.01(0)
$24_{8\,16}$ 2 23	1059261.436(1.745)	$24_{8\,17}$ 1 23	1059261.426(1.745)	0.011	0.009(0)
$19_{7\,13}$ 2 20	706501.215(0.582)	$19_{7\,12}$ 1 20	706501.25(0.582)	0.035	0.009(0)
$22_{9\,13}$ 2 23	1007048.938(1.531)	$22_{9\,14}$ 1 23	1007048.943(1.531)	0.004	0.009(0)
$9_{5\,5\,2}$ 8	223786.135(0.054)	$9_{5\,4\,3}$ 8	223786.161(0.054)	0.025	0.009(0)

$23_{9\,15}$ 2 24	1067584.806(1.809)	$23_{9\,14}$ 1 24	1067584.81(1.809)	0.004	0.008(0)
$24_{9\,15}$ 2 22	1130760.955(2.13)	$24_{9\,16}$ 3 22	1130761.039(2.13)	0.084	0.008(0)
$21_{8\,14}$ 2 19	877569.286(1.043)	$21_{8\,13}$ 3 19	877569.382(1.043)	0.096	0.008(0)
$24_{10\,14}$ 2 25	1210751.172(2.592)	$24_{10\,15}$ 1 25	1210751.176(2.592)	0.003	0.008(0)
$15_{11\,5}$ 2 14	825757.289(0.917)	$15_{11\,4}$ 1 14	825757.268(0.917)	0.021	0.007(0)
$18_{8\,10}$ 2 19	719653.261(0.603)	$18_{8\,11}$ 1 19	719653.266(0.603)	0.005	0.007(0)
$13_{9\,5\,2}$ 12	580886.097(0.368)	$13_{9\,4\,3}$ 12	580886.082(0.368)	0.015	0.007(0)
$19_{8\,12}$ 2 20	769652.245(0.726)	$19_{8\,11}$ 1 20	769652.251(0.726)	0.006	0.007(0)
$21_{9\,13}$ 2 22	949152.342(1.292)	$21_{9\,12}$ 1 22	949152.346(1.292)	0.004	0.007(0)
$24_{8\,16}$ 2 25	1059261.399(1.745)	$24_{8\,17}$ 1 25	1059261.383(1.745)	0.016	0.007(0)
$9_{5\,5\,2}$ 11	223786.146(0.054)	$9_{5\,4\,3}$ 11	223786.126(0.054)	0.020	0.007(0)
$17_{11\,7}$ 2 17	912534.936(1.163)	$17_{11\,6}$ 1 17	912534.936(1.163)	0.000	0.007(0)
$23_{10\,14}$ 2 24	1147595.944(2.216)	$23_{10\,13}$ 1 24	1147595.947(2.216)	0.003	0.006(0)
$19_{10\,10}$ 2 18	921341.693(1.174)	$19_{10\,9}$ 1 18	921341.695(1.174)	0.001	0.006(0)
$20_{9\,11}$ 2 21	893894.043(1.089)	$20_{9\,12}$ 1 21	893894.047(1.089)	0.004	0.006(0)
$12_{8\,4\,2}$ 11	475025.019(0.227)	$12_{8\,5\,3}$ 11	475025.005(0.227)	0.014	0.006(0)
$14_{9\,5\,2}$ 14	617699.275(0.418)	$14_{9\,6\,1}$ 14	617699.275(0.418)	0.000	0.006(0)
$18_{10\,8}$ 2 16	871366.271(1.007)	$18_{10\,9}$ 3 16	871366.275(1.007)	0.004	0.006(0)
$22_{10\,12}$ 2 23	1087078.123(1.89)	$22_{10\,13}$ 1 23	1087078.126(1.89)	0.003	0.005(0)
$17_{8\,10}$ 2 18	672292.43(0.502)	$17_{8\,9\,1}$ 18	672292.434(0.502)	0.004	0.005(0)
$24_{11\,13}$ 2 25	1299202.585(3.157)	$24_{11\,14}$ 1 25	1299202.588(3.157)	0.002	0.005(0)
$19_{10\,10}$ 2 20	921341.7(1.174)	$19_{10\,9}$ 1 20	921341.701(1.174)	0.001	0.005(0)
$19_{9\,11}$ 2 20	841273.116(0.917)	$19_{9\,10}$ 1 20	841273.119(0.917)	0.003	0.005(0)
$15_{7\,9\,2}$ 16	522257.504(0.268)	$15_{7\,8\,1}$ 16	522257.51(0.268)	0.006	0.005(0)
$11_{8\,4\,2}$ 10	443472.623(0.203)	$11_{8\,3\,3}$ 10	443472.594(0.203)	0.029	0.005(0)
$8_{6\,2\,2}$ 9	246512.083(0.069)	$8_{6\,3\,1}$ 9	246512.051(0.069)	0.032	0.005(0)
$9_{5\,5\,2}$ 7	223786.15(0.054)	$9_{5\,4\,3}$ 7	223786.195(0.054)	0.045	0.004(0)
$21_{10\,12}$ 2 22	1029196.953(1.611)	$21_{10\,11}$ 1 22	1029196.956(1.611)	0.003	0.004(0)
$23_{11\,13}$ 2 24	1236061.039(2.721)	$23_{11\,12}$ 1 24	1236061.042(2.721)	0.002	0.004(0)
$8_{5\,3\,2}$ 7	200116.568(0.047)	$8_{5\,4\,3}$ 7	200116.548(0.047)	0.020	0.004(0)
$10_{5\,5\,2}$ 8	250091.4(0.064)	$10_{5\,6\,3}$ 8	250091.455(0.064)	0.055	0.004(0)
$18_{10\,8}$ 2 20	871366.263(1.007)	$18_{10\,9}$ 3 20	871366.257(1.007)	0.007	0.003(0)
$14_{6\,8\,2}$ 12	428011.945(0.173)	$14_{6\,9\,3}$ 12	428012.045(0.173)	0.100	0.003(0)
$21_{11\,11}$ 2 20	1117683.48(2.024)	$21_{11\,10}$ 1 20	1117683.481(2.024)	0.001	0.003(0)
$14_{7\,7\,2}$ 15	482794.302(0.222)	$14_{7\,8\,1}$ 15	482794.306(0.222)	0.004	0.003(0)

$20_{7\,13}$ 2 19	759167.07(0.704)	$20_{7\,14}$ 1 19	759167.031(0.704)	0.039	0.003(0)
$16_{8\,8\,2}$ 17	627568.676(0.42)	$16_{8\,9\,1}$ 17	627568.679(0.42)	0.003	0.003(0)
$19_{11\,9}$ 2 17	1009843.01(1.519)	$19_{11\,8}$ 3 17	1009842.994(1.519)	0.017	0.003(0)
$18_{12\,6}$ 2 18	1056797.11(1.755)	$18_{12\,7}$ 1 18	1056797.11(1.755)	0.000	0.002(0)
$18_{9\,9\,2}$ 19	791288.679(0.774)	$18_{9\,10}$ 1 19	791288.682(0.774)	0.002	0.002(0)
$20_{10\,10}$ 2 21	973951.709(1.374)	$20_{10\,11}$ 1 21	973951.711(1.374)	0.002	0.002(0)
$23_{9\,15}$ 2 21	1067584.8(1.809)	$23_{9\,14}$ 3 21	1067584.888(1.809)	0.088	0.002(0)
$22_{11\,11}$ 2 23	1175554.863(2.346)	$22_{11\,12}$ 1 23	1175554.864(2.346)	0.002	0.002(0)
$20_{8\,12}$ 2 18	822290.517(0.871)	$20_{8\,13}$ 3 18	822290.615(0.871)	0.098	0.002(0)
$17_{7\,11}$ 2 18	609098.383(0.394)	$17_{7\,10}$ 1 18	609098.394(0.394)	0.011	0.002(0)
$24_{12\,12}$ 2 25	1396094.938(3.857)	$24_{12\,13}$ 1 25	1396094.939(3.857)	0.001	0.002(0)
$9_{6\,4\,2}$ 8	270175.315(0.076)	$9_{6\,3\,3}$ 8	270175.29(0.076)	0.025	0.002(0)
$10_{7\,3\,2}$ 9	351295.048(0.124)	$10_{7\,4\,3}$ 9	351295.019(0.124)	0.029	0.002(0)
$12_{7\,5\,2}$ 10	411776.153(0.16)	$12_{7\,6\,3}$ 10	411776.127(0.16)	0.026	0.002(0)
$20_{11\,9}$ 2 18	1062446.367(1.75)	$20_{11\,10}$ 3 18	1062446.375(1.75)	0.008	0.002(0)
$23_{12\,12}$ 2 22	1332962.035(3.36)	$23_{12\,11}$ 1 22	1332962.036(3.36)	0.001	0.002(0)
$15_{10\,6}$ 2 15	737240.689(0.662)	$15_{10\,5}$ 1 15	737240.689(0.662)	0.000	0.002(0)
$23_{9\,15}$ 2 25	1067584.796(1.809)	$23_{9\,14}$ 3 25	1067584.697(1.809)	0.098	0.002(0)
$16_{12\,4}$ 2 17	964758.334(1.402)	$16_{12\,5}$ 1 17	964758.321(1.402)	0.013	0.002(0)
$10_{6\,4\,2}$ 10	296471.387(0.086)	$10_{6\,5\,1}$ 10	296471.386(0.086)	0.000	0.002(0)
$12_{7\,5\,2}$ 14	411776.149(0.16)	$12_{7\,6\,3}$ 14	411776.166(0.16)	0.017	0.001(0)
$13_{6\,8\,2}$ 14	391170.665(0.142)	$13_{6\,7\,1}$ 14	391170.683(0.142)	0.018	0.001(0)
$21_{11\,11}$ 2 22	1117683.486(2.024)	$21_{11\,10}$ 1 22	1117683.487(2.024)	0.001	0.001(0)
$20_{11\,9}$ 2 22	1062446.361(1.75)	$20_{11\,10}$ 3 22	1062446.352(1.75)	0.009	0.001(0)
$11_{6\,6\,2}$ 13	325401.956(0.1)	$11_{6\,5\,3}$ 13	325401.921(0.1)	0.035	0.001(0)
$15_{6\,10}$ 2 16	467493.303(0.212)	$15_{6\,9\,1}$ 16	467493.374(0.212)	0.071	0.001(0)
$13_{10\,4}$ 2 14	660987.021(0.527)	$13_{10\,3}$ 1 14	660987(0.527)	0.020	0.001(0)
$22_{9\,13}$ 2 20	1007048.934(1.531)	$22_{9\,14}$ 3 20	1007049.023(1.531)	0.088	0.001(0)
$12_{8\,4\,2}$ 12	475024.403(0.227)	$12_{8\,5\,1}$ 12	475024.403(0.227)	0.000	0.001(0)

[a] Numbers in parenthesis denotes uncertainty in the unit of MHz.
[b] Numbers in parenthesis denotes uncertainty in the unit of the last significant digit.

Using transitions which are listed in Tables C.2 to C.9, Figure C.1 to C.8 are obtained. The *ortho-para* transitions are shown in red color rows in the tables. There are the corresponding Figures, after each table.

Table C.2: List of the hyperfine transitions and their transition moments resolved rotational transition of $13_{5\,8} - 12_{6\,7}$.

Transition			Frequency (MHz)	Transition moment	Transition			Frequency (MHz)	Transition moment
$13_{5\,8}$ 3 14	-	$12_{6\,7}$ 3 14	12128.6380	0.02	$13_{5\,8}$ 3 11	-	$12_{6\,7}$ 3 10	12127.7625	0.89
$13_{5\,9}$ 2 14	-	$12_{6\,7}$ 1 13	12128.4332	0.02[a]	$13_{5\,8}$ 1 14	-	$12_{6\,7}$ 1 13	12127.6885	1.14
$13_{5\,9}$ 2 15	-	$12_{6\,7}$ 3 14	12128.3798	0.02[b]	$13_{5\,8}$ 3 11	-	$12_{6\,7}$ 3 11	12127.6712	0.02
$13_{5\,8}$ 3 14	-	$12_{6\,7}$ 3 13	12128.3241	1.15	$13_{5\,8}$ 1 14	-	$12_{6\,7}$ 3 14	12127.5904	0.01
$13_{5\,8}$ 3 15	-	$12_{6\,7}$ 3 15	12128.3231	0.02	$13_{5\,8}$ 3 12	-	$12_{6\,7}$ 3 12	12127.5420	0.01
$13_{5\,8}$ 3 13	-	$12_{6\,7}$ 3 12	12128.1872	1.04	$13_{5\,8}$ 3 10	-	$12_{6\,7}$ 3 9	12127.4424	0.83
$13_{5\,8}$ 3 13	-	$12_{6\,7}$ 3 13	12128.1234	0.03	$13_{5\,8}$ 1 13	-	$12_{6\,7}$ 1 12	12127.4062	1.08
$13_{5\,8}$ 1 12	-	$12_{6\,7}$ 1 11	12128.0713	0.98	$13_{5\,8}$ 3 11	-	$12_{6\,7}$ 1 11	12127.3761	0.01
$13_{5\,8}$ 1 12	-	$12_{6\,7}$ 3 12	12128.0306	0.02	$13_{5\,8}$ 3 16	-	$12_{6\,7}$ 3 15	12127.3698	1.33
$13_{5\,8}$ 3 15	-	$12_{6\,7}$ 3 14	12127.9270	1.21	$13_{5\,8}$ 3 10	-	$12_{6\,7}$ 3 10	12127.1454	0.02
$13_{5\,8}$ 3 12	-	$12_{6\,7}$ 3 11	12127.8778	0.98					

[a] $|13_{5\,9}\ 2\ 13\rangle^{P}$- $|13_{5\,8}\ 3\ 13\rangle^{O}$ *ortho-para* mixing states by mixing coefficient $\rho_{mixing} = 0.007$ leads to this transition.

[b] $|13_{5\,9}\ 2\ 15\rangle^{P}$- $|13_{5\,8}\ 3\ 15\rangle^{O}$ *ortho-para* mixing states by mixing coefficient $\rho_{mixing} = 0.014$ leads to this transition.

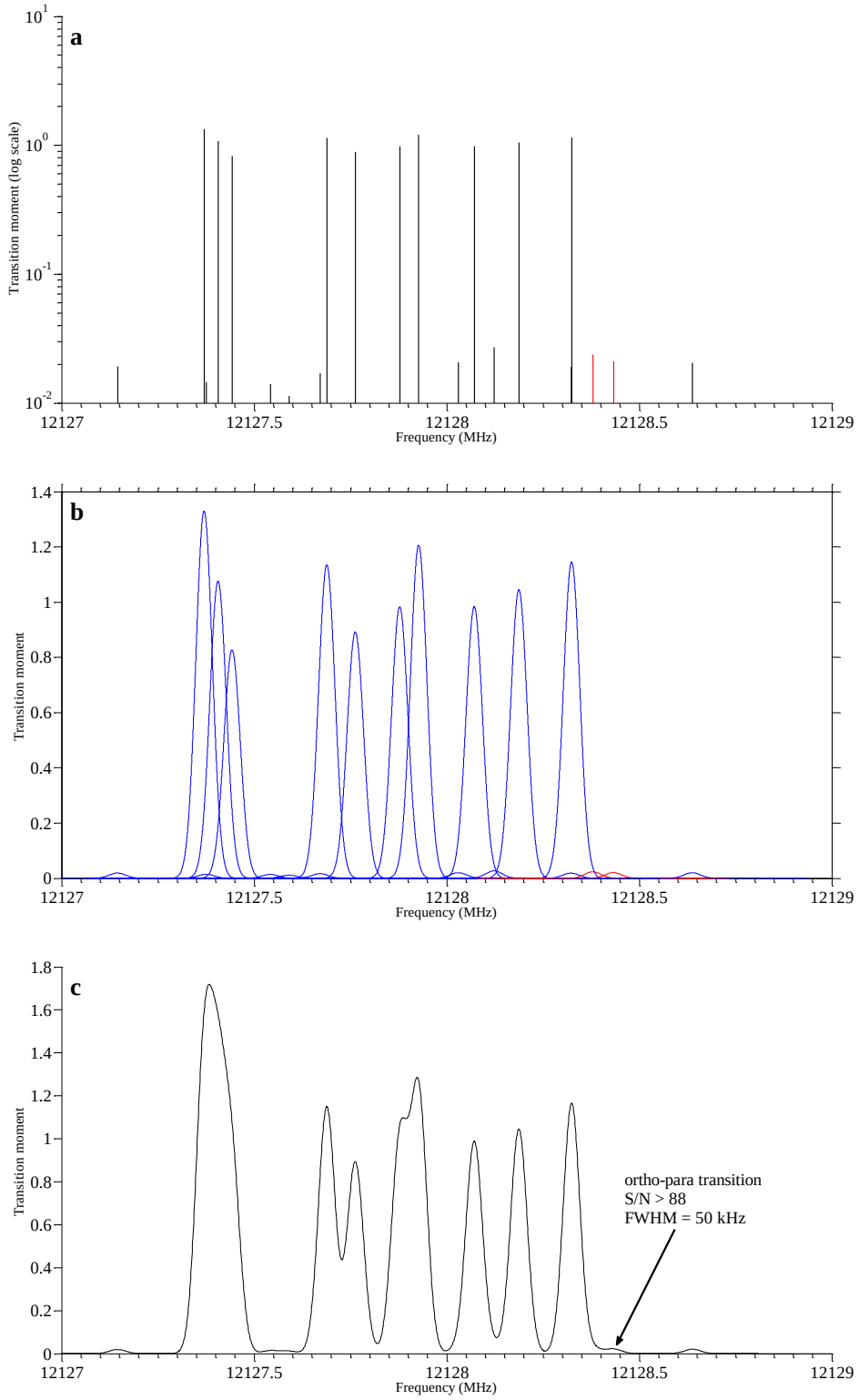

Figure C.1: (a) Blue and red sticks in this Figure correspond to the normal and *ortho-para* transitions respectively, which are listed in Table C.2. (b) Each line shape is estimated as a Gaussian type by the FWHM equal to 50 kHz. (c) Summation of all peaks in Figure C.1.b

Table C.3: List of the hyperfine transitions and their transition moments resolved rotational transition of $13_{5\,8} - 13_{4\,9}$.

Transition	Frequency (MHz)	Transition moment	Transition	Frequency (MHz)	Transition moment
$13_{5\,8}3\ 16$ - $13_{4\,9}3\ 15$	37805.8717	0.10	$13_{5\,8}3\ 15$ - $13_{4\,9}3\ 15$	37804.9185	6.92
$13_{5\,8}1\ 14$ - $13_{4\,9}3\ 13$	37805.8682	0.04	$13_{5\,8}3\ 11$ - $13_{4\,9}3\ 11$	37804.9028	5.10
$13_{5\,8}3\ 11$ - $13_{4\,9}1\ 12$	37805.7951	0.08	$13_{5\,8}3\ 12$ - $13_{4\,9}3\ 12$	37804.8952	5.66
$13_{5\,9}2\ 13$ - $13_{4\,9}3\ 13$	37805.7775	0.04[a]	$13_{5\,8}3\ 10$ - $13_{4\,9}3\ 10$	37804.8638	4.84
$13_{5\,8}1\ 13$ - $13_{4\,9}3\ 12$	37805.7137	0.06	$13_{5\,9}2\ 12$ - $13_{4\,9}1\ 12$	37804.8633	0.01
$13_{5\,8}1\ 13$ - $13_{4\,9}1\ 14$	37805.7042	0.06	$13_{5\,8}3\ 14$ - $13_{4\,9}3\ 13$	37804.8207	0.14
$13_{5\,8}3\ 12$ - $13_{4\,9}3\ 13$	37805.6666	0.08	$13_{5\,8}3\ 15$ - $13_{4\,9}1\ 14$	37804.7509	0.06
$13_{5\,8}3\ 15$ - $13_{4\,9}3\ 14$	37805.6542	0.11	$13_{5\,8}3\ 12$ - $13_{4\,9}3\ 11$	37804.6962	0.09
$13_{5\,8}3\ 10$ - $13_{4\,9}3\ 11$	37805.5199	0.10	$13_{5\,9}2\ 15$ - $13_{4\,9}3\ 15$	37804.4656	0.10[b]
$13_{5\,8}1\ 14$ - $13_{4\,9}3\ 15$	37805.2550	0.06	$13_{5\,8}1\ 14$ - $13_{4\,9}1\ 13$	37804.3210	0.05
$13_{5\,8}1\ 12$ - $13_{4\,9}3\ 13$	37805.1779	0.11	$13_{5\,8}3\ 13$ - $13_{4\,9}3\ 12$	37804.2500	0.07
$13_{5\,8}3\ 13$ - $13_{4\,9}3\ 14$	37805.1439	0.15	$13_{5\,8}3\ 11$ - $13_{4\,9}3\ 10$	37804.2468	0.10
$13_{5\,8}3\ 11$ - $13_{4\,9}3\ 12$	37805.1018	0.09	$13_{5\,8}3\ 13$ - $13_{4\,9}1\ 14$	37804.2405	0.04
$13_{5\,8}1\ 12$ - $13_{4\,9}1\ 12$	37805.0998	5.67	$13_{5\,8}1\ 12$ - $13_{4\,9}3\ 11$	37804.2075	0.08
$13_{5\,8}1\ 14$ - $13_{4\,9}1\ 14$	37805.0874	6.66	$13_{5\,8}3\ 14$ - $13_{4\,9}3\ 15$	37804.2074	0.11
$13_{5\,8}3\ 13$ - $13_{4\,9}3\ 13$	37805.0213	5.92	$13_{5\,9}2\ 11$ - $13_{4\,9}3\ 11$	37804.1387	0.04
$13_{5\,8}3\ 16$ - $13_{4\,9}3\ 16$	37805.0088	7.66	$13_{5\,8}3\ 12$ - $13_{4\,9}1\ 13$	37804.1193	0.05
$13_{5\,8}3\ 13$ - $13_{4\,9}1\ 12$	37804.9433	0.11	$13_{5\,8}3\ 15$ - $13_{4\,9}3\ 16$	37804.0555	0.10
$13_{5\,8}3\ 14$ - $13_{4\,9}3\ 14$	37804.9432	6.55	$13_{5\,8}3\ 13$ - $13_{4\,9}1\ 13$	37803.4741	0.02
$13_{5\,8}1\ 13$ - $13_{4\,9}1\ 13$	37804.9378	6.23			

[a] $|13_{5\,9}\ 2\ 13\rangle^{P}$- $|13_{5\,8}\ 3\ 13\rangle^{O}$ *ortho-para* mixing states by mixing coefficient $\rho_{mixing} = 0.007$ leads to this transition.

[b] $|13_{5\,9}\ 2\ 15\rangle^{P}$- $|13_{5\,8}\ 3\ 15\rangle^{O}$ *ortho-para* mixing states by mixing coefficient $\rho_{mixing} = 0.014$ leads to this transition.

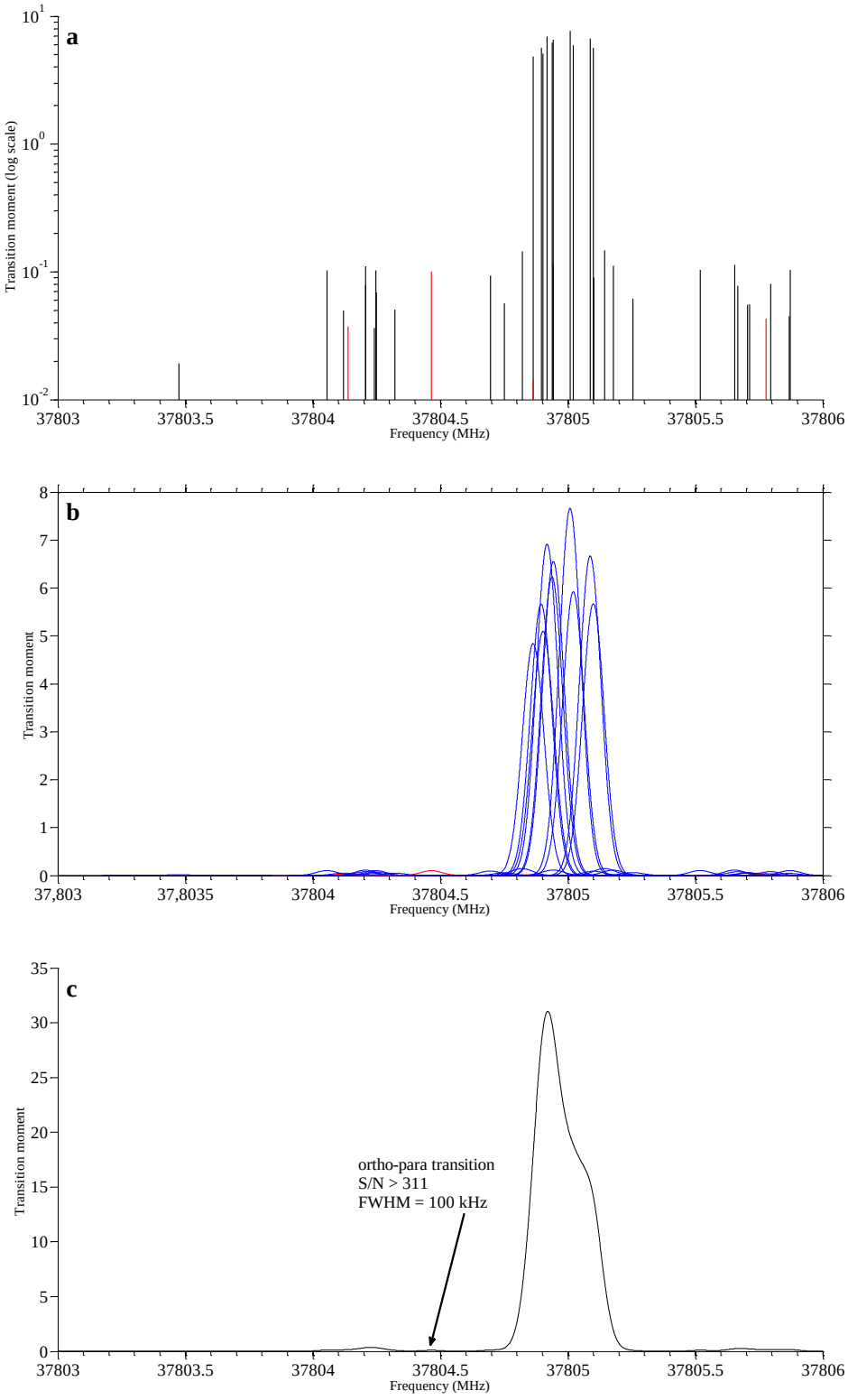

Figure C.2: (a) Blue and red sticks in this Figure correspond to the normal and *ortho-para* transitions respectively, which are listed in Table C.3. (b) Each line shape is estimated as a Gaussian type by the FWHM equal to 100 kHz. (c) Summation of all peaks in Figure C.2.b

Table C.4: List of the hyperfine transitions and their transition moments resolved rotational transition of $13_{5\,9}$– $13_{4\,10}$.

Transition	Frequency (MHz)	Transition moment	Transition	Frequency (MHz)	Transition moment
$13_{5\,9}2\ 14$ - $13_{4\,10}2\ 13$	37834.3596	0.05	$13_{5\,9}2\ 15$ - $13_{4\,10}2\ 15$	37833.4674	7.12
$13_{5\,8}3\ 11$ - $13_{4\,10}2\ 11$	37834.2609	0.04	$13_{5\,9}2\ 15$ - $13_{4\,10}2\ 14$	37833.4375	0.07
$13_{5\,9}2\ 12$ - $13_{4\,10}2\ 13$	37834.1774	0.05	$13_{5\,9}2\ 12$ - $13_{4\,10}2\ 11$	37833.3290	0.07
$13_{5\,9}2\ 13$ - $13_{4\,10}2\ 12$	37834.1550	0.05	$13_{5\,9}2\ 12$ - $13_{4\,10}2\ 12$	37833.3187	5.69
$13_{5\,9}2\ 13$ - $13_{4\,10}2\ 14$	37834.1362	0.05	$13_{5\,9}2\ 13$ - $13_{4\,10}0\ 13$	37833.2805	6.19
$13_{5\,8}3\ 15$ - $13_{4\,10}2\ 15$	37833.9202	0.10[a]	$13_{5\,9}0\ 13$ - $13_{4\,10}2\ 12$	37832.6357	0.05
$13_{5\,8}1\ 12$ - $13_{4\,10}2\ 12$	37833.5553	0.01	$13_{5\,9}2\ 14$ - $13_{4\,10}0\ 13$	37832.6265	0.05
$13_{5\,9}2\ 14$ - $13_{4\,10}2\ 15$	37833.5121	0.07	$13_{5\,9}0\ 13$ - $13_{4\,10}2\ 14$	37832.6170	0.05
$13_{5\,9}2\ 11$ - $13_{4\,10}2\ 11$	37833.4968	5.30	$13_{5\,8}3\ 13$ - $13_{4\,10}2\ 13$	37832.5243	0.05[b]
$13_{5\,9}0\ 13$ - $13_{4\,10}2\ 13$	37833.4944	6.24	$13_{5\,9}2\ 12$ - $13_{4\,10}0\ 13$	37832.4442	0.05
$13_{5\,9}2\ 11$ - $13_{4\,10}2\ 12$	37833.4865	0.07	$13_{5\,9}0\ 13$ - $13_{4\,10}0\ 13$	37831.7613	0.01
$13_{5\,9}2\ 14$ - $13_{4\,10}2\ 14$	37833.4822	6.64			

[a] $|13_{5\,9}\ 2\ 13\rangle^{P}$- $|13_{5\,8}\ 3\ 13\rangle^{O}$ *ortho-para* mixing states by mixing coefficient ρ_{mixing} = 0.007 leads to this transition.

[b] $|13_{5\,9}\ 2\ 15\rangle^{P}$- $|13_{5\,8}\ 3\ 15\rangle^{O}$ *ortho-para* mixing states by mixing coefficient ρ_{mixing} = 0.014 leads to this transition

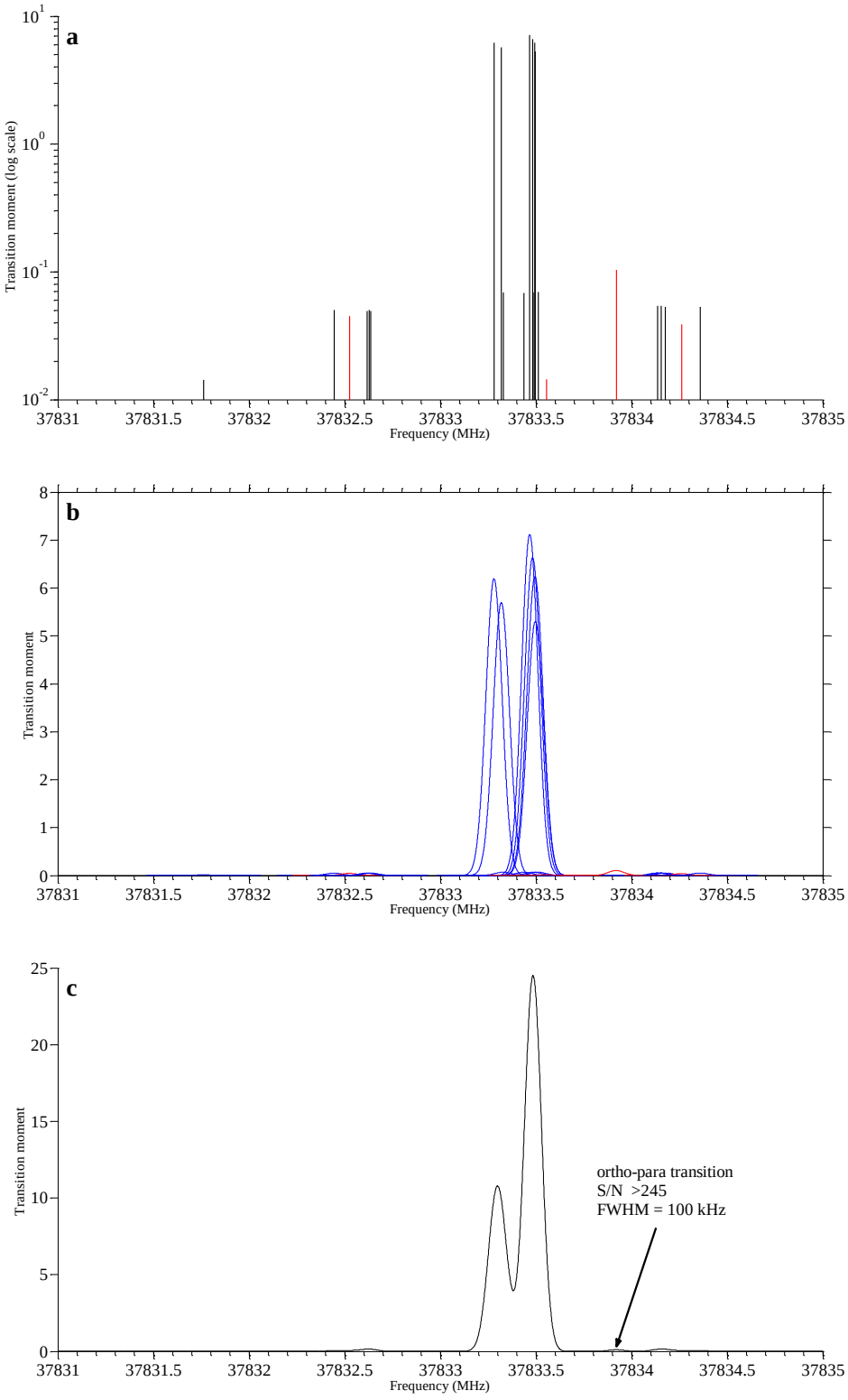

Figure C.3: (a) Blue and red sticks in this Figure correspond to the normal and *ortho-para* transitions respectively, which are listed in Table C.4. (b) Each line shape is estimated as a Gaussian type by the FWHM equal to 100 kHz. (c) Summation of all peaks in Figure C.3.b

Table C.5: List of the hyperfine transitions and their transition moments resolved rotational transition of $13_{5\,8} - 12_{4\,8}$.

Transition	Frequency (MHz)	Transition moment	Transition	Frequency (MHz)	Transition moment
$13_{5\,8}3\ 11$ - $12_{4\,8}2\ 10$	72077.3989	0.03	$13_{5\,9}2\ 11$ - $12_{4\,8}2\ 11$	72076.6134	0.07
$13_{5\,9}2\ 13$ - $12_{4\,8}2\ 13$	72077.2898	0.05	$13_{5\,9}2\ 15$ - $12_{4\,8}2\ 14$	72076.6055	6.29
$13_{5\,9}2\ 12$ - $12_{4\,8}2\ 12$	72077.2504	0.05	$13_{5\,9}0\ 13$ - $12_{4\,8}2\ 12$	72076.5674	5.50
$13_{5\,8}3\ 15$ - $12_{4\,8}2\ 14$	72077.0584	0.09[b]	$13_{5\,9}2\ 13$ - $12_{4\,8}0\ 12$	72076.4843	5.46
$13_{5\,8}1\ 12$ - $12_{4\,8}2\ 11$	72076.6822	0.01	$13_{5\,9}2\ 12$ - $12_{4\,8}2\ 11$	72076.4456	5.04
$13_{5\,9}2\ 14$ - $12_{4\,8}2\ 14$	72076.6502	0.07	$13_{5\,9}0\ 13$ - $12_{4\,8}2\ 13$	72075.7706	0.05
$13_{5\,9}2\ 14$ - $12_{4\,8}2\ 13$	72076.6358	5.89	$13_{5\,8}3\ 13$ - $12_{4\,8}2\ 12$	72075.7281	0.04[a]
$13_{5\,9}2\ 11$ - $12_{4\,8}2\ 10$	72076.6348	4.64	$13_{5\,9}2\ 12$ - $12_{4\,8}0\ 12$	72075.6481	0.05

[a] $|13_{5\,9}\ 2\ 13\rangle^{P}$- $|13_{5\,8}\ 3\ 13\rangle^{O}$ *ortho-para* mixing states by mixing coefficient $\rho_{mixing} = 0.007$ leads to this transition.

[b] $|13_{5\,9}\ 2\ 15\rangle^{P}$- $|13_{5\,8}\ 3\ 15\rangle^{O}$ *ortho-para* mixing states by mixing coefficient $\rho_{mixing} = 0.014$ leads to this transition

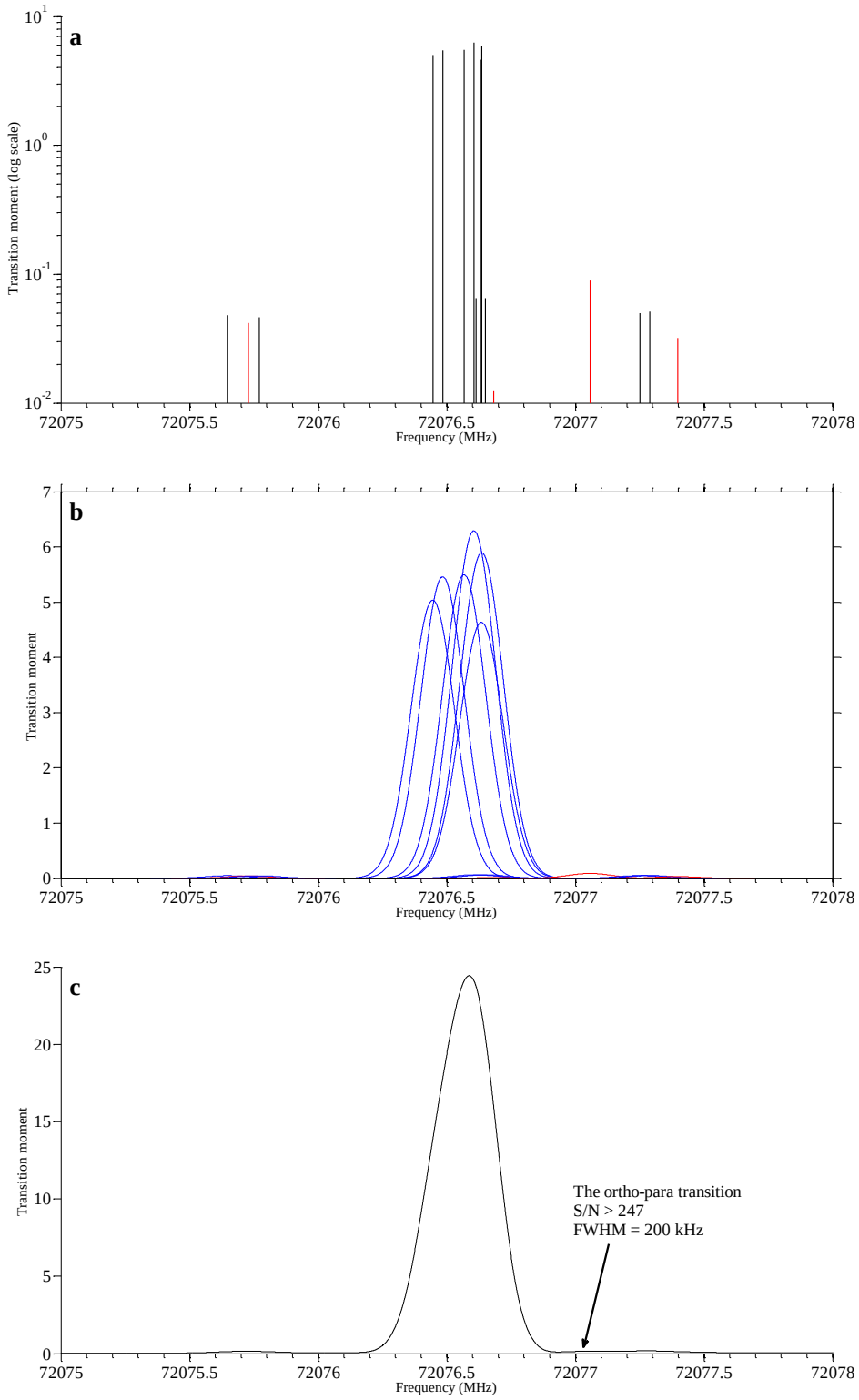

Figure C.4: (a) Blue and red sticks in this Figure correspond to the normal and *ortho-para* transitions respectively, which are listed in Table C.5. (b) Each line shape is estimated as a Gaussian type by the FWHM equal to 200 kHz. (c) Summation of all peaks in Figure C.4.b.

Table C.6: List of the hyperfine transitions and their transition moments resolved rotational transition of $13_{5\,8} - 12_{4\,9}$.

Transition			Frequency (MHz)	Transition moment	Transition			Frequency (MHz)	Transition moment
$13_{5\,8}3\ 11$	-	$12_{4\,9}1\ 11$	72093.6368	0.08	$13_{5\,8}3\ 15$	-	$12_{4\,9}3\ 14$	72092.7248	6.19
$13_{5\,9}2\ 13$	-	$12_{4\,9}3\ 12$	72093.6138	0.04[a]	$13_{5\,9}2\ 12$	-	$12_{4\,9}1\ 11$	72092.7049	0.01
$13_{5\,8}3\ 12$	-	$12_{4\,9}3\ 12$	72093.5028	0.07	$13_{5\,8}3\ 12$	-	$12_{4\,9}3\ 11$	72092.6571	5.02
$13_{5\,8}1\ 13$	-	$12_{4\,9}1\ 13$	72093.5014	0.05	$13_{5\,8}1\ 13$	-	$12_{4\,9}1\ 12$	72092.6559	5.49
$13_{5\,8}3\ 10$	-	$12_{4\,9}3\ 10$	72093.2678	0.10	$13_{5\,8}3\ 11$	-	$12_{4\,9}3\ 10$	72092.6507	4.54
$13_{5\,8}1\ 14$	-	$12_{4\,9}3\ 14$	72093.0614	0.06	$13_{5\,8}3\ 10$	-	$12_{4\,9}3\ 9$	72092.5491	4.22
$13_{5\,8}1\ 12$	-	$12_{4\,9}3\ 12$	72093.0142	0.11	$13_{5\,9}2\ 15$	-	$12_{4\,9}3\ 14$	72092.2720	0.09[b]
$13_{5\,8}3\ 13$	-	$12_{4\,9}3\ 13$	72092.9794	0.14	$13_{5\,8}3\ 13$	-	$12_{4\,9}1\ 13$	72092.0377	0.03
$13_{5\,8}1\ 12$	-	$12_{4\,9}1\ 11$	72092.9415	5.02	$13_{5\,8}3\ 14$	-	$12_{4\,9}3\ 14$	72092.0138	0.10
$13_{5\,8}1\ 14$	-	$12_{4\,9}1\ 13$	72092.8846	5.90	$13_{5\,9}2\ 11$	-	$12_{4\,9}3\ 10$	72091.8866	0.03
$13_{5\,8}3\ 11$	-	$12_{4\,9}3\ 11$	72092.8637	0.09	$13_{5\,8}3\ 12$	-	$12_{4\,9}1\ 12$	72091.8374	0.05
$13_{5\,8}3\ 13$	-	$12_{4\,9}3\ 12$	72092.8576	5.33	$13_{5\,8}3\ 15$	-	$12_{4\,9}3\ 15$	72091.8038	0.10
$13_{5\,8}3\ 14$	-	$12_{4\,9}3\ 13$	72092.7787	5.85	$13_{5\,8}3\ 13$	-	$12_{4\,9}1\ 12$	72091.1922	0.01
$13_{5\,8}3\ 16$	-	$12_{4\,9}3\ 15$	72092.7570	6.79					

[a] $|13_{5\,9}\ 2\ 13\rangle^{P}$- $|13_{5\,8}\ 3\ 13\rangle^{O}$ *ortho-para* mixing states by mixing coefficient $\rho_{mixing} = 0.007$ leads to this transition.

[b] $|13_{5\,9}\ 2\ 15\rangle^{P}$- $|13_{5\,8}\ 3\ 15\rangle^{O}$ *ortho-para* mixing states by mixing coefficient $\rho_{mixing} = 0.014$ leads to this transition

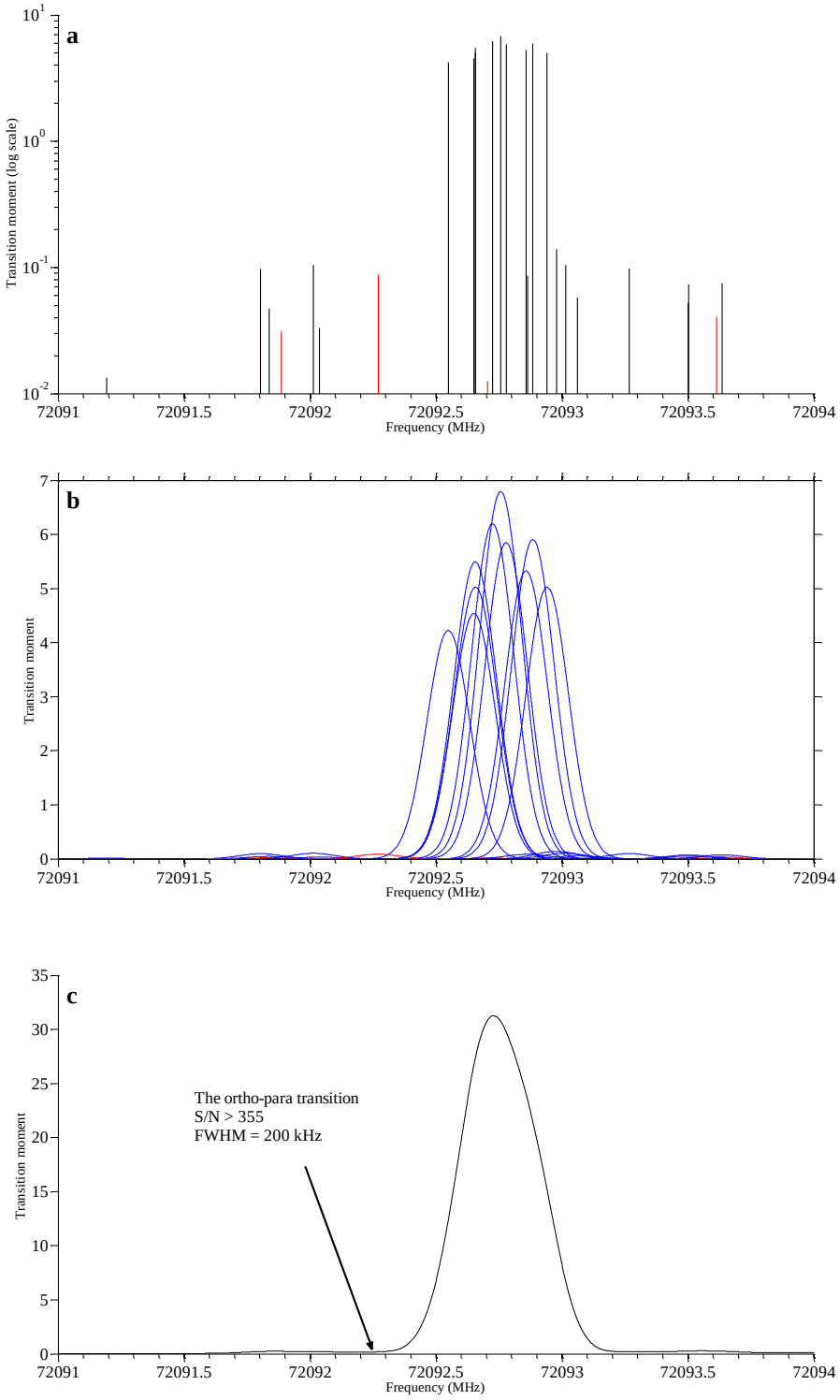

Figure C.5: (a) Blue and red sticks in this Figure correspond to the normal and *ortho-para* transitions respectively, which are listed in Table C.6. (b) Each line shape is estimated as a Gaussian type by the FWHM equal to 200 kHz. (c) Summation of all peaks in Figure C.5.b.

Table C.7: List of the hyperfine transitions and their transition moments resolved rotational transition of $14_{6\,8} - 13_{5\,9}$.

Transition			Frequency (MHz)	Transition moment	Transition			Frequency (MHz)	Transition moment
$14_{6\,8}2\ 13$	-	$13_{5\,9}0\ 13$	83173.3521	0.05	$14_{6\,9}1\ 15$	-	$13_{5\,8}3\ 15$	83172.0900	0.06
$14_{6\,8}2\ 14$	-	$13_{5\,8}3\ 13$	83173.2279	0.04[a]	$14_{6\,9}3\ 15$	-	$13_{5\,8}3\ 14$	83172.0750	6.83
$14_{6\,8}2\ 14$	-	$13_{5\,9}2\ 14$	83173.1257	0.05	$14_{6\,9}3\ 12$	-	$13_{5\,8}3\ 12$	83172.0682	0.09
$14_{6\,8}0\ 14$	-	$13_{5\,9}0\ 13$	83172.7357	6.44	$14_{6\,9}1\ 13$	-	$13_{5\,8}3\ 13$	83172.0348	0.11
$14_{6\,8}2\ 12$	-	$13_{5\,9}2\ 12$	83172.6937	0.07	$14_{6\,9}3\ 14$	-	$13_{5\,8}3\ 13$	83171.9694	6.27
$14_{6\,8}2\ 13$	-	$13_{5\,9}2\ 12$	83172.6691	5.93	$14_{6\,9}3\ 16$	-	$13_{5\,8}3\ 15$	83171.9369	7.14
$14_{6\,9}3\ 13$	-	$13_{5\,8}3\ 13$	83172.5741	0.06	$14_{6\,9}3\ 13$	-	$13_{5\,8}3\ 12$	83171.9289	5.92
$14_{6\,8}2\ 15$	-	$13_{5\,9}2\ 15$	83172.5602	0.07	$14_{6\,9}1\ 13$	-	$13_{5\,8}1\ 12$	83171.8782	5.92
$14_{6\,9}3\ 12$	-	$13_{5\,8}1\ 12$	83172.5569	0.07	$14_{6\,8}0\ 14$	-	$13_{5\,9}2\ 14$	83171.8705	0.05
$14_{6\,8}2\ 16$	-	$13_{5\,9}2\ 15$	83172.5490	7.23	$14_{6\,9}3\ 12$	-	$13_{5\,8}3\ 11$	83171.8616	5.43
$14_{6\,8}2\ 12$	-	$13_{5\,9}2\ 11$	83172.5259	5.53	$14_{6\,8}2\ 13$	-	$13_{5\,9}2\ 13$	83171.8328	0.05
$14_{6\,8}2\ 15$	-	$13_{5\,9}2\ 14$	83172.5154	6.86	$14_{6\,9}3\ 11$	-	$13_{5\,8}3\ 10$	83171.7908	5.06
$14_{6\,9}1\ 15$	-	$13_{5\,9}2\ 14$	83172.4981	0.01	$14_{6\,8}2\ 15$	-	$13_{5\,8}1\ 14$	83171.7708	0.01
$14_{6\,8}2\ 14$	-	$13_{5\,9}2\ 13$	83172.4717	6.40	$14_{6\,9}1\ 15$	-	$13_{5\,8}1\ 14$	83171.7534	6.87
$14_{6\,8}2\ 13$	-	$13_{5\,8}1\ 12$	83172.4325	0.02	$14_{6\,9}1\ 14$	-	$13_{5\,8}1\ 13$	83171.7386	6.44
$14_{6\,9}3\ 11$	-	$13_{5\,8}3\ 11$	83172.4079	0.10	$14_{6\,9}3\ 17$	-	$13_{5\,8}3\ 16$	83171.6880	7.84
$14_{6\,9}3\ 16$	-	$13_{5\,9}2\ 15$	83172.3898	0.16[b]	$14_{6\,9}3\ 15$	-	$13_{5\,8}3\ 15$	83171.3640	0.11
$14_{6\,9}1\ 14$	-	$13_{5\,8}1\ 14$	83172.3553	0.05	$14_{6\,9}3\ 14$	-	$13_{5\,9}2\ 13$	83171.2132	0.04[a]
$14_{6\,9}3\ 14$	-	$13_{5\,8}3\ 14$	83172.1701	0.14	$14_{6\,9}3\ 14$	-	$13_{5\,8}1\ 14$	83171.1225	0.04
$14_{6\,9}1\ 13$	-	$13_{5\,9}2\ 12$	83172.1148	0.02	$14_{6\,9}3\ 13$	-	$13_{5\,8}1\ 13$	83171.1104	0.05
$14_{6\,8}2\ 16$	-	$13_{5\,8}3\ 15$	83172.0961	0.16[b]	$14_{6\,9}3\ 16$	-	$13_{5\,8}3\ 16$	83170.9836	0.10

[a] $|13_{5\,9}\ 2\ 13\rangle^{P}$- $|13_{5\,8}\ 3\ 13\rangle^{O}$ *ortho-para* mixing states by mixing coefficient $\rho_{mixing} = 0.007$ leads to this transition.

[b] $|13_{5\,9}\ 2\ 15\rangle^{P}$- $|13_{5\,8}\ 3\ 15\rangle^{O}$ *ortho-para* mixing states by mixing coefficient $\rho_{mixing} = 0.014$ leads to this transition

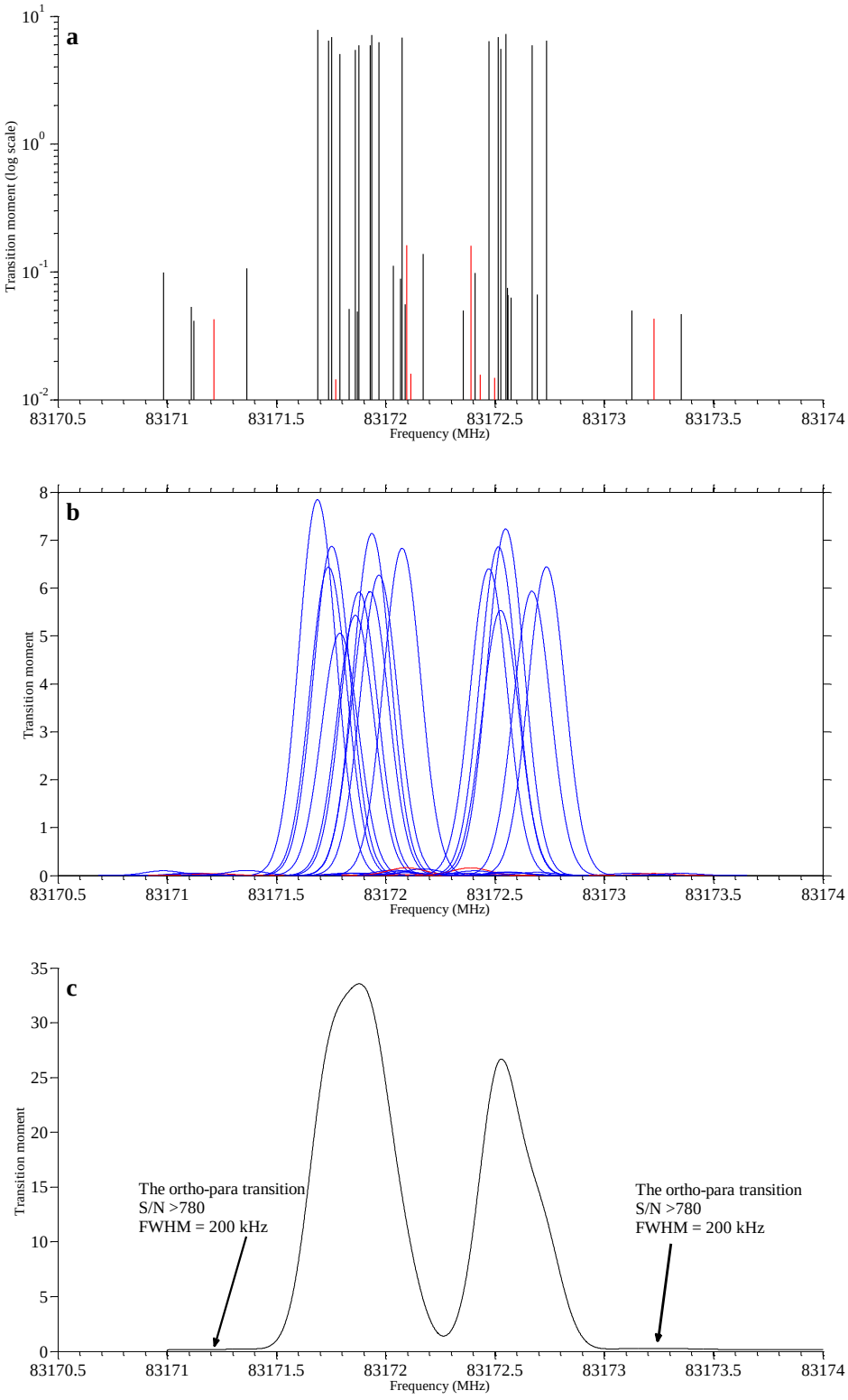

Figure C.6: (a) Blue and red sticks in this Figure correspond to the normal and *ortho-para* transitions respectively, which are listed in Table C.7. (b) Each line shape is estimated as a Gaussian type by the FWHM equal to 200 kHz. (c) Summation of all peaks in Figure C.6.b.

Table C.8: List of the hyperfine transitions and their transition moments resolved rotational transition of $25_{6\ 19} - 24_{7\ 18}$.

Transition			Frequency (MHz)	Transition moment	Transition			Frequency (MHz)	Transition moment
$25_{6\ 19}$ 3 25	-	$24_{7\ 17}$ 2 24	11686.8727	0.03[a]	$25_{6\ 19}$ 3 28	-	$24_{7\ 18}$ 3 27	11689.2900	3.74
$25_{6\ 19}$ 3 25	-	$24_{7\ 18}$ 1 24	11687.4764	0.05	$25_{6\ 19}$ 3 23	-	$24_{7\ 18}$ 3 22	11689.3442	2.88
$25_{6\ 19}$ 3 27	-	$24_{7\ 17}$ 2 26	11688.2005	0.14	$25_{6\ 19}$ 3 25	-	$24_{7\ 18}$ 3 24	11689.3469	3.24
$25_{6\ 19}$ 3 23	-	$24_{7\ 17}$ 2 22	11688.3104	0.18[b]	$25_{6\ 19}$ 3 24	-	$24_{7\ 18}$ 3 24	11689.3759	0.02
$25_{6\ 19}$ 3 27	-	$24_{7\ 18}$ 3 27	11688.5664	0.02	$25_{6\ 19}$ 3 27	-	$24_{7\ 18}$ 3 26	11689.3883	3.46
$25_{6\ 19}$ 3 22	-	$24_{7\ 18}$ 3 21	11688.5714	2.93	$25_{6\ 19}$ 1 26	-	$24_{7\ 18}$ 1 25	11689.4362	3.47
$25_{6\ 19}$ 3 26	-	$24_{7\ 18}$ 3 26	11688.7498	0.02	$25_{6\ 19}$ 3 24	-	$24_{7\ 18}$ 3 23	11689.5793	3.19
$25_{6\ 19}$ 1 24	-	$24_{7\ 18}$ 1 23	11688.8408	3.19	$25_{6\ 19}$ 3 22	-	$24_{7\ 18}$ 3 22	11690.0066	0.02
$25_{6\ 19}$ 1 25	-	$24_{7\ 18}$ 1 24	11688.8538	3.15	$25_{6\ 19}$ 1 25	-	$24_{7\ 17}$ 0 24	11690.0833	0.14[c]
$25_{6\ 19}$ 3 23	-	$24_{7\ 18}$ 1 23	11688.9124	0.01	$25_{6\ 19}$ 3 23	-	$24_{7\ 18}$ 3 23	11690.3197	0.02
$25_{6\ 19}$ 3 26	-	$24_{7\ 18}$ 3 25	11688.9617	3.45	$25_{6\ 19}$ 1 25	-	$24_{7\ 18}$ 3 24	11690.7244	0.05
$25_{6\ 19}$ 3 25	-	$24_{7\ 18}$ 3 25	11688.9982	0.02					

[a] $|24_{7\ 18}\ 3\ 24\rangle^{O}$- $|24_{7\ 17}\ 2\ 24\rangle^{P}$ *ortho-para* mixing states by mixing coefficient $\rho_{mixing} = 0.008$ leads to this transition.

[b] $|24_{7\ 18}\ 3\ 22\rangle^{O}$- $|24_{7\ 17}\ 2\ 22\rangle^{P}$ *ortho-para* mixing states by mixing coefficient $\rho_{mixing} = 0.059$ leads to this transition.

[c] $|24_{7\ 18}\ 1\ 24\rangle^{O}$- $|24_{7\ 17}\ 0\ 24\rangle^{P}$ *ortho-para* mixing states by mixing coefficient $\rho_{mixing} = 0.041$ leads to this transition.

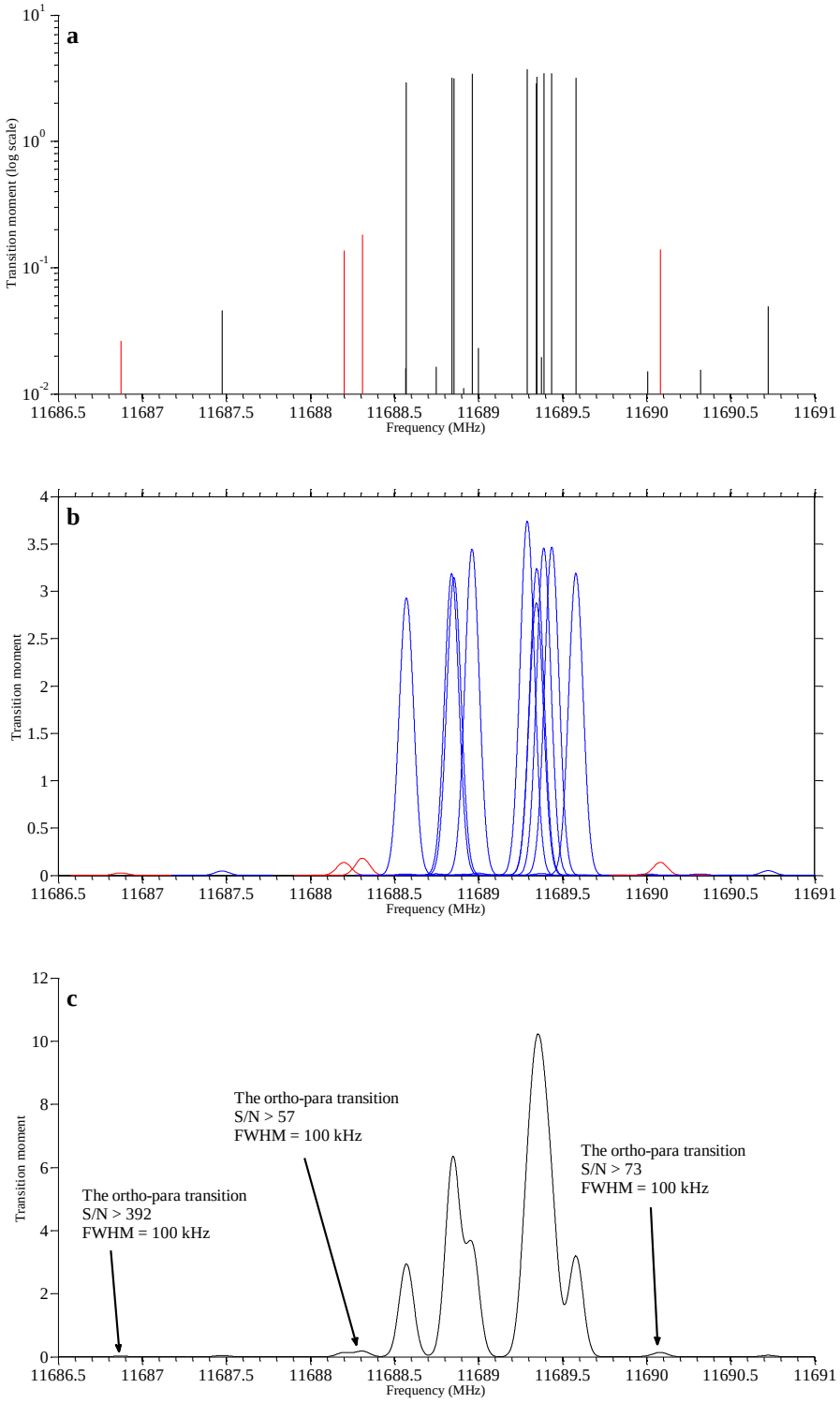

Figure C.7: (a) Blue and red sticks in this Figure correspond to the normal and *ortho-para* transitions respectively, which are listed in Table C.8. (b) Each line shape is estimated as a Gaussian type by the FWHM equal to 100 kHz. (c) Summation of all peaks in Figure C.7.b.

Table C.9: List of the hyperfine transitions and their transition moments resolved rotational transition of $24_{6\,19} - 24_{7\,18}$.

Transition	Frequency (MHz)	Transition moment	Transition	Frequency (MHz)	Transition moment
$24_{6\,19}$ 1 24 - $24_{7\,18}$ 3 24	54335.5428	0.19	$24_{6\,19}$ 3 25 - $24_{7\,18}$ 3 24	54337.0964	0.08
$24_{6\,19}$ 3 22 - $24_{7\,18}$ 3 23	54336.004	0.06	$24_{6\,19}$ 3 24 - $24_{7\,18}$ 3 25	54337.40528	0.09
$24_{6\,19}$ 1 23 - $24_{7\,18}$ 3 23	54336.0844	0.01	$24_{6\,19}$ 3 22 - $24_{7\,18}$ 1 23	54337.41129	0.04
$24_{6\,19}$ 1 24 - $24_{7\,18}$ 1 25	54336.1317	0.03	$24_{6\,19}$ 1 24 - $24_{7\,18}$ 1 24	54337.41328	11.55
$24_{6\,19}$ 3 27 - $24_{7\,18}$ 3 26	54336.1644	0.06	$24_{6\,19}$ 3 25 - $24_{7\,18}$ 3 25	54337.4451	12.63
$24_{6\,19}$ 1 24 - $24_{7\,17}$ 0 24	54336.1838	0.51[c]	$24_{6\,19}$ 1 23 - $24_{7\,18}$ 1 23	54337.49165	11.66
$24_{6\,19}$ 3 21 - $24_{7\,18}$ 3 22	54336.2509	0.06	$24_{6\,19}$ 3 24 - $24_{7\,18}$ 1 25	54337.64552	0.02
$24_{6\,19}$ 1 23 - $24_{7\,18}$ 3 24	54336.2878	0.03	$24_{6\,19}$ 3 25 - $24_{7\,18}$ 3 26	54337.65706	0.06
$24_{6\,19}$ 1 25 - $24_{7\,18}$ 3 24	54336.3137	0.02	$24_{6\,19}$ 3 25 - $24_{7\,18}$ 1 25	54337.68533	0.01
$24_{6\,19}$ 1 24 - $24_{7\,18}$ 1 23	54336.7466	0.03	$24_{6\,19}$ 3 21 - $24_{7\,18}$ 3 21	54337.68607	10.73
$24_{6\,19}$ 3 26 - $24_{7\,18}$ 3 25	54336.7474	0.07	$24_{6\,19}$ 3 26 - $24_{7\,18}$ 3 27	54337.78132	0.06
$24_{6\,19}$ 3 23 - $24_{7\,18}$ 3 23	54336.8219	11.67	$24_{6\,19}$ 3 23 - $24_{7\,18}$ 3 22	54337.79736	0.05
$24_{6\,19}$ 3 24 - $24_{7\,18}$ 3 23	54336.8532	0.08	$24_{6\,19}$ 3 22 - $24_{7\,17}$ 2 22	54338.01334	0.66[b]
$24_{6\,19}$ 1 25 - $24_{7\,18}$ 3 26	54336.8744	0.04	$24_{6\,19}$ 3 26 - $24_{7\,17}$ 2 26	54338.14721	0.50
$24_{6\,19}$ 1 25 - $24_{7\,18}$ 1 25	54336.9027	12.73	$24_{6\,19}$ 1 23 - $24_{7\,17}$ 2 23	54338.15315	0.01
$24_{6\,19}$ 3 26 - $24_{7\,18}$ 3 26	54336.9594	12.67	$24_{6\,19}$ 1 23 - $24_{7\,18}$ 1 24	54338.15834	0.04
$24_{6\,19}$ 3 22 - $24_{7\,18}$ 3 22	54336.9795	10.49	$24_{6\,19}$ 1 25 - $24_{7\,18}$ 1 24	54338.18427	0.04
$24_{6\,19}$ 3 27 - $24_{7\,18}$ 3 27	54336.9863	13.78	$24_{6\,19}$ 3 23 - $24_{7\,18}$ 1 23	54338.22919	0.02
$24_{6\,19}$ 3 26 - $24_{7\,18}$ 1 25	54336.9877	0.03	$24_{6\,19}$ 3 24 - $24_{7\,18}$ 1 23	54338.26043	0.03
$24_{6\,19}$ 3 23 - $24_{7\,18}$ 3 24	54337.0254	0.07	$24_{6\,19}$ 3 22 - $24_{7\,18}$ 3 21	54338.4146	0.06
$24_{6\,19}$ 3 24 - $24_{7\,18}$ 3 24	54337.0566	11.82	$24_{6\,19}$ 3 24 - $24_{7\,18}$ 1 24	54338.92712	0.16
$24_{6\,19}$ 1 23 - $24_{7\,18}$ 3 22	54337.0598	0.04	$24_{6\,19}$ 3 24 - $24_{7\,17}$ 2 24	54339.53076	0.10[a]

[a] $|24_{7\,18}\ 3\ 24\rangle^{O}$- $|24_{7\,17}\ 2\ 24\rangle^{P}$ *ortho-para* mixing states by mixing coefficient $\rho_{mixing} = 0.008$ leads to this transition.

[b] $|24_{7\,18}\ 3\ 22\rangle^{O}$- $|24_{7\,17}\ 2\ 22\rangle^{P}$ *ortho-para* mixing states by mixing coefficient $\rho_{mixing} = 0.059$ leads to this transition.

[c] $|24_{7\,18}\ 1\ 24\rangle^{O}$- $|24_{7\,17}\ 0\ 24\rangle^{P}$ *ortho-para* mixing states by mixing coefficient $\rho_{mixing} = 0.041$ leads to this transition.

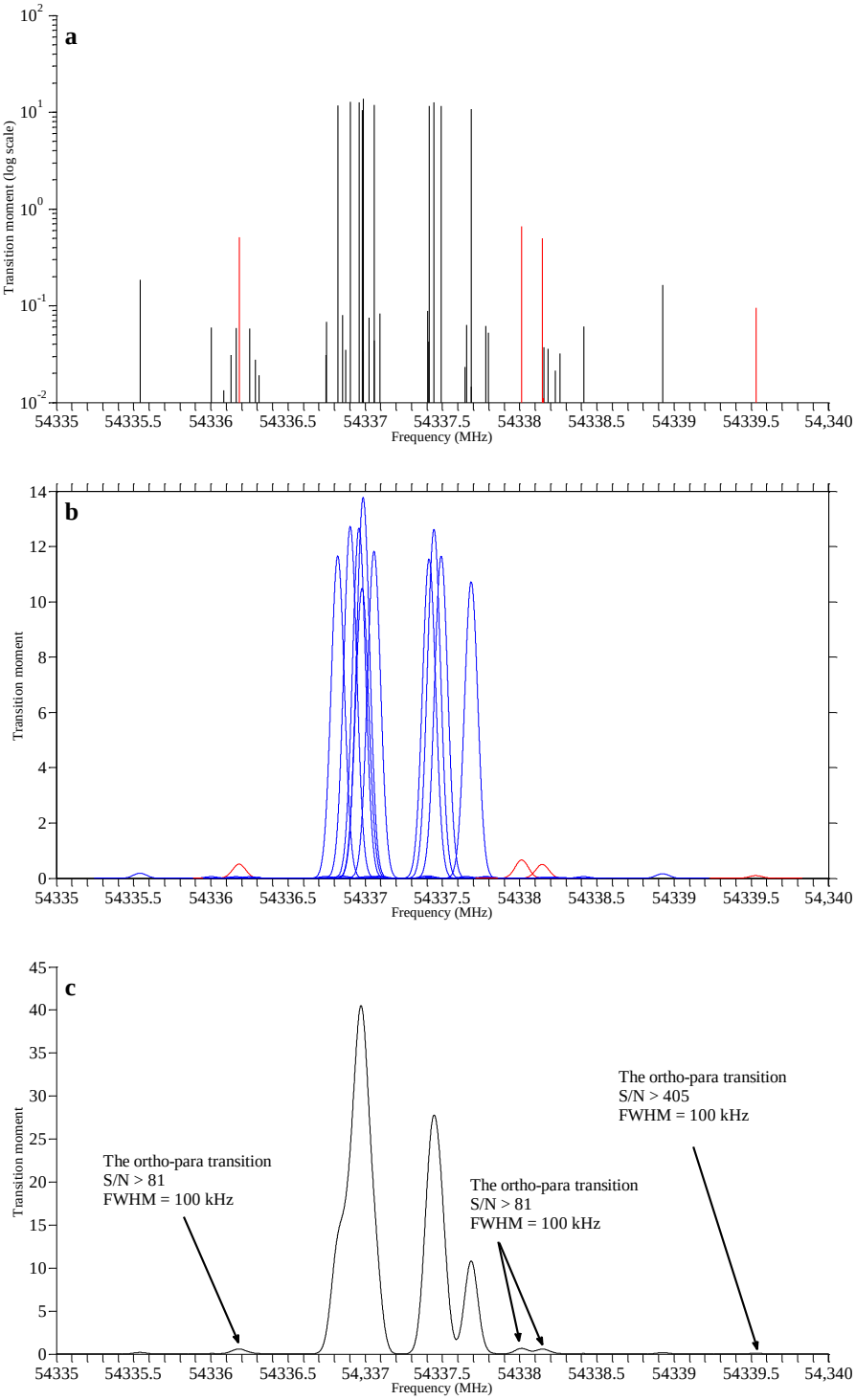

Figure C.8: (a) Blue and red sticks in this Figure correspond to the normal and *ortho-para* transitions respectively, which are listed in Table C.9. (b) Each line shape is estimated as a Gaussian type by the FWHM equal to 100 kHz. (c) Summation of all peaks in Figure C.8.b.

C-2 Investigation on the *ortho-para* mixing coefficient dependency on the F, J and K_a quantum numbers by estimating it with perturbation theorem

Dependency of the *ortho-para* mixing coefficients on the F, J and K_a quantum numbers using the perturbation theorem is investigated in section 5-3-3. The result is summarized in Figure 5-6. As it is described in section 5-3-3, Figure 5-6 shows that using the perturbation theorem finding the dependency of the *ortho-para* mixing coefficient to quantum numbers is not possible.
All ten different combinations of J and I quantum numbers in Figure 5.6 could be found in Figures C.9 to C.18, separately. Details about making these figures is the same as Figure 5-6 and is described in section 5-3-3.

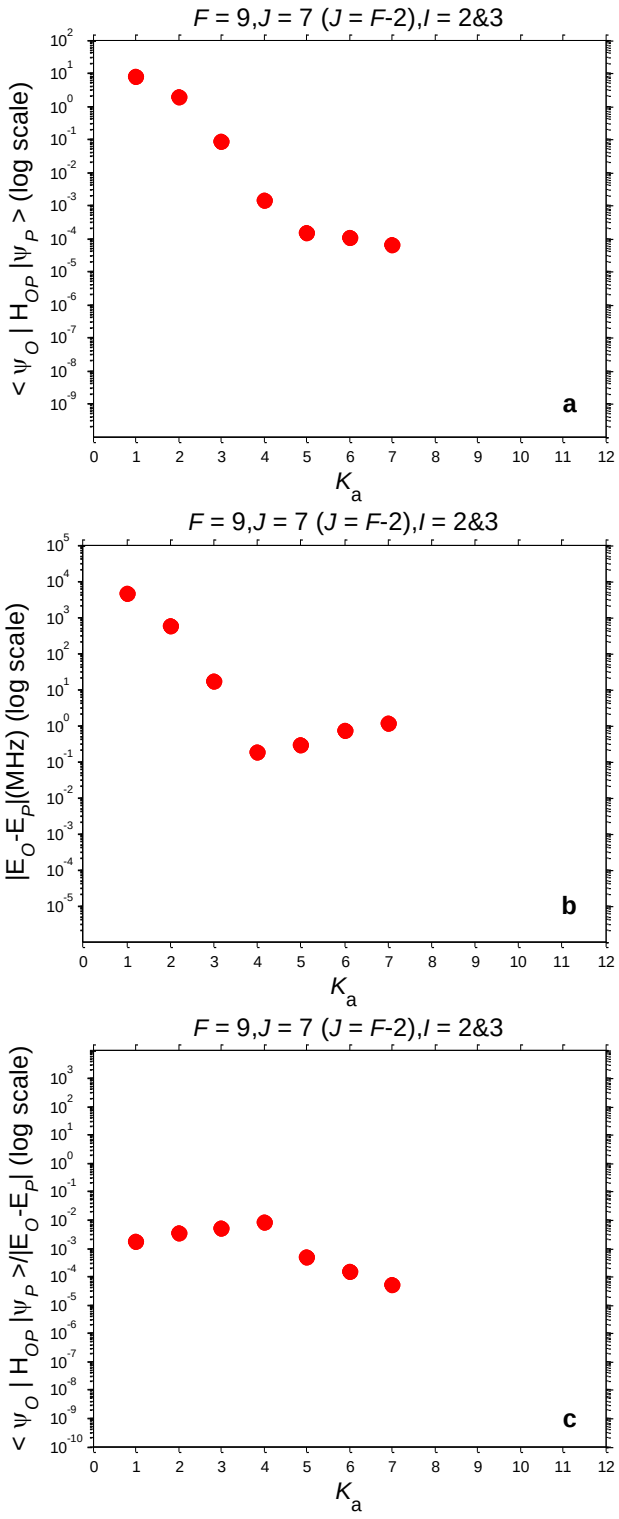

Figure C.9: (a) $\langle \Psi^P | \mathrm{H}_{OP} | \Psi^O \rangle$ versus K_a quantum number for different combinations of J and I quantum numbers for when F=9. (b) $|\mathrm{E}_O - \mathrm{E}_P|$ versus K_a quantum number. (c) $\frac{\langle \Psi^O | \mathrm{H}_{OP} | \Psi^P \rangle}{\mathrm{E}_O - \mathrm{E}_P}$ versus K_a quantum number. The vertical axes are on logarithmic scale.

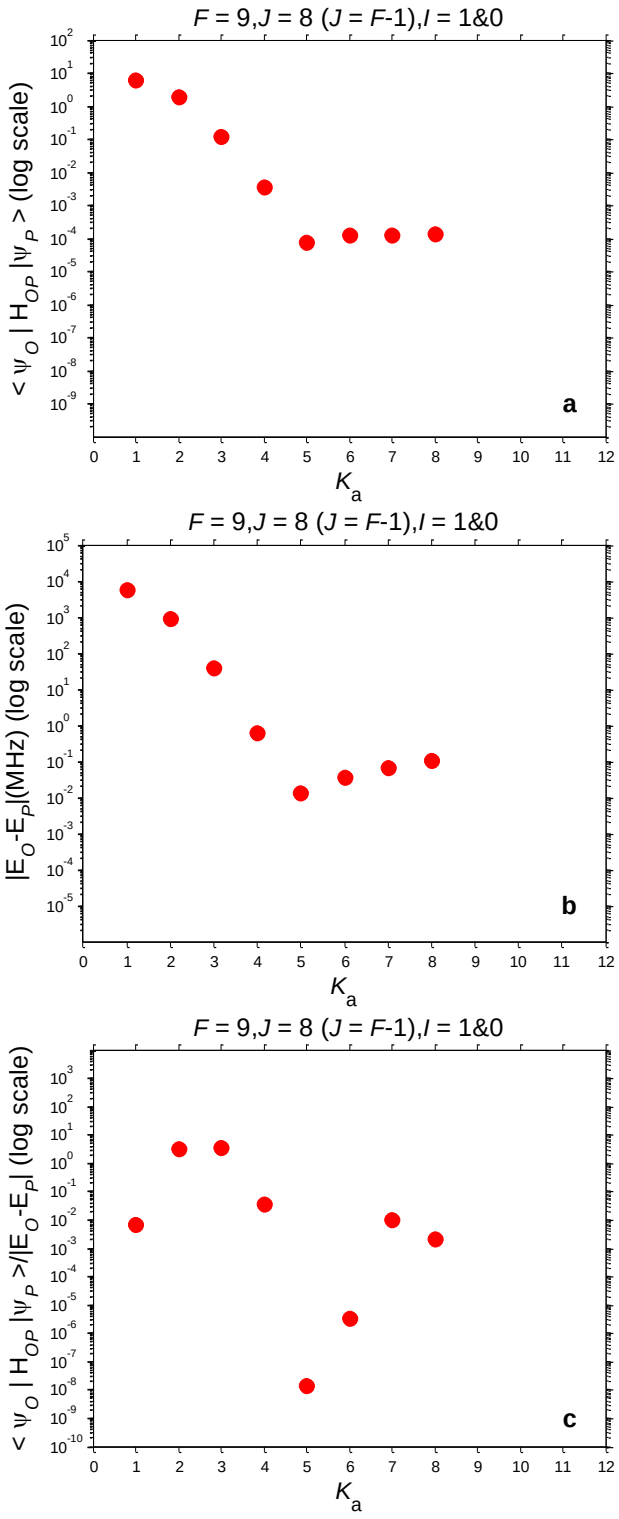

Figure C.10: (a) $\langle \Psi^P | \mathrm{H}_{OP} | \Psi^O \rangle$ versus K_a quantum number for different combinations of J and I quantum numbers for when F=9. (b) $|\mathrm{E}_O - \mathrm{E}_P|$ versus K_a quantum number. (c) $\frac{\langle \Psi^O | \mathrm{H}_{OP} | \Psi^P \rangle}{\mathrm{E}_O - \mathrm{E}_P}$ versus K_a quantum number. The vertical axes are on logarithmic scale.

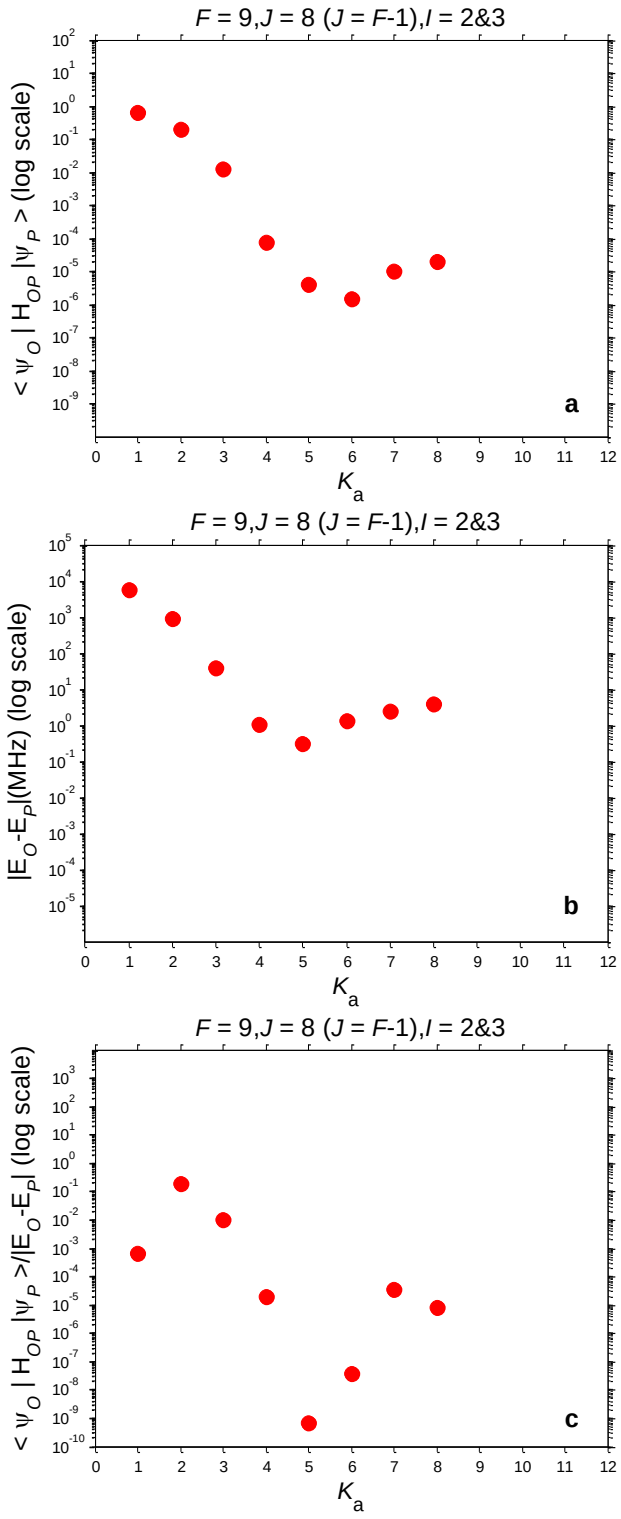

Figure C.11: (a) $\langle \Psi^P | \mathrm{H}_{OP} | \Psi^O \rangle$ versus K_a quantum number for different combinations of J and I quantum numbers for when F=9. (b) $|\mathrm{E}_O - \mathrm{E}_P|$ versus K_a quantum number. (c) $\frac{\langle \Psi^O | \mathrm{H}_{OP} | \Psi^P \rangle}{\mathrm{E}_O - \mathrm{E}_P}$ versus K_a quantum number. The vertical axes are on logarithmic scale.

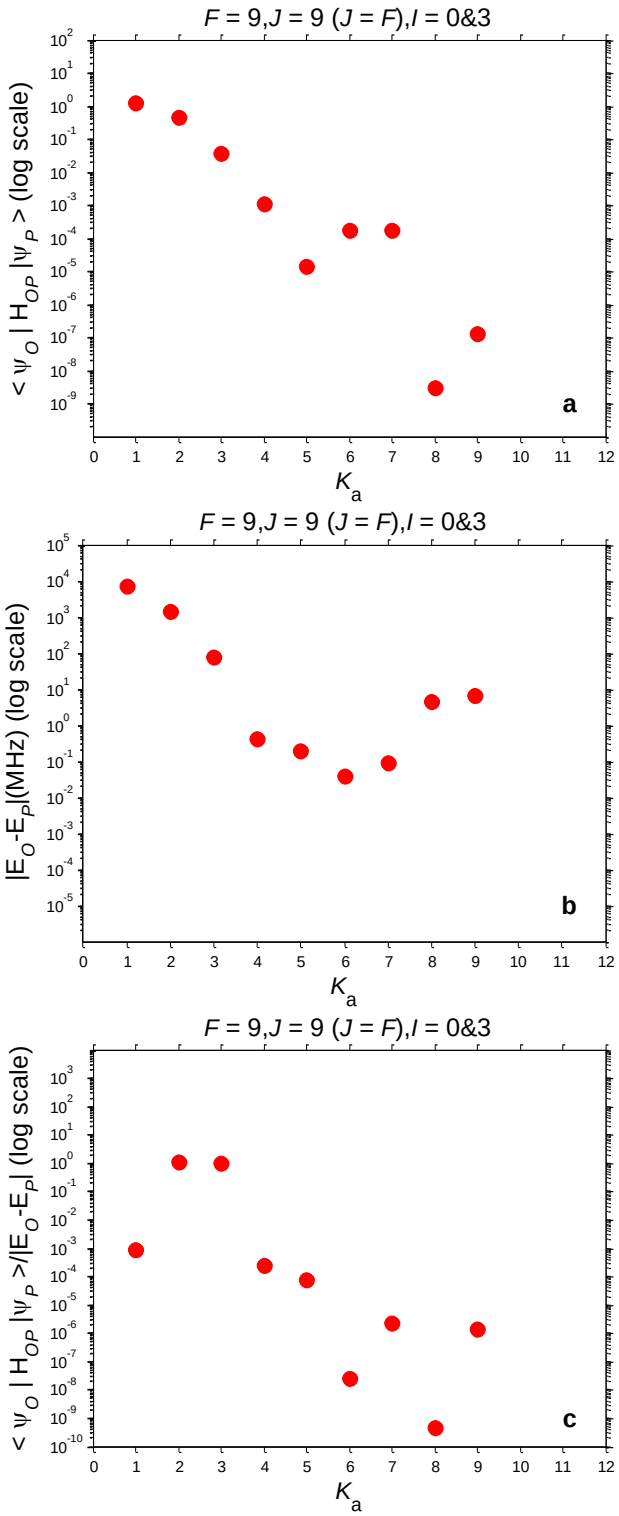

Figure C.12: (a) $\langle \Psi^P | \mathrm{H}_{OP} | \Psi^O \rangle$ versus K_a quantum number for different combinations of J and I quantum numbers for when F=9. (b) $|\mathrm{E}_O - \mathrm{E}_P|$ versus K_a quantum number. (c) $\frac{\langle \Psi^O | \mathrm{H}_{OP} | \Psi^P \rangle}{\mathrm{E}_O - \mathrm{E}_P}$ versus K_a quantum number. The vertical axes are on logarithmic scale.

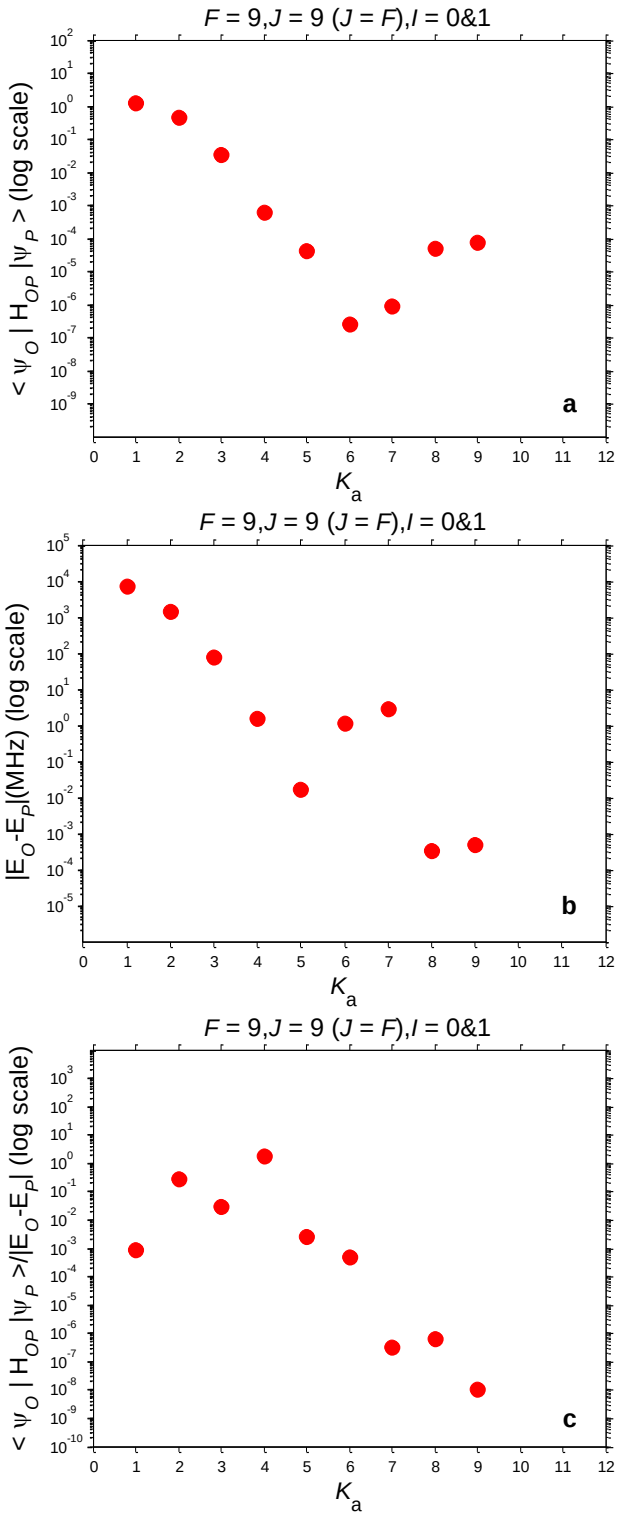

Figure C.13: (a) $\langle \Psi^P | \mathrm{H}_{OP} | \Psi^O \rangle$ versus K_a quantum number for different combinations of J and I quantum numbers for when F=9. (b) $|\mathrm{E}_O - \mathrm{E}_P|$ versus K_a quantum number. (c) $\frac{\langle \Psi^O | \mathrm{H}_{OP} | \Psi^P \rangle}{\mathrm{E}_O - \mathrm{E}_P}$ versus K_a quantum number. The vertical axes are on logarithmic scale.

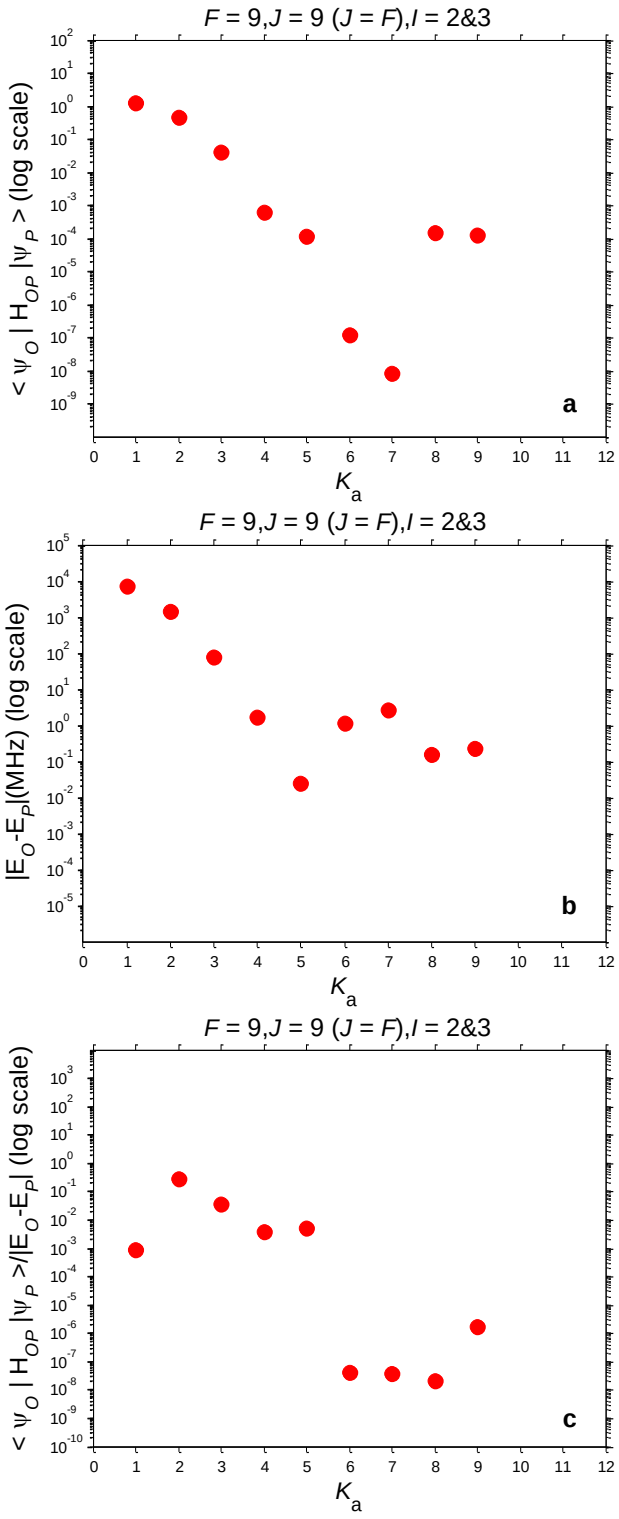

Figure C.14: (a) $\langle \Psi^P | \mathrm{H}_{OP} | \Psi^O \rangle$ versus K_a quantum number for different combinations of J and I quantum numbers for when F=9. (b) $|\mathrm{E}_O - \mathrm{E}_P|$ versus K_a quantum number. (c) $\frac{\langle \Psi^O | \mathrm{H}_{OP} | \Psi^P \rangle}{\mathrm{E}_O - \mathrm{E}_P}$ versus K_a quantum number. The vertical axes are on logarithmic scale.

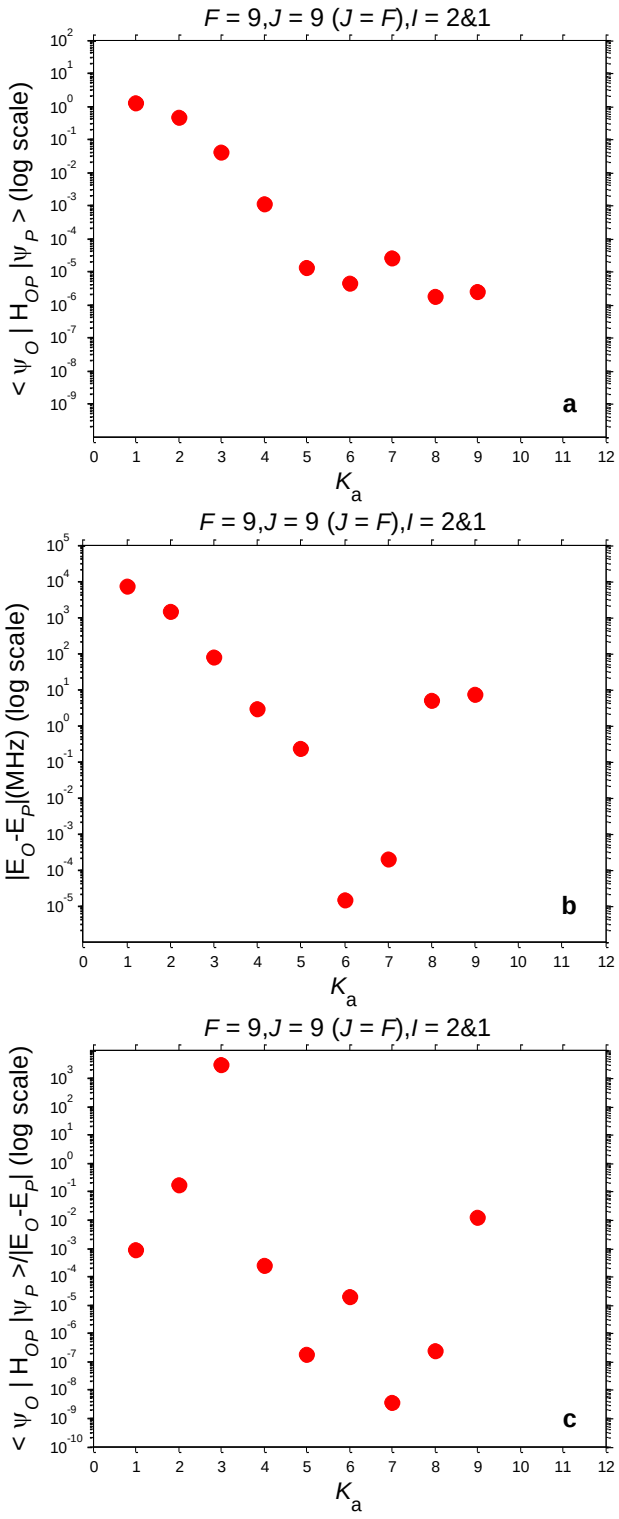

Figure C.15: (a) $\langle \Psi^P | \mathrm{H}_{OP} | \Psi^O \rangle$ versus K_a quantum number for different combinations of J and I quantum numbers for when F=9. (b) $|\mathrm{E}_O - \mathrm{E}_P|$ versus K_a quantum number. (c) $\frac{\langle \Psi^O | \mathrm{H}_{OP} | \Psi^P \rangle}{\mathrm{E}_O - \mathrm{E}_P}$ versus K_a quantum number. The vertical axes are on logarithmic scale.

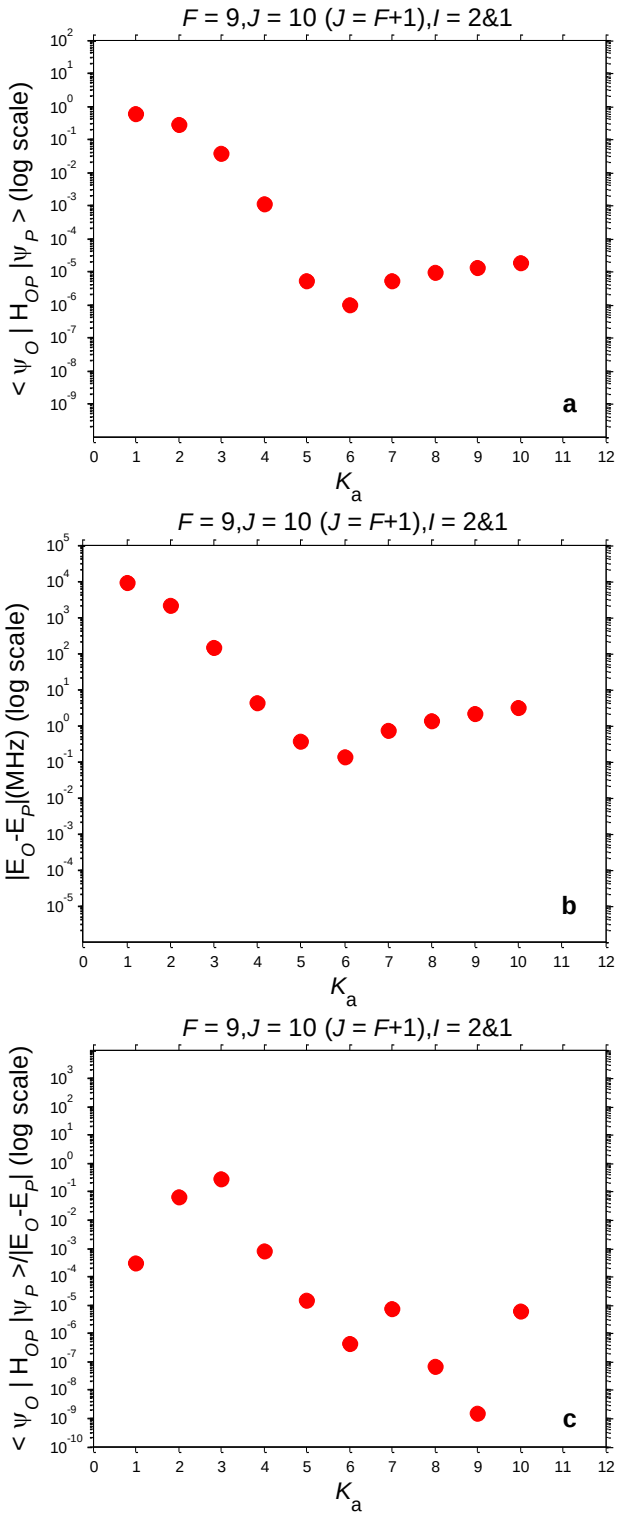

Figure C.16: (a) $\langle \Psi^P | \mathrm{H}_{OP} | \Psi^O \rangle$ versus K_a quantum number for different combinations of J and I quantum numbers for when F=9. (b) $|\mathrm{E}_O - \mathrm{E}_P|$ versus K_a quantum number. (c) $\frac{\langle \Psi^O | \mathrm{H}_{OP} | \Psi^P \rangle}{\mathrm{E}_O - \mathrm{E}_P}$ versus K_a quantum number. The vertical axes are on logarithmic scale.

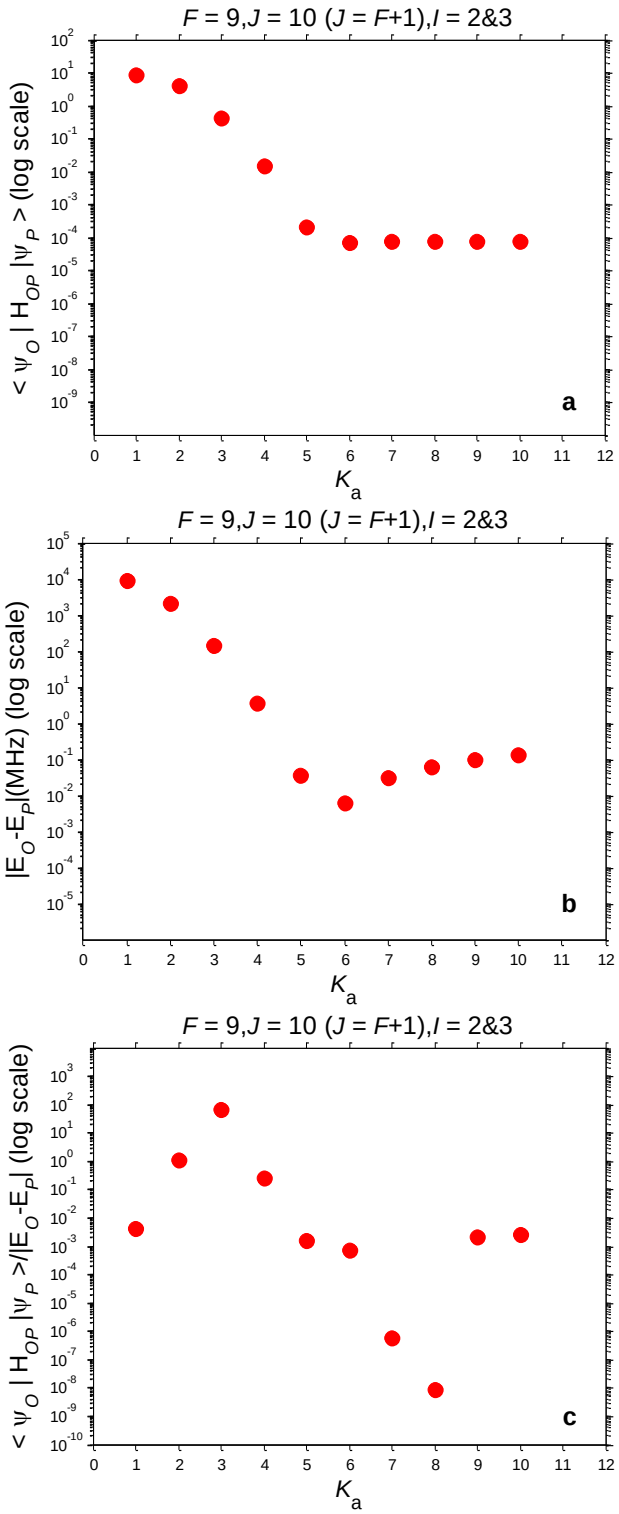

Figure C.17: (a) $\langle \Psi^P | \mathrm{H}_{OP} | \Psi^O \rangle$ versus K_a quantum number for different combinations of J and I quantum numbers for when F=9. (b) $|\mathrm{E}_O - \mathrm{E}_P|$ versus K_a quantum number. (c) $\frac{\langle \Psi^O | \mathrm{H}_{OP} | \Psi^P \rangle}{\mathrm{E}_O - \mathrm{E}_P}$ versus K_a quantum number. The vertical axes are on logarithmic scale.

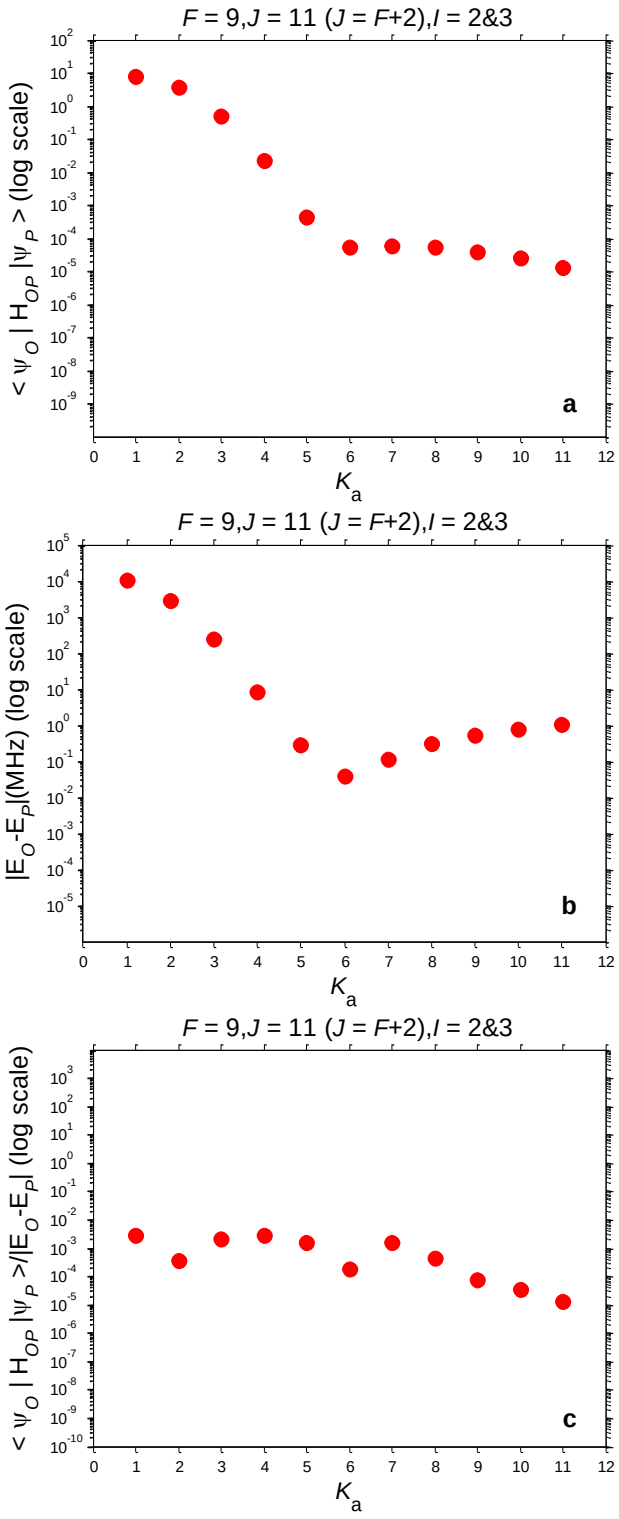

Figure C.18: (a) $\langle \Psi^P | \mathrm{H}_{OP} | \Psi^O \rangle$ versus K_a quantum number for different combinations of J and I quantum numbers for when F=9. (b) $|\mathrm{E}_O - \mathrm{E}_P|$ versus K_a quantum number. (c) $\frac{\langle \Psi^O | \mathrm{H}_{OP} | \Psi^P \rangle}{\mathrm{E}_O - \mathrm{E}_P}$ versus K_a quantum number. The vertical axes are on logarithmic scale.

Appendix D

List of Presentations and Publication on this Study

Millimeter-Wave Spectroscopy of S_2Cl_2: A Candidate Molecule for Measuring *Ortho–Para* Transition
Zeinab Tafti Dehghani , Shinji Ota , Asao Mizoguchi , and Hideto Kanamori
J. Phys. Chem. A, 2013, *117* (39), pp 10041–10046

Theoretical and Experimental Study of the Radiative *Ortho-Para* Transition in Disulfur Dichloride, S_2Cl_2
Zeinab Tafti Dehghani , Asao Mizoguchi , and Hideto Kanamori
15th Symposium on Molecular Spectroscopy Japan, FuKuoka, Kyushu University, 22-23 May 2015

Millimeter-Wave Spectroscopy of S_2Cl_2: A Candidate Molecule for the detection of *Ortho–Para* Transition
Zeinab Tafti Dehghani , Asao Mizoguchi , and Hideto Kanamori
The International Symposium on Molecular Spectroscopy, Urbana, IL, 16-21 June 2014

An Investigation on Possibility of Observing *ortho-para* Transition, Based on New Measurements of Microwave Spectrum of Disulfur Dichloride; S_2Cl_2
Zeinab Tafti Dehghani , Asao Mizoguchi , and Hideto Kanamori
13th Symposium on Molecular Spectroscopy Japan, Tokyo, Sophia University, 18-19 May 2012

THE JOURNAL OF PHYSICAL CHEMISTRY A

Article

pubs.acs.org/JPCA

Millimeter-Wave Spectroscopy of S_2Cl_2: A Candidate Molecule for Measuring Ortho−Para Transition

Zeinab Tafti Dehghani, Shinji Ota, Asao Mizoguchi, and Hideto Kanamori*

Department of Physics, Tokyo Institute of Technology, Ohokayama, Meguro-ku, Tokyo 152-8551, Japan

ABSTRACT: S_2Cl_2 is a candidate for the observation of ortho−para transition. To estimate the ortho−para mixing in a hyperfine-resolved rotational state, pure rotational transitions were measured by millimeter-wave (mm-wave) spectroscopy using two different experimental set-ups. The transitions from the term value around 20 K was measured with a supersonic jet and those around 200 K were measured with a dry ice cooled gas cell. Several hundred peaks were assigned for the naturally abundant $S_2{}^{35}Cl_2$ and $S_2{}^{35}Cl^{37}Cl$ isotopic species and the rotational molecular parameters including the fourth-order and sixth-order centrifugal distortion constants were determined. The hyperfine structures were partly resolved in some *Q*-branch transitions, which were well described with the hyperfine constants determined by FTMW spectroscopy in the centimeter-wave region. With the new rotational constants determined in our study and the previous hyperfine constants, it will be possible to obtain a more reliable ortho−para mixing ratio and to narrow down the possible candidate transitions in the mm-wave region for the observation of ortho−para transition.

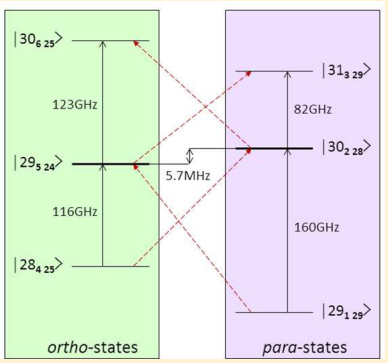

I. INTRODUCTION

Disulfur dichloride (S_2Cl_2) is a chiral molecule with a skew Cl−S−S−Cl type of conformation[1−6] and C_2 symmetry along the *b*-axis.[7] This molecule is of interest from several points of view and can be potentially used for observation of parity violation, which has been confirmed in elementary particle physics[8,9] and in atoms.[10] Despite several experimental attempts to detect the energy difference between optical isomers,[11] it has not been observed in molecular systems until now. The energy difference between the optical isomers of S_2Cl_2 due to parity violation is theoretically predicted to be on the order of 10^{-12} cm^{-1}, which is not measurable experimentally.[12]

Another interest for S_2Cl_2 is interconversion between different nuclear spin states in molecules with identical nuclei,[13] because this molecule is a promising candidate for the observation of ortho−para transition.[7] As the Cl atom has a nuclear spin of I_i = 3/2, the total nuclear spin angular momentum in S_2Cl_2 can be I = 0, 1, 2, 3. According to Pauli's principle, the complete wave functions including spin in S_2Cl_2 are classified as ortho and para states by an interchange of the two identical Cl atoms. The ortho state involves K_aK_c = oe and eo rotational states coupled with odd-I nuclear spin states and the para state involves K_aK_c = oo, ee, and even-I nuclear spin states. In general, the transition between pure ortho and para states is considered to be strictly forbidden. However, the measurement of the ortho−para transition is permitted via an interaction ($\mathbf{H}_{o\text{-}p}$), in which a pure ortho state mixes with pure para states and vice versa. In 2008, Mizoguchi et al. observed hyperfine structures in the pure rotational transitions of S_2Cl_2 in the centimeter-wave (cm-wave) region using Fourier transform microwave (FTMW) spectroscopy.[7] In the analysis of the hyperfine structures based on the effective Hamiltonian with separate block diagonalization of the ortho and para states, unexpected splitting on the order of 50 kHz was observed in several lowest transitions. To figure out these splitting patterns, another effective Hamiltonian that allowed the mixing of the ortho and para states was introduced. Accordingly, the observed spectrum splitting and line shift could be explained by the off-diagonal terms of the nuclear quadrupole interaction. If this interpretation of the hyperfine splitting is physically correct, the ortho−para transitions should be possible in S_2Cl_2; this is because the ortho−para mixing can originate from the off-diagonal hyperfine terms: $\mathbf{H}_{o\text{-}p}$. They estimated the mixing ratio of the wave functions in some low rotational states but found that the transition moments of the ortho−para transitions are very small in the cm-wave region.

The ortho−para transition intensity depends on the mixing ratio of ortho and para state represented as

$$\langle \psi_{ortho} | \mathbf{H}_{o-p} | \psi_{para} \rangle / (E_{ortho} - E_{para}) \quad (1)$$

Therefore, we expect to have an enhancement due to the small energy denominator. As the S_2Cl_2 molecule is an asymmetric top with Ray's κ parameter of −0.92, an accidental near-resonance is expected among the rotational states with higher rotational quantum numbers. In addition, as the transition intensity becomes stronger as the cube of the transition frequency, searching for the weak forbidden transitions is easier in the higher frequency region. Until now microwave spectroscopy of S_2Cl_2 has been restricted to the region below 40 GHz.[6,7] In those studies the rotational constants, the fourth-order centrifugal distortion

Special Issue: Oka Festschrift: Celebrating 45 Years of Astrochemistry

Received: January 19, 2013
Revised: May 1, 2013
Published: May 1, 2013

dx.doi.org/10.1021/jp400632g | *J. Phys. Chem. A* 2013, 117, 10041−10046

constants, and the hyperfine constants were determined. Nonetheless, the centrifuge-based treatment is not enough to predict the transition frequencies in the millimeter wave (mm-wave) region. To have a reliable intensity prediction for ortho−para transitions in the higher frequency region, more precise information on the hyperfine-resolved rotational term energy is needed.

In this work, we extend the rotational spectroscopy of S_2Cl_2 up to 100 GHz. To access as many rotational states as possible, the absorption spectra were measured not only under supersonic jet but also in the gas cell condition. As a result, we were able to observe the transition with the rotational quantum numbers up to $J = 37$ and $K_a = 10$ for $S_2{}^{35}Cl_2$ and up to $J = 41$ and $K_a = 10$ for $S_2{}^{35}Cl^{37}Cl$. The set of molecular parameters including the sixth-order centrifugal distortion constants were determined for the first time and the reproducibility of the hyperfine pattern was confirmed by using the previous hyperfine constants from ref 7.

II. EXPERIMENTAL DETAILS

Pure grade S_2Cl_2 (Wako Pure Chemical Industries) was used without further purification. The naturally abundant isotopes of chlorine, ^{35}Cl, and ^{37}Cl yield three isotopic species for S_2Cl_2 but only $S_2{}^{35}Cl_2$ and $S_2{}^{35}Cl^{37}Cl$ are considered in this work. In the supersonic jet experiment, a pulse-jet nozzle (Parker Hannifin) of 0.8 mm ϕ orifice was used at a repetition rate of 10 Hz. Specified purity Ar gas (99.999%, Nihon Sanso) was bubbled through the liquid sample of S_2Cl_2 and injected into a vacuum chamber evacuated by a 12 in. oil diffusion pump. The back-pressure of the nozzle was chosen to achieve the strongest absorption signal. For example, the pressure of Ar buffer gas was optimized as 0.5 atm for the $^rR_4(15)$ transition, which has the rotational term energy corresponding to $T = 15$ K.

A W-band source module (HP83558A) driven by a synthesized sweeper (HP83620) was used. The output radiation power of a few milliwatts was focused with an elliptical mirror (200 mm × 150 mm) 2.7 cm downstream from the pulse valve. The beam waist of the MW radiation was 2 cm o.d. The MW radiation was frequency modulated at 47 kHz through the synthesizer. By using an InSb detector (QME-2BI) cooled to liquid helium temperature, we demodulated the absorption signal by a lock-in amplifier (SRS SR850) with twice the modulation frequency (2f-detection) and a time constant of 300 μs. The detected signal was recorded by a digital oscilloscope (Tektronix TDS5104B) and sampled for a period of 10 ms with 2 ms delay after opening the pulse valve, for which the absorption signal was strongest. For observing the spectrum the mm-wave frequency was scanned by a 0.05 MHz step, while 100 shots of the pulse jet were averaged. So it took 15 min for sweeping 4 MHz to measure a Doppler broadened isolated line.

The absorption spectrum was also measured with a gas cell to observe the transitions from the higher J-quantum numbers than those covered by the supersonic jet experiment. The gas cell was a 2 m long Pyrex glass tube with a diameter of 10 cm, surrounded by dry ice to maintain the temperature at 220 K. The vapor pressure of the sample at the dry ice temperature is a few millitorr. The pressure of the sample was maintained at a few millitorr using a slow flow and continuous pumping. The measurement was carried out by sweeping the mm-wave frequency over 10 MHz in 150 second, and 4 scans were averaged to attain a good signal-to-noise ratio. Because the depth of the frequency modulation was same as that of the supersonic jet experiment, the accuracy of frequency measurements was ∼100 kHz between 75 and 100 GHz in both the experiments.

III. RESULT AND DISCUSSION

Spectral search for the two isotopic species, $S_2{}^{35}Cl_2$ and $S_2{}^{35}Cl^{37}Cl$, in the 75−100 GHz region was based on a spectral atlas simulated by using the rotational constants reported in the previous FTMW work.[7] For calculating the rotational term values, we used an A-reduced asymmetric-rotor Hamiltonian in I^r representation.[14] The matrix elements were calculated using the Wang basis set.[14] At this point, it was clear that the prediction for the higher rotational states has a large margin of error due to the centrifugal distortion effect, because the transitions observed in FTMW were limited up to $J = 11$ and $K_a = 3$ in $S_2{}^{35}Cl_2$, and $J = 6$ and $K_a = 2$ in $S_2{}^{35}Cl^{37}Cl$. We started with the gas cell experiment but the observed line density was too high to assign them correctly. Therefore, we decided to conduct the supersonic jet experiment first as the cooling effect on the rotational temperature due to supersonic expansion makes it easier to assign the spectra than in the gas cell experiment.

A. Supersonic Jet Experiment. The series of $^rQ_9(J)$-branches of $S_2{}^{35}Cl_2$ and $S_2{}^{35}Cl^{37}Cl$ could be easily observed with a slight shift from the predicted frequencies of the band head; however, they appeared with a distinct triplet spectral pattern as shown in Figure 1. This triplet pattern was attributed

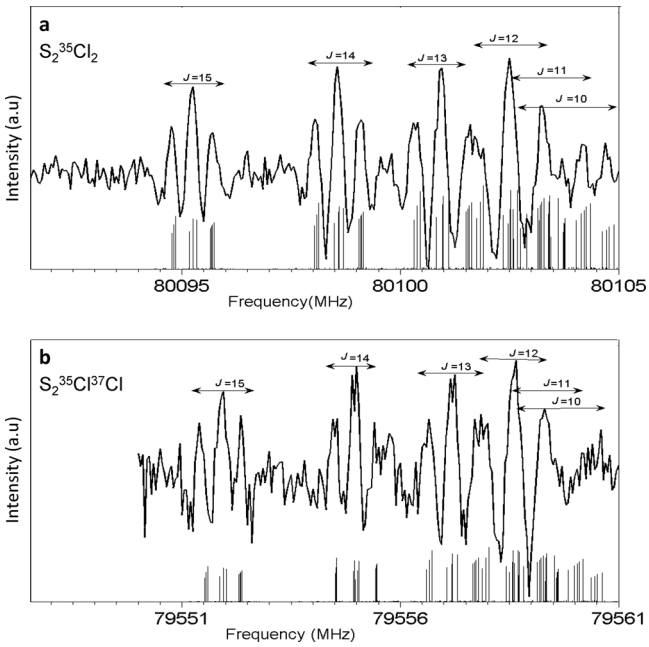

Figure 1. Series of $^rQ_9(J)$-branches of (a) $S_2{}^{35}Cl_2$ and (b) $S_2{}^{35}Cl^{37}Cl$ observed in the supersonic jet experiment. Stick spectrum shows the hyperfine components calculated with the rotational constants from fit II in Table 5 and hyperfine constants reported in ref 7.

to the nuclear quadrupole interaction of the two chlorine nuclei. It was difficult to assign the hyperfine components as they overlapped with other rotational transitions at the band head. More information about the hyperfine structure is described in following section C. The low-J transitions in R-branch could be observed closely at the position of the predicted frequency. Figure 2a shows the observed spectrum of the $^rR_5(13)$ transition of $S_2{}^{35}Cl_2$, in which the asymmetric K-doubling is resolved, and the positions predicted by the rotational molecular constants from ref 7 are marked by a dotted line. The assignment of the K-doubling was also

dx.doi.org/10.1021/jp400632g | J. Phys. Chem. A 2013, 117, 10041−10046

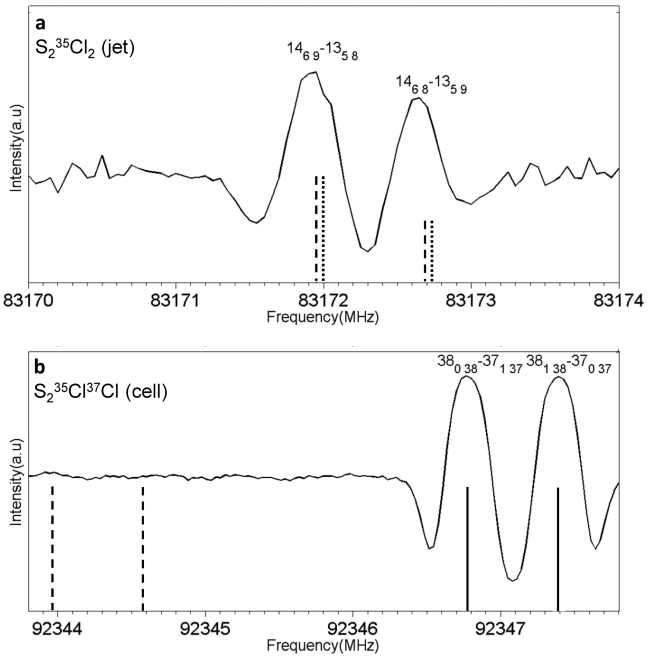

Figure 2. (a) Example of middle-J transition: ${}^rR_5(13)$ transition of $S_2{}^{35}Cl_2$ observed with the supersonic jet experiment. (b) Example of high-J transition: ${}^rR_{K_c=0}(37)$ transition of $S_2{}^{35}Cl^{37}Cl$ observed with the gas cell experiment. The frequency positions predicted by the rotational molecular constants of ref 7, fit I, and fit II in Table 5 are shown with dotted line, dashed line, and solid line, respectively. The solid line is overlapped under the dashed line in case of (a), whereas in case of (b), the dotted line is out of range.

confirmed from the spectral intensity due to the nuclear spin weight of 10:6. The ortho $14_{6,9}-13_{5,8}$ transition was observed to be stronger than the para $14_{6,8}-13_{5,9}$ transition. By adding those observed lines into the least-squares analysis, we improved the molecular parameters step by step. In total 30 R- and 18 Q-lines for $S_2{}^{35}Cl_2$ and 30 R- and 10 Q-lines for $S_2{}^{35}Cl^{37}Cl$ were observed and their central frequencies, ignoring the hyperfine structure are listed in Table 1 and Table 3, respectively. These transitions were analyzed simultaneously with the transitions measured by FTMW.[7] The least-squares fitting was weighted by 1.0 for FTMW and 0.01 for our mm-wave work according to the accuracy of each experimental measurement. As a result, the three rotational constants are improved and the fourth-order centrifugal distortion constants including δ_K are determined, which were not determined in the FTMW experiment. These molecular parameters are listed in Table 5 as fit I. The rotational temperature was also determined from the supersonic jet experiment. From the spectrum intensity distribution of the series of the observed ${}^rQ_9$-branch, the rotational temperature was estimated to be T = 10−20 K. This value corresponds well with the term value of the lower state of the ${}^rR_4(15)$ transition, which was used for optimizing the supersonic jet condition as described in the Experimental Details.

B. Gas Cell Experiment. The gas cell experiment was used to obtain the information about higher rotational states than those populated in the supersonic jet experiment. By using the fit I parameters, we obtained a better simulation atlas for the higher-J and K_a transitions. However, there remain considerable errors for high-J transitions. For example, for the $38_{0,38}-37_{1,37}$ and $38_{1,38}-37_{0,37}$ transitions of $S_2{}^{35}Cl^{37}Cl$ shown in Figure 2b, the frequencies predicted in ref 7 were −33 MHz away from their observed position, and thus off-scale. The frequencies predicted using fit I are also 3 MHz below the observed frequencies and are shown using a dashed line in the figure. However, the assignment of the spectral lines was easier in this case, because the signal-to-noise ratio for the gas cell experiment was better than that of the supersonic jet experiment. Here it might be mentioned that although these

Table 1. Observed Transitions of $S_2{}^{35}Cl_2$ in the Supersonic Jet Experiment[a]

$J'_{K_a'K_c'}-J''_{K_a''K_c''}$	ν_{obs}/MHz	$\nu_{o\text{-}c}$/kHz[b]	$J'_{K_a'K_c'}-J''_{K_a''K_c''}$	ν_{obs}/MHz	$\nu_{o\text{-}c}$/kHz[b]
$8_{7\,1}-7_{6\,2}$	75862.6542	19.2	$17_{5\,13}-16_{4\,12}$	82356.4471	−131.7
$8_{7\,2}-7_{6\,1}$	75862.6542	19.2	$17_{6\,11}-16_{5\,12}$	91002.2187	23.6
$8_{8\,0}-7_{7\,1}$	84290.1207	−13.0	$17_{6\,12}-16_{5\,11}$	90996.2704	−11.7
$8_{8\,1}-7_{7\,0}$	84290.1207	−13.0	$17_{7\,11}-16_{6\,10}$	99481.8676	74.5
$9_{7\,2}-8_{6\,3}$	78491.3932	−8.0	$17_{7\,10}-16_{6\,11}$	99481.8676	−61.3
$9_{7\,3}-8_{6\,2}$	78491.3932	−8.0	$18_{6\,13}-17_{5\,12}$	93591.3109	72.6
$10_{7\,3}-9_{6\,4}$	81119.7699	17.1	$13_{10\,3}-13_{9\,4}$	80100.9271	−48.9
$10_{7\,4}-9_{6\,3}$	81119.7699	17.2	$13_{10\,4}-13_{9\,5}$	80100.9271	−48.9
$11_{6\,5}-10_{5\,6}$	75310.6443	21.2	$14_{10\,4}-14_{9\,5}$	80098.5671	−33.8
$11_{6\,6}-10_{5\,5}$	75310.6443	71.4	$14_{10\,5}-14_{9\,6}$	80098.5671	−33.8
$11_{7\,4}-10_{6\,5}$	83747.4812	30.6	$15_{10\,5}-15_{9\,6}$	80095.2310	−23.4
$11_{7\,5}-10_{6\,4}$	83747.4812	31.0	$15_{10\,6}-15_{9\,7}$	80095.2310	−23.3
$12_{6\,6}-11_{5\,7}$	77933.9542	16.5	$19_{10\,9}-19_{9\,10}$	80068.7021	33.7
$12_{6\,7}-11_{5\,6}$	77933.9542	150.7	$19_{10\,10}-19_{9\,11}$	80068.7021	33.7
$13_{6\,7}-12_{5\,8}$	80554.7429	−73.2	$15_{11\,4}-15_{10\,5}$	88516.0006	28.7
$14_{6\,8}-13_{5\,9}$	83172.6360	−49.7	$15_{11\,5}-15_{10\,6}$	88516.0006	28.7
$14_{6\,9}-13_{5\,8}$	83171.9142	−37.1	$16_{11\,5}-16_{10\,6}$	88513.8224	8.9
$15_{5\,10}-14_{4\,11}$	77307.8974	142.7	$16_{11\,6}-16_{10\,7}$	88513.8224	8.9
$15_{5\,11}-14_{4\,10}$	77252.8717	70.0	$17_{11\,6}-17_{10\,7}$	88510.7738	16.0
$16_{5\,11}-15_{4\,12}$	79911.0801	19.6	$17_{11\,7}-17_{10\,8}$	88510.7738	16.0
$16_{5\,12}-15_{4\,11}$	79816.4151	−19.2	$18_{11\,7}-18_{10\,8}$	88506.6781	11.6
$16_{7\,9}-15_{6\,10}$	96865.2142	−2.8	$18_{11\,8}-18_{10\,9}$	88506.6781	11.6
$16_{7\,10}-15_{6\,9}$	96865.2142	58.9	$19_{11\,8}-19_{10\,9}$	88501.4695	76.5
$17_{5\,12}-16_{4\,13}$	82513.6421	98.6	$19_{11\,9}-19_{10\,10}$	88501.4695	76.5

[a]All transitions are weighted to be 0.01 relative to the previous cm-wave data[7] with weight=1. [b]$\nu_{o\text{-}c}$: difference between the observed frequency and calculation with the molecular constants listed as Fit II in Table 5.

Table 2. Observed Transitions of $S_2{}^{35}Cl_2$ in the Cell Experiment[a]

$J'_{K_a'K_c'}-J''_{K_a''K_c''}$	ν_{obs}/MHz	$\nu_{o\text{-}c}$/kHz	$J'_{K_a'K_c'}-J''_{K_a''K_c''}$	ν_{obs}/MHz	$\nu_{o\text{-}c}$/kHz
$12_{7\,5}-11_{6\,6}$	86374.2504	31.1	$27_{4\,24}-26_{3\,23}$	87820.1320	12.3
$12_{7\,6}-11_{6\,5}$	86374.2504	32.4	$29_{3\,27}-28_{2\,26}$	78303.2312	−44.8
$12_{8\,4}-11_{7\,5}$	94806.0130	−81.3	$31_{4\,28}-30_{3\,27}$	92251.9616	50.2
$12_{8\,5}-11_{7\,4}$	94806.0130	−81.3	$32_{0\,32}-31_{1\,31}$	79686.1565	−4.8
$13_{7\,6}-12_{6\,7}$	88999.6940	−53.3	$36_{3\,34}-35_{2\,33}$	93387.7136	40.2
$13_{7\,7}-12_{6\,6}$	88999.6940	−49.4	$36_{4\,33}-35_{3\,32}$	99071.7233	−43.0
$14_{7\,7}-13_{6\,8}$	91623.6423	−43.6	$37_{3\,34}-36_{4\,33}$	93665.6640	−0.8
$14_{7\,8}-13_{6\,7}$	91623.6423	−33.0	$24_{12\,12}-24_{11\,13}$	96892.5048	−66.1
$15_{6\,9}-14_{5\,10}$	85786.9255	−18.8	$24_{12\,13}-24_{11\,14}$	96892.5048	−66.1
$15_{6\,10}-14_{5\,9}$	85785.4121	18.8	$27_{11\,16}-27_{10\,17}$	88396.3195	5.2
$16_{6\,11}-15_{5\,10}$	88393.9201	42.0	$27_{11\,17}-27_{10\,18}$	88396.3195	5.1
$19_{6\,13}-18_{5\,14}$	96196.0713	−78.9	$31_{11\,20}-31_{10\,21}$	88281.0672	14.4
$20_{6\,14}-19_{5\,15}$	98784.0974	−139.5	$31_{11\,21}-31_{10\,22}$	88281.0672	13.5

[a]All transitions are weighted to be 0.01 relative to the previous cm-wave data[7] with weight=1.

dx.doi.org/10.1021/jp400632g | J. Phys. Chem. A 2013, 117, 10041−10046

Table 3. Observed Transitions of $S_2{}^{35}Cl^{37}Cl$ in the Supersonic Jet Experiment[a]

$J'_{K_a'K_c'}-J''_{K_a''K_c''}$	ν_{obs}/MHz	ν_{o-c}/kHz	$J'_{K_a'K_c'}-J''_{K_a''K_c''}$	ν_{obs}/MHz	ν_{o-c}/kHz
$8_{8\ 0}-7_{7\ 1}$	83388.8932	2.9	$15_{7\ 9}-14_{6\ 8}$	92980.8807	17.7
$8_{8\ 1}-7_{7\ 0}$	83388.8932	2.9	$16_{6\ 11}-15_{5\ 10}$	87129.3776	89.1
$9_{8\ 1}-8_{7\ 2}$	85953.7153	30.2	$16_{7\ 9}-15_{6\ 10}$	95541.3911	−11.4
$9_{8\ 2}-8_{7\ 1}$	85953.7153	30.2	$16_{7\ 10}-15_{6\ 9}$	95541.3911	43.0
$9_{9\ 0}-8_{8\ 1}$	94320.1873	58.5	$17_{6\ 11}-16_{5\ 12}$	89678.7619	−98.0
$9_{8\ 1}-8_{7\ 0}$	94320.1873	58.5	$17_{6\ 12}-16_{5\ 11}$	89673.4668	−88.1
$10_{8\ 2}-9_{7\ 3}$	88523.3944	38.5	$17_{7\ 10}-16_{6\ 11}$	98099.0919	−116.6
$10_{8\ 3}-9_{7\ 2}$	88523.3944	38.5	$17_{7\ 11}-16_{6\ 12}$	98099.0919	3.2
$10_{9\ 1}-9_{8\ 2}$	96890.3953	61.8	$18_{6\ 12}-17_{5\ 13}$	92210.4995	−17.1
$10_{9\ 2}-9_{8\ 1}$	96890.3953	61.8	$18_{6\ 13}-17_{5\ 12}$	92210.8261	18.5
$11_{8\ 3}-10_{7\ 4}$	91092.8041	39.9	$14_{10\ 4}-14_{9\ 5}$	79554.9559	−73.4
$11_{8\ 4}-10_{7\ 3}$	91092.8041	39.9	$14_{10\ 5}-14_{9\ 6}$	79554.9559	−73.3
$11_{9\ 2}-10_{8\ 3}$	99460.5077	44.1	$15_{10\ 5}-15_{9\ 6}$	79551.9202	−30.4
$11_{9\ 3}-10_{8\ 2}$	99460.5077	44.1	$15_{10\ 6}-15_{9\ 7}$	79551.9202	−30.4
$14_{6\ 8}-13_{5\ 9}$	82025.3107	62.4	$15_{11\ 4}-15_{10\ 5}$	87915.2980	45.4
$14_{6\ 9}-13_{5\ 8}$	82024.6334	44.0	$15_{11\ 5}-15_{10\ 6}$	87915.2980	45.4
$14_{7\ 7}-13_{6\ 8}$	90418.1474	51.5	$16_{11\ 5}-16_{10\ 6}$	87913.3423	1.3
$14_{7\ 8}-13_{6\ 7}$	90418.1474	60.8	$16_{11\ 6}-16_{10\ 7}$	87913.3423	1.2
$15_{6\ 9}-14_{5\ 10}$	84580.8246	150.6	$17_{11\ 6}-17_{10\ 7}$	87910.5349	−52.3
$15_{7\ 8}-14_{6\ 9}$	92980.8807	−5.6	$17_{11\ 7}-17_{10\ 8}$	87910.5349	−52.3

[a]All transitions are weighted to be 0.01 relative to the previous cm-wave data[7] with weight=1.

Table 4. Observed Transitions of $S_2{}^{35}Cl^{37}Cl$ in the Cell Experiment[a]

$J'_{K_a'K_c'}-J''_{K_a''K_c''}$	ν_{obs}/MHz	ν_{o-c}/kHz	$J'_{K_a'K_c'}-J''_{K_a''K_c''}$	ν_{obs}/MHz	ν_{o-c}/kHz
$10_{7\ 3}-9_{6\ 4}$	80151.6019	−92.4	$35_{1\ 35}-34_{0\ 34}$	85131.3641	5.3
$10_{7\ 4}-9_{6\ 3}$	80151.6019	−92.3	$35_{2\ 34}-34_{1\ 33}$	86812.6474	148.4
$11_{7\ 4}-10_{6\ 5}$	82719.8291	−89.0	$36_{0\ 36}-35_{1\ 35}$	87535.6900	4.5
$11_{7\ 5}-10_{6\ 4}$	82719.8291	−88.7	$36_{1\ 36}-35_{0\ 35}$	87536.8808	−4.4
$12_{6\ 6}-11_{5\ 7}$	76904.5742	−80.4	$36_{4\ 33}-35_{3\ 32}$	97278.4804	35.7
$12_{6\ 7}-11_{5\ 6}$	76904.5742	40.0	$37_{0\ 37}-36_{1\ 36}$	89941.3017	−81.3
$12_{7\ 5}-11_{6\ 6}$	85287.2030	−60.0	$37_{1\ 37}-36_{0\ 36}$	89942.2300	−6.3
$12_{7\ 6}-11_{6\ 5}$	85287.2030	−58.8	$37_{2\ 36}-36_{1\ 35}$	91604.4582	117.0
$13_{7\ 6}-12_{6\ 7}$	87853.3626	−70.1	$37_{2\ 35}-36_{3\ 34}$	92877.6106	−124.5
$13_{7\ 7}-12_{6\ 6}$	87853.3626	−66.6	$38_{0\ 38}-37_{1\ 37}$	92346.7780	2.6
$13_{8\ 6}-12_{7\ 5}$	96230.0329	−95.7	$38_{1\ 38}-37_{0\ 37}$	92347.3899	8.6
$13_{8\ 5}-12_{7\ 6}$	96230.0329	−95.7	$38_{1\ 37}-37_{2\ 36}$	93973.6773	19.7
$15_{6\ 10}-14_{5\ 9}$	84579.3323	49.6	$38_{2\ 37}-37_{1\ 36}$	94003.0395	−131.5
$19_{3\ 16}-18_{2\ 17}$	78533.2237	43.5	$39_{0\ 39}-38_{1\ 38}$	94751.8435	−25.4
$19_{4\ 16}-18_{3\ 15}$	75327.3603	−54.0	$39_{1\ 39}-38_{0\ 38}$	94752.3290	30.4
$22_{5\ 18}-21_{4\ 17}$	92914.0478	156.0	$39_{1\ 38}-38_{2\ 37}$	96381.5563	−46.7
$23_{5\ 18}-22_{4\ 19}$	96713.5407	−123.6	$39_{2\ 37}-38_{3\ 36}$	97839.4025	77.2
$25_{4\ 22}-24_{3\ 21}$	84238.8556	−66.1	$39_{3\ 36}-38_{4\ 35}$	97344.2910	23.5
$32_{0\ 32}-31_{1\ 31}$	77909.5005	20.0	$40_{0\ 40}-39_{1\ 39}$	97156.6412	−24.5
$32_{1\ 32}-31_{0\ 31}$	77914.1362	6.7	$40_{1\ 40}-39_{0\ 39}$	97157.0656	95.3
$32_{2\ 31}-31_{1\ 30}$	79652.4259	6.5	$40_{1\ 39}-39_{2\ 38}$	98788.2374	−79.3
$33_{0\ 33}-32_{1\ 32}$	80316.5900	−15.6	$26_{10\ 16}-26_{9\ 17}$	79404.9432	83.4
$33_{1\ 33}-32_{0\ 32}$	80319.9282	1.9	$26_{10\ 17}-26_{9\ 18}$	79404.9432	82.2
$34_{0\ 34}-33_{1\ 33}$	82723.3230	1.8	$37_{12\ 25}-37_{11\ 26}$	95935.4072	−11.6
$34_{1\ 34}-33_{0\ 33}$	82725.6787	−11.2	$37_{12\ 26}-37_{11\ 27}$	95935.4072	−12.5
$35_{0\ 35}-34_{1\ 34}$	85129.6832	11.9			

[a]All transitions are weighted to be 0.01 relative to the previous cm-wave data[7] with weight=1.

two lines appear to be a doublet, it is not an accidental doublet but asymmetric doublet with a common K_c = 37. In the case of high J and low K_a limit, even a near-prolate top asymmetric rotor has a rotational term value similar to a near-oblate top.[15] Therefore, the same intensity or an absence of intensity alternation between these two peaks with K_c'' = 37 shows an absence of the equivalent nuclei in $S_2{}^{35}Cl^{37}Cl$.

The transitions thus assigned for $S_2{}^{35}Cl_2$ and $S_2{}^{35}Cl^{37}Cl$ are listed in Table 2 and 4, respectively. Finally, all observed data including those observed by FTMW were analyzed simultaneously with the Hamiltonian including the sixth-order centrifugal distortion terms. The molecular parameters determined by the least-squares analysis are listed in Table 5 as fit II, in which seven parameters for the sixth-order centrifugal distortion terms are determined. As seen in Figure 2b, the new predicted frequency using fit II parameters shows good agreement with the observed. The standard deviation of the fitting was 0.0057 and 0.0067 MHz for $S_2{}^{35}Cl_2$ and $S_2{}^{35}Cl^{37}Cl$, respectively and is not higher than that in ref 7.

C. Spectral Line Profile and Hyperfine Structures. As seen in Figure 1, each line in the series of the $^rQ_9$-branch of both $S_2{}^{35}Cl_2$ and $S_2{}^{35}Cl^{37}Cl$ was observed as a triplet, in which asymmetric K-doubling is degenerate. On the other hand, the most of the R-transition were observed as a singlet, even if the asymmetric K-doubling is clearly resolved. However, the line widths of the R-transition in Figure 3 look different from each other. All these line profiles can be attributed to hyperfine structures in the rotational transition. The hyperfine components calculated by using the previous hyperfine constants reported in ref 7 are shown below the observed spectrum in the Figures 1 and 3. Due to the selection rule of $\Delta J = \Delta F$, each rotational transition of $S_2{}^{35}Cl_2$ is composed of 10 or 6 strong components depending on whether it is the ortho- or para-state. For example, the contribution of the strong components is 98% of the total intensity in the $^rQ_{10}(16)$ transition. The remaining 2% originate from the off-diagonal matrix elements among states with different J and I quantum numbers. In general, the nuclear quadrupole interaction becomes stronger with decreasing J, and stronger with an increase of K_a in the same J. Therefore, the K_a/J ratio is a useful parameter for estimating the size of the hyperfine splitting. Furthermore, the term values of the hyperfine states in this molecule have a tendency of splitting the components into three bundles. This characteristic mainly comes from the nuclear quadrupole interaction parameter of χ_{aa} and the separation between the bundles depends on the K_a/J ratio. If the lower state of a ^rQ-transition and a ^rR-transition is common, the upper state of the ^rQ-transition has large K_a'/J' ratio than that of the ^rR-transition; that is $(K_a'' + 1)/J''$ and $(K_a'' + 1)/(J'' + 1)$, respectively. Therefore, in general, the three-bundle structure is more easily reflected as a triplet spectral pattern in the ^rQ-transition than in the ^rR-transition.

Another example of R-transitions is shown in Figure 3. The calculated hyperfine structure spreads wider in the $16_{6,11}-15_{5,10}$ transition than in the $16_{5,11}-15_{4,12}$ transition as the K_a/J ratio is larger. In addition, the observed spectrum is further broadened due to the Doppler effect in the experimental condition. The former was observed with the gas cell and the latter with the supersonic jet. It is obvious that although the Doppler broadening is narrower in the supersonic jet than in the gas cell, it is still far from complete separation of individual hyperfine structures. Although we did not use this hyperfine information for the least-squares analysis, such line-width and line-profile dependence on the K_a/J ratio helps to confirm the assignment of the rotational quantum numbers. As described above, the hyperfine structures observed in the mm-wave region were well reproduced by the

dx.doi.org/10.1021/jp400632g | J. Phys. Chem. A 2013, 117, 10041−10046

Table 5. Rotational Constants and Centrifugal Distortion Constants of S_2Cl_2

	$S_2{}^{35}Cl^{35}Cl$			$S_2{}^{35}Cl^{37}Cl$		
	fit I[a]	fit II[b]	ref 7	fit I[a]	fit II[b]	ref 7
A/MHz	5533.8937(6)[c]	5533.8934(9)	5533.8964(11)	5475.4350(6)	5475.4349(12)	5475.4344(11)
B/MHz	1393.8461(14)	1393.8512(8)	1393.8436(3)	1361.8654(7)	1361.8651(5)	1361.8640(5)
C/MHz	1232.6697(12)	1232.6640(8)	1232.6728(2)	1205.1932(6)	1205.1908(7)	1205.1953(8)
Δ_J/kHz	0.568(8)	0.585(3)	0.556(3)	0.531(3)	0.511(1)	0.554(9)
Δ_{JK}/kHz	−5.150(47)	−5.219(19)	−5.115(47)	−4.937(13)	−4.727(11)	−4.465(147)
Δ_K/kHz	24.04(4)	24.02(3)	24.70(25)	23.60(2)	23.33(4)	22.68(37)
δ_J/kHz	0.131(6)	0.122(3)	0.144(2)	0.114(17)	0.1109(8)	0.054(20)
δ_K/kHz	1.9(8)	4.8(4)			0.6(1)	
H_J/kHz		0.033(2)			−0.0044(8)	
H_{JK}/Hz		−1.3(1)			1.8(1)	
H_{KJ}/Hz		4.6(5)			−4.5(3)	
H_K/Hz		−3.9(5)			1.9(3)	
h_J/Hz		−0.0144(2)			−0.0015(5)	
h_{JK}/Hz		3.7(3)			0.12(7)	
h_K/Hz		−42(4)			59 (3)	
σ_{fit}/MHz	0.0036	0.0057	0.0039	0.0043	0.0067	0.0045

[a]Determined with the data by the supersonic jet experiment and the previous cm-wave experiment.[7] [b]Determined with the data by both the supersonic jet and the cell experiment and the previous cm-wave experiment.[7] [c]Numbers in parenthesis denotes one standard deviation of least-squares fitting in the unit of the last significant digit.

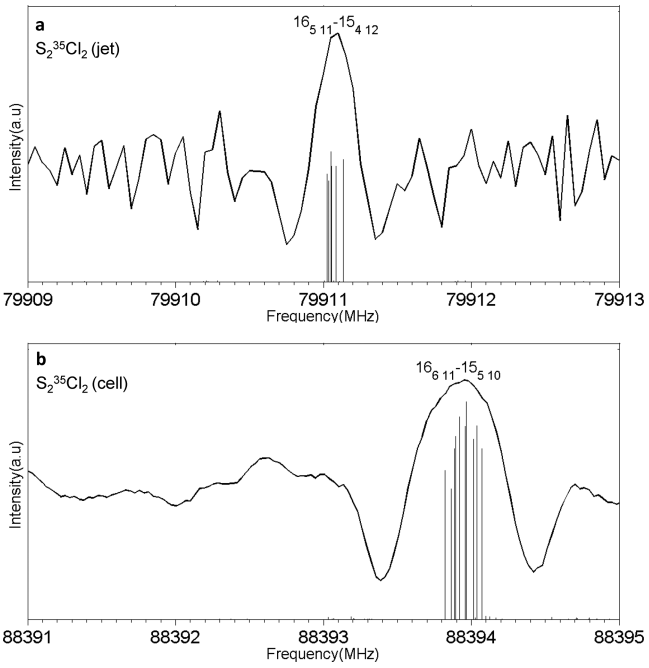

Figure 3. (a) Para $16_{5,11}-15_{4,12}$ transition of $S_2{}^{35}Cl_2$ observed with the supersonic jet experiment. (b) Ortho $16_{6,11}-15_{5,10}$ transition of $S_2{}^{35}Cl_2$ observed with the gas cell experiment. Stick lines show the calculated hyperfine structures. Spreading of the hyperfine components depends on the K_a/J ratio. The observed spectral profile also shows the difference in Doppler broadening between the supersonic jet and the gas cell experiment.

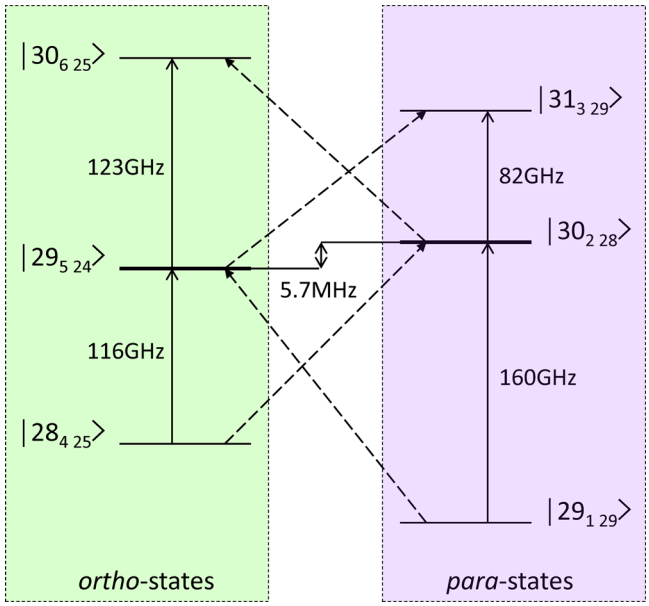

Figure 4. Energy levels of accidentally neighboring pair of ortho-$|29_{5,24}\rangle$ and para-$|30_{2,28}\rangle$ state, and four states related with the rotational transitions. The normal b-type rotational transitions are indicated by vertical arrows in the common symmetry states, and the ortho−para transitions are shown by dashed arrows crossing the different symmetric states. The ortho−para transitions appear beside the normal transition with the energy difference of 5.7 MHz.

nuclear quadrupole interaction parameters determined in the previous cm-wave experiment.[7] It should be enhanced again that the understanding for each hyperfine eigenstate is a key point for surveying the ortho−para transition, even if those structures are buried in the Doppler broadening.

D. Candidate MW Transitions for Ortho−Para Transition. As shown in eq 1, the ortho−para transition intensity depends on the mixing ratio of ortho and para state and energy difference of those mixing state. To have a large intensity borrowing, a large numerator and a small denominator are favorable. Therefore, by using the new rotational constants determined in this work, we searched for accidentally small energy denominator among the rotational states of $J \leq 40$ and $K_a \leq 40$. In the process of searching, the difference in the rotational quantum numbers was restricted to $\Delta F = 0$, $\Delta J \leq 3$, and $\Delta K_a \leq 3$, because otherwise the matrix elements between the ortho and para state have nonzero values. As a result, we found the rotational term energy of ortho-$|29_{5,24}\rangle$ and para-$|30_{2,28}\rangle$ state differs by only

dx.doi.org/10.1021/jp400632g | J. Phys. Chem. A 2013, 117, 10041−10046

5.7 MHz. In Figure 4, the ortho−para candidate transitions are schematically shown by dashed crosswise arrows, whereas the normal *b*-type transitions are shown by vertical arrows. It shows that the ortho−para transitions always go with the normal transition by the energy difference of 5.7 MHz. Therefore, a too small energy difference between ortho and para state makes it difficult to distinguish the very weak transition from strong normal transition consist of many hyperfine components spreading over a few megahertz. Therefore, in the point of frequency measurement, these four transitions are possible candidates in the mm-wave region. About the value of the state mixing, we should be more careful because it demands inherent eigenvectors identification for the case of nearly degenerate solution. On that point we are preparing a new program for the diagonalization of the Hamiltonian matrix involving the hyperfine interaction. More quantitative discussion on the ortho−para transition will be reported elsewhere after confirming the validation of the new program.

IV. CONCLUSIONS

We have extended the frequency region of microwave spectroscopy of S_2Cl_2 up to 100 GHz. The rotational molecular constants including the fourth-order and sixth-order centrifugal distortion constants were determined. These constants improve the prediction of transition frequencies in the mm-wave region. We also confirmed that the previous hyperfine constants determined in the cm-wave region are sufficiently adequate to reproduce the partly resolved spectral profiles observed by Doppler-limited spectroscopy in the mm-wave region. With the new rotational constants from this study and the previous hyperfine constants, it will be possible to predict the ortho−para mixing ratio and to narrow down the possible candidates for the observation of the ortho−para transition in the mm-wave region.

AUTHOR INFORMATION

Corresponding Author

*Tel: 81-3-5734-2615. E-mail: kanamori@phys.titech.ac.jp

Notes

The authors declare no competing financial interest.

ACKNOWLEDGMENTS

It is a great pleasure to dedicate this paper to Prof. T. Oka. We have learned a lot of thing from him about the interconversion between different nuclear spin states in molecules with identical nuclei. His strong interest in our previous S_2Cl_2 study encourages us extensively to promote this ambitious research subject of the ortho−para transition.

REFERENCES

(1) Palmer, K. J. The Electron Diffraction Investigation of Sulfur Monochloride, Sulfur Dichloride, Sulfur Trioxide, Thionyl Chloride, Sulfuryl Chloride, Vanadium Oxytrichloride, Chromyl Chloride. *J. Am. Chem. Soc.* **1938**, *60*, 2360−2369.

(2) Hirota, E. An Electron Diffraction Investigation on the Molecular Structure of Sulfur Monochloride and Monobromide. *Bull. Chem. Soc. Jpn.* **1958**, *31*, 130−138.

(3) Beagley, B.; Eckersley, G. H.; Brown, D. P.; Tomilinson, D. Molecular Structure of S_2Cl_2. *Trans. Faraday Soc.* **1969**, *65*, 2300−2307.

(4) Frankiss, S. G. Vibrational Spectra and Structures of S_2Cl_2, S_2Br_2, Se_2Cl_2 and Se_2Br_2. *J. Mol. Struct.* **1968**, *2*, 271−279.

(5) Frankiss, S. G.; Harrison, D. J. Vapor State Raman Spectra and Thermodynamic Properties of Sulfur Dichloride and Disulfur Dichloride. *Spectrochim. Acta* **1975**, *31A*, 161−167.

(6) Marsden, C. J.; Brown, R. D.; Godfrey, P. D. Microwave Spectrum and Molecular Structure of Disulfur Dichloride, S_2Cl_2. *J. Chem. Soc., Chem. Commun.* **1979**, *9*, 399−401.

(7) Mizoguchi, A.; Ota, S.; Kanamori, H.; Sumiyoshi, Y.; Endo, Y. Analysis of the Nuclear Quadrupole Interaction of Disulfur Dichloride, S_2Cl_2. *J. Mol. Spectrosc.* **2008**, *250*, 86−97.

(8) Lee, T. D.; Yang, C. N. Question of Parity Conservation in Weak Interactions. *Phys. Rev.* **1956**, *104*, 254−258.

(9) Ambler, E.; Hayward, R. W.; Hoppes, D. D.; Hudson, R. P. Experimental Test of Parity Conservation in Beat Decay. *Phys. Rev.* **1957**, *105*, 1413−1415.

(10) Bouchiat, M. A.; Guena, J.; Hunter, L.; Pottier, L. Observation of Parity Violation in Cesium. *Phys. Lett.* **1982**, *117B*, 358−364.

(11) Daussy, Ch.; Marrel, T.; Amy-Klein, A.; Nguyen, C. T.; Bordé, Ch. J. Chardonnet, Ch. Limits on the Parity Nonconserving Energy Difference between the Enantiomers of a Chiral Molecule by Laser Spectroscopy. *Phys. Rev. Lett.* **1999**, *83*, 1554−1557.

(12) Berger, R.; Gottselig, M.; Quack, M.; Willeke, M. Parity Violation Dominates the Dynamics of Chirality in Dichlorodisulfane. *Angew. Chem., Int. Ed.* **2001**, *40*, 4195−4198.

(13) Hougen, J. T.; Oka, T. Nuclear Spin Conversion in Molecules. *Science* **2005**, *310*, 1913−1914.

(14) Gordy, W.; Cook, R. L. *Microwave Molecular Spectra*; John Wiley & Sons: New York, 1970.

(15) Townes, C. H.; Schawlow, A. L. *Microwave spectroscopy*; McGraw-Hill: New York, 1955.